

AGARD

ADVISORY GROUP FOR AEROSPACE RESEARCH & DEVELOPMENT

7 RUE ANCELLE, 92200 NEUILLY-SUR-SEINE, FRANCE

DTIC
ELECTE
MAR 22 1995
G D

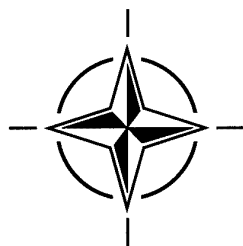
AGARD CONFERENCE PROCEEDINGS 565

Corrosion Detection and Management of Advanced Airframe Materials

(la Détection de la corrosion et la gestion des matériaux
avancés entrant dans la construction des cellules)

*Papers presented at the 79th Meeting of the AGARD Structures and Materials Panel, held in
Seville, Spain, 5-6 October 1994.*

19950321 155



NORTH ATLANTIC TREATY ORGANIZATION

DISTRIBUTION STATEMENT A

Approved for public release;
Distribution Unlimited

Published January 1995

Distribution and Availability on Back Cover

AGARD

ADVISORY GROUP FOR AEROSPACE RESEARCH & DEVELOPMENT

7 RUE ANCELLE, 92200 NEUILLY-SUR-SEINE, FRANCE

AGARD CONFERENCE PROCEEDINGS 565

Corrosion Detection and Management of Advanced Airframe Materials

(la Détection de la corrosion et la gestion des matériaux
avancés entrant dans la construction des cellules)

Papers presented at the 79th Meeting of the AGARD Structures and Materials Panel, held in Seville, Spain, 5-6 October 1994.



North Atlantic Treaty Organization
Organisation du Traité de l'Atlantique Nord

Accession For	
NTIS	CRA&I <input checked="" type="checkbox"/>
DTIC	TAB <input type="checkbox"/>
Unannounced	<input type="checkbox"/>
Justification	
By	
Distribution/	
Availability Codes	
Dist	Avail and/or Special
A-1	

The Mission of AGARD

According to its Charter, the mission of AGARD is to bring together the leading personalities of the NATO nations in the fields of science and technology relating to aerospace for the following purposes:

- Recommending effective ways for the member nations to use their research and development capabilities for the common benefit of the NATO community;
- Providing scientific and technical advice and assistance to the Military Committee in the field of aerospace research and development (with particular regard to its military application);
- Continuously stimulating advances in the aerospace sciences relevant to strengthening the common defence posture;
- Improving the co-operation among member nations in aerospace research and development;
- Exchange of scientific and technical information;
- Providing assistance to member nations for the purpose of increasing their scientific and technical potential;
- Rendering scientific and technical assistance, as requested, to other NATO bodies and to member nations in connection with research and development problems in the aerospace field.

The highest authority within AGARD is the National Delegates Board consisting of officially appointed senior representatives from each member nation. The mission of AGARD is carried out through the Panels which are composed of experts appointed by the National Delegates, the Consultant and Exchange Programme and the Aerospace Applications Studies Programme. The results of AGARD work are reported to the member nations and the NATO Authorities through the AGARD series of publications of which this is one.

Participation in AGARD activities is by invitation only and is normally limited to citizens of the NATO nations.

The content of this publication has been reproduced
directly from material supplied by AGARD or the authors.

Published January 1995

Copyright © AGARD 1995
All Rights Reserved

ISBN 92-836-1011-3



Printed by Canada Communication Group
45 Sacré-Cœur Blvd., Hull (Québec), Canada K1A 0S7

Preface

Advanced materials such as polymer matrix composites, high temperature and low density aluminum alloys and titanium alloys are being used in combination in military aircraft. Environmental degradation decreases mechanical integrity, reduces service life and increases the life cycle costs of these systems. Methods of corrosion detection and management must be established for enhanced longevity of current and future NATO aircraft.

At the 79th Meeting of the Structures and Materials Panel of AGARD, the SMP held a Specialists' Meeting on Corrosion Detection and Management of Advanced Airframe Materials. The purpose of the Specialists' Meeting was to present the current knowledge base of corrosion, degradation, detection and prevention and to identify the research and development issues which must be addressed in order to ensure long service life and low maintenance costs of NATO aircraft. The meeting concentrated on:

- Corrosion Detection
- Test Methodology for Environmental Assessment
- Mechanistic Evaluation
- Corrosion Prevention Methods
- Materials Selection and Design to Prevent Environmental Degradation

The Specialists' Meeting involved four sessions:

- Corrosion Behavior of Aircraft Materials-General
- Methods of Detection
- Prevention
- Recent Field Experience

On behalf of the Structures and Materials Panel, we would like to thank the authors, session chairmen and technical evaluation reporters whose participation made possible the success of the Specialists' Meeting.

Dr. E.A. Starke, Jr.
Dr. J. Waldman
Co-Chairmen, Sub-Committee on
Corrosion Detection and Management
of Advanced Airframe Materials

Préface

Les matériaux avancés tels que les matériaux composites à matrice de polymère et les alliages d'aluminium et de titane de faible densité et de haute température sont utilisés en combinaison dans la construction des avions militaires. La dégradation occasionnée par les conditions ambiantes a pour effet la diminution de l'intégrité mécanique, la réduction de la durée de vie et l'augmentation du coût complet d'utilisation de ces systèmes. Des méthodes de détection et de gestion de la corrosion doivent être établies afin de prolonger la durée de vie des avions actuels et futurs de l'OTAN.

Lors de sa 79^{ième} réunion, le Panel AGARD des structures et matériaux (SMP) a organisé une réunion de spécialistes sur la détection de la corrosion et la gestion des matériaux entrant dans la construction des cellules. Cette réunion a eu pour objet de présenter l'état actuel des connaissances dans le domaine de la corrosion, la dégradation, la détection et la prévention, ainsi que d'identifier les voies de recherche et développement qui seraient à suivre afin d'assurer la longévité et la diminution des coûts de maintenance des avions de l'OTAN. La réunion a examiné les questions suivantes :

- la détection de la corrosion
- les méthodologies de test pour l'évaluation de l'environnement
- l'évaluation mécanistique
- les méthodes de prévention de la corrosion
- le choix des matériaux et des méthodes de conception pour empêcher la dégradation occasionnée par les conditions ambiantes

La réunion de spécialistes s'est déroulée en quatre sessions :

- le comportement en corrosion des matériaux entrant dans la construction des aéronefs — généralités
- les méthodes de détection
- la prévention
- l'expérience récente sur le terrain

Au nom du Panel des structures et matériaux, nous tenons à remercier les auteurs, les présidents de session et les rapporteurs d'évaluation technique, dont la participation a assuré la réussite de cette réunion de spécialistes.

Structures and Materials Panels

Chairman: Mr. R. Labourdette
Directeur Scientifique
des Structures
ONERA
29, Av. de la Div. Leclerc
92322 Châtillon Cedex
France

Deputy Chairman: Dr. O. Sensburg
Chief Engineer
Deutsche Aerospace AG
Militaerflugzeuge
Postfach 80 11 60
81663 Munich
Germany

Sub-Committee Members

Chairman: Prof. Dr. E.A. Starke, Jr.
Earnest Oglesby, Professor & Dean
School of Engineering and
Applied Science
University of Virginia
Charlottesville, VA 22903-2442
USA

Members:	P. Armando	—	FR	L. Kompotiatis	—	GR
	H.J.G. Cavalcinios	—	PO	G. Papakonstantinou	—	GR
	D. Chaumette	—	FR	D. Paul	—	US
	L. Chesta	—	IT	R. Potter	—	UK
	P. Costa	—	FR	T. Ronald	—	US
	D. Coutsouradis	—	BE	D. Simpson	—	CA
	H. Goncalo	—	PO	J. Waldman	—	US
	W. Van der Hoeven	—	NE			
	J.P. Immarigeon	—	CA			
	R. Kochendörfer	—	GE			

Panel Executive

Dr Jose M. CARBALLAL, Spain

Mail from Europe:
AGARD-OTAN
7, rue Ancelle
92200 Neuilly-sur-Seine
France

Mail from US and Canada:
From USA and Canada
AGARD-NATO/SMP
PSC 116
APO AE 09777

Tel: 33 (1) 4738 5790 & 5792
Telefax: 33 (1) 4738 5799
Telex: 610176F

Contents

	Page
Preface/Préface	iii
Structures and Materials Panels	iv
	Reference
Technical Evaluation Report by M. DORUK and R.L. THOMAS	T
SESSION I: CORROSION BEHAVIOR OF AIRCRAFT MATERIALS — GENERAL	
The Corrosion and Protection of Advanced Aluminium-Lithium Airframe Alloys by C.J.E. SMITH, D.L. BARTLETT and J.A. GRAY	1
Exfoliation Corrosion and Stress Corrosion Cracking Behaviour of Al-Li Alloys by R. BRAUN	2
Effect of Loading Direction and Long-Term Aging on Fatigue-Crack Growth in Al-Li Alloy 2090 by M. ANIK and M. DORUK	3
Corrosion of Landing Gear Steels by E.U. LEE, J. KOZOL, J.B. BOODEY, and J. WALDMAN	4
Specific Features of Corrosion Behavior of Stainless Maraging Steels for Aerospace Application by V.B. SPIRIDONOV and V.V. SHARAPOV	5
The Detection and Analysis of Galvanic Damage in BMI/Graphite Fiber Composites by S.R. TAYLOR and G.L. CAHEN, Jr.	6
SESSION II: METHODS OF DETECTION	
Double Pass Retroreflection for Corrosion Detection in Aircraft Structures by J.P. KOMOROWSKI, S. KRISHNAKUMAR, R.W. GOULD, N.C. BELLINGER, F. KARPALA and O.L. HAGENIERS	7
The Use of Electrochemical Impedance Spectroscopy to Predict the Corrosion of Aluminum-Lithium Alloys in Marine Environments by D.R. LENARD, J.G. MOORES, P.R. ROBERGE and E. HALLIOP	8
Non-Destructive Detection of Corrosion for Life Management by D.A. BRUCE	9
Health and Usage Monitoring Systems — Corrosion Surveillance by J.D. SMART and D.C. WEETMAN	10
Eddy Current Detection of Pitting Corrosion Around Fastener Holes by J.H. HEIDA and W.G.J. 't HART	11
In-Situ Detection of Surface Passivation or Activation and of Localized Corrosion: Experiences and Prospectives in Aircraft by A. POURBAIX, JR.	12

Test Method and Test Results for Environmental Assessment of Aircraft Materials by A. POURBAIX, Jr.	13
SESSION III: PREVENTION	
Corrosion Protection Measures for CFC/Metal Joints of Fuel Integral Tank Structures of Advanced Military Aircraft by C.D. HAMM	14
Corrosion Prevention with Environmentally Compliant Materials — A Design Challenge by C.W. MATZ	15
New Nondestructive Techniques for Detection and Quantification of Corrosion in Aircraft Structures by W.P. WINFREE, K.E. CRAMER, P.H. JOHNSTON and M. NAMKUNG	16
Organic Coating Technology for the Protection of Aircraft Against Corrosion by C.R. HEGEDUS, S.J. SPADAFORA and A.T. ENG	17
Problems of Predicting Material Property Retention During Long Term Service by Yu. P. GORDEEV and A.M. KHOMUTOV	18
SESSION IV: RECENT FIELD EXPERIENCE	
Corrosion Detection and Monitoring of Aircraft Structures: An Overview by V.S. AGARWALA, P.K. BHAGAT and G.L. HARDY	19
Paper 20 withdrawn	20
Experience of In-Service Corrosion on Military Aircraft by H.J. VOSS	21
U.S. Navy Operating Experience with New Aircraft Construction Materials by G.T. BROWNE	22
Corrosion In Service Experience with Aircraft in France by M.-J. FRUSTIE and P. GAUTHIER	23
USAF Aging Aircraft Corrosion Program D.E. NIESER	24

TECHNICAL EVALUATION REPORT

R. Doruk
Metallurgical Engineering Department
METU 06531 ANKARA TURKEY

and

R.L. Thomas
Institute for Manufacturing Research
Wayne State University
Detroit, Michigan 48202 USA

1. SUMMARY

This paper presents a technical evaluation of the Specialists' Meeting on "Corrosion Detection and Management of Advanced Airframe Materials, held at the 79th meeting of the AGARD Structures and Materials Panel on October 3-7, 1994 in Sevilla, Spain.

2. INTRODUCTION

The task of maintaining the airworthiness of aircraft in corrosive environments is a challenging one, both for the military and civilian operators. Decreases in defense spending have placed severe constraints on replacement acquisitions of military aircraft, and in turn, these constraints represent a de facto decision to maintain the airworthiness of currently operating military aircraft over unprecedented extend life spans. Aircraft which were originally designed for operating lives in the range 20-30 years are now anticipated to be in service for life spans of 60-80 years (Nieser, Paper 23). If one considers the current distribution of the aging (>20 yrs) USAF fleets, it is clear that several (most notably the C/KC-135 fleet) are already well beyond their original design lifetimes. The magnitude of the projected life extension of such military aircraft calls for a very diligent consideration of new technical problems associated with the combined effects of wide spread corrosion and fatigue damage. Problems associated with corrosion are also important in ensuring long service life and low maintenance costs of current and future NATO aircraft, for which advanced airframe materials are increasingly being utilized. Composite materials and high performance alloys are now frequently used in combination, and such usage raises additional technical problems which must be addressed. The

goal of this AGARD workshop was to provide a forum for discussions and information exchange by specialists in the areas of nondestructive inspection for corrosion, test methodology for accelerated laboratory simulation of long-term corrosion, mechanical testing for the combined effects of corrosion and fatigue, environmentally compliant corrosion protection, and in-service field experience, on both aging (i.e. >20 yrs) and new aircraft.

3. CONTENTS OF PRESENTATIONS

3.1 Corrosion Behavior of Aircraft Materials - General

A series of papers presented data on several aspects of corrosion of aluminum-lithium airframe alloys, including 8090-T81, and 2091-T84 sheet materials, as well as 8090-T8171, 2090-T8E41 and 2901-T8X51 plates. Smith et al (Paper 1) and Braun (Paper 2) have independently concluded that 8090-T81 sheets are susceptible to exfoliation corrosion. Smith et al conclude that this problem is particularly severe in non-recrystallized material where the grains are very elongated. Furthermore, both groups also demonstrated that the exfoliation corrosion which occurs under marine exposure conditions on this material can be reproduced in the laboratory using the intermittent acidified salt fog test (the so-called MASTMAASIS test). Such laboratory testing also indicated that 8090-T81 and 2091-T84 sheet materials are sensitive to stress corrosion cracking. Similar studies on 8090-T8171 and 2901-T8X51 plates yielded the conclusion that there is little environmentally assisted cracking when the stress is applied in the longitudinal and long transverse directions, but that when loaded in the short transverse direction, both plate materials are susceptible to stress corrosion cracking, with threshold stresses below 100 MPa. Observations by Doruk on the 2090 plates (Paper 3) indicated that there is no significant orientation-dependence of fatigue-crack growth behavior, but that long-term aging has a pronounced effect on the growth kinetics, with an observed acceleration of up to 8-fold following aging for 1000 hr. The latter studies indicated that crack growth may be impeded either by the passivation of the crack front under the effect of high anodic currents or the removal of hydrogen ions from the crack-tip region, resulting in a retardation of hydrogen embrittlement. Studies by Lenard et al (Paper 8) suggest that electrochemical impedance spectroscopy (EIS) can be a useful

technique for rapidly assessing the relative corrosion resistance of different aluminum alloys. Using these techniques, the authors found that 8090-T851 material undergoes severe intergranular cracking, associated with the pitting initiated at the edges of the specimens, and concluded that unless care is taken to seal the edges of components made from this material and to deny access of sea water to crevices, then corrosion failures can be expected to occur even though exposed surfaces of the alloy may appear undamaged. Their data indicate that 2090 sheet appears to be more resistant to corrosion at the edges than is 7075 material, and that the corrosion of the rolled surfaces of the 2090 sheet can easily be controlled by the proper application of protective coatings.

Two papers were devoted to the corrosion behavior of steel alloy materials, one (Lee et al, Paper 4) dealing with landing gear steels, the second, (Spiridonov and Sharapov, Paper 5) considering the behavior of stainless maraging steels. Of the five landing gear steels studied, AF1410 steel was found to be most resistant to stress corrosion cracking, with its higher strength derivative, AerMet 100, being next. The AerMet 100 steel was found to have a better combination of high fracture toughness and high tensile strength than AF1410, and was found to be less susceptible to hydrogen embrittlement than 300M steel, one of the materials which has been used in the past for highly loaded structural components in US Navy aircraft. The study of stainless Cr-Ni "maraging" steels, i.e., steels strengthened by transformation of austenite to martensite, followed by aging of the martensite matrix, found satisfactory agreement with a model which suggests an accelerated testing for susceptibility to stress corrosion cracking using an alternating electrochemical polarization technique. The study concluded that exposure of stainless Cr-Ni steels to nitrogen tetroxide produces corrosion damage in the form of intergranular oxidizing embrittlement, a model for which was discussed by Spiridonov and Sharapov (Paper 5).

Throughout the Specialists' Meeting, it was noted that galvanic damage is possible in multi-material assemblies. Taylor and Cahen (Paper 6) studied the detection and analysis of this type of damage for bismaleimide (BMI)-graphite fiber composites when galvanically coupled to an active metal such as aluminum, a situation which occurs more and more frequently in modern aerospace structures. Cathodic polarization of such material was found to degrade the fiber/matrix interface,

producing a porous interface which can be observed via sensitive EIS techniques. Although the prevailing view prior to this research has speculated that hydroxyl ion production may be the damaging species in this phenomenon, the research presented in Paper 6 indicates that oxygen reduction reaction intermediates may in fact play a key role in the damage. Additionally, although titanium has a smaller galvanic coupling to BMI-graphite fiber material, their experimental findings indicate that the galvanic coupling is not necessarily benign in this case, either, and should be studied further as a function of temperature and in the presence of crevices.

3.2 Methods of Detection

The task of detecting corrosion in aircraft structures is an important one, and in light of the fact that the corrosion is often hidden beneath the surface of the structure, it is also a challenging one. The role of nondestructive evaluation (NDE) is essential in ensuring airworthiness of aircraft whose age approach design lifetimes, or whose environmental operating conditions diverge from those under which major airframe static and fatigue tests to verify those lifetimes may have been conducted. New challenges are presented as new materials, such as aluminum-lithium alloys and various composites are used. As noted by Bruce (Paper 9), utilization of NDE can only be relied upon to ensure safety once it has been demonstrated to be effective, with a standard introduced by the USAF some years ago as part of its damage tolerance procedures requiring a "probability of detection" (POD) of 90% to be demonstrated at the 95% confidence level at the desired detection level. These procedures have been applied successfully for the detection of fatigue cracks, but are more difficult to apply to the case of corrosion damage, since comparable information on the reliability of corrosion detection NDE methods is not yet available.

Several authors broadly reviewed the current status of NDE of aircraft structures for hidden corrosion, e.g., Bruce (Paper 9), Winfree et al (Paper 16), Agarwala et al (Paper 19), and Nieser (Paper 23). As noted in Paper 19, current methods can require over 1,000 man-hours of disassembly, inspection, and reassembly for areas that cannot be inspected in-situ. Thus, disassembly remains a high priority research and development issue. Traditional techniques for subsurface inspection include

eddy current, ultrasonic, and radiographic methods. Winfree et al (Paper 16) summarized the comparative features of four techniques as follows: eddy current - capable of determining material loss in first and second layers; ultrasonic - capable of accurate quantification of material loss in the first layer of the structure; thermal (a large-area technique, capable of locating regions with 10% or more material loss; and X-ray - for detection throughout the full thickness of the structure. Two emerging techniques for rapid, wide-area inspection for subsurface corrosion were discussed in some detail during the Meeting: an optical double pass retroreflection surface inspection technique (D-sight), described in detail by Komorowski et al (Paper 7), and infrared thermal wave imaging techniques, presented briefly by Winfree et al (Paper 16) and Agarwala et al (Paper 19). The D-sight technique might seem to be limited to surface corrosion, but because of the fact that it is very sensitive to the surface bulging ("pillowing") effects caused by the confinement of subsurface corrosion products, the authors conclude that it has good potential for lap splice subsurface corrosion detection. Data were presented which compared the technique favorably to results using X-ray, shadow Moiré, and eddy current inspections of a series of test specimens exposed to accelerated corrosion. Thermal wave imaging was also presented as a rapid, wide-area inspection technique, capable of imaging subsurface corrosion in lapsplines, tear straps and other areas of aircraft fuselages. Thermal wave images of pitting and exfoliation corrosion in the vicinity of wing fasteners were shown as preliminary indication of the utility of the NDE technique for such difficult corrosion damage inspection tasks. The difficulty of the inspection was presented by Heida and 't Hart (Paper 11), who studied the eddy current detection of pitting corrosion around fastener holes on F-16 lower wing skins, and concluded that despite its high sensitivity, the corrosion clean-up limit of only 1.5 - 2.5% (0.08 - 0.32 mm), the eddy current technique is considered not applicable for in-service depth assessment of countersink edge corrosion in such skins. Smart and Weetman (Paper 10) presented data from laboratory trials that have shown that electrochemical noise and impedance monitoring techniques can be used for the detection and characterization of corrosion processes. They installed a prototype monitoring system in an aircraft and used it to monitor the localized corrosion activity occurring in specific areas of the aircraft. Considerable progress has been made in recent years in establishing reliable NDE methods

for the detection of corrosion and environmental degradation of composite materials in aircraft. The complexity of the problems, the increasing age of aircraft fleets, and the increasing use of new materials and combinations of materials, suggests that corrosion detection in airframe materials should remain a high priority.

3.3 Prevention

In addition to the corrosive effects of exposure to salt water, high humidity, and atmospheric pollutants, military aircraft are exposed to a wide variety of corrosive chemicals used in maintenance and operational activities. The current status of organic coating technology for protection against such environmental exposure was reviewed by Hegedus and Spadafora (Paper 17), who, along with Matz (Paper 15), pointed out the special challenges presented by the need to eliminate carcinogenic chromates and cadmium, and hexavalent chromium, all proven to be particularly effective in current coating technology. Other environmentally compliant coatings issues relate to the minimization of volatile organic compounds and halogenated solvents. A self-priming topcoat, satisfying these requirements, has been used successfully by the U.S. Navy and Air Force. Hamm (Paper 14) discussed the corrosion protection of dissimilar materials, with the example of carbon fiber composite/metal joints in integral fuel tank structures on advanced military aircraft. Non-adhesive sealing tapes have been adopted for application on faying surfaces of some such joints, combined with glass fiber scrim and polyurethane primer on the CFC side of the joint.

3.4 Recent Field Experience

Recent field experience was reported by Agarwala et al (Paper 19), Voss (Paper 20), Browne (Paper 21), Frustie and Gautier (Paper 22), and Nieser (Paper 23). The review by Browne pointed out that the U.S. Navy operates more aircraft containing carbon epoxy composite, new aluminum alloy/tempers and steels in the naval operating environment than any other organization in the world. The operating conditions cover wide ranges of temperature, exposure to sea water, and the general problems associated with world-wide atmospheric pollution, and thus provide a material testing lab that is second to none. Among the field problems surveyed by Browne were composite degradation

resulting from attachment to conventional alloys, and water ingress. One class of problems was associated with the necessity of providing electromagnetic interference (EMI) shielding - leading to inevitable galvanic corrosion problems, which were met by the development of a conductive , corrosion inhibiting sealant: polythioether, filled with Ni-coated carbon fibers. Initial experience on this sealant seems promising. He also provided examples of corrosion on steel fasteners, Al components, and crevices. Air Force field experience, reported by Nieser, was concentrated on the combined effects of wide spread corrosion damage and wide spread fatigue damage, the effects of which on structural integrity are not currently fully understood. As exemplified by the C/KC-135 fleet, which is scheduled to operate to the year 2040. This aircraft has a unique construction (spot-welded lap joints/doublers) which makes it very susceptible to hidden corrosion. Such corrosion is said to be a real problem in the field today, and will worsen as the fleet continues to age. A major corrosion program is currently underway by the Air Force, Navy, FAA, NASA, industry, and academia to address this problem. Preliminary results of the program were discussed.

4. CONCLUSIONS

1. Corrosion detection and management is a problem of growing significance, because of the aging of the world's existing aircraft fleets, the pervasiveness of corrosive environments in which they must operate, and the comparatively limited experience in assessing the structural effects of wide-spread corrosion.
2. New materials, both alloys and composites, and combinations of these materials in aircraft structures, present new challenges for the detection and management of corrosive degradation.
3. Of the various techniques for accelerated corrosion testing of aluminum alloy materials, the cyclic acidified salt fog (MASTMAASIS test according to ASTM G85, Annex A2) appears best to reproduce marine exposure results for conventional materials and seems also to be a promising testing technique to predict the service performance of high strength aluminum-lithium based alloys.

4. There exist a variety of inspection techniques for the detection of hidden corrosion, each having complementary benefits with respect to the other. Several emerging inspection techniques show promise for more rapid and more quantitative detection of hidden corrosion. A challenge remains to develop assessments of the reliability with which these methods can be applied.
5. The careful utilization of coatings technology plays an important role in the prevention of corrosion. Many of the most effective treatments are not environmentally benign, however, and while good progress has been made, the replacement treatments should be improved through additional research and development.

5. RECOMMENDATIONS

1. This AGARD workshop should be repeated in about four years. Possible new problems associated with operation of aging aircraft and more wide-spread introduction of new materials should be addressed periodically.
2. The AGARD community should participate actively in the ongoing aging aircraft programs aimed at understanding the fundamentals of the corrosion of aerospace materials, the development of corrosion protection coatings, and the development and application of nondestructive inspection for hidden corrosion.

The Corrosion and Protection of Advanced Aluminium - Lithium Airframe Alloys

C J E Smith, D L Bartlett and J A Gray

Structural Materials Centre

Defence Research Agency

Farnborough, Hampshire GU14 6TD

United Kingdom

1. SUMMARY

The corrosion and stress corrosion cracking behaviour of 8090-T81 and 2091-T84 sheet and 8090-T8171 plate aluminium - lithium alloys tested under laboratory and marine exposure conditions are compared with aerospace aluminium alloys currently in service. Initial results are also presented on the corrosion performance of a metal matrix composite aluminium alloy. The corrosion protection of aluminium - lithium alloys is discussed and progress on the development of chromate-free systems and their application to advanced aluminium alloys is described.

2. INTRODUCTION

One of the main advances in aerospace structural metallic materials during the last twenty years or so has been the development of aluminium - lithium alloys. The original targets set were to produce materials which matched the performance of conventional 2000 and 7000 series aluminium - copper and aluminium - zinc -magnesium alloys whilst giving significant reductions in density and improvements in stiffness. International Conferences held between 1980 and 1992 have mapped the advances made in the production, fabrication and physical metallurgy of these materials. The AGARD meeting held in Mierlo in 1988 (1) reviewed progress being made throughout the NATO countries on aerospace materials, in particular aluminium - lithium alloys. Individual components and structures for advanced airframes are now being designed and manufactured from these alloys (2).

A second area where significant progress has been made in lightweight aerospace materials is metal matrix composite (MMC) materials. Developments include the use of continuous fibres, short fibres, whiskers and particles to give reinforcement. Silicon carbide reinforced aluminium alloy MMC materials are currently being evaluated for various aerospace applications. The gains in stiffness and strength are modest in comparison with what can be achieved from the use of continuous fibres but more uniformly isotropic properties may be developed.

The corrosion and protection of advanced aerospace materials are important factors controlling the lifecycle

costs of military aircraft. Estimates published by Kinzie (3) for the USAF indicate that aging airframes require a high level of corrosion control maintenance and repair if they are to remain airworthy. Problems are not necessarily confined to older aircraft. Examples have been found of corrosion developing on aircraft after relatively short periods in service. Before new materials can be introduced it is essential that a detailed study is made of factors influencing the corrosion behaviour. The effectiveness of currently used schemes must also be established. A further consideration is the need to replace chromate based pretreatments and paints with materials which will meet future environmental legislation.

This paper presents the results of studies made on the corrosion and stress corrosion of two commercially produced sheet aluminium - lithium alloys and a plate aluminium - lithium alloy. Emphasis is given to the corrosion behaviour under marine exposure conditions. Some early results are also given relating to an aluminium - copper based MMC material strengthened with silicon carbide particles.

3 MATERIALS

Details of the compositions and heat treatments of the two sheet and plate aluminium - lithium alloys investigated are given in table 1.

The alloys were prepared commercially and in the case of the 8090 sheet and plate materials were supplied in the heat treated condition. The 2091 sheet was obtained in the T3 condition and was aged to give the T84 temper. For comparison several conventional 2000 and 7000 series aluminium alloys were also examined and details of these are included in table 1.

A commercially produced aluminium based metal matrix composite was also evaluated. The material was available as plate and the matrix composition (table 1) was equivalent to 2124. The volume percentage silicon carbide was 17% and the average particle size was 3 μ m. An extruded 2124 alloy was included in the programme which had been prepared using a powder metallurgy route.

Table 1 Compositions and tempers of alloys investigated

Alloy	Composition - weight percentage							
	Li	Cu	Mg	Zr	Si	Fe	Zn	Mn
SHEET 8090 T81	2.43	1.02	0.88	0.05	0.01	0.04		
2091 T84	1.77	1.76	1.31	0.07	0.02	0.02		
2024 T3		4.14	1.50					
2014 T6		4.40	0.50		0.74	0.29		
PLATE 8090 T8171	2.45	1.13	0.71	0.14	0.01	0.04		
2124 MMC		4.16	1.62	0.10	0.15	0.19	0.29	0.6

4. CORROSION BEHAVIOUR UNDER MARINE EXPOSURE

4.1 Corrosion Resistance

4.1.1 Aluminium - lithium Sheet

Coupons 75mm X 50 mm cut from sheet 8090-T81 and 2090-T84 aluminium - lithium alloys together with various control samples were placed on test at the Exposure Trials Station at Eastney in September 1991 and in December 1991. Prior to testing the coupons were degreased and weighed. The coupons were mounted on wooden frames using ceramic bushes so that the longer dimension was in the vertical plane. The frames faced due south and were inclined at an angle of 45° to the ground. The frames were positioned so that all the coupons were at least 1 metre above ground level and were within 100 metres of high water on both the east and west sides of the exposure site. Three coupons of each alloy type were returned to DRA (Farnborough) after approximately 6, 12, 18 and 24 months exposure for metallographic examination.

Examination of the 8090-T81 coupons showed the presence of well defined blisters after 6 months exposure. Evidence of corrosion pitting was found on the 2014-T6 control alloy placed on test at the same time. Tests on the 2091-T84 alloy commenced at a later date but after 6 months, evidence of corrosion attack was found on the underside of the coupons. At the end of the 24 months exposure a large number of exfoliation blisters were visible on the 8090-T81 sheet. Blisters were also apparent on the 2091-T84 coupons.

Table 2 Weightloss and pitting data for 2124 MMC material and controls following 18 months marine exposure.

Alloy	Weightloss (mg/cm ²)	Average Pitting Depth μ m	Average Pitting Density pits/cm ²
2024-T4	6.4	38.5	18
2124 PM	12.3	51.4	15
2124 MMC	8.1	32.6	30

Estimates have been made of the depth of attack from the metallographic sections and the most probable depth of attack computed from the deepest 10% using extreme value statistics. Results obtained are shown in fig.1. Included are data for sheet 2024-T3 alloy obtained from earlier exposure trials. The results indicate that the depths of attack are similar for the two commercial sheet aluminium - lithium alloys and lie between the two control alloys. However the number of sites of attack is far fewer in the case of the 2091-T84 than for the 8090-T81 alloy.

Weightlosses were measured for the two control alloys which showed predominately pitting and intergranular attack. Weight gains however were recorded for the aluminium - lithium alloy coupons resulting from trapped corrosion products.

4.1.2 Metal Matrix Composite

It was found that corrosion pits initiated on the MMC test pieces during exposure at the Eastney marine site but subsequent examination of cross sections showed that the pits were blunted by the presence of silicon carbide particles. Data comparing the average pit depths, average pit density and weight losses after 18 months exposure are given in table 2. The weightlosses are higher in the MMC material than in the plate 2024-T4 control alloy but the average depth of pitting is less. The pits formed in the 2124 MMC material are generally wide, shallow and open. By comparison pits in the non-reinforced materials were much deeper and the weightlosses higher.

4.2 Resistance to Stress Corrosion Cracking

4.2.1 Sheet Aluminium - lithium Alloys

Two sets of tensile specimens were prepared, one set machined with the stress axis parallel to the longitudinal (L) direction and one set with the axis parallel to the long transverse (LT) direction. Specimens were stressed in modified Alcoa rigs which were protected with a wax based coating. They were placed at the Eastney marine site in July 1992 and have

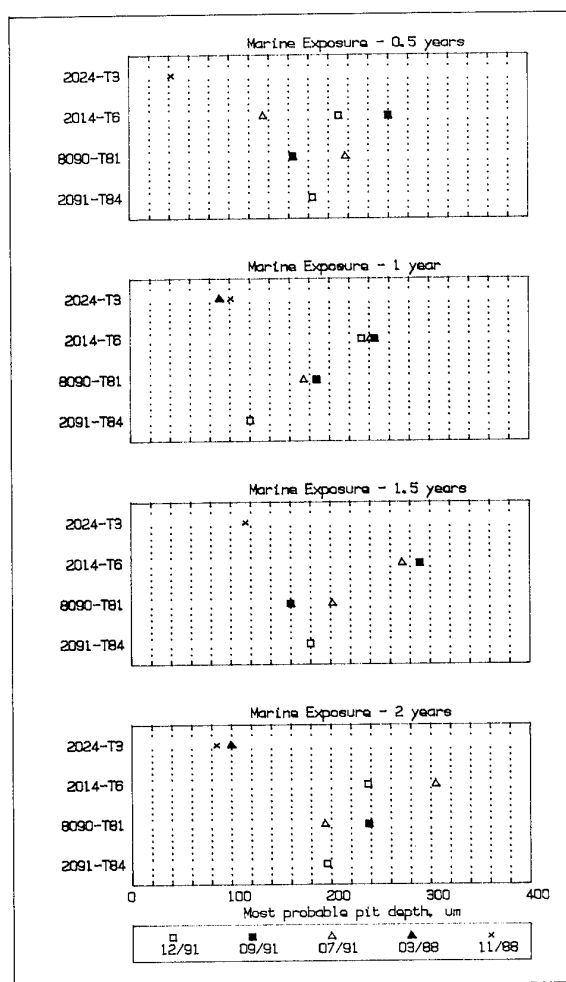


Fig.1 Most probable depths of attack determined for sheet coupons exposed in a marine environment.

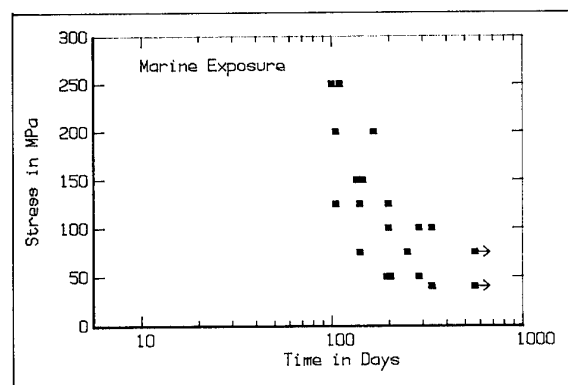


Fig.2 Stress corrosion cracking behaviour of 8090-T8171 plate. Time to failure for specimens stressed parallel to the short transverse direction (ST) and exposed in a marine environment.

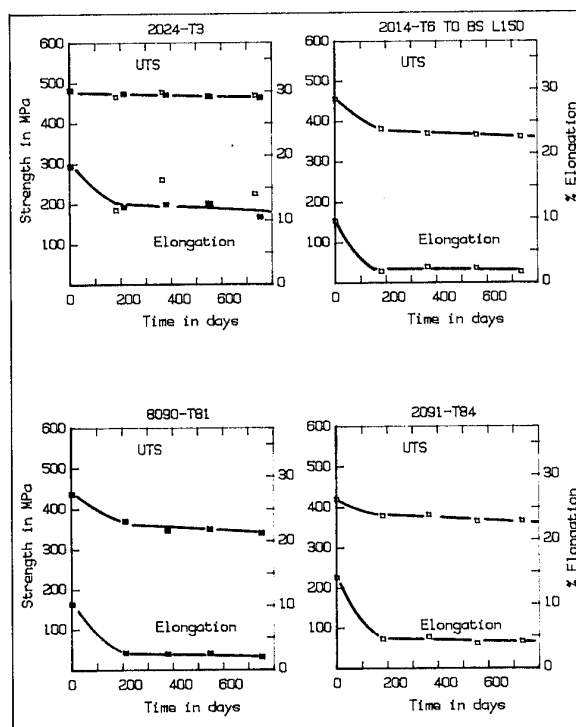


Fig.3 Effect of marine exposure on the tensile properties and elongation of aluminium - lithium sheet and control alloys.

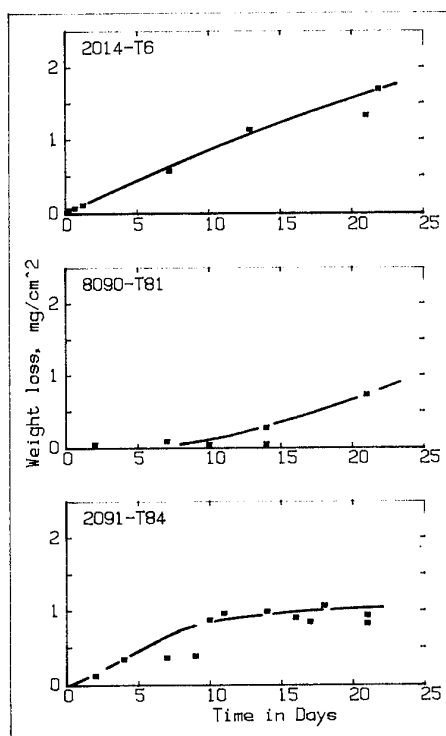


Fig.4 Variation in weightloss with time for coupons immersed in 600 mM/l sodium chloride solution.

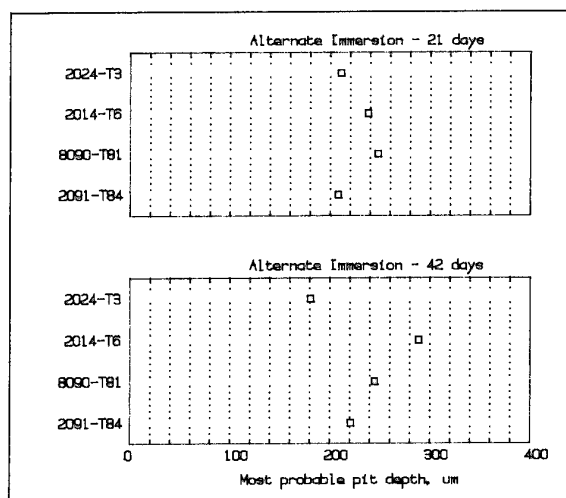


Fig.5 Most probable depth of attack determined for sheet coupons tested by alternate immersion in 600mM/l sodium chloride solution

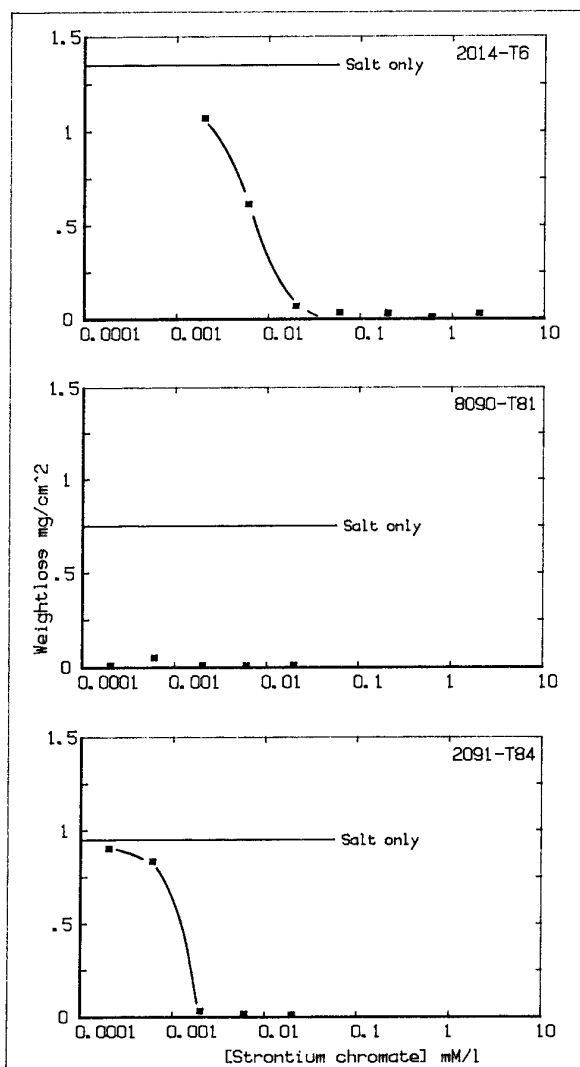


Fig.6 Effect of sodium chromate concentration on the weightloss of aluminium alloy coupons tested by total immersion in 600mM/l sodium chloride solution.

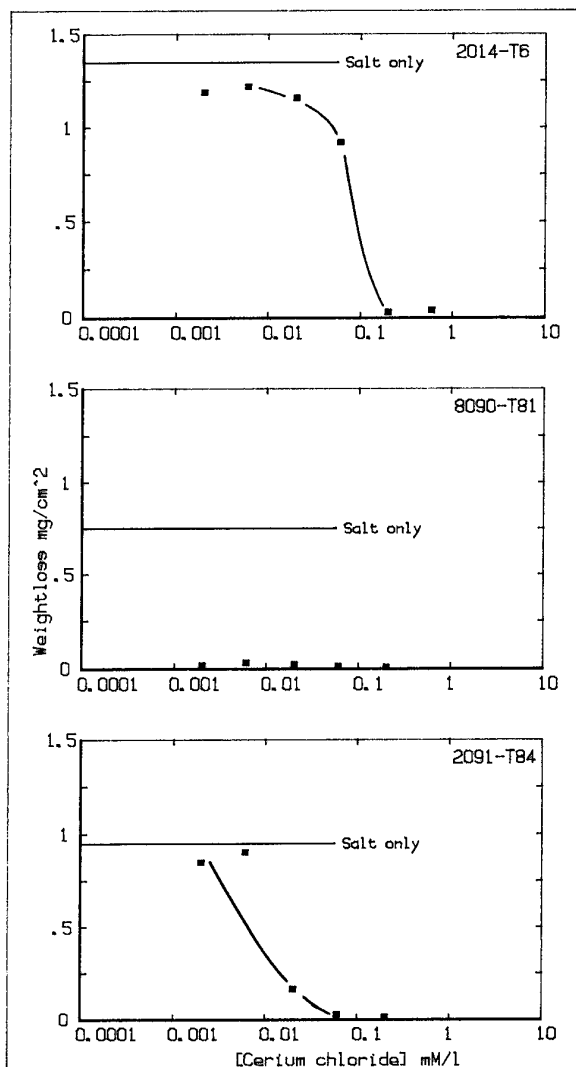


Fig.7 Effect of cerium chloride concentration on the weightloss of aluminium alloy coupons tested by immersion in 600 mM/l sodium chloride solution.

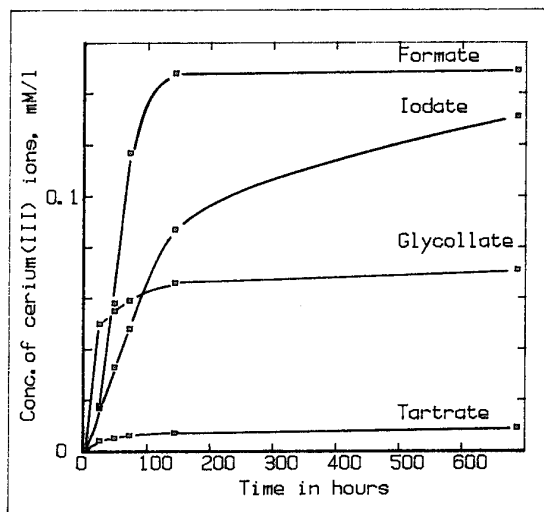


Fig.8 Leaching behaviour of experimental paint schemes containing cerium based pigments.

been inspected monthly for signs of cracking. Limitations with the number of stress jigs available meant that a complete range of stresses could not be employed. Hence in the case of the 8090-T81 alloy the highest stress applied was 125 MPa whilst for 2091-T84 a maximum stress of 250 MPa was employed. So far no failures have been found for either alloy.

4.2.2 Plate Aluminium - lithium Alloy

Cylindrical tensile bars were machined from 8090-T8171 plate material with axis parallel to the short transverse direction. Results obtained are presented in fig.2. Failures have occurred at stresses as low as 40 MPa and after 550 days exposure only two specimens remained on test at stresses of 80 and 40 MPa.

4.3 Effect of Exposure on Mechanical Properties

4.3.1 Sheet Aluminium - lithium Alloys

Tensile test pieces with a 12.5mm gauge width were machined from the two aluminium - lithium sheet alloys and from 2024-T3 and 2014-T6 sheet control alloys. The test pieces were mounted in the same manner as the test coupons described in 4.1.1 and were returned to DRA(Farnborough) after 6, 12, 18 and 24 months exposure. Sufficient specimens were placed on test to allow triplicates of each alloy type to be tested for each exposure period. Tensile testing was carried out using a type 1474 Zwick Tensile Test machine. The 0.2% proof stress ultimate tensile strength and elongation were determined for each specimen.

Data showing the effect of marine exposure on the ductility and strength of 2091-T84 and 8090-T81 sheet alloys are presented in fig.3.

After 6 months exposure a fall in elongation of 10% to 3% was recorded in the case of the 8090-T81 sheet and 14% to 4.5% for 2091-T84 alloy. With longer periods, however, further losses in elongation were relatively small. The 2014-T6 control alloy showed similar losses in elongation but the 2024-T3 sheet alloy maintained a relatively high elongation even after 18 months exposure.

Losses in ultimate tensile strength resulting from marine exposure were recorded for both aluminium - lithium alloys. The drop in strength was most severe in the 8090-T81 alloy, 435 MPa to 350 MPa after 12 months exposure. In the case of the 2091-T84 sheet alloy, the UTS determined after 12 months was 360 MPa which corresponded to a loss of strength of about 60 MPa. The 2014-T6 sheet control was also found to be susceptible to marine exposure but the strength of the 2024-T3 was only marginally reduced. Even after 18 months the UTS was determined to be in excess of 470 MPa.

4.3.2 Metal Matrix Composite

Tensile test specimens machined from plate 2124 MMC material were exposed at the Eastney marine site. Sofar specimens have been on test 18 months and the effect of exposure on mechanical properties is summarised in table 3. The tensile strength is reduced from 480 MPa to 367 MPa after 18 months and the reduction in area data show that there is a significant loss in ductility.

Table 3 Summary of mechanical properties of 2124 MMC material after marine exposure

Exposure time (months)	0.2% PS (MPa)	Tensile Strength (MPa)	Reduction in area %
0	326	480	6.4
6	304	401	2.9
12	296	384	2.5
18	277	367	2.3

5. ACCELERATED CORROSION TESTS

The corrosion behaviour of the aluminium - lithium alloys, the 2124 MMC material and several control alloys were assessed using a series of accelerated corrosion tests.

5.1 Total Immersion Tests

Total immersion tests were conducted on the two sheet aluminium - lithium alloys, 8090-T81 and 2091-T84 and on the control alloy 2014-T6. Small coupons 40 x 25 mm were immersed in 110 ml of 600 mM/l sodium chloride solution contained in polyurethane beakers. Coupons were removed at various times upto 3 weeks, cleaned by immersion in chromic-phosphoric acid solution and weighed.

Fig.4 shows the change in weightloss with time. The degree of attack was least on the 8090-T81 sheet whilst the weightlosses recorded for the 2091-T84 and 2014-T6 materials were similar after 3 weeks immersion. Examination of the coupons showed that the attack was predominately pitting corrosion. Sectioning indicated that some intergranular attack had developed in the 2014-T6 alloy.

5.2 Alternate Immersion Tests

Testing was carried out in accordance with ASTM G44(4). After weighing test panels were immersed for 10 minutes every hour in a 3.5% sodium chloride solution maintained at 30°C. The relative humidity and temperature of the laboratory were maintained at 45±6% RH and at 27±3°C respectively. At the end of the test period panels were removed, cleaned, reweighed and then sectioned and examined

metallographically.

5.2.1 Sheet Aluminium - lithium Alloys

Depths of attack were determined from the metallographic sections prepared from panels which had been tested for 3 and 6 weeks. In each case the data were analysed to enable the most probable depth of attack to be determined. The results are presented in fig.5.

5.2.2 Metal Matrix Composite

Coupons prepared from MMC material together with extruded PM2124 alloy and plate 2024-T3 were tested for 30 days. Weightloss, average pit depth and pit densities are given in table 4. Under these test conditions the MMC material suffers the highest degree of corrosion attack. The depth of pitting is not so great as for the control alloys.

Table 4 Weightloss and pitting data for 2124 MMC and controls following 30 days alternate immersion testing

Alloy	Weightloss (mg/cm ²)	Average Pitting Depth μm	Average Pitting Density pits/cm ²
2024-T4	2.3	58.5	56
2124 PM	5.8	55.8	171
2124 MMC	10.5	43.5	293

5.3 Neutral Salt Fog

Testing was conducted in accordance with ASTM B117 (5). Test panels were exposed to a continuous 5% neutral salt spray for upto 6 weeks in a cabinet maintained at a temperature of 35°C.

5.3.1 Sheet Aluminium - lithium Alloys

Two sets of triplicate panels were tested for each alloy. One set was removed after 3 weeks and the second set was given a full 6 weeks exposure. Each panel was examined optically after corrosion testing and then cleaned by immersion in chromic-phosphoric acid solution. The panels were subsequently rinsed in distilled water and alcohol, dried and reweighed. Data presented in table 5 showing the weightlosses and most probable depths of attack.

5.3.2 Plate Aluminium - lithium Alloy

Blocks 40mm x30mm were machined from the plate 8090-T8171 material. The blocks were then sectioned parallel to the plate surface to allow the quarter thickness (T/4) and half thickness (T/2) surfaces to be exposed. Two sets of samples were exposed for 21

days and 42 days. Areas of pitting could be identified on all of the specimens.

Table 5 Weightlosses and pitting data for sheet aluminium - lithium alloys exposed to neutral salt fog

Alloy	3 weeks exposure		6 weeks exposure	
	Wt-loss mg/cm ²	Depth of attack μm	Wt-loss mg/cm ²	Depth of attack μm
8090-T81	0.35	52	0.38	52
2091-T84	0.34	17	0.40	20
2024-T3	0.74	4	0.89	16
2014-T6	4.95	136	10.32	161

5.3.3 Metal Matrix Composites

Samples prepared from the 2124 MMC material and control materials were tested for 30 days in neutral salt fog. Weightloss and pitting depth data determined are summarised in table 6. The results indicate that the level of corrosion calculated from the weightloss data is much higher than for the control alloys. Metallographic sectioning shows that there is a higher density of pits although the depth of attack is less.

Table 6 Weightloss and pitting data for 2124 MMC material and control alloys following 30 days neutral salt fog.

Alloy	Weightloss (mg/cm ²)	Average Pitting Depth (μm)	Average Pitting Density pits/cm ²
2024-T4	2.4	58.5	48
2124 PM	4.3	61.4	75
2124 MMC	10.6	42.6	160

5.4 Intermittent Acidified Salt Fog

A test procedure developed by Lifka and Sprowls (6) was used to assess the susceptibility to exfoliation corrosion of aluminium - lithium sheet and plate materials. Test samples were exposed for 7 and 14 days to repeated 6 hour test cycles consisting of a 45 minute spray with 5% salt solution acidified to pH3 with acetic acid, a 2 hour direct air purge followed by a 3 hour 15 minute soak when the relative humidity rose to between 90 and 95%. At the end of the test, samples were cleaned and photographed and then sectioned to enable the depth of attack to be

determined.

5.4.1 Sheet Aluminium - lithium Alloys

The most probable depths of attack after 7 and 14 days exposure are given in table 7. The 8090-T81 sheet alloy showed extensive exfoliation blistering and the depth of attack after 14 days exposure was estimated to be in the region of 370 μm . Exfoliation blisters were visible on the surface of the 2091-T84 sheet after 7 days and after 14 days the depth of attack was estimated to be 500 μm . Under the same conditions the 2024-T3 alloy showed only slight pitting attack. Extensive intergranular corrosion occurred in the sheet 2014-T6 material to a depth of 177 μm .

Table 7 Depth of attack for sheet aluminium - lithium alloys and controls exposed to intermittent acidified salt spray.

Alloy	Depth of attack (μm)	
	7 days exposure	14 days exposure
8090-T81	314	370
2091-T84	281	500
2024-T3	16	26
2014-T6	94	177

5.4.2 Plate Aluminium - lithium Alloy

Samples similar to those detailed in section 5.3.2 were exposed to intermittent acidified salt fog for 7 and 14 days. Extensive exfoliation corrosion was found to develop on all of the specimens with attack being most severe (ED) on samples where the original plate surface was exposed.

6. PROTECTION AGAINST CORROSION

6.1 Standard Protective Treatments

Preliminary investigations into the protection of aluminium - lithium alloys using conventional pretreatments and paint schemes were undertaken during the development of the alloys. Work carried out at the DRA by Chambers (7) compared the performances of 2014-T6 sheet aluminium - copper alloy with an aluminium - lithium sheet alloy similar in composition to 8090. Corrosion tests on unprotected material showed that under acidified conditions the aluminium - lithium material was susceptible to exfoliation corrosion. Trials were conducted on material which had been pretreated using two different chromate conversion coatings and an etch primer. A standard chromate pigmented epoxy primer was applied and where appropriate a polyurethane top coat was also

applied. Chambers concluded that the performances of the aluminium - lithium alloy and the control alloy were very similar. Results obtained with the aluminium - lithium sheet for a filiform test were difficult to interpret as extensive exfoliation corrosion developed and the type of filament growth produced was different.

Some marine exposure trials have also been conducted by DRA on primed and top coated aluminium - lithium sheet panels. The sheet was pre-production material with a composition close to 8090. The panels were exposed at the Eastney test site together with panels cut from a 2014-T6 control alloy. After three years exposure there was no evidence of corrosion on either the aluminium - lithium or control panels.

In the present research programme neutral salt fog and intermittent acidified salt spray tests were conducted on 8090-T81 and 2091-T84 test coupons which had been given either a chromate conversion coating or had been anodised in a chromic acid bath. Standard treatments used on conventional aerospace materials were used in each case. After 6 weeks exposure to neutral salt fog, the samples which had received a chromate conversion coating were free from any form of corrosion. Some corrosion pits were visible on the 2091-T84 samples which had been anodised but the anodised 8090-T81 samples showed few signs of corrosion. By comparison unprotected specimens of both alloys showed many areas where corrosion pits had initiated. In the intermittent acidified salt spray tests the unprotected panels developed exfoliation corrosion blisters after 14 days exposure as described in section 5.4.1. No attack was visible on coupons which had been pretreated using a chromate conversion coating but some areas of corrosion could be identified on the anodised coupons especially on the 2091-T84 alloy.

6.2 Chromate-free Protective Treatments

Chromates are the key factor in the protection of aerospace aluminium alloys against corrosion. They find applications in pretreatments as well as being the main inhibiting pigment incorporated into aircraft paint primers. Concern about the carcinogenic nature of chromates has led to renewed efforts to identify alternative inhibitors for use with aluminium alloys.

Research is currently being directed towards the development of chromate-free conversion coatings for use on aluminium alloys and anodising treatments based on boric - sulphuric acid solutions. The work has initially focussed on 2000 and 7000 series alloys but is now considering aluminium - lithium alloys and metal matrix composite materials.

The underlying problem with the development of

chromate free primers continues to be the identification of inhibitors or combinations of inhibitors which match the efficiency of chromates at low concentrations in the presence of high levels of chloride.

As part of the programme to develop non-chromate primers for aerospace applications, experiments were conducted to determine the critical concentrations of some of the more promising inhibitors which have been found for aluminium alloys. The total immersion test described in section 5.1 was used in this work. Test coupons were totally immersed in 600mM/l sodium chloride solution to which had been added various levels of inhibitor. The duration of the test was three weeks, after which coupons were washed and cleaned to remove corrosion products. The results plotted in fig.6 show changes in weight due to corrosion on 2014-T6, 8090-T81 and 2091-T84 coupons for different strontium chromate concentrations. In the case of the 2014-T6 alloy, a minimum concentration of 0.02mM/l strontium chromate is required to prevent corrosion. For the two aluminium - lithium alloys studied much lower concentrations of strontium chromate are required.

Much of the research carried out commercially on chromate-free primers has involved the formulation and testing of paint schemes incorporating fairly conventional inhibitor systems. The more academic approach has been to try to understand in more detail the mechanisms by which chromates inhibit. This it is hoped will provide a sounder basis for selecting and developing replacement systems. Simple screening tests have identified several compounds which give a high level of protection when present in dilute concentrations. Cerium salts, organic compounds containing sulphur and zinc salts of mercapto-carboxylic acids have been found to inhibit corrosion on aluminium (8,9,10) however the minimum concentration required is an order of magnitude higher than for strontium chromate. This can be seen in fig.7 which gives data obtained for cerium chloride. For both 2014-T6 and 2091-T84 alloys the minimum concentration is at least 10 times higher than for strontium chromate. In the case of the 8090 a minimum concentration was not determined. Little corrosion could be detected when the concentration was as low as 0.002mM/l.

The high solubility of cerium chloride makes it an unsuitable inhibitor for use in a paint formulation. Data published by Smith et al.(11) for a 2014-T6 aluminium - copper alloy show that cerium formate, cerium iodate, cerium glycollate and cerium tartrate give similar degrees of inhibition as cerium chloride. One of the factors determining the effectiveness of a paint scheme to give corrosion protection is the leachability of the inhibitive pigment. For protection to be given at

areas where the paint becomes damaged and the underlying metal substrate is exposed the concentration of inhibitor leached out must be greater than the minimum level. In an idealised system where the salt concentration is 600mM/l, a minimum cerium ion concentration of 0.2mM/l is necessary to inhibit corrosion on 2014-T6. Leaching curves obtained from experimental primers containing various cerium compounds are reproduced in fig.8. The results indicate that the rate of leaching for paints pigmented with cerium formate, cerium iodate and cerium glycollate may be sufficiently high to be effective in the protection of 8090 and 2091 alloys. Experiments conducted on proprietary epoxy primers indicate that sufficient chromate may be leached from these paints to exceed the minimum levels indicated in fig.6.

7. DISCUSSION AND CONCLUSIONS

The results obtained from the marine exposure trials and accelerated corrosion tests confirm earlier work on experimental and pre-production materials that under some conditions sheet 8090 may be susceptible to exfoliation corrosion (1). The problem is particularly severe in non-recrystallised material where the grains are very elongated. Robinson (12) has determined the conditions in terms of grain shape and aspect ratio for exfoliation blisters to develop in aluminium alloys. In the present study the aspect ratio of the grains in the 8090-T81 sheet varied from 1.8 at the surface to 3.8 at the centre of the sheet. In the case of the 8090-T8171 plate much higher aspect ratios were measured and increased from 33 at the T/2 position to 41 at the surface. The ratios determined exceed the values calculated by Robinson to be necessary for exfoliation blisters to form. The exfoliation corrosion found under marine exposure conditions on the aluminium - lithium sheet alloys can be reproduced in the laboratory using the intermittent acidified salt fog test. Recently published data comparing the corrosion behaviour of clad and unclad 2000 and 7000 series alloys in a marine environment found that the alternate immersion test gave a good correlation on terms of the relative weightlosses and depths of attack (13). Similar agreement was obtained in the present work for the depths of attack measurements although no evidence of exfoliation corrosion was found on the aluminium - lithium alloys using the alternate immersion test.

The 8090-T8171 plate aluminium - lithium alloy shows a relatively low threshold stress for stress corrosion cracking under marine exposure conditions. The results obtained are compared in table 8 with previously published data (14) for plate 2014-T651, 7075-T651 and 2024-T351 alloys. The performance of the 8090-T8171 plate in terms of the initiation of stress corrosion cracking is similar to 2024-T351. Further data on the growth of stress corrosion cracks in plate material is required.

Table 8 Stress corrosion cracking threshold data for conventional plate materials exposed in a marine environment for 2 years. Stressed in ST direction. Reference 14.

Alloy	Threshold Stress (MPa)
2014 - T651	121
7075 - T651	56
2024-T351	<15

Results of the corrosion tests show that the MMC material forms a higher density of pits than the non-reinforced alloy. A microstructural study carried out by Immeson and Bartlett (15) indicates that the silicon carbide particles play little if any role in the initiation of pits. It is proposed that a magnesium rich phase developed during the powder processing is mainly responsible for pit initiation.

Under total immersion conditions and on exposure to neutral salt fog the aluminium - lithium sheet and plate materials suffer pitting corrosion to a level no more severe than found on conventional aerospace alloys. Results obtained indicate that strontium chromate is an effective inhibitor preventing the initiation of corrosion pits. Trials conducted further show that the pretreatments and paint schemes currently employed give a high degree of protection to aluminum - lithium alloys. Some progress on non-chromate based paint schemes is being made and cerium based compounds show some potential as inhibitors for these alloys.

8. REFERENCES

- 1) Proc. of the AGARD Conference No.444 on "New Light Alloys" held at Mierlo, The Netherlands (1998)
- 2) A F Smith, Proc. of the Sixth International Aluminium - lithium Conference held at Garmisch - Partenkirchen, Germany (1991) pp 1305 - 1310
- 3) R C Kinzie, Proc. of Second Symposium on Aerospace Corrosion Control, Amsterdam, The Netherlands (1992) pp8/1 - 8/9
- 4) ASTM G44-75, "Alternate immersion stress corrosion testing in 3.5% sodium chloride solution", American Society for Testing of Materials, Philadelphia.
- 5) ASTM B117 "Salt spray (fog) testing", American Society of Testing of Materials, Philadelphia.
- 6) B W Lifka and D O Sprowls, Corrosion (1966) 22 7
- 7) A Chambers, unpublished data
- 8) B R W Hinton, D R Arnott and N E Ryan, Metals Forum, (1984) 7(4), 221
- 9) K R Baldwin, M C Gibson, P L Lane, and C J E Smith, published in the Proc. of the 7th European Symposium on Corrosion Inhibitors (7SEIC) Ann. Univ. Ferrara. N.S. Sez. V. Suppl. N.8. (1990) pp 771 - 785
- 10) C J E Smith, M A H Hewins, K R Baldwin and V C R McLoughlin published in the Proceedings of the 6th European Symposium on Inhibitors (6SEIC) Ann. Univ. Ferrara. N.S. Sez. V. Suppl. N.8 (1985) pp 641 -654
- 11) C J E Smith, K R Baldwin, M A H Hewins and M C Gibson, published in "Progress in the Understanding and Prevention of Corrosion" (1993) pp 1652 -1663
- 12) M J Robinson, Corrosion Science (1982) 22(8), pp 775 - 790
- 13) C J E Smith, J A Gray and M A H Hewins to be published in Corrosion Reviews
- 14) J A Gray, RAE Technical Report 79117 (1979)
- 15) D Immeson and D L Bartlett, to be published in Journal of Microscopy.

(c) British Crown Copyright 1994/DRA
Published with the permission of the Controller
of Her Britannic Majesty's Stationery Office

Exfoliation Corrosion and Stress Corrosion Cracking Behaviour of Al-Li Alloys

Reinhold Braun

German Aerospace Research Establishment (DLR)

Institute of Materials Research

Linder Höhe

D-51147 Köln

Germany

1. SUMMARY

The exfoliation corrosion and stress corrosion cracking (SCC) behaviour of damage tolerant sheet and plate materials of aluminium-lithium based alloys in underaged tempers was studied performing different accelerated tests. The EXCO test (ASTM G34) produced blistering and mild exfoliation corrosion. The modified EXCO test suggested by Lee and Lifka proved to be more severe than the standard EXCO test. When exposed to the cyclic acidified salt fog (MASTMAASIS test according to ASTM G85, Annex A2), the Al-Li alloys studied suffered severe exfoliation. The MASTMAASIS test reproduced marine exposure results for conventional 2024-T351 and 7075-T7351 plates and the limited data for aluminium-lithium based 8090-T81 and 2091-T84 sheets published in the literature. Therefore, it seems to be a promising testing technique to predict the service performance of high strength aluminium alloys. Static loading tests indicated very high SCC resistance for 8090-T8171 and 2091-T8X51 plates in longitudinal and long transverse directions. Environmentally assisted cracking occurred in the latter alloys when stress was applied in the short transverse direction. Threshold stresses below 100 MPa were obtained from alternate immersion tests (ASTM G44) and from permanent immersion tests in an aqueous solution of 0.5 M NaCl + 0.1 M LiCl + 0.05 M NaHCO₃ + 0.05 M Na₂CO₃. Using the latter synthetic environment, the slow strain rate testing technique indicated sensitivity to stress corrosion cracking for recrystallized 8090-T81 and 2091-T84 sheet materials.

2. INTRODUCTION

For the last fifteen years the aluminium industry has been strongly engaged in the development of aluminium-lithium based alloys for substitution of established 2XXX and 7XXX series aluminium alloys used in aircraft and space vehicle structures. These efforts have been slowed down, some of the Al-Li products have attained commercial status [1-4]. The most advanced materials are the quaternary Al-Li-Cu-Mg alloys 8090 and 2091, developed by

British Alcan Aluminium and Cégédur Pechiney, respectively, and Alcoa's Al-Li-Cu alloy 2090. Semi-fabricated product forms, such as sheet, plate, extrusions and forgings are being offered [2-4]. However, extensive applications of Al-Li alloys are still prevented by shortcomings, including low cracking resistance and an unusual crack deviation behaviour [5]. Besides the mechanical properties the corrosion behaviour of the lithium bearing materials is crucial for use in aircraft structures. Exfoliation corrosion and stress corrosion cracking (SCC) are two types of environmental attack occurring in heat treatable aluminium alloys.

The present paper summarizes results of exfoliation corrosion and stress corrosion cracking tests performed on damage tolerant sheet and plate materials of the alloys 8090 and 2091.

3. EXPERIMENTAL

Sheet and plate materials of the Al-Li alloys 8090 and 2091 were investigated in underaged tempers. The microstructure of the 1.6 mm thick 8090-T81 and 2091-T84 sheets was recrystallized (2091 CPHK sheet was received in the as-quenched condition T351. It was aged at 135°C for 12 h to the T84 temper). In the centre of the 2091 CPHK sheet, a partially recrystallized thin layer was observed. The plate materials of the alloys 8090-T8171 (52 mm thick) and 2091-T8X51 (38 mm thick) exhibited the typical pancake structure of wrought aluminium alloys. Products of the Al-Li alloys 8090 and 2091 were supplied by Alcan Aluminium International, England, and Cégédur Pechiney, France, respectively. Tensile properties of the materials investigated are given in Table 1.

The exfoliation corrosion behaviour was studied performing EXCO tests according to ASTM G34, modified EXCO tests as proposed by S. Lee and B.W. Lifka [6], and cyclic acidified salt fog (MASTMAASIS) tests according to ASTM G85, Annex A2. Size of the specimens used in these tests was 50 by 100 mm. The surface and the half-thick-

Table 1
Tensile properties of sheet and plate materials of the Al-Li alloys 8090 and 2091
in damage tolerant tempers

Alloy	Orientation	0.2% proof stress [MPa]	Ultimate tensile strength [MPa]	Fracture elongation [%]
sheet				
8090-T81	longitudinal	333 ± 5	443 ± 6	11.3 ± 0.9
	long transverse	286 ± 4	432 ± 7	16.3 ± 0.6
2091-T84	longitudinal	350 ± 5	445 ± 6	12.0 ± 1.1
	long transverse	338 ± 4	472 ± 7	13.0 ± 1.5
plate				
8090-T8171	longitudinal	394 ± 5	477 ± 7	6.1 ± 0.5
	long transverse	346 ± 3	467 ± 1	7.8 ± 0.7
	short transverse	285 ± 3	449 ± 4	7.0 ± 0.7
2091-T8X51	long transverse	328 ± 2	438 ± 3	8.6 ± 0.8
	short transverse	295 ± 5	445 ± 11	7.7 ± 1.6

Table 2
Visual ratings for aluminium alloy sheet and plate panels which were exposed to the standard EXCO
solution (ASTM G34-90), an modified EXCO solution [6], and the cyclic acidified salt fog
(ASTM G85, Annex A2) for different time periods

Alloy	EXCO Test		Modified EXCO Test		MASTMAASIS Test	
	48 h	96 h	48 h	96 h	2 weeks	4 weeks
sheet						
8090-T81	B ⁻	B ⁺	EA	EB	B/EA	EB
2091-T84	B ⁻	B	B ⁺	EA	B ⁺	EA
2024-T3	P ⁻	P/B	B ⁻	B	P	P
plate						
8090-T8171	B ⁺	B/EA	EA	EA	EA	EB/EC
2091-T8X51	B	EA	EA/EB	EB	EA/EB	EB/EC
2024-T351	P/EA	EA	EA	EB	EB/EC	EC
7075-T7351	EA	EA	P ⁻	P/B	P	P

Abbreviations of ratings according to ASTM G34-90: N = no appreciable attack, P = pitting, B = blistering, EA = superficial exfoliation, EB = moderate exfoliation, EC = severe exfoliation. Suffices attached to ratings indicate slight (-) and strong (+) attacks, respectively, within the same category

ness subsurface were exposed for sheet and plate, respectively. Compared to the standard EXCO solution, the pH of the modified solution was increased to 3.2 using HCl, and aluminium ions were added whilst chloride and nitrate ions concentrations were maintained [6]. For lithium bearing and 2XXX series aluminium alloys, the modified EXCO tests were carried out at an elevated temperature of 52°C, whereas temperature was kept at 25°C for 7XXX series aluminium alloys. Corrosion attack was visually rated using the reference photographs presented in ASTM G34-90. To discriminate between different levels of attack at the lower end of the scale (slight exfoliation), the classification recommended in ASTM G34 was expanded by a further category B which describes blistering. When the blisters broke open forming slivers or flakes, the less favourable rating EA was given. To indicate slight changes within the same category, the suffices - (slight) and + (strong) were attached.

The SCC behaviour was investigated conducting static loading tests under constant deformation and constant load conditions and employing the slow strain rate (SSR) testing technique. The synthetic environments used were near neutral 3.5% NaCl solution (alternate immersion according to ASTM G44), an aqueous solution of 2% NaCl + 0.5% Na₂CrO₄ at pH 3, an aqueous solution of 0.5 M NaCl + 0.1 M LiCl + 0.05 M NaHCO₃ + 0.05 M Na₂CO₃, and substitute ocean water without heavy metals according to ASTM D1141 (when tested in the latter three environments, specimens were permanently immersed). SSR tests were performed at free corrosion potential. Nominal strain rates were in the range $5 \cdot 10^{-8}$ to $5 \cdot 10^{-5}$ s⁻¹. Reference tests were carried out in dry laboratory air (inert environment), generated by embedding the specimens in Mg(ClO₄)₂ powder. The fracture energy was used to assess the sensitivity to stress corrosion cracking. Pre-exposure tests were carried out to evaluate the degradation of the specimens caused by corrosion in the absence of applied strain. Details of the SSR testing technique are described elsewhere [7].

4. RESULTS AND DISCUSSION

4.1 Exfoliation corrosion behaviour

Results of EXCO, modified EXCO and cyclic acidified salt fog testing are summarized in Table 2. These accelerated tests indicated sensitivity to exfoliation corrosion for the aluminium-lithium alloys investigated. Ratings were generally worse in the modified than in the standard EXCO solution. In

the MASTMAASIS tests, damage tolerant Al-Li alloys suffered similar or more extensive exfoliation than in the modified EXCO tests. The exfoliation corrosion resistance of aluminium-lithium based sheet was lower than that of the conventional 2024-T3 sheet. Alloy 8090-T81 was found to be more susceptible than 2091-T84. Both Al-Li plates exhibited a similar or slightly better exfoliation corrosion behaviour than the conventional 2024-T351 plate. Fig. 1 shows aluminium alloy plate panels after two weeks MASTMAASIS testing. The overaged 7075-T7351 alloy exhibited pitting, whereas the other alloys suffered exfoliation.

Sheet of the alloys 8090-T81 and 2091-T84 were found to be prone to exfoliation corrosion in marine atmosphere [8]. 8090-T81 was more susceptible than 2091-T84. Conventional 2024-T3 sheet suffered pitting. Exfoliation corrosion was not observed for 7075-T7351 plate during 12 years of exposure in seacoast environment, whereas 2024-T351 plate suffered very severe exfoliation within two years [6]. Outdoor corrosion data for damage tolerant Al-Li plate were not found in the literature.

The EXCO test according to ASTM G34 does not accurately predict the atmospheric results for 2XXX and modern 7XXX series aluminium alloys in tempers revealing intermediate exfoliation corrosion resistance [6]. This test is also considered to be unreliable for predicting the exfoliation corrosion behaviour of aluminium-lithium based alloys, since correlation with exposure data in seacoast environment is poor [9,10]. Recently, Lee and Lifka suggested a modified EXCO solution appearing capable of reproducing marine exposure performance of the conventional alloy 2024, the Al-Li-Cu alloy 2090, and the high-strength alloys 7050 and 7150 in various commercial tempers [6]. Compared to the standard EXCO test, the modified EXCO test better reproduced the marine exposure data for the conventional 2024-T351 and 7075-T7351 plates, although the ratings for 2024-T351 still were not severe enough (Table 2). Ratings for the recrystallized 8090-T81 and 2091-T84 sheet materials were in accordance with results in seacoast environment. However, unrecrystallized medium-strength 8090-T6 sheet suffered severe exfoliation in the modified EXCO solution, not observed when exposed in marine atmosphere [11]. Therefore, further long-term outdoor exposure tests with Al-Li alloys are required to assess the applicability of the modified EXCO testing proposed by Lee and Lifka.

Results of the MASTMAASIS tests gave the best

correlation with marine exposure data. For conventional 2024-T351 and 7075-T7351 plate materials, the performance in seacoast environment was correctly reproduced. The cyclic acidified salt fog test also predicted the corrosion behaviour in marine atmosphere for Al-Li sheet, in particular alloy 8090-T6 [11], and for the control sheet 2024-T3. The MASTMAASIS test seems to be the most appropriate testing technique to evaluate the exfoliation corrosion behaviour of age-hardening aluminium alloys.

4.2 Stress corrosion cracking behaviour

Using two-point loaded bent-beam specimens, alternate immersion tests according to ASTM G44 indicated high SCC resistance for sheet of the Al-Li alloys 8090-T81 and 2091-T84 and the control alloy 2024-T3. During 40 days exposure, no crack initiation was detected at stresses up to 300 MPa applied in longitudinal and long transverse directions (on the surfaces of 2024-T3 specimens corrosion products deposited after 14 days exposure impeding the visual detection of possible cracks). However, sensitivity to stress corrosion cracking was found for the alloy 8090-T81 in a previous investigation, using two-point loaded bent-beam specimens of the same sheet which were alternately immersed in 3.5% NaCl solution at a temperature of 22°C, but under uncontrolled relative humidity conditions. In the latter tests, SCC initiation threshold stresses between 100 and 150 MPa and between 150 and 200 MPa were determined in longitudinal and long transverse directions, respectively. The different results demonstrate that temperature and relative humidity play an important role when SCC threshold stresses are determined under alternate immersion conditions. Furthermore, the results can depend upon the loading method. Constant loading and uniaxial tension straining provide more severe testing conditions than bending. For the same 8090-T81 sheet material, a long transverse threshold stress of about 150 MPa was obtained from automated stress corrosion ring (ASCOR) tests conducted under environmental conditions according to ASTM G44 [12]. Smith et al. reported threshold stresses below 100 MPa and above 200 MPa in longitudinal and long transverse directions, respectively, using 8090-T81 sheet tensile specimens which were tested under ASTM G44 conditions [8].

Figs. 2 and 3 show results of the SSR tests for 8090-T81 and 2091-T84 sheets, respectively. Long transverse tensile specimens were dynamically strained in an aqueous solution of 0.5 M NaCl +

0.1 M LiCl + 0.05 M NaHCO₃ + 0.05 M Na₂CO₃. As proved by pre-exposure tests, the reduction of fracture energy observed at strain rates below $5 \cdot 10^{-7} \text{ s}^{-1}$ is caused by stress corrosion cracking. Similar fracture energy vs. strain rate curves were obtained when longitudinal tensile specimens of both alloys were tested [13,14]. Using chloride-carbonate-hydrogencarbonate solutions, the SSR testing technique indicated sensitivity to environmentally assisted cracking for damage tolerant aluminium-lithium based sheet.

Whilst service problems with environmentally assisted cracking are not known for 2024-T3 sheet, damage tolerant 2091 sheet with a fully recrystallized equiaxed grain structure was found to be highly sensitive to stress corrosion cracking in the underaged T84 temper. A threshold stress below 100 MPa was found [15]. The SCC resistance of 2091 sheet (CPHK version) in the T84 heat treatment was improved by metallurgical adjustments, at slight expense of fracture toughness and strength [3]. The microstructure of the CPHK version exhibits grains flattened in the rolling plane and a partially recrystallized layer in the centre of the sheet. The SCC behaviour of 8090 sheet also depends upon the grain structure. Whereas unrecrystallized medium-strength 8090-T6 alloy was found to be immune in alternate immersion tests [16], recrystallized 8090-T81 sheet materials were prone to environmentally assisted cracking [8,12]. The SCC sensitivity of damage tolerant aluminium-lithium based materials is a further issue which has to be resolved for the successful use of these products in aircraft applications.

Under the environmental conditions of alternate immersion according to ASTM G44 and of permanent immersion in an aqueous solution of 0.5 M NaCl + 0.1 M LiCl + 0.05 M NaHCO₃ + 0.05 M Na₂CO₃, static loading tests indicated very high SCC resistance for both 8090-T8171 and 2091-T8X51 plates when stress was applied in longitudinal and long transverse directions (Table 3; as proved by fractography, one specimen has failed by overload fracture resulting from a reduction of the cross section caused by intergranular corrosion and pitting). When loaded in the short transverse direction, both Al-Li alloy plates were susceptible to stress corrosion cracking. Their SCC behaviour was similar to that of conventional 2024-T351 plate. Threshold stresses below 100 MPa were measured in alternate immersion tests [17]. As illustrated in Fig. 4, results of the alternate immersion tests correlated with those of outdoor exposure tests in

Table 3

Time-to-failure data for 8090-T8171 and 2091-T8X51 plates obtained from constant deformation tests under alternate immersion conditions according to ASTM G44 and from constant load tests under permanent immersion conditions in an aqueous solution of 0.5 M NaCl + 0.1 M LiCl + 0.05 M NaHCO₃ + 0.05 M Na₂CO₃ (n# = number of specimens tested)

Alloy	Orientation	Applied stress	Time-to-failure data	
			alternate immersion	permanent immersion
8090-T8171	longitudinal	350 MPa	5# > 40 days	5# > 40 days
		290 MPa	5# > 40 days	4# > 40 days
	long transverse	310 MPa	5# > 40 days	5# > 40 days
		260 MPa	5# > 40 days	27 days, 4# > 40 days
2091-T8X51	long transverse	330 MPa	3# > 40 days	
		300 MPa	3# > 40 days	5# > 40 days

urban industrial environments. Cracks induced by natural environment propagated along grain boundaries (Fig.5). A similar correlation between data of alternate immersion tests and marine exposure was found for 8090-T8171 plate [8].

Fig. 6 shows time-to-failure data obtained from alternate immersion tests for 8090 and 2024 plate materials in different tempers. Whereas artificial aging to the T851 temper significantly improved the SCC resistance of 2024 alloy, heat treatment had a reduced influence on the crack initiation behaviour of 8090 plate. A short transverse threshold stress slightly below 100 MPa was measured for the peak-aged alloy 8090-T8771. Time-to-failure data for a 30 mm thick 8090 plate in different heat treatments are plotted in Fig. 7 (the plate was received in the T351 condition and aged to the listed tempers using a heating-up rate of 10°C/h). Short transverse orientated C-ring specimens were alternately immersed in 3.5% NaCl solution (22°C temperature, not controlled relative humidity). In all tempers studied ranging from underaged to extremely overaged conditions, SCC initiation threshold stress was below 100 MPa. Similar results were reported by Dorward and Hasse for a 25 mm thick Al-Li-Cu-Mg-Zr plate [18]. For a 50 mm thick plate, however, these authors found that the SCC resistance improved with aging (the latter plate was tested using smooth tensile specimens). An influence of isothermal aging was also observed by Gray [19]. In underaged tempers Al-Li alloys revealed greater sensitivity to environmentally assisted cracking than in peak or overaged tempers. The SCC resistance can be further enhanced applying complex heat treatments

[20], thermal mechanical processing sequences [21], or by the addition of zinc to the Al-Li-Cu-Mg alloys [20].

Fig. 8 presents time-to-failure data for the alloy 8090-T8171 obtained from constant load tests under permanent immersion conditions. A short transverse threshold stress slightly below 50 MPa was measured in the chloride-carbonate-hydrogencarbonate solution. The SCC resistance seemed to be higher using substitute ocean water. However, the specimens which passed the maximum exposure length of 1000 h were severely embrittled, as found in subsequent tensile tests. Therefore, a lower threshold stress might have been determined if the tests had run longer.

For the alloy 2091-T8X51, constant load tests in 0.5 M NaCl + 0.1 M LiCl + 0.05 M NaHCO₃ + 0.05 M Na₂CO₃ indicated a short transverse threshold stress below 50 MPa [17]. Fig. 9 shows results of constant load tests for the 2091-T8X51 plate performed under permanent immersion conditions in substitute ocean water and in an aqueous solution of 2% NaCl + 0.5% Na₂CrO₄ at pH 3. Data obtained from constant load tests under alternate immersion in 3.5% NaCl solution are included. When immersed in substitute ocean water, specimens either failed approximately within the first 100 h of exposure or they passed the maximum exposure length of 1000 h. The unfailed specimens were not significantly embrittled, as found in subsequent tensile testing. The scatter in time-to-failure data might be related to surface condition effects (prior to immersion in substitute ocean water, the 2091-T8X51

tensile specimens were only degreased). Using the chloride-carbonate-hydrogencarbonate solution, time-to-failure lives were found to be influenced by the surface condition of smooth specimens [17]. However, the data obtained from constant load tests in the chloride-chromate solution also exhibited scatter, although the specimens were etched prior to immersion in this synthetic environment. Therefore, mechanical effects or changes of the synthetic environments can also play a role.

Results of SSR tests for the alloys 8090-T8171 and 2091-T8X51 are plotted in Figs. 10 and 11. Short transverse tensile specimens were dynamically strained in an aqueous solution of 0.5 M NaCl + 0.1 M LiCl + 0.05 M NaHCO₃ + 0.05 M Na₂CO₃. The SSR testing technique indicated sensitivity to environmentally assisted cracking for the 2091-T8X51 plate. In contrast to static loading tests, a rather slight SCC susceptibility was found for the 8090-T8171 plate. Similar results were obtained for both alloys from SSR tests using substitute ocean water [17,22]. The poor correlation between the results of static loading tests and those of the SSR testing technique for the alloy 8090-T8171 might be related to relatively long SCC incubation periods. As found by Buis and Schijve for the alloy 2090-T83, crack initiation in substitute ocean water depended on the passive film breakdown by pitting [23].

5. CONCLUSIONS

1. Recrystallized 8090-T81 and 2091-T84 sheets are prone to exfoliation corrosion, as indicated by laboratory tests. In these tests, control 2024-T3 sheet suffers predominantly pitting.
2. Damage tolerant 8090-T8171 and 2091-T8X51 plates are susceptible to exfoliation corrosion. Their behaviour is similar or slightly better than that of conventional 2024-T351 plate.
3. Using an aqueous solution of 0.5 M NaCl + 0.1 M LiCl + 0.05 M NaHCO₃ + 0.05 M Na₂CO₃, the SSR testing technique indicates sensitivity to stress corrosion cracking for damage tolerant 8090-T81 and 2091-T84 sheet materials.
4. As found in static loading tests, 8090-T8171 and 2091-T8X51 plates are virtually immune to environmentally assisted cracking when stress is applied in longitudinal and long transverse directions.
5. When loaded in the short transverse direction, both plates are susceptible to stress corrosion cracking. The SCC initiation resistance is similar to that of 2024-T351 plate. Threshold stresses below 100 MPa are determined.

6. REFERENCES

1. R. Grimes, T. Davis, H.J. Saxty, J.E. Faeron, in "4th International Aluminium Lithium Conference", *Journal de Physique*, 48 (1987) C3-11.
2. R. Grimes, M.A. Reynolds, A.P. Titchener, M.S. Greaves, I. Strassheim, D. Warrington, in "Aluminium-Lithium", M. Peters and P.-J. Winkler (eds.), DGM, Oberursel, 1992, p.3.
3. M. Doudeau, P. Meyer, D. Constant, in "New Light Alloys", AGARD-CP-444, 1989, paper 2.
4. R.H. Graham, R.J. Rioja, J.M. Newman, as ref. 2, p.15.
5. P. Fournier, Y. Barbaux, K.H. Rendigs, as ref. 2, p.1271.
6. S. Lee, B.W. Lifka, in "New Methods for Corrosion Testing of Aluminum Alloys, ASTM STP 1134, V.S. Agarwala and G.M. Ugiansky (eds.), American Society for Testing and Materials, Philadelphia, 1992, p.1.
7. R. Braun, H. Buhl, in "Advanced Aerospace Materials", H. Buhl (ed.), Springer-Verlag, Berlin, 1992, p.296.
8. C.J.E. Smith, J.A. Gray, M.A.H. Hewins, "GARTEUR - Final Report, Corrosion and Stress Corrosion of Commercial Aluminium-Lithium Alloys", Working Paper MS4-93-WP-26, DRA, Farnborough, 1993.
9. P.L. Lane, J.A. Gray, C.J.E. Smith, in "Aluminium-Lithium Alloys III", C. Baker, P.J. Gregson, S.J. Harris, C.J. Peel (eds.), The Institute of Metals, London, 1986, p.273.
10. E.L. Colvin, S.J. Murtha, in "Aluminium-Lithium Alloys", T.H. Sanders, E.A. Starke (eds.), MCEP, Birmingham, 1989, p.1251.
11. R. Braun, to be published.
12. L. Schra, F.F. Groep, *J. Test. Eval.*, 21 (1993) 44.
13. R. Braun, *Mater. Sci. Eng.*, (1994)
14. R. Braun, H. Buhl, as ref. 2, p.807.
15. K. Welpmann, H. Buhl, R. Braun, M. Peters, as ref. 1, p.C3-677.
16. R. Braun, *Werkst. Korros.*, 40 (1989) 661.
17. R. Braun, in "Aluminum Alloys (ICAA4), Volume II", T.H. Sanders and E.A. Starke (eds.), The Georgia Institute of Technology, Atlanta, GA, 1994, p.519.
18. R.C. Dorward, K.R. Hasse, *Corrosion* 43 (1987) 408.
19. A. Gray, as ref. 1, p.C3-891.
20. A. Gray, N.J.H. Holroyd, J. White, as ref. 10, p.1175.
21. D.J. Chellman, R.A. Rainen, J.J. Witters, R.S. James, as ref. 2, p.993.
22. R. Braun, as ref. 2, p.697.
23. A. Buis, J. Schijve, as ref. 2, p.703.

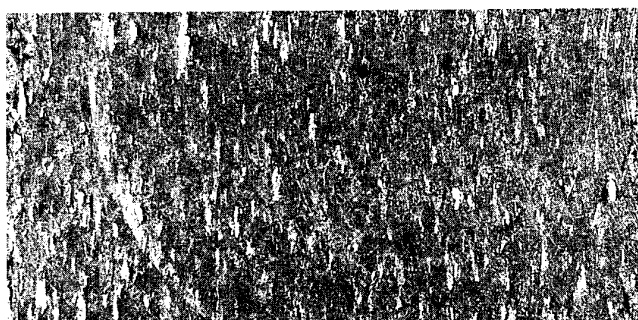
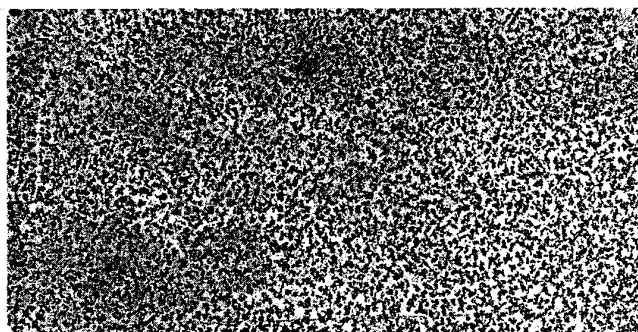
**8090-T8171****2091-T8X51****2024-T351****7075-T7351**

Fig. 1. Appearance of half-thickness subsurface panels of aluminium alloy plate after two weeks of exposure to cyclic acidified salt fog according to ASTM G85, Annex A2 (size of the panels was 50 by 100 mm).

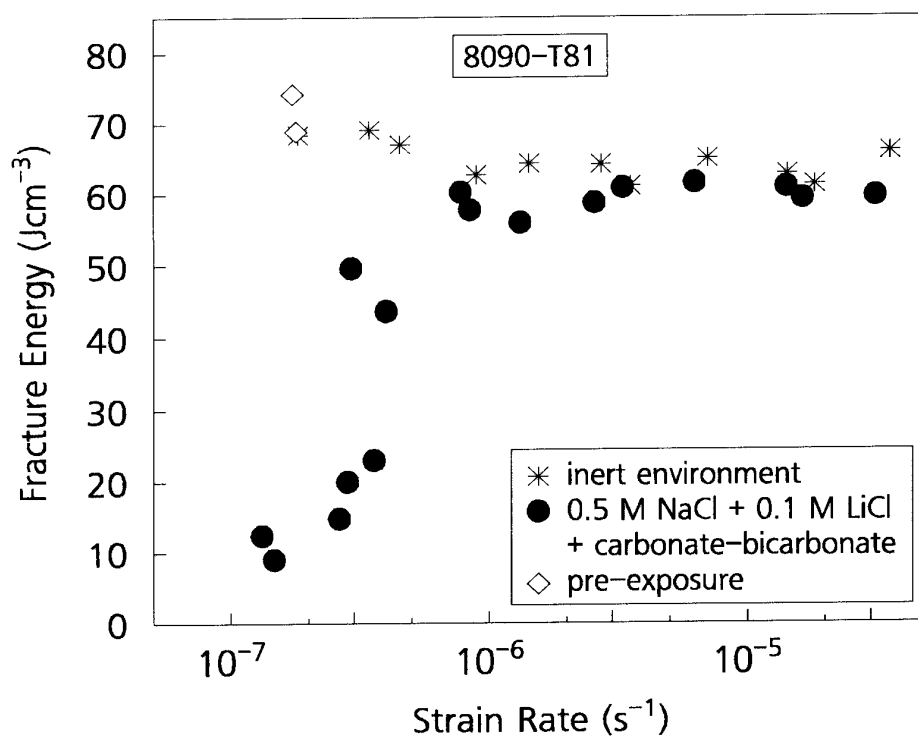


Fig. 2. Fracture energy vs. strain rate for 8090-T81 sheet. Long transverse tensile specimens were dynamically strained in an aqueous chloride-carbonate-hydrogencarbonate solution. Data for pre-exposed specimens are included.

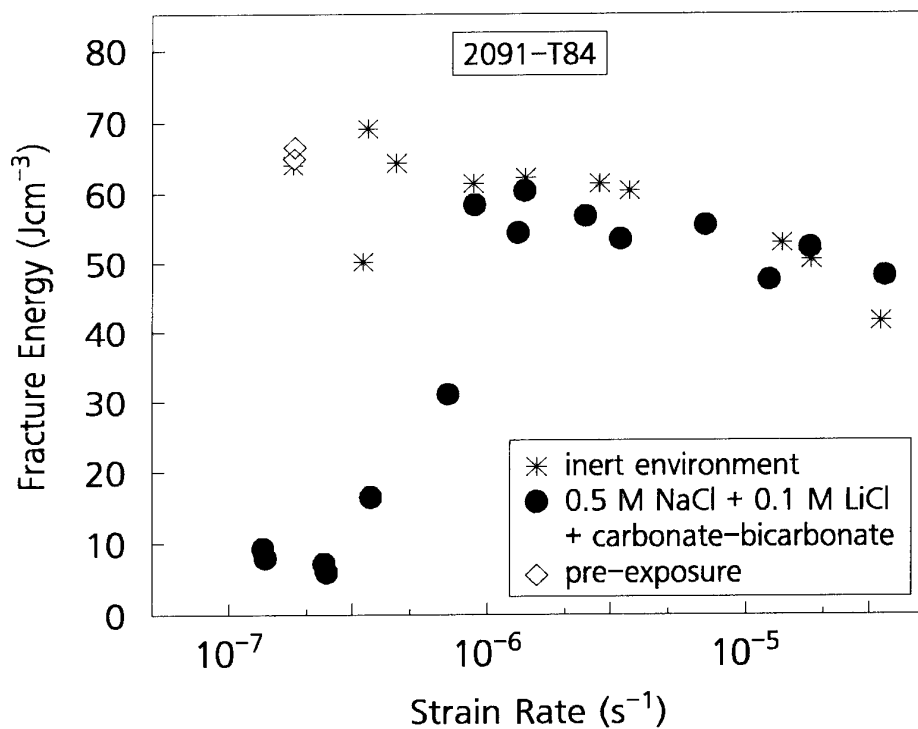


Fig. 3. Fracture energy vs. strain rate for 2091-T84 sheet. Long transverse tensile specimens were dynamically strained in an aqueous chloride-carbonate-hydrogencarbonate solution. Data for pre-exposed specimens are included.

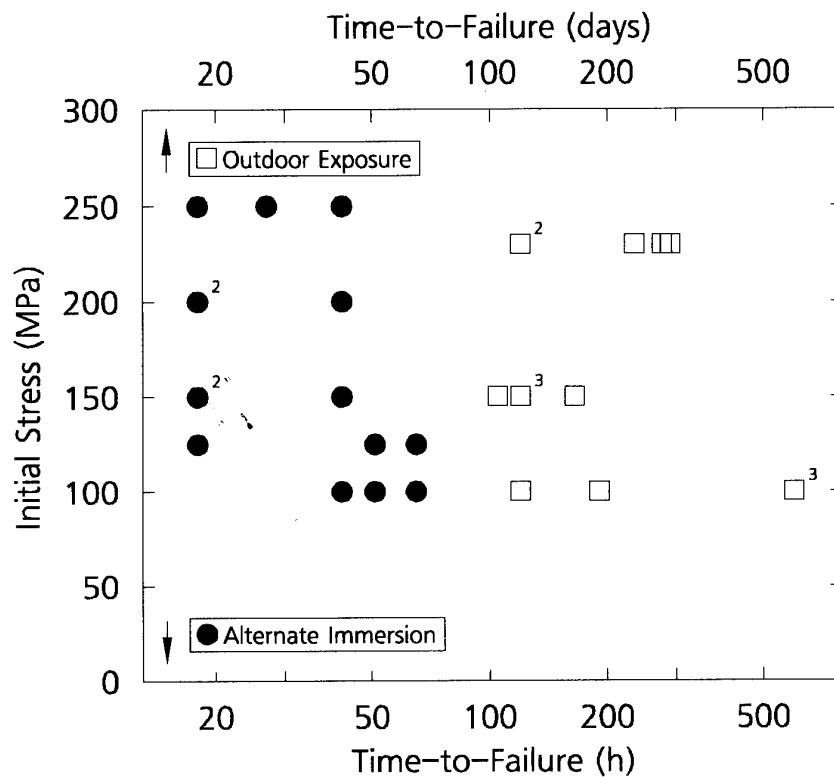


Fig. 4. Time-to-failure data for 2091-T8X51 plate. Short transverse tensile specimens were exposed to the urban industrial environment at Cologne and alternately immersed in 3.5% NaCl solution according to ASTM G44 under constant deformation conditions. Numbers indicate the numbers of specimens tested.

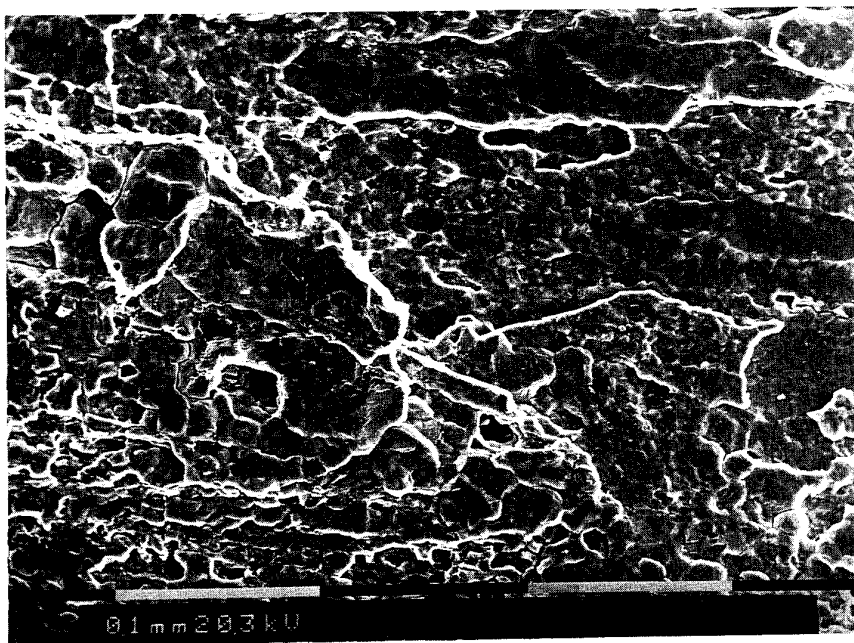


Fig. 5. Scanning electron fractograph of a 2091-T8X51 specimen showing intergranular stress corrosion cracking. The short transverse tensile specimen failed after 120 days of exposure to urban industrial environment at an applied stress of 150 MPa.

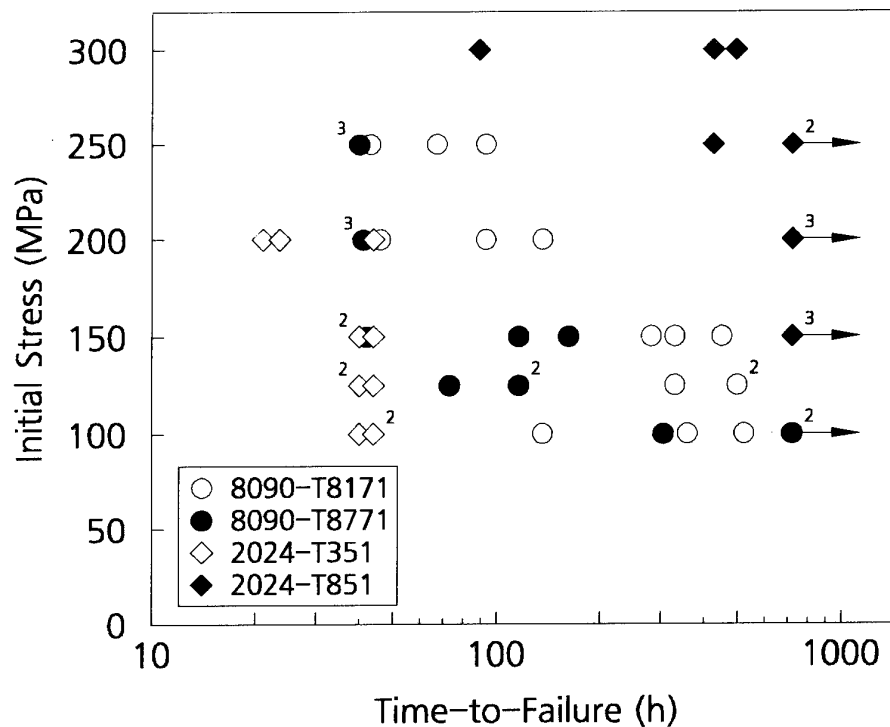


Fig. 6. Time-to-failure data for 8090 and 2024 plate materials in different tempers. Short transverse tensile specimens were alternately immersed in 3.5% NaCl solution according to ASTM G44 under constant deformation conditions. Numbers indicate the numbers of specimens tested.

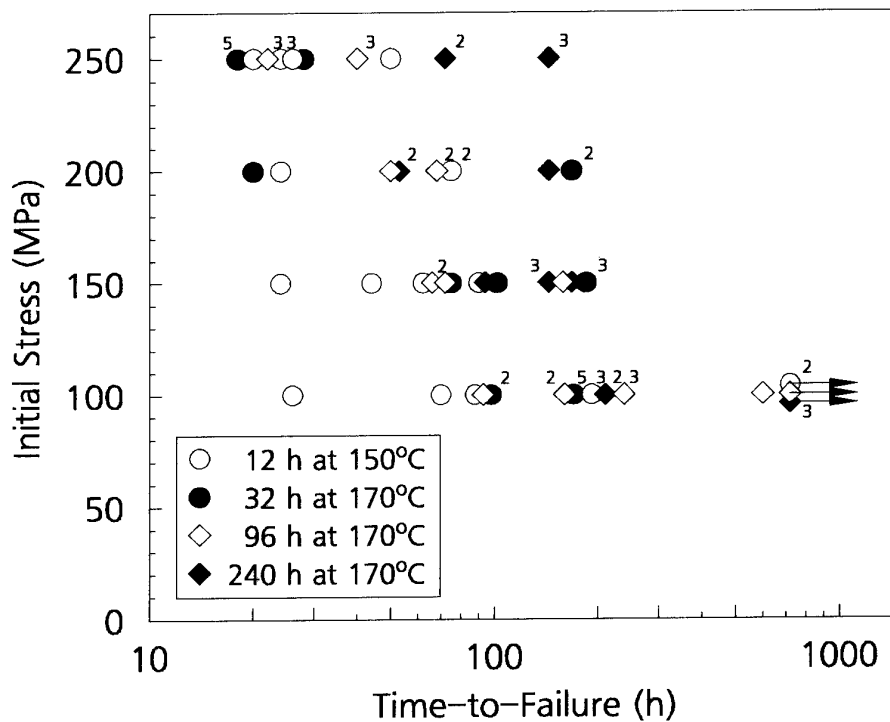


Fig. 7. Time-to-failure data for a 30 mm thick 8090 plate which was received in the T351 condition and aged to different tempers. Short transverse orientated C-ring specimens were alternately immersed in 3.5% NaCl solution at a temperature of 22°C and under uncontrolled relative humidity.

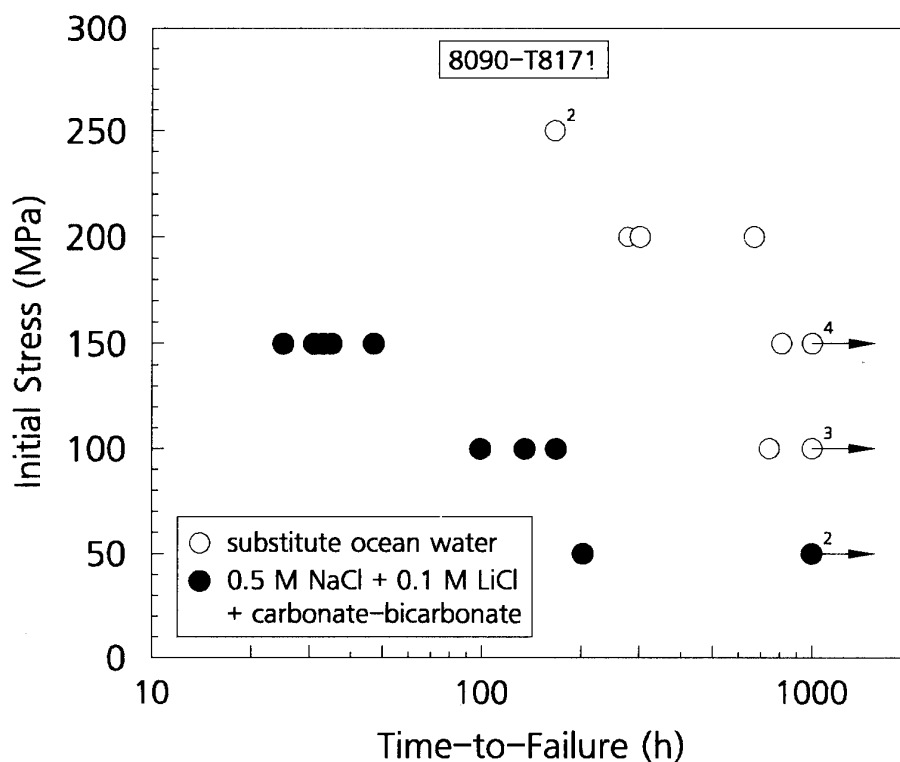


Fig. 8. Time-to-failure data for 8090-T8171 plate. Short transverse tensile specimens were permanently immersed in substitute ocean water and in an aqueous chloride-carbonate-hydrogencarbonate solution under constant load conditions. Numbers indicate the numbers of specimens tested.

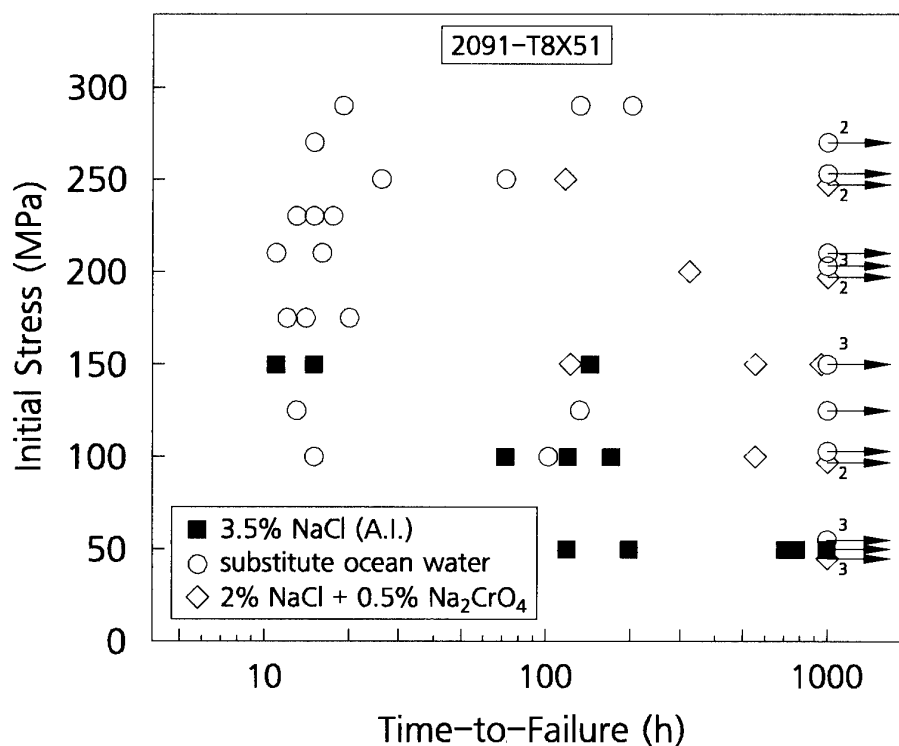


Fig. 9. Time-to-failure data for 2091-T8X51 plate. Short transverse tensile specimens were alternately immersed in 3.5% NaCl solution or permanently immersed in substitute ocean water and in an acidified aqueous chloride-chromate solution under constant load conditions.

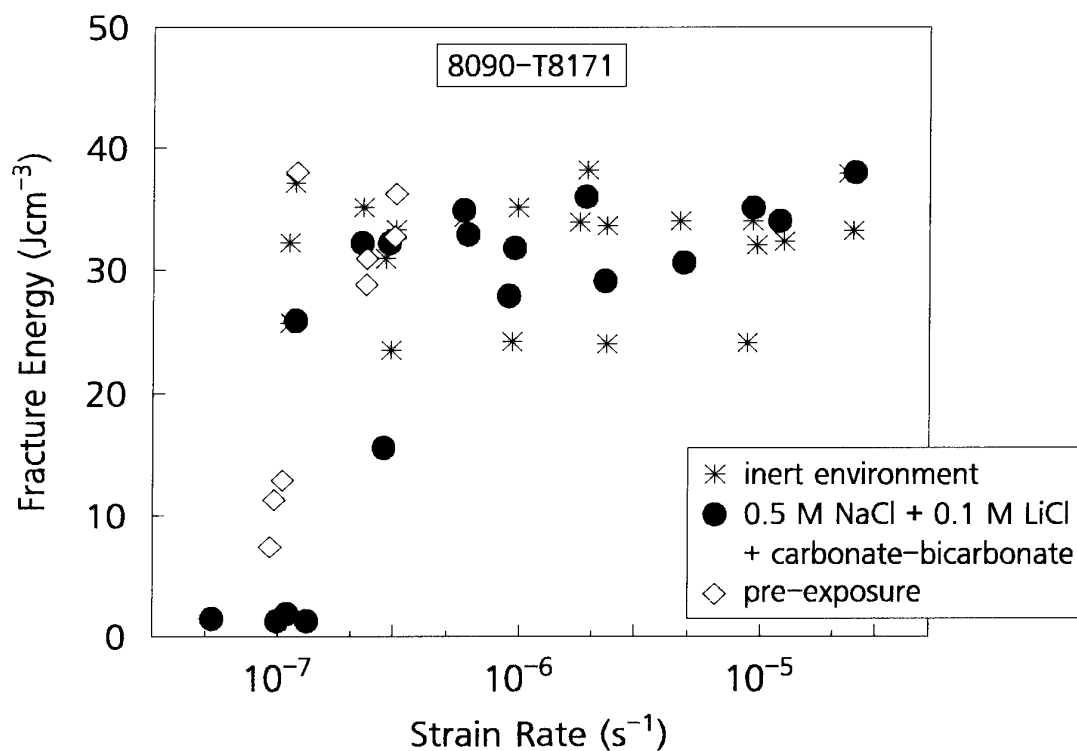


Fig. 10. Fracture energy vs. strain rate for 8090-T8171 plate. Short transverse tensile specimens were dynamically strained in an aqueous chloride-carbonate-hydrogencarbonate solution. Data for pre-exposed specimens are included.

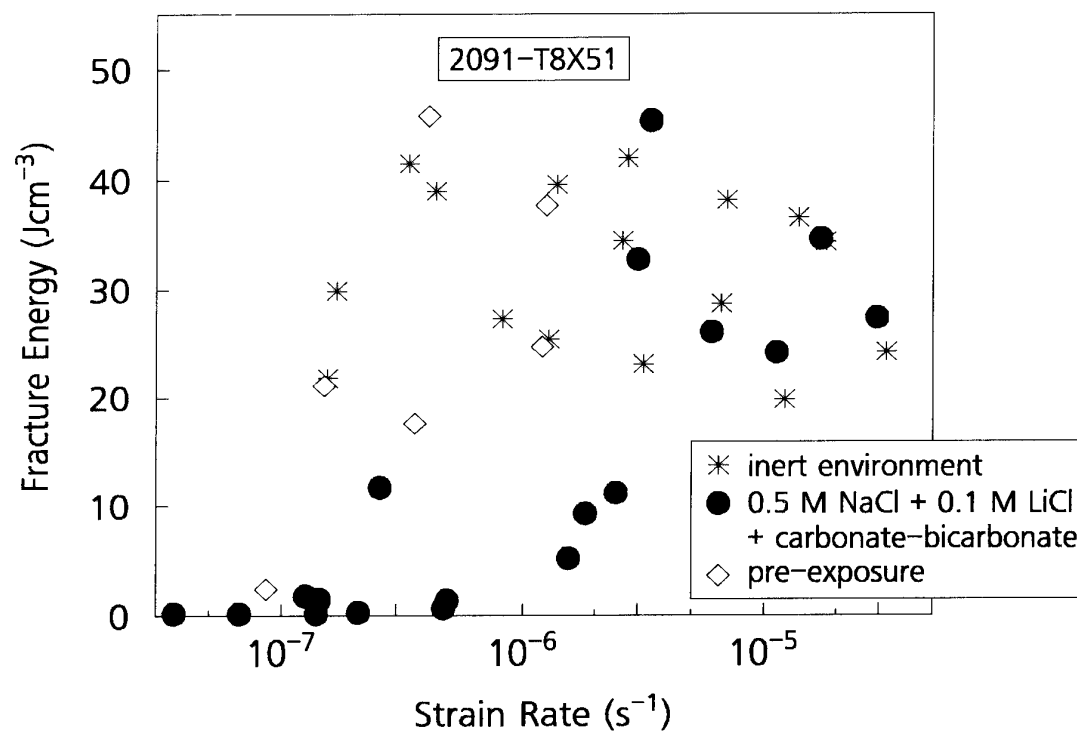


Fig. 11. Fracture energy vs. strain rate for 2091-T8X51 plate. Short transverse tensile specimens were dynamically strained in an aqueous chloride-carbonate-hydrogencarbonate solution. Data for pre-exposed specimens are included.

EFFECT OF LOADING DIRECTION AND LONG-TERM AGING ON FATIGUE-CRACK GROWTH IN Al-Li ALLOY 2090

M. Anık and M. Doruk
Metallurgical Engineering Department
Middle East Technical University
06531 Ankara
Turkey

1. SUMMARY

The effect of prolonged exposures up to 1000 Hr at 150, 165 and 180°C on the fatigue-crack growth were studied in the Al-Li alloy 2090 using the direct current potential drop technique, and results compared with crack growth rates determined in salt-water. The CCT specimens, 40x200 mm in size, were taken from the sheet material with a thickness of 1.6 mm. Since one of the purposes of this work was to investigate the directionality of fatigue-crack growth behavior, the specimens were machined in the grainflow direction (L-T), long-transverse direction (T-L) and 45° to rolling direction (L+45°). The pretreatment applied before the aging consisted of solutionizing at 550°C for one hour followed by 6% stretching.

According to the air results, the fatigue-crack growth behavior did not vary significantly with specimen orientations tested in this study. On the other hand, the long-term aging was found to have a pronounced effect on the crack growth kinetics, demonstrated by growth rates which increased up to about 8 fold following aging for 1000 Hr. The rate of the salt-water induced fatigue-crack growth was higher at low values, but lower at high values of ΔK , relative to those obtained in air. Whereas the reduction in roughness induced crack closure effect is believed to be responsible for enhancement at low stress intensity ranges the retardation at high ΔK -values may be attributed to crack-tip electrochemistry, whereby intermetallics with high cathodic efficiency are thought to play a role.

2. INTRODUCTION

The precipitation hardening Al-Li-Cu alloys are known for their superior fatigue-crack growth resistance as compared to traditional high-strength aluminum alloys such as 2000 and 7000 series [1-5]. As far as the long cracks are concerned the so-called extrinsic toughening through the crack tip shielding is considered to be responsible for this behavior. Crack deflection and wedging through the crack surface roughness or corrosion products induced crack closure appear as the most effective mechanisms that may result in crack tip shielding in Al-Li alloys. The high propensity to coarse planar slip is considered to be the major cause both of the tortuous crack path and crack branching that may reduce the crack driving force [6-7]. On the contrary, the initiation phase of fatigue cracks in Al-Li alloys has been documented to be shorter than that of conventional alloys [8]. This behavior is attributed to the extensive strain localization and strong texture found in these alloys. The optimum microstructure for fatigue crack initiation was claimed to be consistent with that required for high fracture toughness [9].

Despite their high fatigue-crack growth resistance, the Al-Li alloys exhibit a high degree of anisotropy especially when they are loaded in the short-transverse direction. In this orientation the crack extension would follow the rolling plane and occur basically by intergranular delamination. Experiments

with a 12.7 mm thick plate of Al-Li-Cu-Zr alloy 2090-T8E41 revealed about 20 percent reduction in the threshold level when tested in S-L and S-T orientations as compared to L-T, T-L and T-S orientations with fracture plane perpendicular to the rolling plane [5].

Another question of considerable interest is the effect of prolonged heating on the fatigue behavior of Al-Li alloys. Experiments with lightly overaged (100 hrs heating at 163°C) and overaged (1000 hrs heating at 163°C) Al-Li alloy 2090 showed that, above around 10^{-8} m/cycle, the fatigue crack rates progressively increase with aging time, whereas near threshold growth rates below about 10^{-8} m/cycle were found to be comparatively unchanged [10]. This behavior was attributed to the reduced crack closure in overaged compared to the peak-aged alloys.

In conventional high-strength aluminum alloys, the fatigue-crack propagation is enhanced by aqueous environments. Of particular interest is the crack growth kinetics induced by aggressive solutions such as sea water. Some conventional alloys exposed to salt-water showed no significant degradation in fatigue-crack growth behavior when tested in the low ΔK -region. This behavior was attributed to the crack closure effect induced by corrosion products that remain within the crack [11].

The situation with the Al-Li alloys, however may be significantly different from that experienced with the conventional alloys. The limited data available in this area show that the tortuosity of fracture path, characteristic for Al-Li alloys, (especially for 2090-T8E41) may be reduced by combined action of fatigue load and corrosive environment [11]. This may reduce the roughness induced crack closure and result in an enhancement of crack extension. However, this situation would be complicated by the adverse effect of the corrosion product. Evidently, further research is needed to elaborate these questions.

The present study was undertaken to generate further data on the fatigue-crack growth behavior of a conventional high-strength Al-Li-Cu alloy whereby a special emphasis was devoted to the effect of specimen orientation and the long-term aging on fatigue-crack propagation in the air and under salt-water exposure.

3. EXPERIMENTAL DETAILS

The material investigated was an Al-Li-Cu-Zr alloy 2090 in the form of a 1.6 mm thick sheet. Strips 42 mm wide and 440 mm long cut from the sheet in three different direction (parallel, normal and inclined by 45° to rolling direction) were solution heat treated at 550°C in a specially prepared salt bath. Following stretching by 6 percent the strips were halved and machined to final shape and the dimensions of specimens are depicted in Figure 1. Then, the specimens were aged at 150, 165 and 180°C for 20, 100 and 1000 Hr. The aging treatment was carried out in a heating bath circulator filled with a silicon based oil. The aging temperature could be held constant within

Table 1. Orientation of and heat-treatment applied to specimens used in the fatigue tests.

Specimen Orientation and Aging Temperature		Aging time, Hours		
L-T	150°C	20	100	1000
	165°C			
	180°C			
T-L	150°C	20	100	1000
	165°C			
	180°C			
L+45°	150°C	20	100	1000
	165°C			
	180°C			

$\pm 0.01^\circ\text{C}$. As indicated by the Table 1, the experimental programme consisted of fatigue testing 27 specimens with different orientation and different heat treatment.

All fatigue tests were carried out on a closed loop servo-hydraulic machine with a load capacity of 10.000 kg operating under load control. Sinusoidal loading was applied at a frequency of 5 Hz and the stress ratio R was 0.05, which was kept constant through the whole experiments. The maximum load was 500 kg, which corresponded to a maximum nominal stress of 76.61 MPa.

The starter notch in the center of specimens produced by electrical discharge machining (EDM) was converted to an initial crack through applying fatigue load until the crack grew to a length of approximately 5 mm. Fatigue tests were continued up to unstable failure. The critical crack length at which unstable failure was initiated was always lower than 0.7 W, i.e. within the validity range of the stress intensity equation.

The propagation of fatigue cracks was measured both by a travelling microscope and the direct current-potential drop (dc-pd) technique to calibrate the potential drop according to crack length. Furthermore, the data generated by these measurements were fitted with the polynomial,

$$(V/V_0) / (V_{ref}/V_{ref0}) = 0.970204 + 0.262386 (2a/W) - 3.88706 (2a/W)^2 + 40.7865 (2a/W)^3 - 110.555 (2a/W)^4 + 136.94(2a/W)^5 - 62.9274 (2a/W)^6$$

where V and V_{ref} are the potential drop and the reference potential drop, and V_0 and V_{ref0} are their initial values. The reference potential drop was monitored also to compensate for temperature changes. In addition, the potential drop was recorded twice through reversing the polarity at the power source every time. In all dc-pd measurement the excitation current was 10 A and could be kept constant within the limits ± 30 mA. Potential was measured to a precision of $\pm 1 \mu\text{V}$ and the crack length measurement resolution was better than $\pm 50 \mu\text{m}$.

The effect of salt-water exposure on the fatigue-crack propagation was one of the objectives that would be achieved in this study. Therefore, the experimental programme outlined in Table 1 was duplicated whereby 3.5% NaCl aqueous solution was circulated through the crack in the specimen. The plexiglas cell that was used in salt-water experiments is illustrated in Figure 2. The design of the two-piece cell is such that the contact with salt-water of the spot welded regions on both faces of specimens is avoided.

4. RESULTS AND DISCUSSION

4.1. Microstructures

In order to follow-up the microstructural changes upon artificial aging in alloy 2090, transmission electron microscopy (TEM) was applied extensively. The results of the TEM study are summarized briefly before the fatigue-crack growth behavior is discussed in detail.

In as-received condition the microstructure of alloy 2090 consisted of very small and homogeneously distributed phases whereas no precipitation was observed at the grain boundary regions. Spherical δ' , δ' encapsulating spherical Al_3Zr , coating the plate-like θ' , θ' on Al_3Zr and T_1 were types of precipitates identified with the help of TEM. After the solutionizing heat treatment prior to artificial aging the only visible phase was Al_3Zr .

The aging at 150°C resulted in the formation of the spherical δ' which was identified as the major precipitate at this temperature. Its number density increased when the aging time was extended to 100 hr. The further extension of the aging time to 1000 hr, however, induced a coarsening of this phase, and while the number density decreased the diameter of precipitates grew two or three fold. A δ' precipitate free zone (PFZ) was identified adjacent to grain boundaries and also some δ at grain boundary regions when the aging time was sufficiently long (100 and 1000 Hr). Generally, the grain boundary precipitates were coarser for the 1000 hours aging. The plate-like θ' precipitates were observed following 20 and 100 Hr aging, and most of them are coated by δ' phase. Upon aging for 1000 Hr, however, they disappeared almost completely, so that the δ' precipitates appeared to be associated with Al_3Zr instead of the θ' phase. The aging for 100 Hr resulted in the plate-like T_1 precipitates being much coarser for the longer aging time.

The dominant phases in aging at 165°C were the plate-like T_1 and θ' , and δ' showing a homogeneous distribution over the matrix. There was δ' PFZ near to grain boundaries and around T_1 precipitates as well. Precipitates both in matrix and at grain boundaries appeared coarser when compared to aging at 150°C . Up to 100 Hr aging time δ' was observed to be associated with θ' and Al_3Zr while in 1000 Hr aging only with Al_3Zr precipitates.

The aging treatments at 180°C caused a general coarsening of precipitates. This was exhibited clearly by the coarse precipitates at grain boundaries induced by aging for 1000 Hr. Also the spherical δ' precipitates showed a very coarse distribution especially when the aging times were long. The T_1 phase appeared to be dominant in the matrix, and there was a δ' PFZ around the large T_1 precipitates. θ' precipitates were observed in specimens aged for shorter periods of time (20 and 100 Hr) with the little amount of δ' precipitates coating this particular phase whereas the majority of δ' encapsulated Al_3Zr .

4.2. Fatigue-Crack Growth Behavior

Fatigue-crack growth data for specimens of the alloy 2090 prepared according to Table 1 and tested in the laboratory air are shown in Figures 3-5. As seen from these data, the ΔK -range that could be covered in the experiments begins at about 7 and extends to about $22 \text{ MPa}\sqrt{\text{m}}$. Evidently, da/dN - ΔK plots included in these figures give no information on the threshold stress intensities ΔK_{th} , and the evaluation of results has to be accomplished by direct comparison of da/dN - ΔK curves. An additional approach used in this study was to compare the crack growth rates for an intermediate value of ΔK , which was selected as $12 \text{ MPa}\sqrt{\text{m}}$.

4.2.1. Effect of Orientation

According to the crack length-number of cycles data that are not presented here, the T-L orientation appears to have the highest fatigue-crack growth resistance especially for specimens with lower degree of aging. For example, the specimens aged for 20 Hr at 165 and 180°C showed almost the same growth rates in L-T and L+45°, which were higher than that in T-L orientation. These differences tend, however, to diminish with increasing aging times as illustrated by specimens treated for 100 and 1000 Hr at 165°C . Although the specimen aged for 20 Hr exhibited a slightly higher fatigue-crack growth resistance in T-L over the other two orientation, this difference disappeared almost completely when the aging

Table 2. Enhancement of fatigue-crack growth as a function of aging and specimen orientation (for $\Delta K = 12 \text{ MPa}\sqrt{\text{m}}$).

Aging		Specimen Orientation			K _{max} (MPa $\sqrt{\text{m}}$)
Time (Hrs)	Temperature (°C)	L-T	T-L	L+45°	
20	150	1	1	1	23.63
	165	1	1	1	23.62
	180	1	1	1	22.84
100	150	1.59	1.34	1.58	23.42
	165	1.78	2.02	1.44	20.74
	180	2.96	2.13	1.67	20.84
1000	150	8.79	7.73	4.93	17.58
	165	6.86	7.46	5.57	18.84
	180	7.60	5.46	3.35	17.47

time was increased up to 1000 Hr. An exception to this were the specimens aged at 180°C. As seen from Figure 6, the crack growth tends to be faster in L-T direction, relative to other orientations. At the first glance these results may be found to be contradictory to the fairly well established fact that the crack path in L-T orientation is deflected and branched while it remains more straight in T-L orientation, consistent with the higher fatigue-crack growth resistance in L-T, compared to T-L orientation [12]. This may be due to the partial, not necessarily a true reflection of fatigue-crack growth behavior provided by the comparison in Figure 6.

To get a more realistic view on the effect of orientation on the fatigue-crack growth rates, the da/dN - ΔK curves obtained in three different orientations are plotted on the same graph to enable a direct comparison. Figure 7 constructed for 20, 100 and 1000 Hr aging times (aging temperature 165°C) separately exhibit a fairly close overlapping of the da/dN - ΔK curves that belong to different specimen orientations.

The present study was carried out with a sheet of 1.6 mm thickness. Therefore, measurement in S-L and S-T orientations could not be conducted. As pointed out earlier, a study with a 12.7 mm thick plate of alloy 2090-T8E41 revealed about 20 percent reduction in ΔK_{TH} when tested in latter orientations, compared to L-T, T-L and T-S whereby the intergranular delamination was identified as the principal crack growth mechanism [5]. All these results may be interpreted to mean that the anisotropy of the fatigue crack growth resistance of alloy 2090 confines essentially to orientations S-L and S-T with thick-sectioned parts that are loaded also in the short-transverse direction.

4.2.2. Effect of High Temperature Exposure

The overwhelming effect of the high temperature exposure on the fatigue-crack growth resistance of alloy 2090 can be deduced directly from da/dN - ΔK curves included in Figures 3-5. The specimens aged at 150°C exhibited the highest resistance to fatigue-crack propagation, and it was found to degrade with the increasing temperature as illustrated by the enhancement of crack growth. Comparing the crack growth at $\Delta K = 12 \text{ MPa}\sqrt{\text{m}}$ one may find that the increase in crack growth rate was roughly two fold when the aging temperature was changed from 150 to 180°C for the same exposure times.

On the contrary, the exposure time which was extended up to 1000 Hr appeared to be the dominant factor causing rapid increase of fatigue-crack growth rate. Using again the data that corresponds to $\Delta K = 12 \text{ MPa}\sqrt{\text{m}}$, Figure 8 was constructed to show the effect of aging time, compared to temperature and specimen orientations. In addition, the ratios of crack growth rates for 20 Hr aging to that following aging for 100 Hr and exposures for 1000 Hr were given in Table 2.

In the present study no attempt was made to measure the fracture toughness of alloy 2090 as a function of aging treatment and specimen orientation. Instead, the maximum values of stress intensity at which the unstable fracture was initiated were determined. Since they were very similar for the three orientations, but the same aging temperature and time,

their average was taken and added to the last column of Table 2, to show the correlation between K_{max} and the degree to which the fatigue-crack growth was enhanced following the prolonged heating. According to these, compared to aging for 20 and 100 Hr, exposures for 1000 Hr are found to induce about 20 to 25 and 10 to 16 percent reductions in K_{max} respectively. The degradation reflected by these data was attributed to the coarsening of matrix precipitates, the formation of subgrain boundary and grain boundary precipitates and Cu-rich precipitates which resulted in Cu-depleted and PFZs [10].

The progressive increase of the fatigue-crack growth rates following high-temperature exposure for extended periods of time was explained in terms of crack closure. According to this, a reduction in crack closure in over-aged, compared to under or peak-aged structures in conformity with the microscopic change from branched to linear crack paths was claimed to be responsible for the enhancement of fatigue-crack propagation [10]. In the present study, however, no data were generated that might be in support of this type of mechanism.

4.2.3. Effect of Salt-Water Exposure

Fatigue-crack growth rate data for alloy 2090 tested in 3.5%NaCl aqueous solution, compared to those obtained in air are given in Figures 9-11 for specimens in the L-T orientation, but aged differently. As far as the detrimental effect of the salt water is concerned, it is apparent, that at low ΔK -values the fatigue-crack growth rates are higher than those determined in air. This type of behavior was exhibited most clearly by the specimens aged at 150°C (Figure 9). For example, a comparison for $\Delta K = 8 \text{ MPa}\sqrt{\text{m}}$ reveals that the rates of salt-water enhanced fatigue-crack growth are about two fold over those in air. The differences between the crack growth rates, tend, however, to diminish with the increasing stress intensity range, and they become equal at a ΔK which is observed to shift to lower values upon increasing the aging time (As inferred from the Figures 8a-c, for specimens aged at 150°C, ΔK -values at which the crack growth rates both in air and salt water become equal are about 20, 15 and 12 MPa $\sqrt{\text{m}}$ for aging times of 20, 100 and 1000 Hr respectively). At higher ΔK -values, however, the crack-growth rates in salt-water appear to be lower than those in air. The da/dN - ΔK curves obtained with specimens aged at 165 and 185°C show the same type of behavior. Although the salt-water induced degradation following aging at 165°C appears to be less, the rates of fatigue-crack growth tend to increase at low ΔK -values. For example, specimens that were aged at 165°C for 1000 Hr yielded slower crack propagation in salt water at ΔK -values higher than about 8 MPa $\sqrt{\text{m}}$ (Figure 10c).

The salt-water enhancement of the fatigue-crack growth at low stress intensity range appears to be consistent with the results of previous investigations [11]. This behavior was attributed to the reduction of the roughness induced crack closure caused by the combined action of fatigue stresses and corrosive environment. There is now sufficient evidence in the literature that the stress intensity has an effect on the stress intensity range ratio defined as $\Delta K_{eff}/\Delta K$. Since this ratio tends to decay with decreasing ΔK , a reduction in the tortuosity of the fracture surfaces through the proposed fretting-like mechanism may cause a fast increase in the magnitude of ΔK_{eff} when the crack length is small. This may explain why the salt-water induced crack growth faster than that in air at small ΔK -values.

When the attention is focussed on slower growth of fatigue cracks at high stress intensity ranges under the salt-water exposure, the crack tip chemistry may be found to play a role. In this context, it would be worthwhile to examine the scanning electron micrographs of fracture surfaces shown in Figure 12. The intermetallics that are known to be present prior to aging treatment become visible on the fracture surfaces when the stress intensity range is sufficiently high (Figure 12c). The intermetallics that may contribute to crack deflection at low stress intensities are cut at higher ΔK -values. The intermetallics are expected to be electrochemically nobler than the alloy and to act as cathodic sites in a cell established

between these regions and the crack front. A model that may explain the slower fatigue-crack growth in salt water and at higher stress intensities may require the passivation of the crack front under the effect of high anodic current densities in this region. Or, if the hydrogen cracking is adopted as the basic mechanism that underlies the corrosion fatigue of alloy [13-14], this model would be consistent with the removal of hydrogen ions from the crack tip. Obviously, more research is needed to develop a better understanding of environmental effect on the fatigue-crack growth in Al-Li alloys.

5. CONCLUSIONS

Based on a study of the fatigue-crack growth behavior of Al-Li alloy 2090 as a function of specimen orientation and long-term aging the following conclusions can be drawn:

1. By the direct comparison of the da/dN - ΔK curves it can be confirmed that the fatigue-crack growth behavior is not significantly different for specimen orientations L-T, T-L and L+45°.
2. Long-term aging appears to have a pronounced effect on fatigue-crack growth kinetics. Whereas the specimens in the underaged condition exhibited the highest resistance to crack growth, the exposure times up to 1000 Hr caused a progressive increase in rates of crack advance in all specimen orientations tested. A comparison for $\Delta K = 12$ MPa \sqrt{m} reveals accelerations in the crack growth up to about 8 fold following aging for 1000 Hr.
3. The rate of salt-water induced fatigue-crack growth was higher at low values but lower at high values of ΔK , compared to those obtained in air. The enhancement in crack growth at low ΔK -values is attributed to a decrease in the roughness induced crack closure effect caused by the combined action of the fatigue load and corrosion. The retardation observed at high ΔK -values, however, may be related with the cathodic effectiveness of intermetallics that would be exposed directly to the environment, since they are cut by the advancing crack rather than serve to deflect the crack path. Accordingly, the crack growth may be impeded either by the passivation of the crack front under the effect of high anodic currents or the removal of hydrogen ions from the crack-tip region resulting in a retardation of hydrogen embrittlement.

6. ACKNOWLEDGEMENT

This work was supported by the Structure and Materials Panel of AGARD under the Additional Support Programme to South-Flank NATO Countries. Thanks are due to

Dr.J.Waldman of the Naval Air Warfare Center, (NAWC) for supplying the 2090 sheet. Several discussions with Dr. E.W. Lee of NAWC, especially during the preparation of experimental programme, is also gratefully acknowledged.

7. REFERENCES

1. Stoltz, R.E. and Pelloux, R.M., Corrosion 29, 1973, p.13.
2. Bucci, R.J., Eng.Fract.Mech. 12, 1979, p.407.
3. Lin, F.S. and Starke, Jr.,E.A., Mater.Sci. Eng. 43, 1980, p.65.
4. Gao, M., Pao, P.S. and Wei, R.P., Metall. Trans. A, 1988, Vol. 19A, p.1739.
5. Venkateswara Rao, K.T., Yu, W. and Ritchie, R.O., Metall.Trans. A, 1988, Vol.19A, p.549.
6. Jata, K.V. and Starke, Jr.,E.A., in Aluminum-Lithium Alloys III, ed.by C.Baker, P.J. Gregson, S. J. Harris and C.J. Peel, The Institute of Metals, London, 1986, p.247.
7. Venkateswara Rao K.T. , Yu, W. and Ritchie, R.O., Scripta Met., 20, 1986, p.1459.
8. Peters, M., Welpmann, K., Zinc, W. and Sanders,Jr., T.H., in Aluminum-Lithium Alloys III, ed. by C.Baker, P.J. Gregson, S.J. Harris and C.J.Peel, The Institute of Metals, London, 1986, p.239.
9. Starke, Jr., E.A. and Luetjering, G., "Cyclic Plastic Deformation and Microstructure", ed. M. Meshii, ASM, Metals Park, Ohio, 1979, p.205.
10. Venkateswara Rao, K.T. and Ritchie, R.O., Mater. Sci. Eng. 100, 1988, p. 23.
11. Pao, P.S., Imam, M.A., Cooley, L.A. and Yoder, G.R., Corrosion 45, 1989, p.530.
12. Eswara Prasad, N.,Kamat, S.V. and Malakondaiah, G., Intern. J. Fract., 61, 1993, p.55.
13. Dervenis, C.P., Meletis, E.I. and Hochman, R.F., Mater. Sci. Eng. A, 102, 1988, p.151.
14. Piascik, R.S. and Gangloff, R.P., Metall. Trans. A, 1991, Vol. 22A, p.2415.

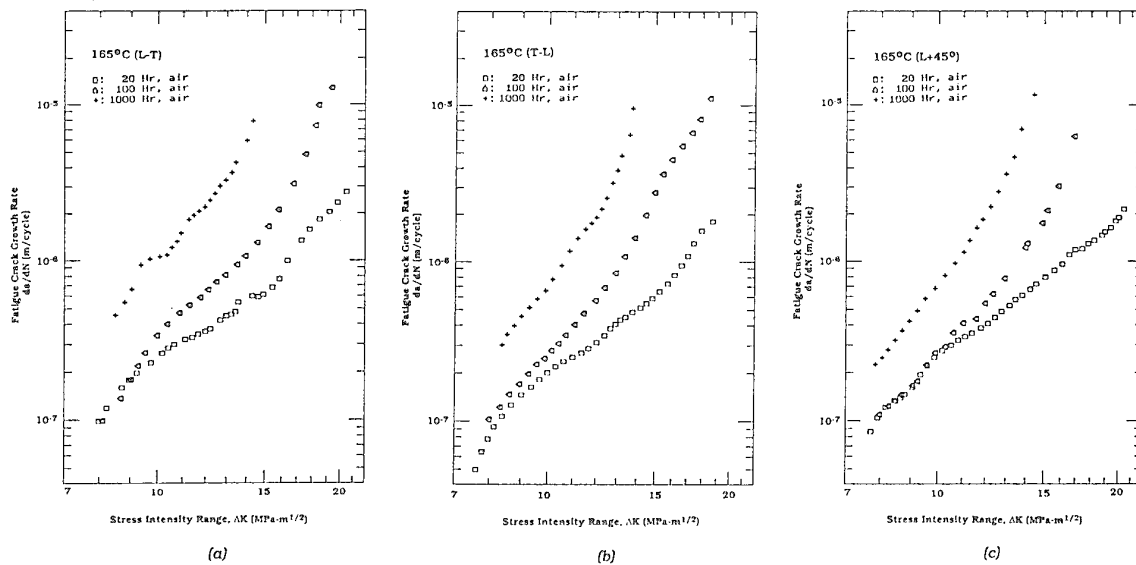


Figure 4. Crack growth behavior of fatigue cracks in alloy 2090 as a function of nominal stress intensity range showing the effect of long-term aging at 165°C, for (a) L-T, (b) T-L and L+45° orientations.

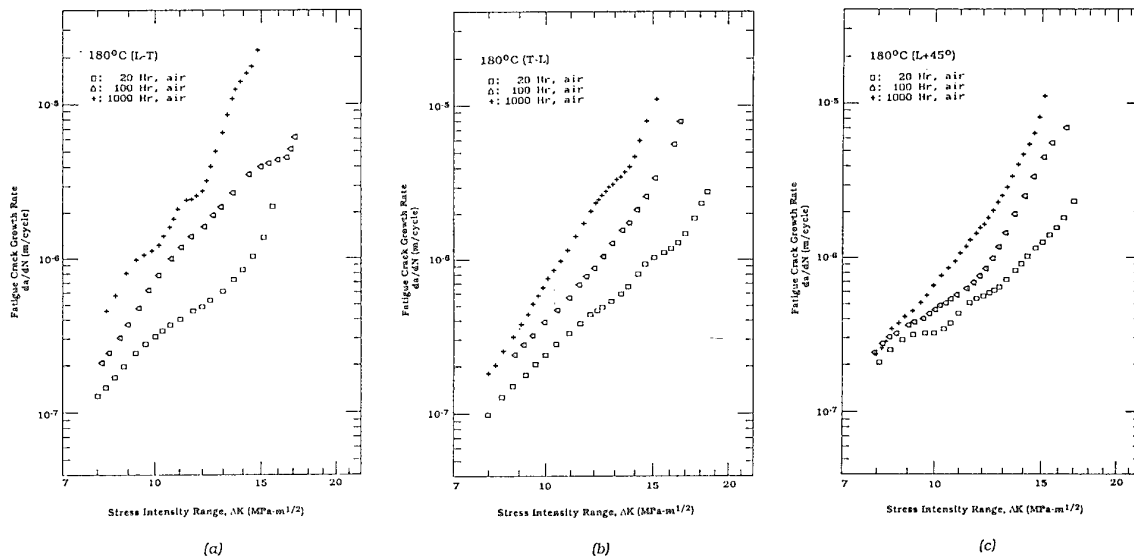


Figure 5. Crack growth behavior of fatigue cracks in alloy 2090 as a function of nominal stress intensity range showing the effect of long-term aging at 180°C, for (a) L-T, (b) T-L and L+45° orientations.

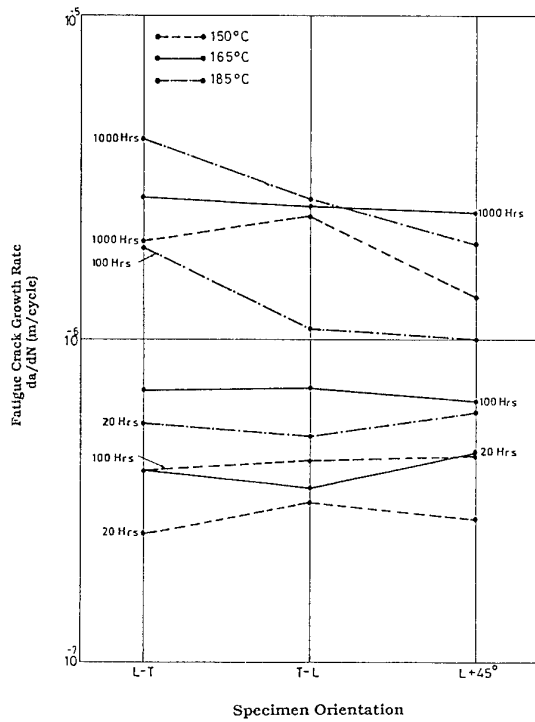


Figure 6. A comparison of the fatigue-crack growth rates showing the effect of specimen orientation (for $\Delta K=12 \text{ MPa}\sqrt{\text{m}}$).

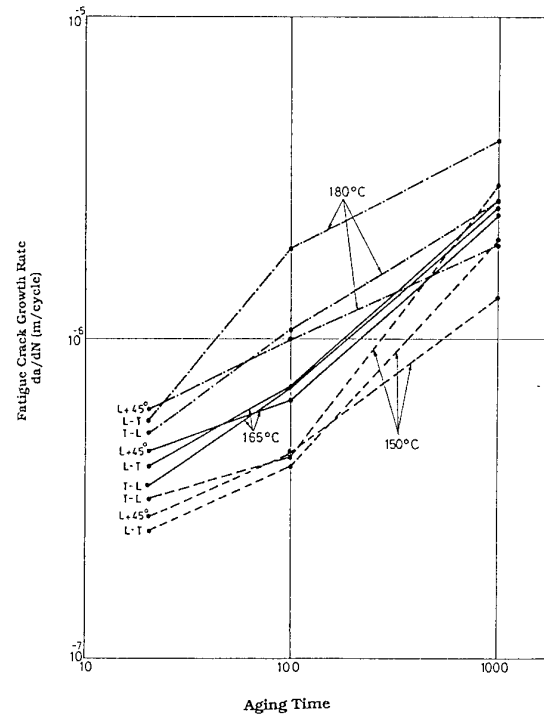


Figure 8. A comparison of the fatigue-crack growth rates showing the effect of prolonged aging (for $\Delta K=12 \text{ MPa}\sqrt{\text{m}}$).

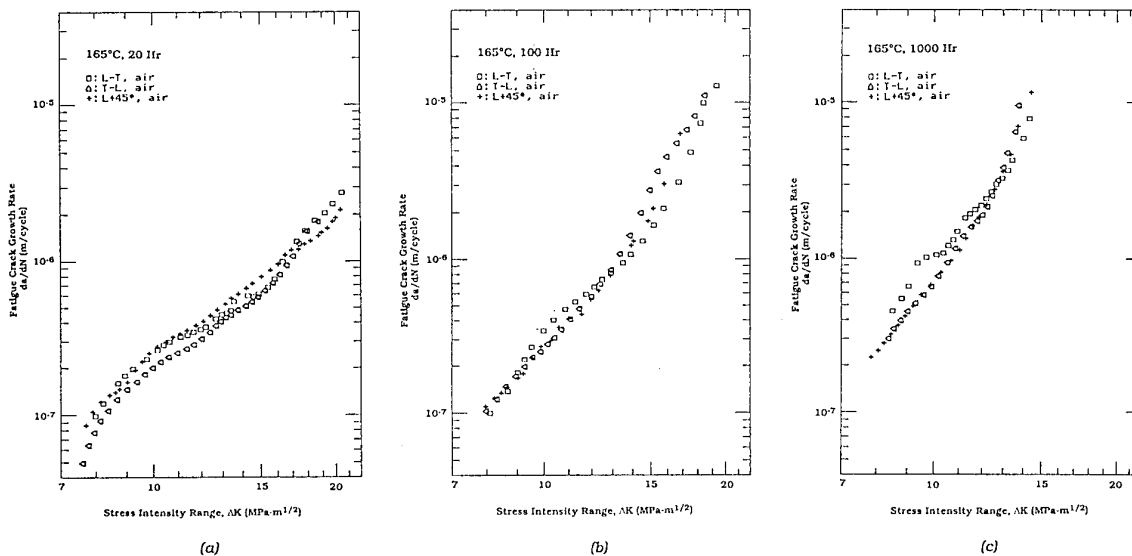


Figure 7. Variation of fatigue-crack growth rates in 2090 as a function of orientation, for specimens aged at 165°C for (a) 20, (b) 100 and (c) 1000 Hr.

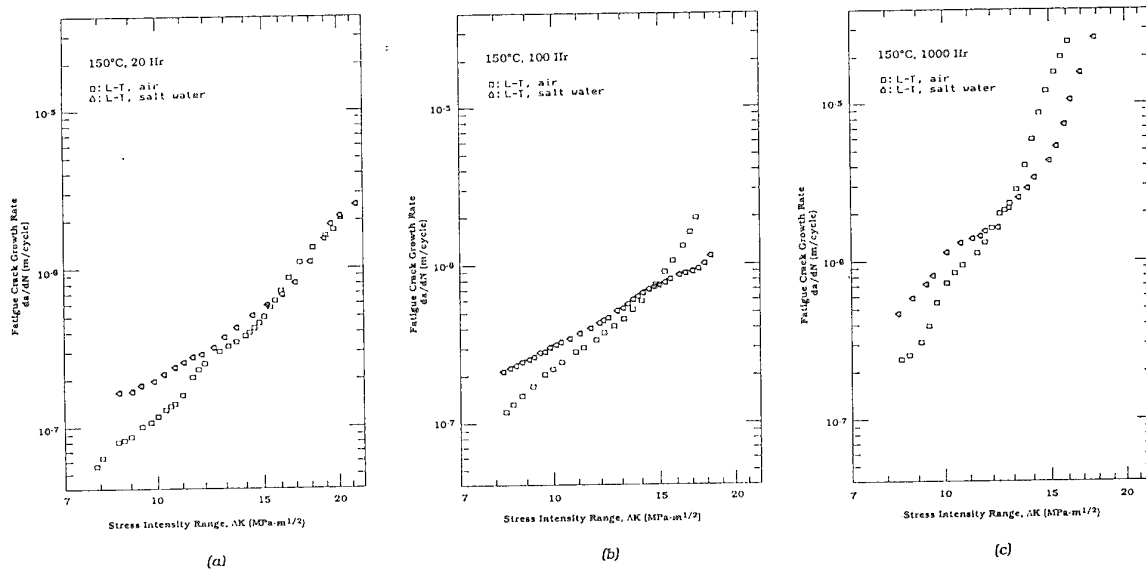


Figure 9. Comparison of the fatigue-crack growth behavior of alloy 2090 in air and 3.5% NaCl solution, for specimens in L-T orientation and aged at 150°C for (a) 20, (b) 100 and (c) 1000 Hr.

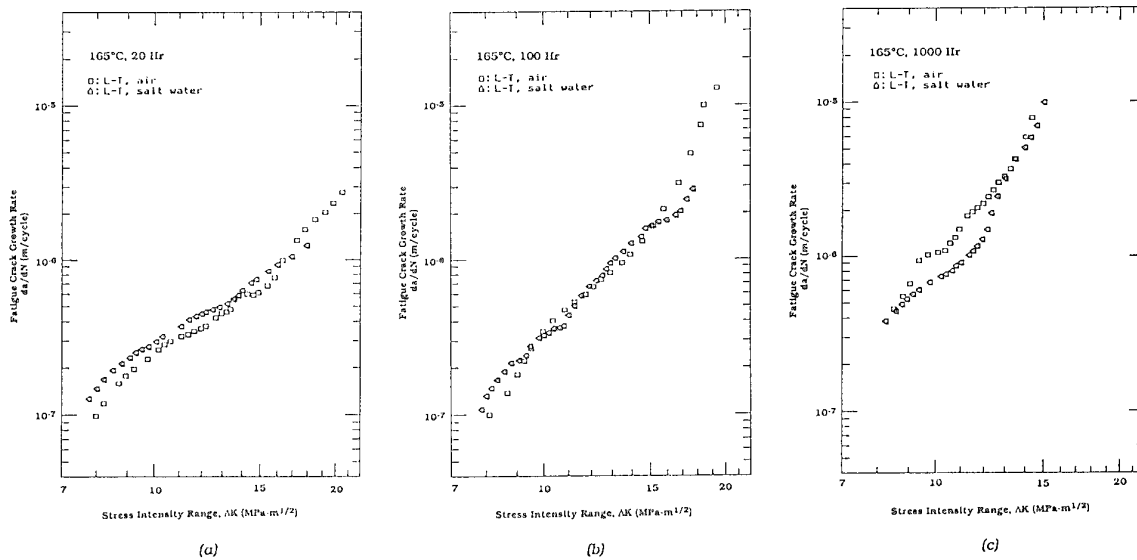


Figure 10. Comparison of the fatigue-crack growth behavior of alloy 2090 in air and 3.5% NaCl solution, for specimens in L-T orientation and aged at 165°C for (a) 20, (b) 100 and (c) 1000 Hr.

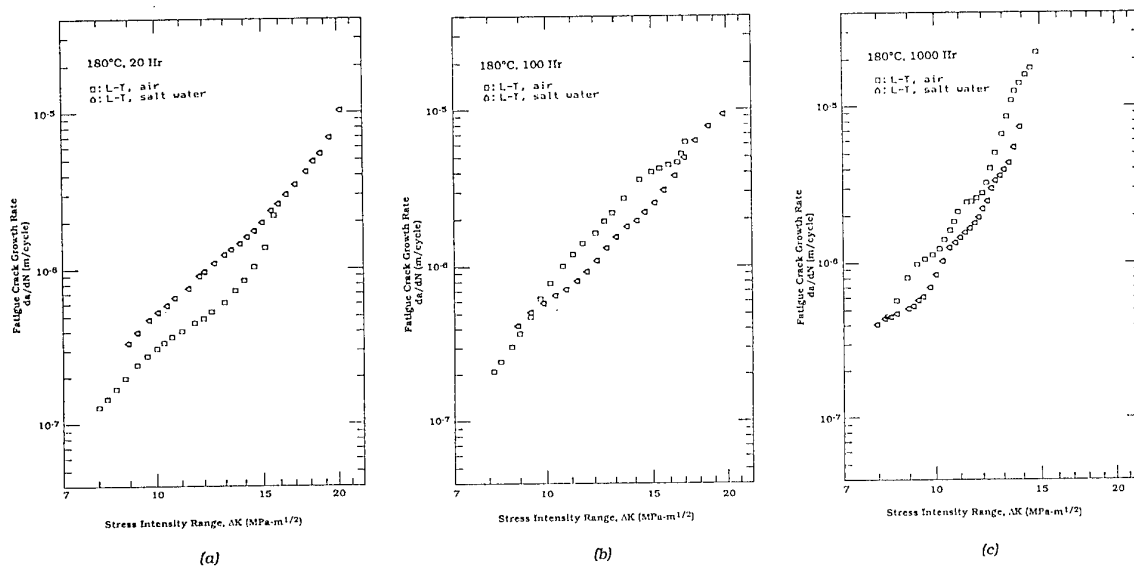


Figure 11. Comparison of the fatigue-crack growth behavior of alloy 2090 in air and 3.5% NaCl solution, for specimens in L-T orientation and aged at 180°C for (a) 20, (b) 100 and (c) 1000 Hr.

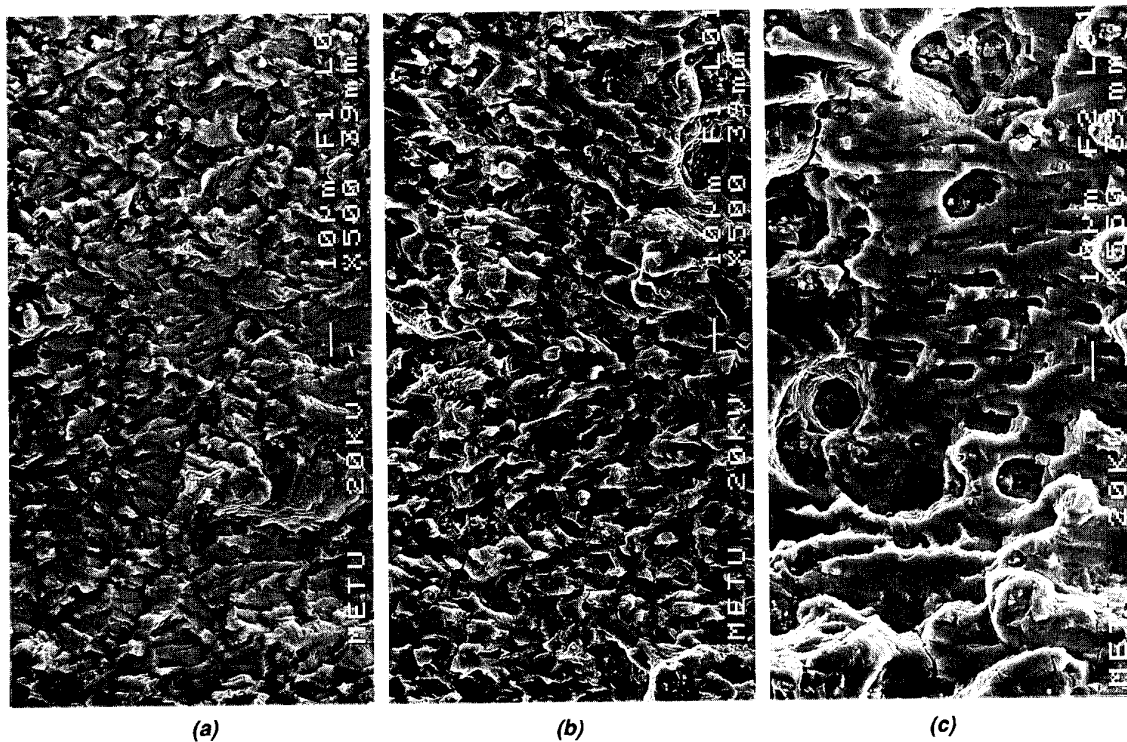


Figure 12. Scanning electron microfractographs of alloy 2090 (in T-L orientation) aged at 165°C for 20 Hr; (a) Fracture surfaces at low (7.4 $\text{MPa}\sqrt{\text{m}}$), (b) intermediate (11.3 $\text{MPa}\sqrt{\text{m}}$), and (c) high (15.0 $\text{MPa}\sqrt{\text{m}}$) values of ΔK .

CORROSION OF LANDING GEAR STEELS

E. U. Lee
J. Kozol
J. B. Boodey
J. Waldman
Naval Air Warfare Center
Aircraft Division Warminster
Warminster, PA 18974, USA

SUMMARY

A study was conducted on the corrosion behavior of landing gear steels, AerMet 100, 300M, AF1410, HYTUF and 4340. This study included investigations of stress corrosion cracking and immersion corrosion in an aqueous 3.5% NaCl solution, salt spray corrosion in a fog chamber of atomized aqueous 5% NaCl solution, humidity corrosion in an atmosphere of vapor from distilled water and hydrogen embrittlement.

AF1410 steel is most resistant to stress corrosion cracking, and it is followed by AerMet 100, 0.20C AF1410, HYTUF, 300M and 4340 steels. The immersion corrosion and salt spray corrosion rates of an AerMet 100 steel are 33-40% and 13-20% those of a 300M steel. In a humidity chamber, AerMet 100 steel is not corrodible in 110 days, whereas 300M steel is quite susceptible to humidity corrosion. Compared to 300M steel, AerMet 100 steel is less susceptible to hydrogen embrittlement.

LIST OF SYMBOLS

a	crack length
B	specimen thickness
D	deflection of specimen arms at load line in DCB specimen
E	modulus of elasticity
H	half-width of DCB specimen
K _I	mode I stress intensity factor
K _{IC}	plane strain fracture toughness
K _{ISCC}	threshold stress intensity for stress corrosion cracking
L	depth of single edge notched cantilever bend type specimen
M	bending moment
t	time

INTRODUCTION

Ultra-high strength steels are the materials of choice for highly loaded structural components with volume restriction in US Navy aircraft. Examples of such

components are landing gear, catapult and arresting structure, wing attach fitting and horizontal stabilator spindle. In the past, landing gear was made from low alloy steels with tensile strength above 260 ksi (1793 MPa), such as 4340 and 300M. However, service failures due to low fracture toughness and poor resistance to corrosion and hydrogen embrittlement led to the prohibition of their use in new designs. Alternatives are more damage tolerant steels, such as HYTUF and AF1410 and its higher strength derivatives. The higher strength derivatives of AF1410 are 0.20C modified AF1410 and AerMet 100.

AerMet 100 steel has a better combination of high fracture toughness (exceeding 110 ksi*in^{1/2}) and high tensile strength (280-300 ksi) than 0.20C modified AF1410. Consequently, it has a greater potential for application to landing gear and other fracture critical components. However, its corrosion behavior was not been fully understood. A study was initiated to characterize the corrosion behavior of AerMet 100 and the other landing gear steels. The characterization efforts included clarification of stress corrosion cracking, immersion corrosion, humidity corrosion, salt spray corrosion and hydrogen embrittlement. The results are reported in this paper.

EXPERIMENTAL PROCEDURE

1. Materials

AF1410, 0.20C AF1410, AerMet 100, HYTUF, 4340, and 300M steels were employed in this study. Their chemical compositions are shown in Table 1. These steels were subjected to heat treatments, consisting of austenitizing, quenching to martensitic condition, and then tempering (for low alloy steels) or refrigerating and aging to provide hardening from formation of various metallic (M₂C) carbides (for Co-Ni steels). The heat treatments are described in Table 2.

2. Specimens

Double cantilever beam (DCB) and single-edge notched cantilever bend (SENCB) specimens were used for the stress corrosion tests. The immersion corrosion, humidity corrosion, and salt spray corrosion tests were conducted with square sheet specimens. The hydrogen embrittlement

susceptibility was evaluated with round tensile specimens. The specimens are shown in Fig. 1.

3. Tests

a. Stress Corrosion Cracking Test

The stress corrosion cracking test was performed employing two different methods, one with a double cantilever beam (DCB) specimen and the other with a single-edge notched cantilever bend (SENCB) specimen. The method with a DCB specimen introduces a constant crack opening displacement with stress intensity decreasing for increasing crack length. The threshold stress intensity for stress corrosion cracking, K_{ISCC} , is defined as the stress intensity at crack arrest. The method with a SENCB specimen introduces a constant bending moment with stress intensity increasing with increasing crack length. The K_{ISCC} is defined as the stress intensity of no failure in an arbitrarily selected test period, e. g., 1000 or 10000 hours.

DCB specimens of AerMet 100 and 300M steels were precracked by tension-tension fatigue loading. The precrack length was approximately 0.068 in. beyond the notch. Subsequently the specimen was bolt loaded. The load was provided by opposing bolts inserted across the notch with a steel ball between the bolts, which gives uniform loading. The specimens were continuously immersed in an aqueous 3.5% NaCl solution at room temperature. They were removed from the solution at periodic intervals and crack lengths were measured visually on each surface with a traveling optical microscope. The crack length versus time data was used to determine the crack growth rate, da/dt. The stress intensity, K_I , was determined for each measured crack length, employing the following equation.

$$K_I = (EL/L^3)^{1/2} / [4\sqrt{H} \{ (a/H) + 0.673 \}^2]$$

where

- E : modulus of elasticity
- H : half-width of the specimen
- L : deflection of specimen arms at the load line
- a : crack length, defined as the distance from the center of the loading bolts to the crack tip

SENCB specimens of AerMet 100, 300M, AF1410, 0.2C AF1410, HYTUF, and 4340 steels were fatigue precracked in three point bending. The precrack depth was approximately 0.050 inch (1.3 mm) below the notch tip. The precracked portion of each specimen was encased in a polyethylene cell, which was then filled with an aqueous 3.5% NaCl solution. The specimen was dead weight loaded in cantilever bending, and time to fracture was recorded in accordance with a method developed by B. F. Brown.

(Ref 1). The aqueous 3.5% NaCl solution was changed weekly during the test. After failure, notch-plus-crack lengths were measured at mid- and quarter-thicknesses and averaged for entry into the stress intensity calculation. Applied stress intensity, K_I , was calculated from a formula developed by Kies et al (Ref 2):

$$K_I = [4.12M \sqrt{(1/\alpha) - \alpha^3}] / BD^{3/2}$$

where

- α : $1 - a/D$
- M : applied bending moment
- B : specimen thickness
- a : crack length, defined as the notch length plus the crack depth
- D : specimen depth

b. Immersion, Humidity, Salt Spray Corrosion Tests

Prior to environmental exposure, the dimension of each square sheet specimen of AerMet 100 and 300M steels was measured to permit accurate calculation of the exposed area, and weighed. Subsequently specimens were suspended in an aqueous 3.5% NaCl solution at room temperature for the immersion corrosion test, in a humidity chamber of 100% relative humidity and 120°F for the humidity corrosion test, and in a fog chamber of atomized aqueous 5% NaCl solution and 95°F for the salt spray corrosion test, respectively. Specimens were removed from the respective corrosive environments after each of the preset exposure periods. The exposure periods were 10 - 101 days for the immersion corrosion test, 110 days for the humidity corrosion test, and 17 - 209 hours for the salt spray corrosion test. Specimens were cleaned in a solution of 1000 ml hydrochloric acid, 20 g antimony trioxide, and 50 g stannous chloride to remove corrosion products, dried and weighed. From the weight loss and the exposure period, the corrosion rate was determined.

c. Hydrogen Embrittlement Test

The specimens of AerMet 100 and 300M steels were electrochemically charged at 5 mA/cm² for 24 hours in 0.2M NaOH + 0.2M NaCN prior to testing. Subsequently, they were bright cadmium plated to a thickness of 0.3 mil to prevent egress of hydrogen. Tensile tests were conducted at strain rates of 1x10⁻³, 5x10⁻⁵, and 1x10⁻⁶ in/in/sec. The hydrogen embrittlement susceptibility was measured by losses in ultimate tensile and yield strengths, percent elongation and percent reduction in area. Fractographic comparisons were made between as-received and hydrogen-charged specimens to determine changes in failure mechanisms.

d. Metallographic and Fractographic Examination

Metallographic specimens were prepared by standard techniques, and were examined via optical microscopy. The fracture modes of stress corrosion cracking and hydrogen embrittlement were determined via scanning electron microscopic examination of the fracture surfaces.

RESULTS AND DISCUSSION

1. Stress Corrosion Cracking

a. DCB Specimen Test

The variation of crack length with time of exposure to an aqueous 3.5% NaCl solution is shown for AerMet 100 steel specimens of L-R and C-L orientations and a 300M steel specimen of T-L orientation in Fig. 2. The initial crack growth and the final crack length are much greater in the 300M steel than in the AerMet 100 steel, indicating better SCC resistance of the AerMet 100 steel. In the AerMet 100 steel, the crack plane orientation, L-R or C-L, results in little difference in the crack growth behavior, except an incubation period prior to the initial crack growth in the C-L orientation.

The plots of crack growth rate, da/dt , vs. stress intensity, K_I , are presented for the aforementioned specimens in Fig. 3. The values of SCC threshold stress intensity, K_{ISCC} , are determined to be 33 and 19 $\text{ksi}\cdot\text{in}^{1/2}$ for the AerMet 100 and 300M steels, respectively. Furthermore, the crack growth rate is much greater for a given stress intensity in the 300M steel than in the AerMet 100 steel. A comparison in terms of K_{ISCC} and da/dt shows that the SCC resistance of the AerMet 100 steel is superior to that of the 300M steel in an aqueous 3.5% NaCl solution. Previously, a lower value of K_{ISCC} , 21 $\text{ksi}\cdot\text{in}^{1/2}$, was reported by Atrens (Ref 3) for an AerMet 100 steel tested in a 3.5% NaCl solution. Prior to the SCC test, the steel was solution treated at 1625°F, air cooled, refrigerated at -108°F, aged at 900°F and air cooled.

During fatigue precracking in air, the crack grew straight from the notch tip in the longitudinal direction of the DCB specimens of both AerMet 100 and 300M steels. However, in the AerMet 100 steel, as soon as a specimen was dipped in an aqueous 3.5% NaCl solution and stress corrosion cracking started, the crack deviated in the transverse direction of the specimen, Fig. 4(a). The crack deviation occurred in both smooth-faced and side-grooved specimens. The side groove had a depth of 10% of the specimen thickness but could not stop the crack deviation. Crack deviation was also observable during the later stage of SCC growth in the 300M steel, Fig. 4(b). Optical microscopy examinations of a cross-section of the crack revealed that the crack deviated along nearly parallel light and dark alternating bands, Fig. 5. These bands, exposed by

overetching the metallographic specimen, are here referred as "ghost bands," and are known to result from micro segregation of alloying elements in the original ingot (Refs 4 and 5). Working of the ingot accounts for the banding orientation in the deformation direction (Refs 4 and 5). A greater portion of the crack appears to align with the darker bands. Olson et al (Ref 6) also observed similar bands in ESR 4340 steel forgings and association of the brittle behavior with regions of intergranular fracture aligned with the banding. An electron microprobe analysis of ghost bands shows lower amounts of Cr, Ni and Mo in the dark band than in the light band, as shown in Table 3. The SEM fractographic features of a crack surface in a DCB specimen indicate that the SCC mode is predominantly intergranular cracking, Fig. 6.

b. SENCB Specimen Test

The combined results of SENCB specimen tests, variations of stress intensity K_I with time to failure and K_{ISCC} values, are shown in Fig. 7 and Table 4. Among the steels tested, the AF1410 steel has the best SCC resistance. However, the carbon content increases from 0.15 to 0.20% in the 0.20C AF1410 results in a decreased SCC resistance. The AerMet 100 steel, a high strength derivative of AF1410, shows a SCC resistance comparable to the 0.20C version of AF1410. The 300M steel, commonly used in landing gear applications in the past, shows poorer SCC resistance, even at 10,000 hours. Evidence of a slight anisotropy is seen in the behavior of HYTUF steel between specimens oriented in the LT and TL directions. As shown in Table 4, the K_{ISCC} values are less in the TL direction than in the LT direction. This effect is not apparent in the AF1410 steel. The difference in anisotropy may reflect the difference in cleanliness of the steels, associated with melting practice. The HYTUF steel was air melted plus vacuum arc melted, the 4340 electroslog remelted (ESR), and the other steels vacuum induction melted plus vacuum arc remelted.

2. Immersion and Humidity Corrosion

The variation of immersion corrosion rate with time of exposure in an aqueous 3.5% NaCl solution is shown for the AerMet 100 and 300M steels in Fig. 8. The corrosion rates are expressed by the reduction rates of specimen size and weight. The immersion corrosion rate of the AerMet 100 steel is 33 - 40% that of the 300M steel. This indicates that the AerMet 100 steel has better resistance to immersion corrosion than the 300M steel. The immersion corrosion rate is greatest at the initial stage of corrosion and it decreases with exposure time for both steels.

In a humidity chamber of 100% relative humidity and 120°F, the AerMet 100 steel specimens did not show any measurable corrosion in 110 days. On the other

hand, the 300M steel specimens showed noticeable corrosion with size reduction rate of 2.0413 mills per year (mpy) and weight reduction rate of 0.0447 milligrams per square decimetre per day (mdd).

3. Salt Spray Corrosion

The variations of corrosion rate with exposure time in a salt spray chamber of atomized aqueous 5% NaCl solution are shown for the AerMet 100 and 300M steels in Fig. 9. The salt spray corrosion rate of the AerMet 100 steel is 13-20% that of the 300M steel. As for immersion corrosion, the corrosion rate is greatest at the beginning of the exposure and it decreases with time.

4. Hydrogen Embrittlement

The mechanical properties of hydrogen-charged and uncharged AerMet 100 and 300M steels are presented in Table 5. In the uncharged steels, the mechanical properties did not vary significantly with strain rate. The starting ultimate tensile strength of the 300M steel was high and the ductility was unusually low. The AerMet 100 steel exhibited excellent strength and ductility. The 24 hour electrochemical charging deteriorated the mechanical properties of both steels. The ductility and strength of the 300M steel dropped off rapidly even at the highest strain rate. At the lowest strain rate, no ductility remained, and the yield and ultimate tensile strengths are reported as the fracture strength. The AerMet 100 steel did lose a great amount of its starting ductility with the hydrogen-charge. Its strength did not significantly decrease with decreasing strain rate.

The fractographic examination revealed an intergranular fracture initiation site for the hydrogen-charged 300M steel. On the other hand, the AerMet 100 steel did not exhibit any intergranular fracture. However, its fracture surface morphology became more brittle in appearance, and indicated that the specimen was not completely saturated with hydrogen. A uniform region, approximately 1/3 of the radius deep, was observed to be more embrittled than the remainder of the fracture surface at the two slower strain rates. This indicates that the diffusivity of hydrogen in AerMet 100 steel is smaller than in 300M steel.

CONCLUSIONS

1. With DCB specimens in an aqueous 3.5% NaCl solution, the K_{ISCC} values of the AerMet 100 and 300M steels are determined to be 33 and 19 ksi*in^{1/2}, respectively. In the AerMet 100 steel, the stress corrosion crack grows along an intergranular path in the direction of forging deformation.
2. With SENCB specimens in an aqueous 3.5% NaCl solution, the AF1410 steel exhibits the highest SCC

resistance, and it is followed by AerMet 100, 0.20C AF1410, HYTUF, 300M and 4340 steels.

3. The immersion corrosion and salt spray corrosion rates of the AerMet 100 steel are 33-40% and 13-20% those of the 300M steel, respectively.
4. In a humidity chamber, the AerMet 100 steel is not corrodible within the employed test period 110 days. But the 300M steel is susceptible to corrosion, and its rate is 2.0413 mpy or 0.0447 mdd.
5. The resistance of AerMet 100 steel to hydrogen embrittlement is superior to that of 300M steel.

REFERENCES

1. Brown, W. F., "A New Stress Corrosion Cracking Test for High Strength Alloys," Materials Research and Standards, 6, 1966, pp. 129-133.
2. Kies, J. A., Smith, H. L., Romine, H. E., and Bernstein, H., "Fracture Testing of Weldments," Fracture Toughness Testing and Its Applications, ASTM STP 381, Philadelphia, PA, American Society for Testing and Materials, 1965, PP. 328-356.
3. Andej Atrens: Private Communication
4. Rostoker, W. and Dvorak, J. R., "Interpretation of Metallographic Structures," New York, N. Y., Academic Press, 1965, p. 17.
5. Pokorny, A. and J., "Solidification and Deformation of Steels, Metallographic Atlas of Iron, Steels and Cast Irons," III, Philadelphia, PA, W. B. Saunders Co., 1967, pp. 50-55.
6. Olson, G. B., Anctil, A. A., DeSisto, T. S., and Kula, E. B., "Anisotropic Embrittlement in High-Hardness ESR 4340 Steel Forgings," Met Trans A, 14A, 8, Aug. 1983, pp. 1661-1669.

Table 1. Chemical Compositions of Specimen Steels (wt %)

Steel	C	Ni	Co	Cr	Mo	Mn	Si
AF1410	0.15	10.21	14.18	2.08	0.98	0.03	0.01
0.20C	0.20	10.17	14.31	2.04	1.03	<.01	<.01
AF1410							
AerMet 100	0.24	11.26	13.4	3.11	1.15	0.01	<.01
HYTUF	0.26	1.76	-	0.38	0.38	1.36	1.49
4340	0.40	1.8	-	0.80	0.25	0.75	0.25
300M	0.40	1.8	-	0.85	0.4	0.7	1.6

Table 2. Heat Treatment Conditions

Steel	Austenitize	Quench	Temper, Age	Hardness (R _c)
(For DCB Specimen Test and Hydrogen Embrittlement Tests)				
AerMet 100	1600F	OQ, -320F, 1Hr	900F, 5Hr, AC	51-53
300M	1600F	OQ	575F, 4Hr	51-53
			Double Temper	
(For SENCB Specimen Test)				
AF1410	1530F	OQ, -100F, 1Hr	950F, 5Hr, AC	46-49
0.20C	1550F	OQ, -100F, 1Hr	900F, 5Hr, AC	52-53
AF1410				
AerMet 100	1600F	OQ, -100F, 1Hr	900F, 5Hr, AC	51-53
HYTUF	1600F	OQ	550F, 2Hr	45-46
			535F, 2Hr	
4340	1500F	OQ	500F, 2Hr	50-53
			Double Temper	
300M	1600F	OQ	575F, 4Hr	51-53
			Double Temper	

Table 3. Chemical Composition of Ghost Bands (wt %)

	Cr	Ni	Mo	Co
		Light Band		
	3.17	12.27	1.70	13.90
		Dark Band		
	2.86	11.44	1.37	13.90
(Light - Dark) = 0.31	0.31	0.83	0.33	0.00

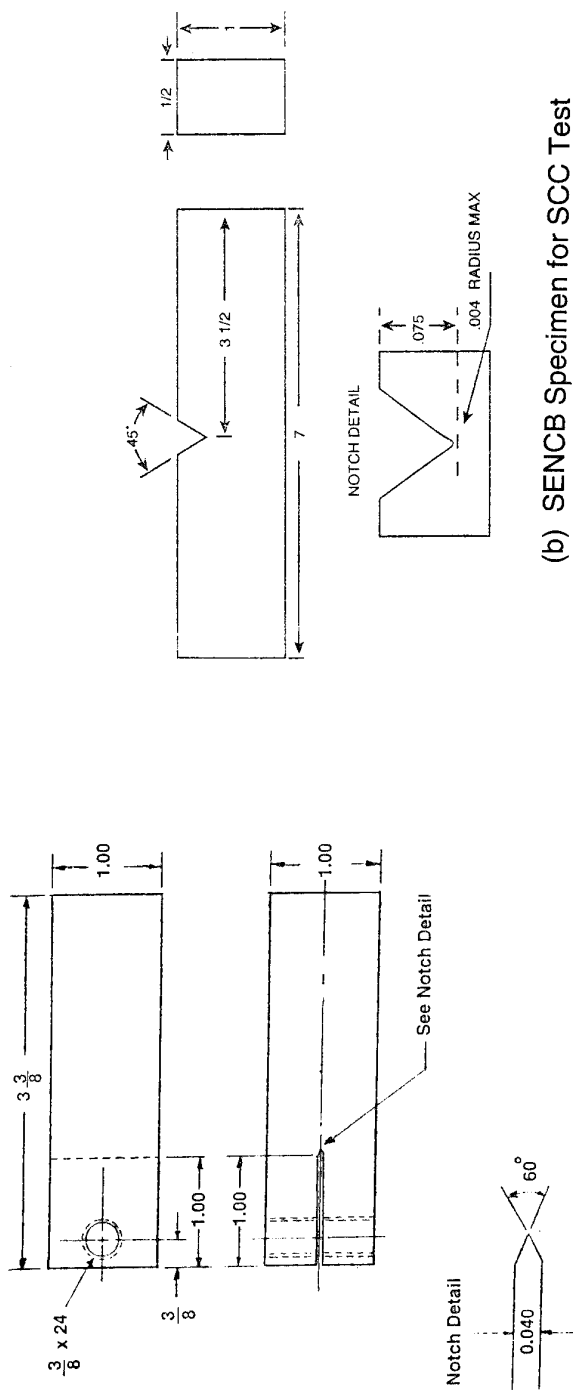
Table 4. Threshold Stress Intensity for Stress Corrosion Cracking, K_{ISCC}, Determined by SENCB Specimen Test

Steel	K _{ISCC} , ksi*in ^{1/2} (MPa*M ^{1/2})	
	1000 Hrs	10000 Hrs
AF1410	55 (60)	40-45 (44-49)
0.20C AF1410	25 (27)	16-20 (18-22)
AerMet 100	30 (33)	15-22 (16-22)
HYTUF LT	25 (27)	15-20 (16-22)
HYTUF TL	19 (21)	<15 (<16)
300M	15-18 (16-20)	11-14 (12-15)
4340	10 (11)	<9 (<10)

Table 5. Mechanical Properties of Hydrogen-Charged and Uncharged AerMet 100 and 300M Steels

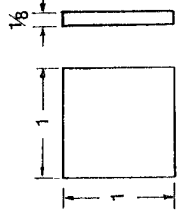
Material Condition	%Elong	%RA	YS(ksi)	UTS(ksi)
300M				
Uncharged				
All Strain Rates	2.15	2.95	240	320
Hydrogen-Charged				
1x10 ⁻³ in/in/sec	0.37	0.39	240	250
3x10 ⁻⁵ in/in/sec	0.14	0.00	180	213
1x10 ⁻⁶ in/in/sec	0.00	0.00	170*	170*
AerMet 100				
Uncharged				
All Strain Rates	11.0	64.5	254	280
Hydrogen-Charged				
1x10 ⁻³ in/in/sec	2.80	7.55	260	280
3x10 ⁻⁵ in/in/sec	1.50	6.81	254	265
1x10 ⁻⁶ in/in/sec	1.15	3.17	217	223

* Yield Strength and Ultimate Tensile Strength Equal Fracture Strength

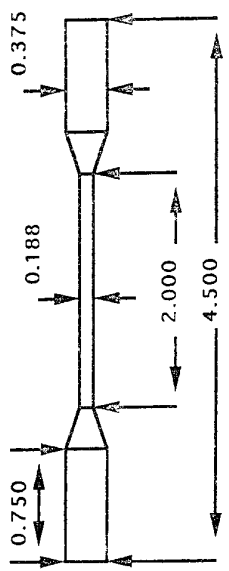


(a) DCB Specimen for SCC Test

(b) SENCB Specimen for SCC Test



(c) Square Sheet Specimen for Immersion and Salt Spray Corrosion Tests



(d) Tensile Specimen for Hydrogen Embrittlement Test

Figure 1. Specimen

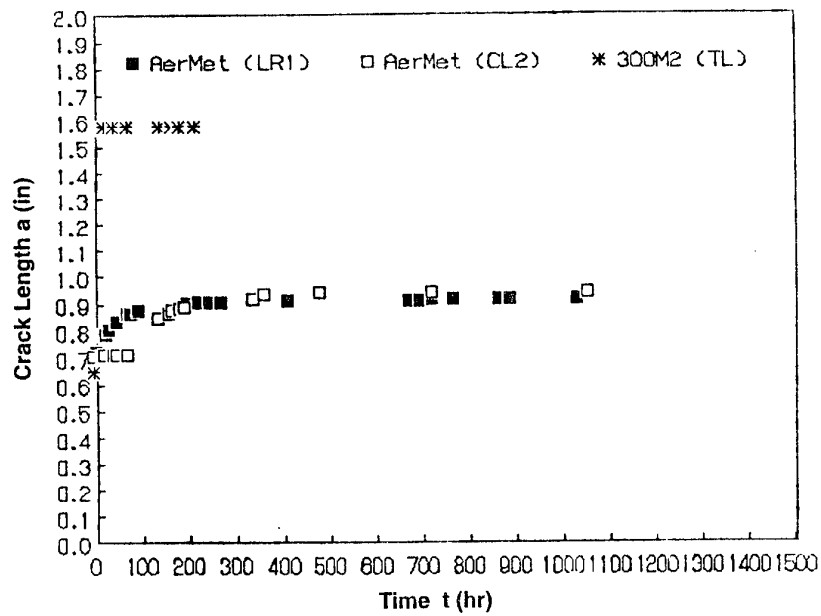


Figure 2. Stress Corrosion Crack Growth during DCB Specimen Test

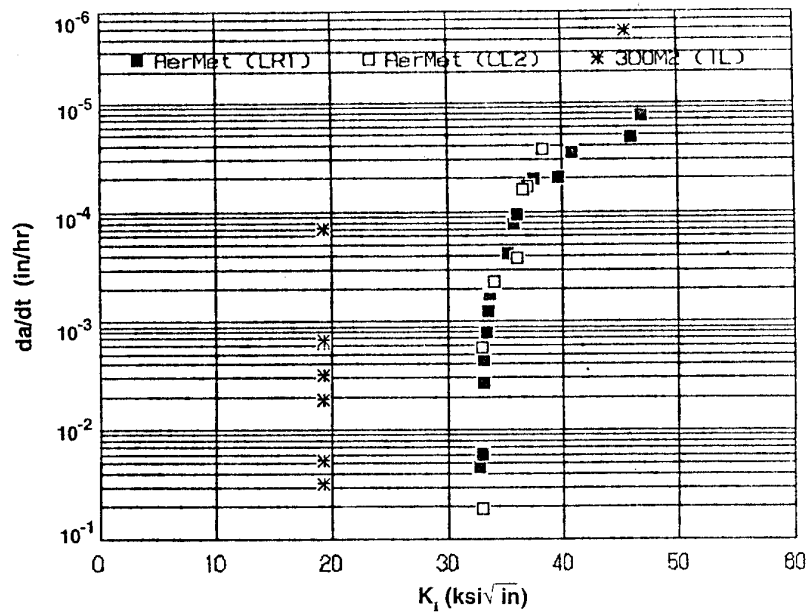
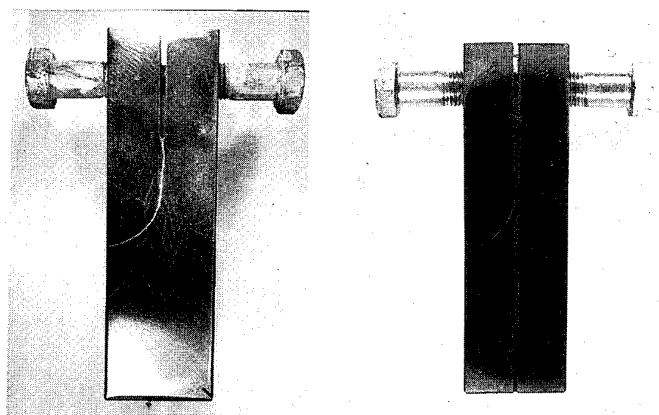


Figure 3. Variation of Stress Corrosion Crack Growth Rate da/dt with Stress Intensity K_I during DCB Specimen Test



(a) AerMet 100 Steel



(b) 300M Steel

Figure 4. Crack at Surface of Fatigue Precracked and SCC Tested DCB Specimen

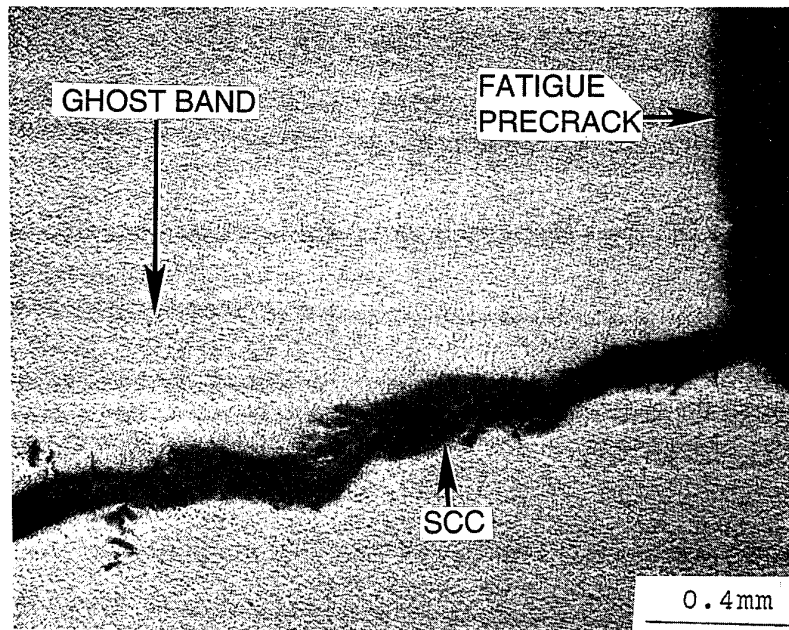


Figure 5. Ghost Bands, Fatigue Precrack and Stress Corrosion Crack in AerMet 100 Steel

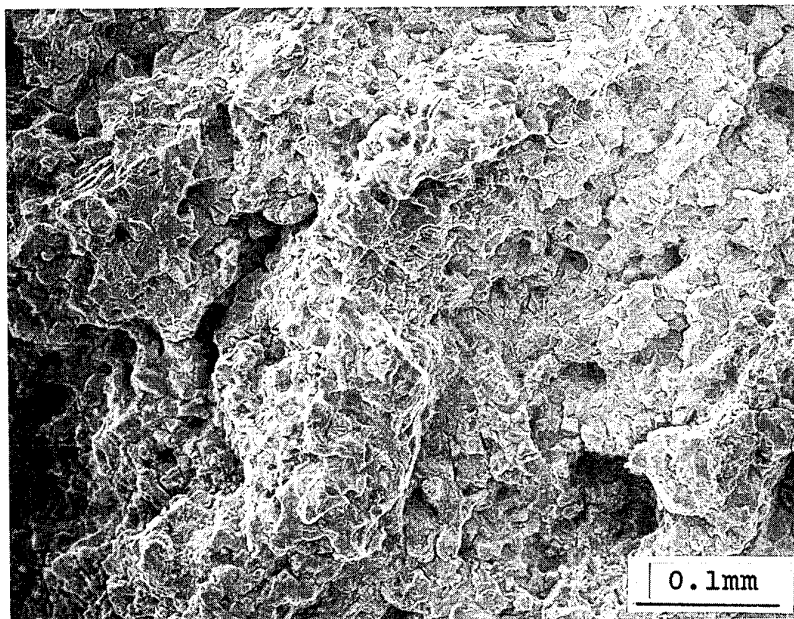


Figure 6. SEM Fractograph of DCB Specimen of AerMet 100 Steel

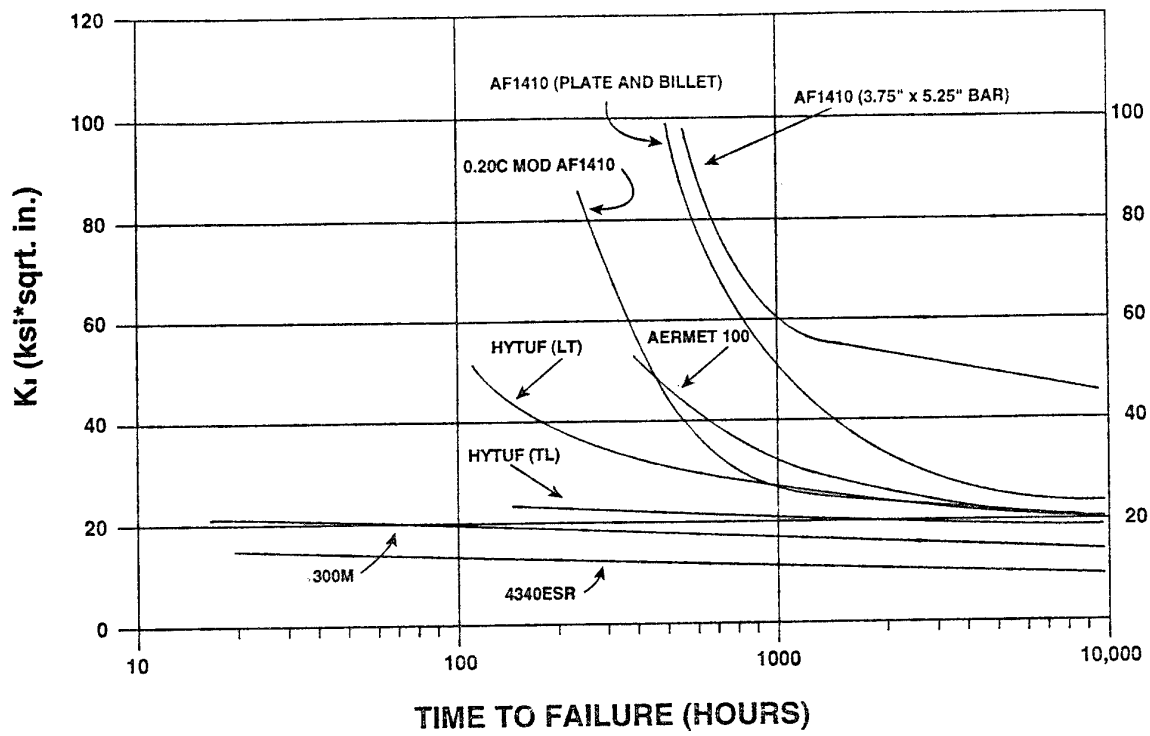
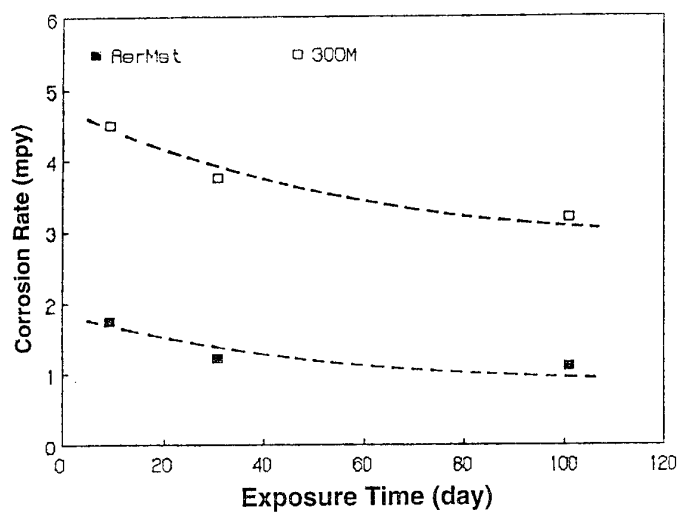
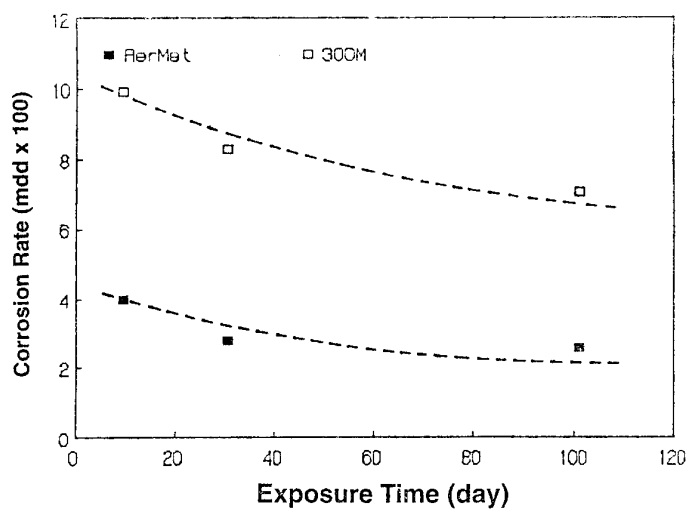


Figure 7. Combined Results of SENC B Specimen Tests



(a)



(b)

Figure 8. Immersion Corrosion Rates of AerMet 100 Steel and 300 Steels**(a) Size Reduction Rate****(b) Weight Reduction Rate****(mpy: mils per year, mdd: milligrams per square decimetre per day)**

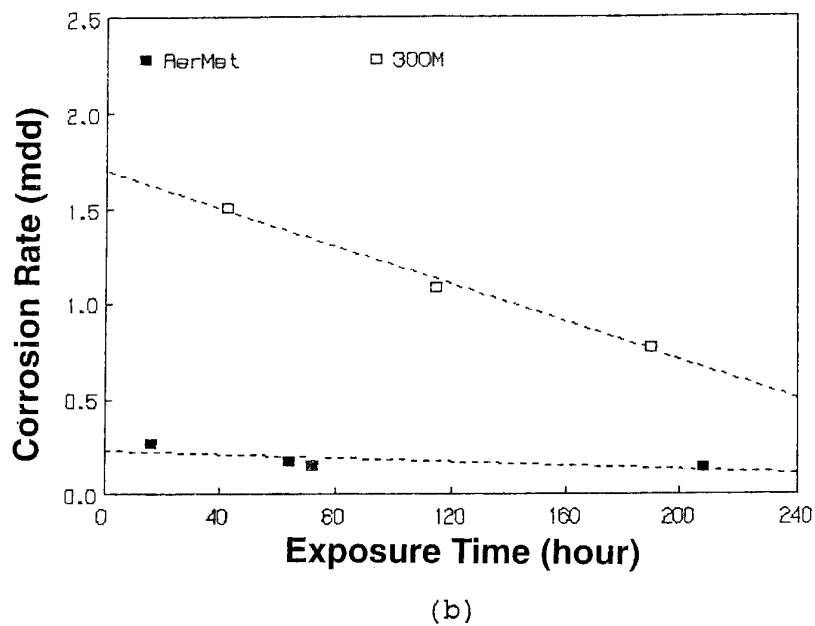
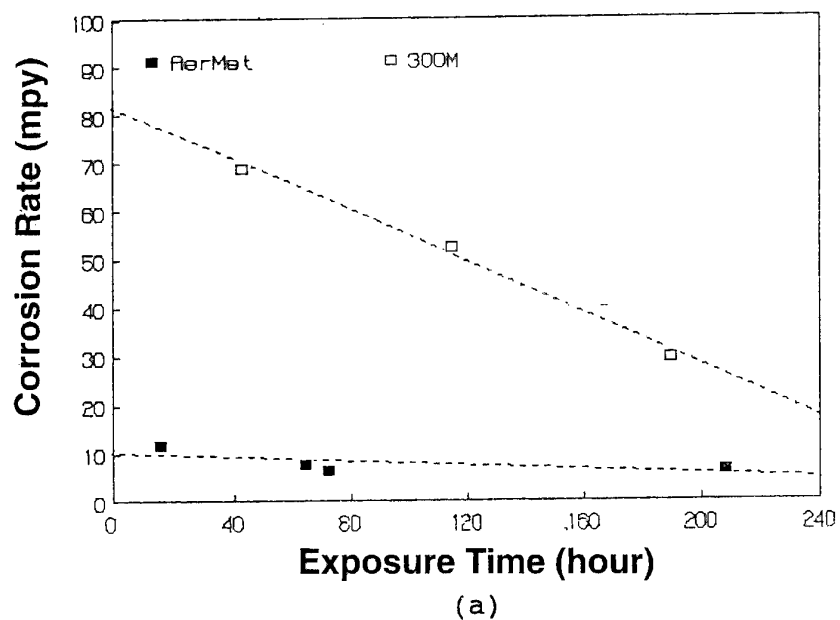


Figure 9. Salt Spray Corrosion Rates of AerMet 100 and 300M Steel
(a) Size Reduction Rate
(b) Weight Reduction Rate

Specific Features of Corrosion Behavior of Stainless Maraging Steels for Aerospace Application

V.B.Spiridonov and V.V.Sharapov

KOMPOZIT Corp.

4, ulitsa Pionerskaya

141070 Kaliningrad, Moscow Region, Russia

SUMMARY

Specific features of the embrittlement of stainless Cr-Ni maraging steels by environmental or N_2O_4 media are considered by the example of steel 03Kh11N10M2TU-VD. Results of corrosion tests and fractographic and microanalytical investigations are presented. The method of accelerated testing of these steels for stress corrosion cracking is described.

1. INVESTIGATED MATERIALS

The term "maraging" means that these steels gain the final strength by the transformation of austenite to martensite followed by aging of the martensite matrix. Alloying of solid solution also slightly contributes to the strength.

Nowadays a number of compositions are used in fabricating maragings. Particularly, maragings with useful strength up to 2000 MPa based on the composition 18Ni - 9Co - 5Mo - Ti are popular. However, chromiumless maragings are susceptible to the general corrosion that set limits on their application in the aerospace industry. The resistance to corrosion may be abruptly increased by chromium alloying. Steels with 10-12% of chromium and 8-10% of nickel have a sufficient corrosion resistance both in industrial environment and in aggressive media. Maragings based on the composition 0.03C - 11Cr - 10Ni - 2Mo - Ti are widely used and well studied in Russia. The chemical composition of the steel 03Kh11N10M2TU-VD (EP678U-VD) is presented in Table 1.

The hardening effect in this steel is due to precipitation of ϵ -Fe₃Ti phase with hcp structure. The aging of this steel at 540°C for 3 hours (overaging heat-treatment) allows one to reach strength level of 1400-

1500 MPa along with high plasticity (ultimate elongation of 11-15%), ductility (impact toughness at room temperature of 0.85 MJ/m²) and the resistance to crack growth (impact toughness of a precracked specimen at room temperature of 0.5 MJ/m²).

Practical applicability of maragings is limited to a great extent by their susceptibility to the environmental embrittlement. A simple dependence of susceptibility to the environmental embrittlement on aging temperature is shown in Fig.1. This dependence is not often taking into account by producers, although is seen that equal tensile properties obtained by under- and overaging do not guarantee equal serviceability of

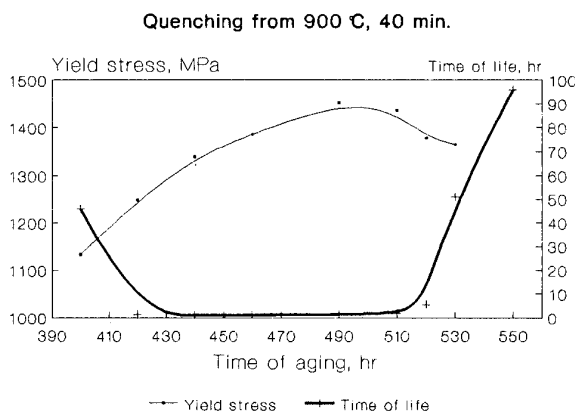


Fig.1

Dependences of yield strength and lifetime under accelerated SCC testing on aging temperature.

Table 1

Chemical Composition (Main Alloying Elements) of Investigated Steels

Steel	Concentrations of Main Alloying Elements, Mass %						Class of Steel
	C	Cr	Ni	Mo	Ti	Others	
03Kh11N10M2T	< 0.03	9.5-10.5	10.5-11.5	2.0-3.0	0.8-1.2	0.15-0.35 Al	Maraging
03Kh11N8M2F	<0.03	11-12	8.3-8.6	2.3-2.8	-	0.05-0.3 V	Martensitic, weakly aging

these steels in marine medium, hydrogen, etc.

The main reason for increasing susceptibility to the environmental embrittlement for underaging and peak hardening treatments is the appearance of large internal stresses, especially, at grain boundaries due to martensite transformation and formation of precipitates. According to indirect data, the values of these stresses may almost approach the yield strength of the steel. Chemical compositions of grain boundaries and adjacent volumes seem to have no significant effect on the resistance to the embrittlement of Cr-Ni maragings. It is known that many processes of the intergranular embrittlement are related to grain boundary segregations. We did not reveal grain boundary segregations of any impurities or alloying elements in steels of this type. The absence of impurity segregations is caused by the presence of molybdenum in solid solution and the presence of titanium which may be considered as a strong internal getter actively bounding nitrogen, sulfur, oxygen, and phosphorus in the compounds.

2. CORRELATION BETWEEN STRESS CORROSION CRACKING (SCC), HYDROGEN EMBRITTLEMENT (HE), AND PITTING FORMATION (PF)

Modern theoretical and experimental possibilities do not allow determination of all features of the HE mechanism for high-strength steels. We can only flatly assert that mechanisms assumed for carbon low-alloyed steels attributed to the formation of molecular hydrogen on collectors, formation of methane bubbles, etc. are invalid for high-strength steels.

In our opinion, SCC of high-strength steels in water-containing media is the particular case of HE. Only the source of hydrogen is replaced. Of course, it is necessary to take into account that different sources support, respectively, different parameters of hydrogen charging. These are the form of introducing hydrogen (H , H_2 , H^+), paths and mechanisms of hydrogen permeation, etc. In final score, these distinctions affect the fracture processes that is corroborated by fractographical data. For example, we observed that in many cases of electrochemical hydrogen charging cracks propagated along the boundaries of martensite colonies but in gaseous hydrogen-containing media at the same structural state of the steel cracks propagated along the primary austenite boundaries.

According to the hypothesis proposed, at the first stage of SCC of high-strength steels the hydrogen is generated in pits during PF. In addition, these pits and microcracks initiated near pits double as mechanical notches. Higher hydrogen content near pits together with stress concentration hear sharp notches activate the crack propagation according to the HE mechanism. Using these approaches, we developed an accelerated

method for testing maragings for SCC resistance [1]. According to this method, the steel plate measuring the size of 110 mm x 22 mm is loaded by bending and, at the first stage, undergone anode polarization in 3% NaCl water solution for about 30 min. with current density of 10 mA/cm² to activate PF. At the second stage, cathode polarization with the same current density is used to activate the HE effects. The second stage lasted during a given base time or ended with the failure of the specimen.

The good correlation between the results of accelerated and long-term testings not only shorten the durations of corrosion tests to 1-2 days (specimens with this lifetime are considered as unsusceptible to SCC) but proved the validity of theoretical approaches used in consideration. This method is successfully used by a number of rocket-space institutes and plants in Russia.

At the same time, it should be noted that the efforts to use this method for high-strength austenitic-martensitic steel 0.07C - 16Cr - 6Ni have failed. The reasons for this difference in the corrosion behavior may consist both in the different distinctive features of SCC mechanisms of steels of even closed strength levels and in pure quantitative distinctions, for example, in the rate of the transport of hydrogen necessary for the crack growth.

The importance of the PF stage estimated in the course of the development of the accelerated method forced us to investigate this phenomenon thoroughly.

According to Manning [2] and some other authors, the main sites of PF in the steels containing manganese sulfides are interfaces MnS/matrix and, according to [3], "PF in stainless steels is possible only near non-metal inclusions".

Chromium-nickel maragings of high purity have no MnS inclusions. The main nonmetal inclusions are titanium carbides, nitrides and carbonitrides, and titanium sulfides and oxysulfides.

The following method was used to estimate the sites of preferential PF in the steel 03Kh11N10M2TU-VD in SCC conditions. Plates of the size of 110 mm x 22 mm with mechanically polished tested (tensile) surface were loaded by bending and during few minutes undergone anode polarization in 3% NaCl water solution. Then the specimens were extracted from the solution, rinsed by water and ethanol, and their tested surface was observed by light and scanning electron microscopes. This cycle was repeated several times for each specimen.

The data below were obtained regardless the concentration of nonmetal inclusions in the metal charges:

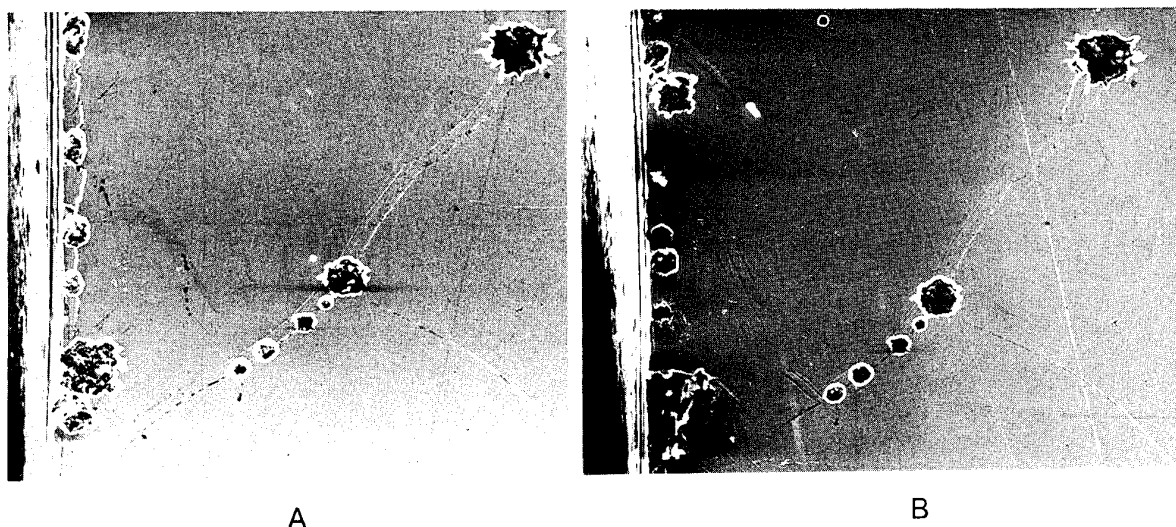


Fig.2

Scanning electron micrographs of the specimen surface after anode polarization with mechanical loading, x150.

A - after 30 min of testing;

B - after 65 min of testing, new pits are shown by arrows.

- as a rule, nonmetal inclusions are not the sites of PF;

- in most cases pits initiate at fresh scratches and at specimen edges;

- "old" pits do not increase during subsequent cycles of testing, only new pits appear that is clearly seen in Fig.2.

These results are in good agreement with known data for aluminum alloys. To a certain extent, they can explain the effects of so called probabilistic nature of PF [4] and the great scatter of lifetimes at SCC observed in practice because the key item of PF and subsequent failure is the occasional appearance of the nonpassivated mechanical defect or the deterioration of protective oxide film.

3. EMBRITTLEMENT OF STAINLESS STEELS BY NITROGEN TETROXIDE (NTO) AT MODERATE TEMPERATURES AND PRESSURES

It is considered that stainless steels are not susceptible to some types of local corrosion in NTO at moderate (20-70°C) temperatures and pressures [5]. However, we established that under these conditions steels may be damaged by a specific type of corrosion for which we proposed a name "intergranular oxidizing embrittlement (IOE)". This type of corrosion results both in the crack formation and embrittlement of the subsurface layer (about several hundreds micrometers

thick). The maraging 03Kh11N10M2T and martensitic steel with weak effect of aging 03Kh11N8M2F (see Table 1) are especially susceptible to this type of corrosion.

Investigations of a number of specimens of these steels and their weld joints showed that cracks initiated during the contact with NTO in the sites of maximum stresses, including stresses introduced by active loading, residual welding stresses, internal stresses due to structural transformations in the main metal, etc. The "lashes-like" cracks are the most typical example of the cracks initiated by welding stresses (Fig.3).

Loading by bending or impact bending in air or vacuum of the specimens contacted for a long time with NTO results in the formation of the subsurface cracks. The cracks appear in the site of application of the bending load (Fig.3). The intensity of crack formation and depths of the cracks correlates with susceptibility of the specimen to cracking in NTO. The maximum depth of such cracks was 0.9 mm. We named the cracks formed in NTO as the cracks of Type 1 and those formed in air or vacuum as the cracks of Type 2.

The complex microanalytical investigation of tested in NTO specimen was carried out by means of scanning electron microscopy, X-ray microanalysis, Auger-electron microscopy, X-ray photoelectron

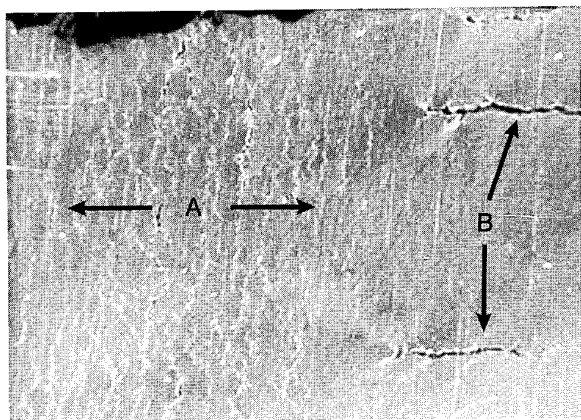


Fig 3

Surface of the thermally-affected zone of EP678 weld joint after contact with NTO during 450 days and following impact bending in air. Scanning electron microscopy. x14.

A - area of cracks of Type 2, directions of tensile stresses under the impact are shown by white arrows;

B - opened "lashes-like" cracks of Type 1.

spectroscopy, and secondary ion mass-spectroscopy to determine the reasons for the steel embrittlement in NTO.

A schematic representation of the IOE mechanism suggested is shown in Fig.4. It is based on the combined effect of chemical reactions of formation of unstable oxynitrate compounds of iron in the top of the crack (submicrocrack) growing along a grain boundary and formation of the protective film of chromium oxides on the walls of the crack (submicrocrack).

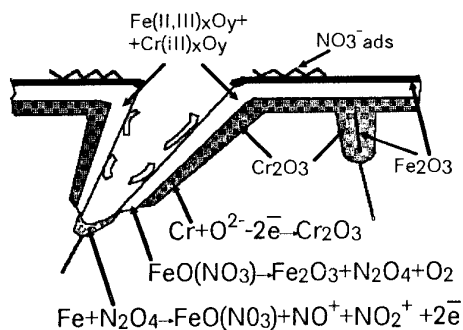


Fig.4 Schematic representation of IOE mechanism.

Regarding the level of total effective stresses on the grain boundary the IOE can result in the embrittlement of grain boundaries in the subsurface layer of metal or, at a high level of stresses, in the

embrittlement of grain boundaries accompanied with the crack formation.

We estimated that the surface multilayer oxide film with limited protective properties and probably permeable to NTO or its components is forming during the interaction of Cr-Ni steels with NTO until the formation of the 15-30-nm sublayer of chromium oxide adjacent to the metal. The inhibition of NTO by nitrogen monoxide affects the adsorption stage of the interaction and causes relatively fast formation of the 5 nm protective film.

The susceptibility of steels to the formation of the cracks of Type 2 may be used to develop the methods of accelerated testing of steels for IOE susceptibility.

4. CONCLUSIONS

1) The main features of behavior of stainless Cr-Ni maragings in water-containing media are in satisfactory agreement with the model assuming that SCC is the particular case of HE when the pitting formation in sites of protective oxide film deteriorations is the source of hydrogen charging.

2) This model allowed us to develop the method of accelerated testing of high-strength steels to SCC susceptibility using the alternating electrochemical polarization.

3) Stainless Cr-Ni steels contacting with NTO at moderate temperatures and pressures may be damaged by a specific type of corrosion that was named "intergranular oxidizing embrittlement (IOE)".

REFERENCES

1. Spiridonov, V.B., et al. "A Method of Testing of High-Strength Steels to SCC Susceptibility", USSR Author's Certificate N 641327, 1978.
2. Manning, P.E., Duquette, D.J., and Savage, W.F. "The Role of Sulfide Inclusions Morphology in Pit Initiation of Several Type 300 Series Stainless Steels", Corrosion (USA), 36, 6, 1980, pp.313-319.
3. Structure and Corrosion of Metals and Alloys. Ed. by E.A.Ul'yanin, Metallurgiya, Moscow, 1989.
4. Shibata Tosio, "Pitting as Probabilistic Phenomenon", J. Metal Finish. Soc. Jap., 31, 6, 1980, pp. 336-344.
5. Handbook on Corrosion Resistance of Chemical Equipment. Ed. by A.M.Sukhotin, Khimiya, Moscow, 1988.

THE DETECTION AND ANALYSIS OF GALVANIC DAMAGE IN BMI/GRAPHITE FIBER COMPOSITES

S.R. Taylor

G.L. Cahen, Jr.

Center for Electrochemical Science and Engineering

Department of Materials Science and Engineering

University of Virginia

Charlottesville, VA 22903, USA

SUMMARY

The use of graphite fiber polymer matrix composites (GFPMC) in multi-material assemblies which must maintain mechanical integrity in aqueous environments has focused attention on the galvanic degradation of these materials. Of recent concern to the aerospace industry is the galvanic degradation of bismaleimide (BMI)-graphite fiber (GF) composites when galvanically coupled to an active metal (e.g. aluminum). A detailed understanding of the damage process, both in terms of mechanism and extent, has not been possible because of the lack of a sensitive method to detect, quantify, and characterize damage in this material system. This study has used electrochemical impedance spectroscopy (EIS) to monitor material interfacial changes in an 8-ply, 0°, unidirectional BMI-GF composite subjected to cathodic and anodic polarization in NaCl solutions, exposure to caustic solutions, and galvanic coupling to a series of metals (Al, Fe, Cu, Ti) in NaCl solutions. Cathodic polarization was found to produce porous electrode behavior which was attributed to breakdown of the fiber/matrix interface and subsequent moisture ingress. This is in contrast to caustic exposure which did not show a porous electrode response, presumably due to general BMI solvation. These electrochemical results in combination with mechanical shear tests performed in an array of chemical and electrochemical conditions indicate that long-lived reaction intermediates, e.g. peroxide and superoxide radicals, generated during the oxygen reduction reaction on graphite, not hydroxyl ions, are the key damaging species. This will have important implications to the development of more damage resistant polymer chemistries. The sensitivity of EIS has also indicated that couples to titanium, proposed to be a benign couple, caused changes in the impedance spectra similar to those for low cathodic overpotentials. The long term implications of these latter changes on composite durability are not known at this time, but warrant further evaluation.

1. INTRODUCTION

The high specific strength, specific modulus, and toughness of graphite fiber-polymer matrix composites (GFPMC) have made this material an important, if not optimum, candidate for certain structural applica-

tions in the aerospace, marine, and automotive industries. The analysis of composite durability has traditionally focused on structural stability following exposure to impact damage, cyclic stress, heat, or moisture. However, the expanding applications to aqueous environments combined with sophisticated multi-material construction methods have made it evident that the long term mechanical integrity of PMC's will ultimately depend on their stability to a host of environmental factors which may include: wet/dry cycling, caustic exposure (as encountered in aircraft cleaning solutions), and galvanic polarization¹⁻³. A recent and significant example of the latter condition is the electrochemical degradation of polyimide/graphite fiber composites when galvanically coupled to an active metal⁴⁻⁷.

Bismaleimide, a polyimide-based polymer with a high glass transition temperature of 200° to 400° F⁸⁻¹¹, is an attractive matrix material for high temperature aerospace applications due to the reduced amount of volatile compounds and hence void production in the final curing stage^{10,12}. It has been observed that when a bismaleimide (BMI)/graphite fiber composite is coupled to an active metal such as aluminum, and immersed into an electrolyte, there is damage not only to the aluminum anode, but to the cathodically polarized graphite-filled composite as well⁴⁻⁷. Because of the known susceptibility of imide linkages to hydroxyl attack^{13,14}, one explanation for galvanic degradation of BMI/graphite composites has been the alkaline hydrolysis of the imide backbone by OH⁻ ions generated by oxygen reduction on the cathodically polarized graphite fibers⁷. This mechanism, however, has not been thoroughly investigated and the controlling variables have not been well defined.

To date, the effects of polarization on the degradation of PMC's has been examined by coupling it to various metals having different positions in the Galvanic series. Although this methodology has practical advantages, it provides little mechanistic information and does not uniquely address the importance of polarization on the degradation process. The use of galvanic couples creates questions concerning the effect of adsorbed metal ions (released from oxidation of the anode) on the reaction kinetics on the graphite fiber surface, as well as the repeatability of the potential established by the couple. The crevice geometry formed in the composite/metal contact area

plays an important role in the crevice chemistry which develops between the composite and metal, so that subtle changes in couple assembly may effect the resulting potential.

An additional concern in characterizing the effects of polarization on the degradation of BMI-GF composites is the separation of the effects of overpotential and time. If a thermodynamic barrier exists such that below a certain overpotential, damage does not occur, then there may be "safe" metals which would cause minimal polarization and hence no damage when coupled to BMI-GF. Titanium has been proposed as such a material. On the otherhand, if all potentials are deleterious, the extent of polarization may only effect the rate, so that with sufficient time, any amount of polarization will lead to composite failure. Therefore, it is important to characterize the effects of overpotential and time.

Compounding the questions regarding degradation mechanism is the need for a quantitative method to sensitively measure material changes in a nondestructive manner. Current methods for measuring environmental damage in BMI-GF composites involve visual inspection, tensile testing, and scribing methods. These methods are limited to either subjective interpretation, low sensitivity, sample destruction, or large data scatter¹⁵ each of which can mask the delineation of subtle changes. The sensitivity of these methods is sometimes augmented by accelerated tests, however, results from accelerated tests are often criticized if it is unclear whether the damage mechanism remains unaltered¹⁶. Thus, in addition to understanding the chemical and electrochemical damage processes in polymer matrix composites, there is a need for a sensitive and quantitative method to nondestructively detect the material changes caused by these conditions.

Electrochemical impedance spectroscopy (EIS) has recently been used to sensitively and nondestructively detect fatigue damage and moisture absorption in epoxy-graphite fiber composites¹⁷. Since the degradation phenomenon associated with galvanic couples of BMI-GF composites is electrochemical in nature, it has been logical to apply EIS in the analysis of this material degradation process. EIS has the added advantage of acquiring data *in situ* and continuously without cell disassembly and sample destruction.

The objective of this research is to examine the efficacy of EIS to monitor interfacial changes in BMI-GF composites exposed to chemical (caustic) and electrochemical environments. A primary interest is to compare the effects of overpotential, specifically cathodic polarization, to the damage characteristics of alkaline solutions, two environments in which hydroxyl ions are present. For purposes of comparison, the effects of anodic polarization will also be examined. Finally, the effect of galvanic coupling to various

metals (i.e. aluminum, steel, copper, and titanium) will be investigated.

II. EXPERIMENTAL METHODS

Materials

A continuous, 0°, 8-ply composite of bismaleimide 5250-4 resin and IM7 carbon fibers was used throughout this study. Test samples consisted of 2 cm square coupons which were wet polished using 240 grit SiC paper to remove the gelcoat. All electrochemical testing was performed on the broad face of the composite sheet and not on the coupon edges. Electrical contact was made with a copper sheet which was pressed against the back of the sample. Fiber loading was approximately 60 vol.% which provided electrical conduction to the sample surface exposed to solution.

Electrochemical Impedance Spectroscopy

EIS testing was performed in a 300 cm³ cell which exposed 1 cm² geometric area of composite via a knife-edge teflon gasket. A platinum coated niobium counter electrode and saturated calomel reference electrode were used. Impedance measurements were made in a three electrode configuration under potentiostatic control using a Schlumberger 1255 Frequency Response Analyzer and PAR 273 potentiostat under computer control. Data were collected from 65 kHz to 0.1 Hz using a 10 mV rms sine wave superimposed on a 0 V_{SCB} DC potential. This DC potential was determined to be a typical open circuit value for these composites. Impedance scans were collected at various times of exposure in the environments described below.

Potentiostatic Polarization

The effect of polarization on composite behavior was examined by holding samples at a constant DC potential. Both anodic and cathodic overpotentials of large (e.g. 1.5 V) and small (e.g. 20 mV) values were examined. The noble character of graphite makes anodic polarization from a galvanic couple improbable in engineering applications, however, it is conceivable that this condition could be produced by a stray current. This mode of polarization was examined to add to the general understanding of electrochemical degradation. The majority of polarizations were 24 hours in length with impedance scans collected at various time intervals. Samples were held at the potential of interest before and after EIS testing, but held at 0 V_{SCB} (open circuit potential) during the time of the impedance test. All experiments were performed in aerated 0.6M NaCl made with ACS grade sodium chloride and 18 Mohm distilled water.

Caustic Exposure

In order to compare the effects of cathodic polarization to chemical attack by OH⁻, composite samples were exposed to 0.1M, 1.0M, and 2.0M NaOH solu-

tions. Samples were removed periodically, rinsed in distilled water, and subjected to impedance testing as described previously in 0.6M NaCl.

Galvanic Couples

EIS was used to monitor the effect of galvanic coupling to the composite samples using a series of alloys from various positions in the galvanic series: 1100 aluminum, 1010 steel, copper, and titanium (listed in order of decreasing activity). Eight-ply composite samples measuring 4 cm by 0.7 cm (2.8 cm²) were electrically coupled to 20 cm² metal coupons using alligator clips and external wiring. The composite and metal coupons were immersed in aerated 0.6M NaCl leaving the electrical connections out of solution. Composite samples were disconnected from the metal samples during EIS testing.

III. RESULTS AND DISCUSSION

Potentiodynamic Polarization

The anodic and cathodic polarization behavior of BMI-GF composite in aerated 0.6M NaCl is shown in Figure 1. A polarization scan was started at an initial open circuit potential of 250 mV_{SCE}, scanned cathodically, reversed at -1.7 V_{SCE} and then scanned in the anodic direction. A second open circuit potential is seen at about -100 mV_{SCE}. These two values are consistent with the range of open circuit potentials measured (ca. -100 to +300 mV_{SCE}) on these materials^{17,24}. The precise cause of this shift in the open circuit value is unknown, but may be attributable to potential induced alterations in the prismatic edge functional groups on the graphite which in turn control the subsequent electrochemistry on the surface^{18,24}. Graphite also has a certain degree of polarizability within this potential range in neutral aqueous environments²⁴ which would also account for the observed range of open circuit potentials.

During cathodic polarization, the oxygen reduction reaction becomes mass transport limited between -0.5 and -1.5 V_{SCE}. Below -1.5 V_{SCE}, the hydrogen evolution reaction becomes the dominant cathodic process. Hydrogen evolution could potentially introduce an additional damage process over and above that caused by oxygen reduction (e.g. damage caused by bubble evolution). Although a cathodic overpotential greater than -1.5 V is beyond the range expected for any galvanic couple, potentials greater than this value were investigated.

The current resulting from anodic polarization of graphite in NaCl solution at potentials less than 0.9 V_{SCE} could result from oxidation of functional groups, oxygen adsorption and carbon oxidation²⁴⁻²⁶. The increased current at potentials above 0.9 V_{SCE} is attributed to oxygen evolution, and above approximately 1.1 V_{SCE}, chlorine evolution can occur. The consequences of these levels of polarization on materi-

al damage will be discussed subsequently.

Effects of Cathodic Polarization

Figure 2 shows the Nyquist and Bode plots for a composite sample polarized to -1.4 V_{SCE} for 0, 6, and 16 h. The general response is that of a constant phase element in parallel with a resistor. This resistance is initially very large as evidenced by the nearly constant phase angle and large low-frequency real axis intercept, but decreases with time. Several basic changes in the impedance data occur with time under these polarization conditions: (1) the impedance at a specific frequency decreases, (2) the slope of the Bode magnitude plot decreases, and (3) the peak in the phase angle plot decreases. The most plausible explanation for the general decrease in impedance is that the electrochemically active surface area is increasing. This idea is supported by a linear increase in the double layer capacitance as a function of time. This increased electrode area could result from either roughening of the exposed fiber surfaces or from breakdown of the fiber/matrix interface. No surface roughening of the fibers was observed in the scanning electron microscope, however a small gap (ca. 0.1 μm) could be seen between the fiber and matrix. Additional electrochemical evidence for breakdown of the fiber/matrix interface is the decreasing slope of the magnitude plot and decreasing phase angle peak which are indicative of the "squaring effect" observed in porous electrodes²⁷⁻²⁹. One could argue that these impedance changes might result from heterogeneous modifications in the functional chemistry of the graphite. However, it is neither clear how surface chemistry alone could lead to such a dramatic distributed response, nor is it clear that chemical heterogeneities would evolve over such an extended period of time. It is more logical that extended polarization would lead to uniformity in surface chemistry.

Further support for the idea that the porous electrode response is due to fiber/matrix interfacial breakdown, comes from an analysis of the impedance phase angle data to determine moisture penetration distance and rate. Although changes in the double layer capacitance could be used to calculate moisture penetration of the fiber/matrix interface, this approach requires precise knowledge of the initial number and area of exposed fibers - information which is not easily attainable. A more convenient approach is to use the phase angle data, since the phase angle will be insensitive to the number or area of fibers exposed, i.e. the phase angle is an intrinsic parameter and will be the same for a single fiber or many millions of fibers. The phase angle of the impedance vector can also be a more sensitive indicator of interfacial changes. If we assume a right cylindrical fiber surrounded by an insulating matrix, moisture penetration of the interface can be envisioned as creating an annular groove around the fiber (Figure 3). A model which explores a fiber intersecting the sample surface at a glancing angle will be examined in later work. If it is assumed

that interfacial breakdown causes the groove to grow deeper with time, and that the groove opening remains constant, the phase angle can be used to calculate the geometric angle²⁹ subtended by the fiber surface and the disbonded matrix. This geometric angle can then be used to calculate a penetration depth at different times of exposure, which can in turn be used to calculate a penetration distance. The details of this procedure have been described elsewhere³⁰.

The phase angle data was used to calculate the moisture penetration rate for a BMI-GF composite polarized to $-1.2 V_{\text{SCB}}$ for 24 hours in aerated 0.6M NaCl and is shown in Figure 4. There appears to be an increase in the rate of moisture penetration after 20 hours, however it is unclear whether this change is real or an artefact introduced by certain assumptions in the calculation parameters³⁰. For example it has been assumed that the groove opening did not change with time, when in reality it probably does. This could lead to errors at early times when small changes in groove opening distance might have a larger impact on the depth calculation of shallow grooves. Note, however, that the penetration rate for samples exposed to $-1.4 V$ follows the same trend as the $-1.2 V_{\text{SCB}}$ samples in the first 20 hours. Unfortunately, longer term data was not taken for this ($-1.4 V_{\text{SCB}}$) sample. If the penetration rate between 0 and 20 hours and between 20 and 70 hours is extrapolated to 1 year, penetration distances between 1.8 cm/year and 9 cm/year respectively are found. This compares relatively well to moisture penetration distances of 0.8 cm/year observed in epoxy matrix/graphite fiber composites which were galvanically coupled to magnesium and exposed to seawater¹. The fact that the measured penetration depth for the epoxy composite is less than that for the BMI-GF is plausible for several reasons. First, the potential established by a galvanic couple to magnesium will be approximately -0.9 to $-1.0 V_{\text{SCB}}$, a condition which is slightly less damaging than the condition tested here. It is also possible that the salts which can precipitate from seawater at high pH act as diffusion barriers and decrease the damage process. Finally, it is known that the bond between epoxy and graphite is significantly better than between graphite and BMI³¹. The fact that calculated moisture penetration rates are approximately equal to measured values is further evidence that cathodic polarization causes breakdown of the fiber/matrix interface and that the interpretation of the "squaring effect" in the phase angle data is correct. Note in Figure 5 that the penetration rates calculated for samples polarized to $-1.73 V_{\text{SCB}}$ and $-1.4 V_{\text{SCB}}$ are positioned as one would expect from the cathodic polarization behavior (Figure 1). The potentials of -1.2 and $-1.4 V_{\text{SCB}}$ both lie in the diffusion limited region for oxygen reduction and would be expected to produce similar levels of damage, whereas the damage produced by $-1.73 V_{\text{SCB}}$, a potential which is in the hydrogen evolution region, is severe and occurs

rapidly. Future experiments will attempt to directly measure moisture penetration depths in the BMI-GF system.

To further confirm that the polarization induced changes in the impedance spectra were indicative of changes at the material interface, a series of experiments were performed in which the applied potential was interrupted and then re-established. Figure 5 shows the phase angle as a function of log frequency for a composite sample which was polarized to $-1.7 V_{\text{SCB}}$ for 5 hours. The peak phase angle is reduced from -80 degrees to ca. -45 degrees in an EIS measurement made immediately following the 5 hour polarization. After the sample remained in solution for 7 hours at open circuit, EIS was repeated. As can be seen in Figure 5, the interfacial changes brought about by the initial cathodic polarization remained essentially unchanged when the sample was allowed to sit at open circuit. When the cathodic potential was reapplied, the phase angle decreased further to ca. -35 degrees in the mid-frequency range (ca. 20 Hz). This phase angle response was essentially retained following 21 hours of exposure at open circuit. The phase angle at low frequency (< 1 Hz) increased slightly as the sample sat at open circuit following polarization. Although a precise interpretation of this behavior is unclear, other experiments suggest that this may be related to the depletion of a reactive intermediate generated during the oxygen reduction reaction.

Figure 6 shows the Bode phase angle plot for a BMI-GF composite immersed in aerated 0.6M NaCl at open circuit for four days. Note that the response remains capacitive and that there is essentially no evidence of fiber/matrix interfacial breakdown in this time period. Thus, interfacial breakdown is directly facilitated by cathodic polarization, however it is unclear whether this breakdown is caused solely by a cathodic reaction product or whether other processes (e.g. electrostatic debonding, direct reduction of the BMI) are also involved.

Rather than pursue a rigorous analysis of the constant phase element response, a more qualitative approach was taken for purposes of comparison. A review of the experimental data indicated that the phase angle was the most sensitive indicator of changes (damage) in the composite. Therefore, comparisons of interfacial changes (or material damage) as a function of exposure conditions were facilitated by producing "delta phase angle" plots. The delta phase angle plot is produced by subtracting the phase angle value at some time t_1 from the initial value for each frequency examined:

$$\Delta\theta(\omega_{t=t_1}) = \theta(\omega_{t=t_1}) - \theta(\omega_{t=t_0}) \quad (1)$$

The delta phase angle plots for several cathodic overpotentials at different times of exposure are shown in Figure 7. In this plotting format, the closer

the response is to zero, the smaller the degree of interfacial change from initial conditions. It can be seen that for a given time of polarization, the degree of damage increases with increasing cathodic overpotential, and that for a given overpotential, damage increases with time. Cathodic polarization produces a delta phase angle plot which has a characteristic peak between 10 and 100 Hz and a gradually increasing value below 1 Hz. This latter region is referred to as a low frequency "tail". The peak results from a parallel shift of the phase angle response to lower frequencies with increasing damage (caused by increasing time or potential), while the tail results from the decreased impedance and accompanying phase angles at lower frequencies. As mentioned, this tail may be associated with the accumulation of cathodically produced electroactive species.

It is interesting to note that even though the $-1.2 V_{SCB}$ and $-1.4 V_{SCB}$ polarizations lie in the diffusion limited region for oxygen reduction and thus support the same cathodic current, the delta phase angle plot and the moisture penetration data of Figure 4 indicate more change for $-1.4 V$ than for $-1.2 V$. The effect of fiber polarization beyond its role in cathodic kinetics needs further examination.

Effects of Anodic Polarization

The Nyquist and Bode plots for a composite sample polarized to $+1.5 V_{SCB}$ are shown in Figure 8. These data show a marked deviation from the response observed for cathodic polarization. Anodic polarization produces: (1) a decrease in the impedance with increasing time, (2) a parallel shift in the capacitive region of the magnitude to lower frequencies, and (3) very little depression of the peak phase angle.

As in cathodic polarization, the decrease in impedance for anodically polarized samples can be interpreted as an increase in capacitance resulting from an increase in active surface area. However, the lack of porous electrode behavior suggests that the surface remains electrochemically "planar". An anodic overpotential of this magnitude is expected to combust the graphite^{25,26} and produce a rough topography, however it is possible that the BMI is also susceptible to oxidation and ablation in a manner that maintains larger "pore" sizes which are easily penetrated by the frequencies used in these experiments, thus minimizing porous electrode behavior.

The delta phase angle plot for anodic polarization (Figure 9) reveals that very little change occurs at low frequencies in contrast to the delta phase angle plot for a cathodically polarized sample. The significant phase angle peak at ca. 100 Hz is much more pronounced than in the cathodic data and is attributed to the very uniform shift of the phase angle data to lower frequencies at longer times of exposure.

Caustic Exposure

The impedance spectra of BMI composite samples exposed to 0.1M, 1.0M, and 2.0M NaOH was very similar to that following anodic polarization. The spectra showed essentially no depression of the phase angle and parallel shifts in the magnitude and phase angle response to lower frequencies as the severity of the environment increased. The similarity to anodic polarization was also borne out in the delta phase angle plot as seen in Figure 10. A delta phase angle peak has been clearly observed in caustic solutions as dilute as 10 mM.

In keeping with the previously proposed theory for electrochemical damage, it was initially predicted that caustic exposure should create damage similar to cathodic polarization, if OH^- ions are the key damaging species. However, there is an absence of porous behavior in the caustic exposure in contrast to cathodic polarization. The uniform shifts in the magnitude and phase angle plot indicate that the electrode is uniformly accessible, i.e. no porosity is developing. One possible explanation of this is that bulk dissolution of the BMI by the caustic solution is occurring so as to expose new fiber area but not create small pores between the fiber and matrix. In contrast, the locally generated hydroxyl ions (or reaction intermediates) produced during cathodic polarization cause matrix damage in the immediate proximity of the graphite fiber, thus creating a groove or pore adjacent to the fiber. However, this does not explain the significant low frequency tail observed in the cathodically polarized samples but not in the samples exposed to caustic solution.

It is well documented that in neutral or alkaline environments, the oxygen reduction reaction can take one of two possible pathways: "Pathway 1" also known as the "peroxide pathway", and "Pathway 2", also known as the "direct 4-electron pathway"^{32,33}. What is immediately relevant about these reactions, however, is that Pathway 1 forms a peroxide intermediate which desorbs from the catalyst surface, while in Pathway 2, the peroxide remains adsorbed on the surface. Pathway 2 is viewed as a less damaging mechanism since highly damaging peroxide intermediates do not enter into the solution phase. The implications with regards to BMI-GF composites are extremely important. Catalysts on which Pathway 1 is clearly dominant include carbon and graphite^{33,34}, and gold (in alkaline electrolytes)³⁵. Carbon is a very effective catalyst for reduction of O_2 to peroxide in alkaline solutions as might occur during cathodic polarization in a restricted geometry such as the disbanded region between the fiber and matrix. The exchange current density, i_0 , for the production of peroxide on graphite and carbon is very high, ca. 10^{-4} to $10^{-3} A/cm^2$ [33,34]. But more importantly, the kinetics for further reduction or decomposition of peroxide on carbon and graphite are slow compared to the desorption process, resulting in the build-up of substantial peroxide in the

electrolyte within a porous or creviced geometry^{33,34}. The reason that peroxide becomes important in the degradation of polyimide based composites is because high peroxide concentrations can lead to high concentration of superoxide radical species (e.g. $O_2^{\bullet-}$ and OH^{\bullet}) within the pore or crevice. In air saturated concentrated NaOH containing 0.1M HO_2 , the equilibrium concentration of $O_2^{\bullet-}$ would be ca. 10^{-4} M which exceeds the concentration of oxygen by an order of magnitude^{33,34}. These superoxide radical intermediates produced during homogeneous peroxide decomposition have a lifetime of approximately 200 sec. at 20° C and are much more damaging than peroxide. An additional property of superoxide radicals which make them excessively deleterious to polymers is that they can react with labile hydrogens on the polymer surface to produce a more highly reactive hydroperoxyl radical (HOO^{\bullet}) which is hydrocarbon soluble and can readily diffuse through the polymer where it is converted by further reaction with labile hydrogens to peroxide³⁶.

Preliminary fracture studies of cathodically polarized BMI composites have shown evidence of bulk polymer degradation not seen in samples exposed to caustic alone³⁷ (Figure 11). In fact, exposures to caustic solutions over the same time frame as the cathodic polarization caused an increase in fracture strength probably as a result of plasticization of the brittle BMI matrix. In the presence of light, this peroxide can undergo photolysis to form hydroxyl radicals which can further initiate oxidation. Thus, although the overall oxygen reduction reaction produces OH^- ions which can degrade polyimides, the electrochemical reduction of oxygen on graphite quite likely leads to the production of aggressive intermediates which desorb from the surface, become hydrocarbon soluble, and are much more damaging. Because of these extremely aggressive intermediates, it is probable that all polymer matrices will be susceptible to damage to varying degrees *unless* efforts are made to control the electrochemistry on the graphite. This laboratory has observed similar electrochemical degradation of epoxy matrix composites using EIS, however the kinetics were slower than that of BMI-based materials. Several possible compounds and surface treatment procedures have been identified which can change the oxygen reduction pathway on graphite from the deleterious Pathway 1 to Pathway 2.

Galvanic Couples

The Nyquist and Bode plots for a composite sample which has been galvanically coupled to an 1100 aluminum in aerated 0.6M NaCl showed that, with time, the overall impedance decreases, the slope of the magnitude plot decreases, and the phase angle decreases. As before, these changes have been attributed to an increase in active surface area (i.e. fiber area) and the development of porosity, suggesting similar damage as that for cathodic polarization. Some difference, however, is noted in the delta phase

angle plot (Figure 12) where the peak in the 200 Hz range is more pronounced for the galvanic couples resulting from an added parallel shift in the magnitude plot. Both galvanic couples and cathodic polarization produce a low frequency tail in the delta phase angle plot which is proposed to result from the electrochemically generated peroxide intermediates which are not present in the caustic exposures.

The impedance changes observed for couples to aluminum, steel, copper, and titanium follow the sequence predicted from the metal activity in NaCl solution. The potentials established by the various metals were as follows: Al = -0.81 V_{SCB} , Fe = -0.70 V_{SCB} , Cu = -0.20 V_{SCB} , and Ti = -0.05 to +0.12 V_{SCB} . It should be noted that the variable potentials observed with titanium couples also resulted in variations in the delta phase angle plots. In some tests, the delta phase angle showed positive phase angle changes as opposed to negative changes observed in cathodically polarized samples. This variability may arise from the high polarizability of titanium. Although titanium is regraded as a benign couple for the construction of composite aerospace structures, the data presented here raises some very critical questions. The subtle changes observed by EIS for titanium couples may produce unnoticeable visual or mechanical alterations in a time frame of several months or several years. Questions remain, however, as to how these changes will extrapolate over the lifetime of the structure. Issues of crevice geometry, crevice chemistry, and temperature should be examined in future studies.

IV. SUMMARY AND CONCLUSIONS

The growing range of working environments and applications encountered by graphite fiber/polymer matrix composites necessitates information about the environmental durability of these materials. Present methods for testing environmental effects on polymer matrix composites are limited in sensitivity and are destructive, while accelerated tests raise skepticism with regard to the fidelity of the mechanism.

Present evidence suggests that electrochemical impedance spectroscopy is a rapid and sensitive method for monitoring changes in surface morphology and surface chemistry in graphite fiber filled polymer matrix composites in the conditions of interest. This claim is based on direct correlation of EIS data with polarization conditions as well as general agreement between calculated moisture penetration rates and field data. This method has been particularly useful in analyzing the chemical and electrochemical degradation processes of BMI-GF composites.

Cathodic polarization of BMI-GF samples causes a degradation process which appears to degrade the fiber/matrix interface and produces a porous interface as observed via EIS. The damage is dependent on the

rate of oxygen reduction and on overpotential. Electrochemical changes observed at low overpotentials are less clearly understood and may result from a combination of physical changes and oxidation/reduction of prismatic edge functional groups. Although hydroxyl ion production is regarded by many to be the damaging species, this research indicates that oxygen reduction reaction intermediates (e.g. peroxide, superoxide radicals) may be the key damaging species. Caustic exposure and anodic polarization produced EIS spectra in which no porosity was observed. Because of the aggressiveness of the proposed damaging species, it is believed that the development of composite materials which are immune to electrochemical degradation will require an approach that controls the initial electrochemistry on the graphite. Several methods for this control have been identified by these authors.

Galvanic couples to aluminum, steel, copper, and titanium resulted in spectra similar to, but not identical to cathodic polarization. It is possible that the metal ions released in the oxidation of the metal may be responsible for the observed differences. The degree of interfacial change observed via EIS corresponded to the potential established by the galvanic couple (Al > Fe > Cu > Ti). Of particular importance is the fact that galvanic coupling of a BMI-GF composite sample to titanium produced impedance changes which are not necessarily benign. The impact of this result in combination with temperature and crevice effects should be examined further.

ACKNOWLEDGMENTS

The authors would like to thank D.F. Wall and K.C. Stewart for their efforts in the acquisition of electrochemical and mechanical test data. We would also like to express our appreciation to the Virginia Center for Innovative Technology and the Naval Air Warfare Center for their support of this research.

References

1. F.E. Sloan and J.B. Talbot, *Corrosion*, 48(10):830 (1992).
2. W.C. Tucker and R. Brown, *J. Comp. Mater.*, 23:389 (1989).
3. W.C. Tucker, R. Brown and L. Russell, *J. Comp. Mater.*, 24:92 (1990).
4. M.A. Dornheim, *Aviation Week and Space Technology*, 133:122 (Nov. 26, 1990).
5. R.C. Cochran, R.E. Trabocco, L. Boodey, J. Thompson and T.M. Donnellan, "Degradation of Imide Based Composites", Proc. 36th Intl. SAMPE Symp., San Diego, CA (1991).
6. D. Kinard, "Corrosion of Polyimides", High Temple Workshop XI, Reno, NV (1991).
7. E.M. Woo, J.S. Chen and C.S. Carter, *Polymer Composites*, 14(5):395 (1993).
8. T.L. St. Clair, in High Temperature Polymer Matrix Composites, T.T. Serafini, Editor, Noyes Data Corp., Park Ridge, NJ (1987) p.35.
9. M.A. Meador, P.J. Cavano, D.C. Malarick, in Structural Composites - Vith ASM-ESD, Oct.8-11 (1990) Detroit, ASM, Metals Park, Ohio.
10. J.A. Parker, D.A. Kourtides and G.M. Fohlen, in High Temperature Polymer Matrix Composites, T.T. Serafini, Editor, Noyes Data Corp., Park Ridge, NJ (1987) p.54.
11. C.L. Hamermesh and P.J. Dynes, in High Temperature Polymer Matrix Composites, T.T. Serafini, Editor, Noyes Data Corp., Park Ridge, NJ (1987) p.169.
12. P. Delvigs, in High Temperature Polymer Matrix Composites, T.T. Serafini, Editor, Noyes Data Corp., Park Ridge, NJ (1987) p.23.
13. W.P. Pawlowski and D.D. Coolbaugh, *Polym. Mat. Sci. and Engr.*, 59:68 (1988).
14. G.E. Zaikos, Developments in Polymer Degradation, Vol. 6, (1985).
15. G.S. Springer, in Environmental Effects on Composite Materials, Vol. 2, G.S. Springer, Editor, Technomic Publishing Co., Lancaster, PA (1984), p.6.
16. E.C. Edge, in Environmental Effects on Composite Materials, Vol. 2, G.S. Springer, Editor, Technomic Publishing Co., Lancaster, PA (1984), p.230.
17. R.C. Glass, S.R. Taylor, G.L. Cahen, Jr. and G.E. Stoner, *J. Nondestructive Eval.*, 6(4):181 (1987).
18. R.E. Panzer and P.J. Elving, *Electrochimica Acta*, 20:635 (1975).
19. W.J. Blaedel and R.A. Jenkins, *Anal. Chem.*, 46:1952 (1974).
20. R.M. Wightman, M.R. Deakin, P.M. Kovach, W.G. Kuhr and K.J. Stutts, *J. Electrochem. Soc.*, 132(7): 1578 (1984).
21. E. Theodoridou, J.O. Besenhard and H.F. Fritz, *J. Electroanal. Chem.*, 122:67 (1981).
22. J.F. Rusling, *Anal. Chem.*, 56:575 (1984).
23. J.P. Randin, Comprehensive Treatise of Electrochemistry, Vol.4, Chapter 10, Plenum Press, NY (1981).
24. S.M. Lipka, "A Fundamental Study of the Kinetic Behavior of Ensembles of Carbon-Based Microelectrodes", Ph.D. Dissertation, University of Virginia (1985).
25. J.P. Randin, "Carbon", in The Encyclopedia of Electrochemistry of the Elements, A.J. Bard, Editor, Vol. VII, Marcel-Dekker, NY (1976).
26. K. Kinoshita, Carbon - Electrochemical and Physicochemical Properties, Wiley-Interscience, NY (1988).
27. R. de Levie, *Electrochimica Acta*, 8:751 (1963).
28. R. de Levie, *Electrochimica Acta*, 9:1231 (1964).
29. R. de Levie, *Electrochimica Acta*, 10:113 (1965).
30. S.R. Taylor, *Composite Interfaces*, (in press).
31. J.H. Underwood and A.A. Kapusta, *J. Composites Technol. and Res.*, 13(3):179 (1991).
32. E. Yeager, J.A. Molla and S. Gupta, *Electrochem. Soc. Proc.*, Vol. 84-5 (1984).

33. E. Yeager, C. Krouse and K. Rao, *Electrochim. Acta*, 10:57 (1964).
34. I. Moreos and E. Yeager, *Electrochimica Acta*, 15:953 (1970).
35. R. Zurilla, R.K. Sen and E. Yeager, *J. Electrochem. Soc.*, 125:1103 (1978).
36. F. Kawai, in *Biodegradable Polymers and Plastics*, M. Vert, J. Feijen, A. Albertsson, G. Scott, and E. Chiellini, Editors, The Royal Society of Chemistry, Redwood Press, Wiltshire, UK, pp.20-29 (1992).

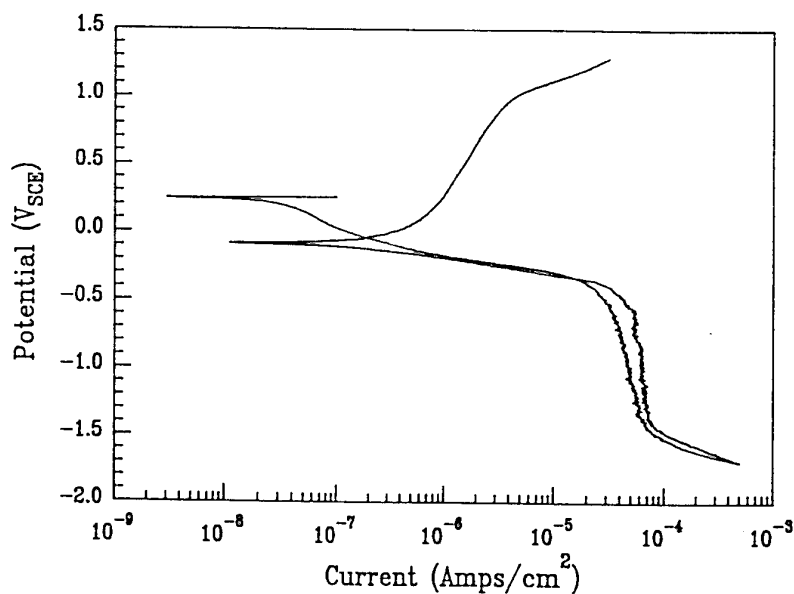


Figure 1. Potentiodynamic polarization scan (0.2 mV/s) of BMI composite in 0.6 M NaCl.

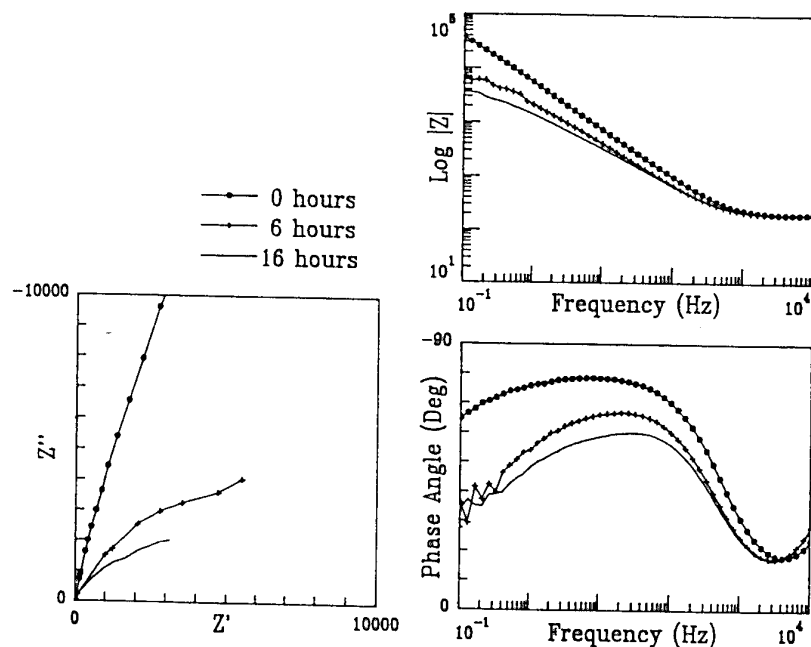


Figure 2 Nyquist and Bode plots for BMI composite sample which has been polarized to $-1.4 V_{SCE}$. EIS was performed at $0V_{SCE}$.

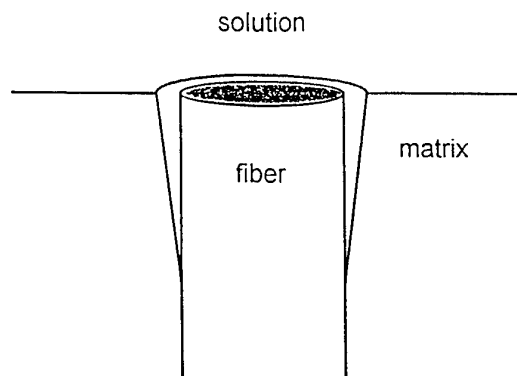


Figure 3. Schematic of proposed source of porous electrode effect in cathodically polarized samples.

Figure 4. Calculated moisture penetration for various levels of cathodic polarization using phase angle data and the annular groove model.

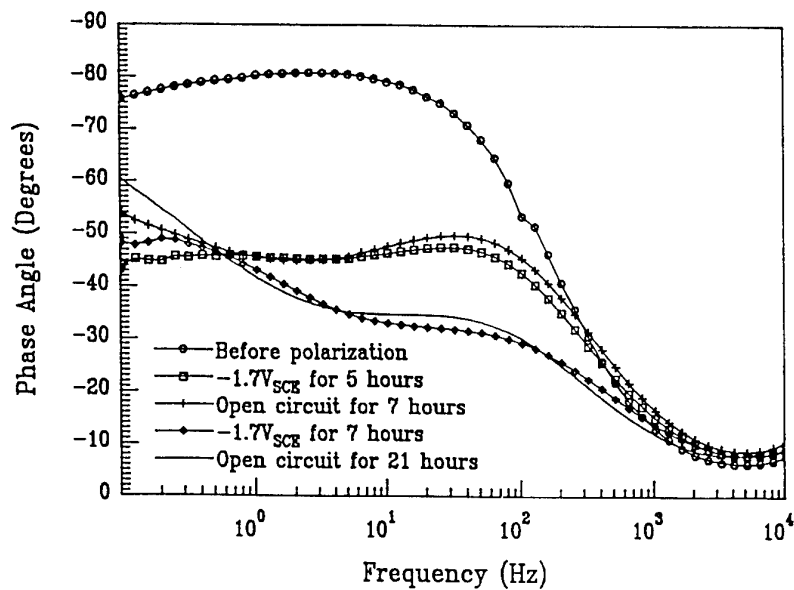
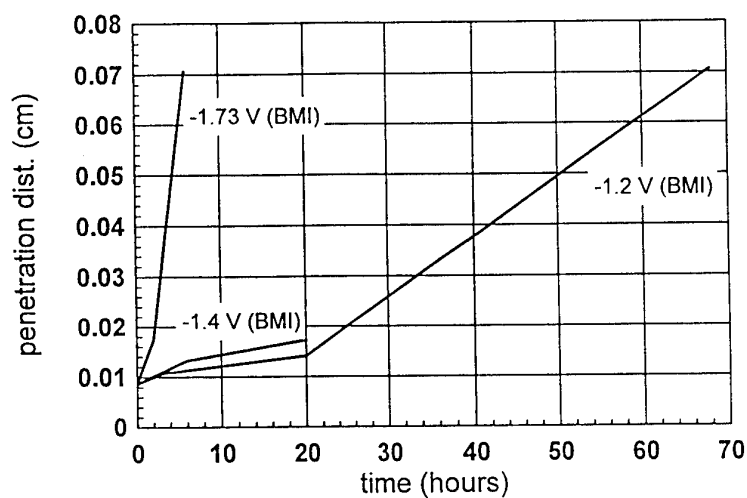


Figure 5. Bode phase angle plot for BMI composite which has been subjected to intermittent cathodic polarization.

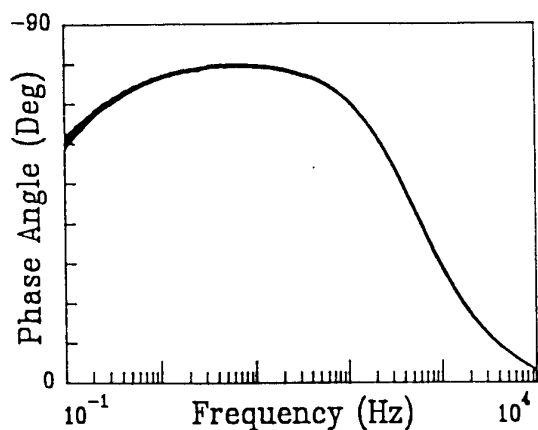


Figure 6. Bode phase angle plots for BMI composite exposed to aerated 0.6M NaCl for 4 days under open circuit conditions (18 experiments).

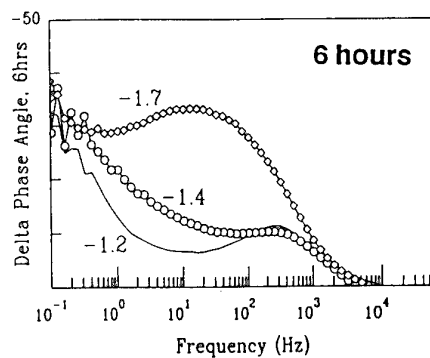
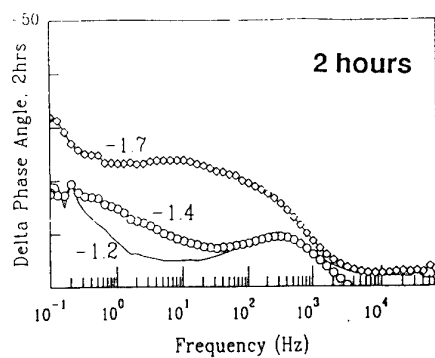


Figure 7. "Delta phase angle" plots for several cathodic overpotentials at different times of exposure in aerated 0.6M NaCl.

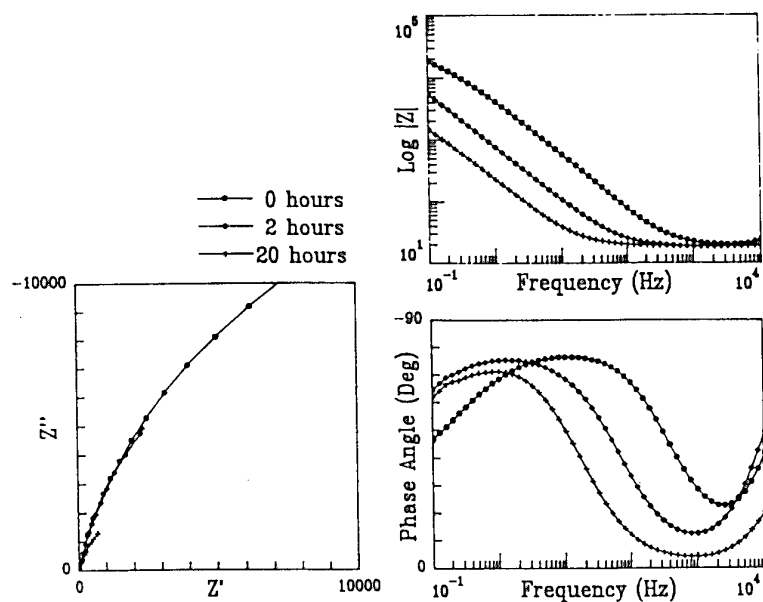
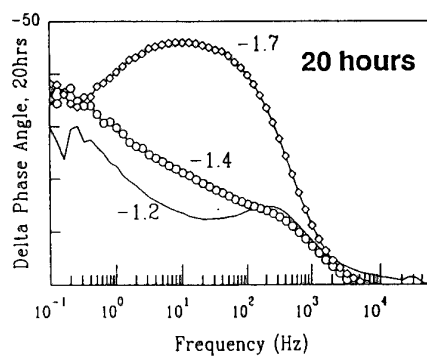


Figure 8. Nyquist and Bode plots for BMI composite sample polarized to +1.5 V_{SCE} in aerated 0.6M NaCl.

Figure 9. Delta phase angle plot for BMI composite sample polarized to $+1.5 V_{SCE}$ in aerated 0.6M NaCl.

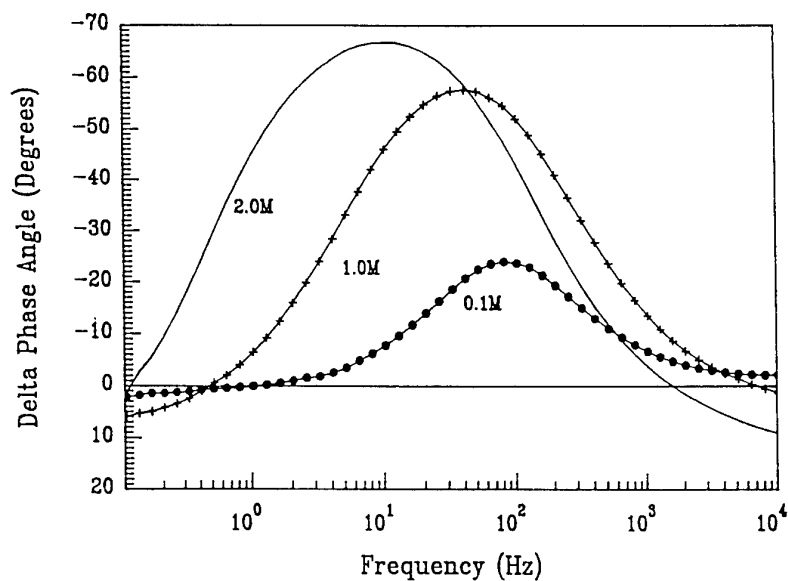
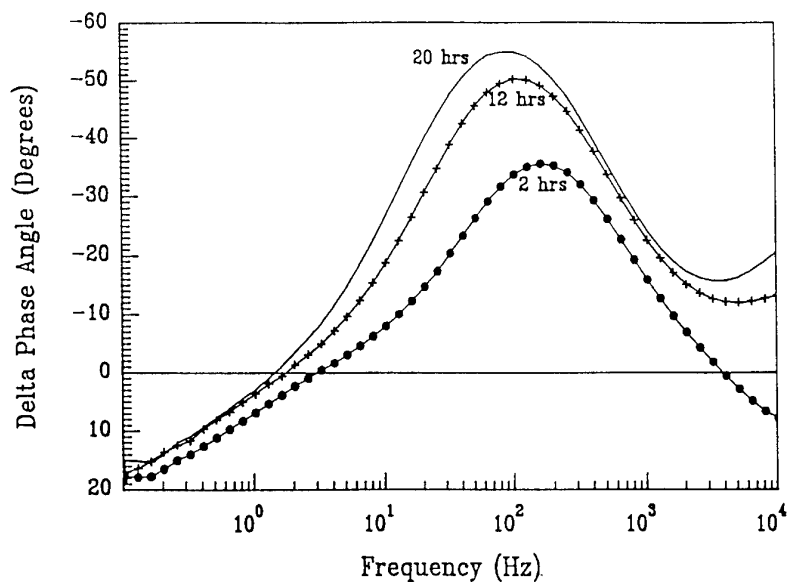
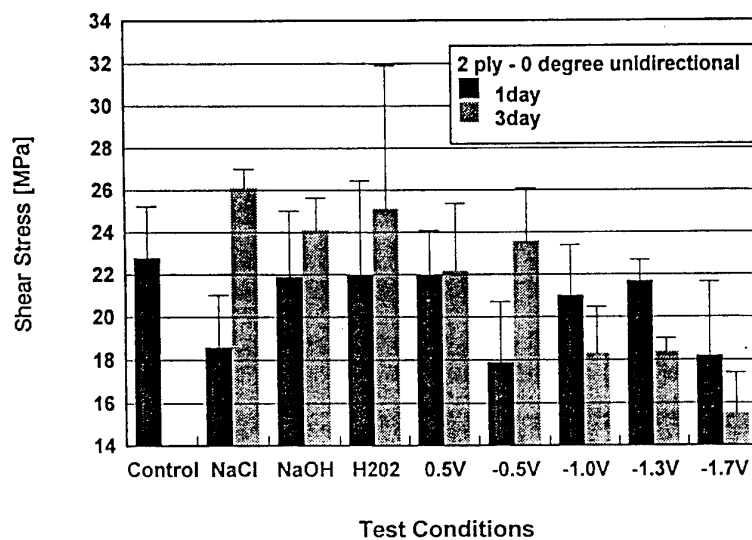


Figure 10. Delta phase angle plot for BMI composite exposed to various concentrations of NaOH at room temperature for 114 hours.

Figure 11. Summary of shear strength data taken from notched 2-ply, 0 degree BMI samples exposed for 1 and 3 days to various chemical and electrochemical environments: air (control), 0.6M NaCl, 0.4M NaOH, 0.4M NaOH + 0.1M H_2O_2 , 0.6M NaCl + anodic polarization ($+0.5 V_{SCE}$), 0.6M NaCl + cathodic polarization ($-1.0, -1.3, -1.7 V_{SCE}$).



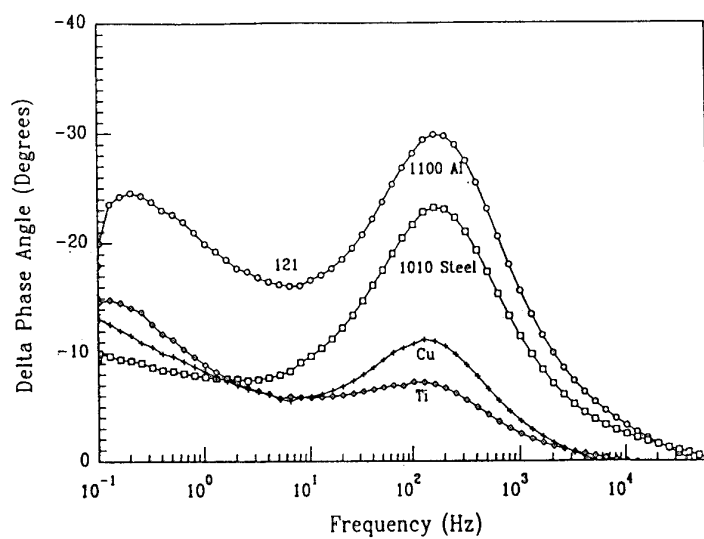


Figure 12. Delta phase angle plot for BMI composite samples which have been galvanically coupled to aluminum steel, copper, and titanium.

Double Pass Retroreflection for Corrosion Detection in Aircraft Structures

J.P.Komorowski, S.Krishnakumar, R.W.Gould, N.C. Bellinger

Structures, Materials and Propulsion Laboratory
Institute for Aerospace Research, National Research Council Canada
Montreal Rd. M 14, Ottawa, ON., K1A 0R6, CANADA

F.Karpala, O.L.Hageniers
Diffracto Ltd., 2835 Kew Drive, Windsor, ON., N8T 3B7, CANADA

1. SUMMARY

An optical double pass retroreflection surface inspection technique (D Sight) used for visualizing surface distortions, depressions or protrusions has been adapted as a rapid, enhanced visual inspection method inspection of large external aircraft surfaces. A project to fully characterize the D Sight indications of corrosion damage in lap splices is currently active. Over 150 large transport aircraft fuselage lap splice specimens have been collected. D Sight Aircraft Inspection System - (DAIS) 250C has been developed and tested both in the laboratory and in the field. In laboratory tests lap splices retrieved from retired aircraft and subjected to accelerated corrosion and lap splices naturally corroded in-service were inspected with DAIS, eddy current, X-ray, shadow moiré and subjected to tear down. It has been shown that the DAIS 250C is capable of locating corrosion pitting indicative of a thickness loss as low as 2%. The first field trial of the DAIS 250C was based on two service bulletins requiring inspection of longitudinal and circumferential lap splices on the 737-200 aircraft from BS 259.5 to BS 1016. The DAIS 250C inspection, including analysis and report, took 36 man-hours. The recommended technique in the SB was close visual inspection and the time required according to the service bulletins, was 278 man-hours.

Computer modelling of the bulging of fuselage skins due to corrosion and D Sight image simulation is also being conducted as a tool for inspection interpretation.

2. INTRODUCTION

The age of an aeroplane can generally be measured in terms of its major design goals: years of service, number of flights or number of flying hours. In 1993 the airlines, for various economic reasons, continued to operate more than 3000 jet aeroplanes with more than twenty years service [1]. The military operators are in a similar position as exemplified by US Air Force C/KC-135 which was produced in the late 1950s and 60s, and is currently projected for service through the first half of the next century [2]. A series of conferences on aging aeroplanes, the first of which was held in 1988 [3], have established that multiple-site fatigue cracking and corrosion are the major issues affecting the airworthiness of these aeroplanes. Often large areas of the airframe are affected and need to be inspected with increased frequency as compared with new aeroplanes. Continued airworthiness of these aging aeroplanes requires improved non-destructive testing (NDT) techniques.

At the 1989 AGARD-SMP on emerging NDT techniques, the D Sight optical set up and its potential as a technique for inspecting composite aircraft structure were introduced for the first time [4][5]. Later, D Sight's potential as an aircraft corrosion detection method was documented in [6]. At the time, it was shown that filiform, exfoliation and fuselage lap splice corrosion could be detected. Subsequently the authors were invited to participate in USAF sponsored corrosion NDT equipment

evaluations. The D Sight based 'breadboard' system designed for composite materials was used and although not optimized for lap splice corrosion it performed very well ("enhanced visual method" in [2]).

Each D Sight application area requires that the system limitations and sensitivity be determined. As well, a specialized inspection optical arrangement is desirable and should be developed for each important application category. Since addressing all potential D Sight applications simultaneously was not feasible, it was decided that fuselage lap splices would be the focus for D Sight corrosion detection development. A 1993 survey of 16 North American airlines conducted by Diffracto Limited confirmed that lap splice corrosion is the most significant corrosion problem in large jet transport aeroplanes. The results of Phase I of a three phase project initiated early in 1993 to develop the D Sight Aircraft Inspection System (DAIS) for lap splice corrosion detection are summarized in this paper.

3. LABORATORY VALIDATION

3.1 Specimen Library

a) Specimen collection

The first step in gaining confidence in a new NDT technology is to test it in the laboratory on as many as possible representative specimens containing defects - in this case corrosion. Such evaluations are needed to establish the limits of the method's applicability and sensitivity. There are three basic types of fuselage lap splices as shown in Figure 1. An aeroplane fuselage design may have two or all three of these basic joints with a number of doublers and substructure (stiffeners, frames and tearstraps) attached. Some manufactures rivet and seal the splices (Douglas) while others use a combination of riveting and bonding (Boeing, Lockheed). Nearly all transport aeroplane skins are made of 2024-T3 aluminium alloy, the stringers are typically 7075-T6 alloy while some tearstraps are made of titanium. A typical jet transport aeroplane contains nearly 200 lap splice configurations. For practical reasons it was decided that only a representative selection of splices would be retrieved from retired aeroplane types. Over the course of a year, the National Research Council (NRC) has established a lap splice specimen library containing over 150 specimens and representing the following aeroplane types: Douglas DC-9, DC-10, Boeing B-727, 737 and Lockheed 1011 [7]. Further additions to the library are planned. The DC-9 lap splice specimens collected for the library are shown in the shaded areas in the schematic ('turtle diagram') in Figure 2.

b) Laboratory Corrosion Exposure

Laboratory D Sight inspections of the library of specimens indicated that about 60% of the specimens contained varying degrees of corrosion. This was confirmed by limited tear down inspections. These specimens were used to develop specifications for the DAIS corrosion inspection head optics.

Accelerated corrosion processes were reviewed and their ability

to simulate the corrosion occurring in aeroplane lap slices was verified experimentally. On that basis, the ASTM Standard B368 Copper-Accelerated Acetic Acid-Salt Spray (CASS) Testing Method has been selected as the most suitable for this program.

A number of constructions representing longitudinal and circumferential lap splices from the non-corroded specimens were prepared for accelerated corrosion testing. In general, these had a nominal surface area of about 1400 cm² (1.5 ft²). A few specimens were subjected to corrosion testing in their original unaltered condition, i.e., without disassembly and removal of corrosion protection from the inner surfaces. The majority of specimens were disassembled and inspected for existing corrosion. Protective coatings on selected surfaces were removed and the specimens were reassembled and introduced into the corrosion chamber. Specimens with thin skin material had their original stiffener structure included in the reconstruction. The exterior surfaces of all specimens were coated using an easily strippable paint system which protected these surfaces from the corrosive environment and facilitated periodic NDT. Table 1 lists specimens subjected to the accelerated corrosion process. The aim of this effort was to produce controlled levels of corrosion to better establish D Sight corrosion sensitivity and resolution.

c) Chemical Characterisation of Corrosion Products

Chemical characterization tests were conducted on corrosion product samples extracted from the lap splices of aging aeroplanes and also those produced by exposure to acidified salt fog in the laboratory. The objective of these tests was to determine precisely the chemical compositions of the two corrosion products [8], which was desirable for two reasons: one, to establish the degree of similitude between corrosion occurring naturally in an aging aeroplane and that produced artificially by exposure to salt fog in the laboratory; and two, for the development of a mathematical model of the "pillowing" deformation of the outer skin caused by the accumulation of corrosion products within aging fuselage skin splices. Three methods were used for the chemical analysis of the corrosion products: x-ray diffraction (XRD), x-ray photoelectron spectroscopy (XPS) and Auger electron spectroscopy (AES).

It is generally believed that the usual product of corrosion of aluminium and aluminium alloys in a humid atmosphere is some form of hydrated aluminium oxide [9]. The opinion most favoured by researchers is that the initial product is amorphous aluminium hydroxide (Al(OH)₃) which crystallizes with time to become a hydrated oxide or a mixture of oxides. The major crystalline phases commonly identified are aluminium oxide monohydrate Boehmite (α -Al₂O₃·H₂O or AlO.OH) and aluminium oxide trihydrate, the latter existing in both alpha form as Gibbsite or Hydrargillite (α -Al₂O₃·3H₂O) and beta form as Bayerite (β -Al₂O₃·3H₂O, monoclinic) [10,11]. Based on thermodynamic considerations, Deltombe and Pourbaix [12] suggest that the form of the product progressively moves to less soluble oxides: from Boehmite to Bayerite to Gibbsite. The studies of Hart [13] and Shipko and Haag [14] appear to support this hypothesis. The results of the chemical analysis tests conducted partly at the NRC Institute for Aerospace Research and partly at the NRC Institute for Microstructural Studies are also in general agreement with this point of view. They indicate that the major portion of the corrosion product is either amorphous or crystalline aluminium oxide trihydrate, while a small fraction is in the monohydrate form, which appears to be an intermediate transition state.

Table 2 contains information on molecular volume ratio for aluminium and its different oxides. It should be noted that aluminium oxide trihydrate has the highest volume increase ratio (6.45).

The most significant result from the x-ray diffraction analysis was the similarity of the spectra generated by the natural corrosion product and the laboratory sample, which confirmed that exposure to acidified salt spray in the laboratory quite closely duplicated the process of corrosion in aging aeroplane.

3.2 DAIS 250C Specifications and Design

The schematic of the DAIS 250C inspection head is shown in Figure 3. The weight of the first model made of aluminium alloy sheet metal was 5.5 kg. Production models are expected to weigh less. The length of the head spans slightly more than the typical body station distance between frames. The inspection head is attached to a portable PC computer running dedicated software, a power supply and a remote pendant. The pendant includes a small video display and an LCD touch sensitive screen through which the inspector can control the system operation (eg. light level, image saving and annotation etc). D Sight images are saved as bitmaps in the popular TIFF format. The DAIS inspection requires two person operation: one manipulating the inspection head and the other operating the pendant. The scanning rate is approximately 1.2 m/min. The image interpretation can be performed at a later time either by viewing images on a monitor, or from prints.

3.3 Specimen Test Results

The specimens which were subjected to accelerated corrosion testing in the laboratory were inspected with D Sight before, at one or two intermediate stages, and at the end of the corrosion application. Several of these specimens were also inspected by other NDT techniques for comparison with the D Sight results. The main techniques other than D Sight employed for monitoring the growth of corrosion in the specimens were x-ray radiography, eddy current and shadow moiré.

a) X-ray

The radiography was performed with a LORAD LPX-160 Series Portable Industrial x-ray Unit capable of applying an x-ray Potential of up to 160 kV and a maximum tube current of 5 mA. The specimens were placed at a distance of 43 inches from the x-ray tube on a table lined with lead to prevent back-scattering of the radiation. For most of the aircraft lap splice specimens, the applied voltage was 55 kV with the tube current at 2.5 mA for an exposure time of 60 secs. For some of the heavier specimens, 60 kV was applied. The x-ray images were recorded on Kodak Industrex M x-ray film and developed in-situ for immediate inspection. Several naturally corroded specimens retrieved from aging aircraft were also inspected. The x-ray results were largely disappointing, in that they failed to detect any corrosion in most of these specimens, even those that revealed significant amounts of corrosion on tear down and during visual inspection. Radiography was therefore employed only on two of the accelerated corrosion specimens: Boeing 727 specimen 43L6 and DC-9 specimen 56T21A.

Significant amounts of corrosion were obvious in the ambient views of the interior and exterior surfaces of both specimens. Virtually no corrosion was identified in the x-ray of the DC-9 specimen 56T21A. The x-ray of the Boeing 727 specimen 43L6 however, exhibited several dark areas which are indicative of corrosion within the lap splice.

b) Shadow Moiré

Shadow moiré is a simple and efficient means of obtaining whole-field contour maps of out of plane deformations. The surface topology of several of the corrosion specimens was mapped and recorded using this technique before, at an intermediate stage, and at the end of the accelerated corrosion process. The location and alignment of the grid over the specimen with consistent repeatability was achieved by mounting the grid on a frame with locating screws and supporting legs fitted with dial gauges for accurate recording of their vertical movements. The specimen was illuminated with a collimated light source from an angle of 45° and viewed through a high resolution CCD camera from vertically above. A grid with 200 lines per inch was used for the corrosion studies, which provided a sensitivity of 0.127 mm (0.005") per fringe.

Shadow moiré was found to be very sensitive to the pillowing deformation caused by artificially induced corrosion. Typical photographs of the moiré fringes obtained at different stages of exposure are displayed side by side for specimen 43L6 in Figure 4. The increase in the number of fringes with increasing periods of exposure is readily observable. The shadow moiré technique not only indicates the presence of corrosion, but also provides a quantitative measure of the corrosion buildup, since the moiré fringes are contours of constant lateral deflection. It may be noted that since a fringe of the opposite intensity lies halfway between two fringes of the same colour (black or white) one can reliably estimate changes in lateral heights equal to half the fringe sensitivity, i.e., of the order of 0.050-0.075 mm. The maximum pillowing deflections calculated from the fringe data are tabulated in Table 3, along with some remarks on the qualitative nature of the results observable from the images of each specimen. For most of the Boeing specimens the maximum pillowing was observed between fasteners in the same row rather than across the rows. In the case of the Douglas specimen (56T21A) the shadow moiré showed evidence of appreciable upward curling (of the order of 0.12 mm) of the free lip of the top skin, but did not indicate significant deformation of the skin between the top and bottom rivet rows. This appears to be due to the fact that the distance between the rivet rows in this specimen is three times that between the rivets in the same row, which causes the curvature to be restricted to the ends, and the middle segments of the strip to remain relatively flat (the modelling, described later, indicates that in the case of a rectangular panel of aspect ratio 2 pinned at the four corners, the deformation due to uniform lateral pressure at the midpoints of the long edges is 99% of that at the centre of the panel, while it is only 18% at the midpoint of the short edges [15]). This significantly reduces the ability of the inspector to detect pillowing visually in these joints and makes the enhanced capability of D Sight even more attractive. Based on the modelling results and shadow moiré measured deformations the specimens in the accelerated corrosion group contained from 2 to 7% corrosion.

c) Eddy Current

The eddy current inspection was performed as per Douglas specifications [16] using a Zetec MIZ-40 multi-frequency eddy current test instrument attached with a Tyvin LFSL-D low frequency differential eddy current probe (880 Hz to 10 KHz). A 450 mm manual XY positioner was used to locate the probe over the specimen. The data from the positioner and the analog XY information from the MIZ-40 was fed into a Dupont PortaScan PS1 portable colour scan imaging system, equipped with PS1S-MIZ40 Eddy Current Software. The PortaScan system provides an instant two-dimensional mapping of the information from the

eddy current probe filtered through gates which can be set to a desired value to display flaws. The following settings were used on the MIZ-40 system for inspecting the corrosion specimens: Frequency = 10 KHz, Gain 25 dB, Phase 80, H 2.0, V 1.6, Samples 500. The set up was calibrated using a reference specimen which consisted of two pieces of aircraft skin fastened together with bolts, one of which had rectangular grooves of different depths cut into its inner surface at regular intervals. It was found that the sensitivity of the eddy current probe was limited to a minimum thickness loss of about 0.23 mm (0.009 inches), so this value was used to set the gates in the PS1 imaging software for the corrosion samples. In aircraft NDT practice, it is accepted that eddy current methods are limited to about 10% loss of thickness in the first layer. There is evidence, confirmed at NRC after the tests described here were completed, that newer probes in a laboratory setting are capable of resolving corrosion thickness loss in the first layer down to approximately 5%. An example of a comparison of an eddy current result with a D Sight inspection is illustrated in Figure 5.

The eddy current testing was less effective on some Douglas specimens than on the Boeing specimens. The Boeing lap splices normally have rivet spacing equal to about an inch in length (25 mm), in the longitudinal as well as circumferential direction. The inter-rivet spacing on the Douglas specimens is about an inch and a half (37 mm) in the circumferential direction and only a third of that in the longitudinal direction. This close spacing caused spurious results in the eddy current tests since a probe with a diameter of 10 mm had to be used for scanning these specimens (rather than the 13 mm probe). Similarly, the proximity of the rivet row to the edge of the outer skin of the Douglas joints also resulted in a loss of sensitivity of the eddy current probe in this region.

The comparison of D Sight, shadow moiré and eddy current inspections carried out on specimens exposed to accelerated corrosion is summarized in Table 3. As should be expected the results show an excellent correlation between D Sight and shadow moiré since both are sensitive to bulging. Corrosion mapping from shadow moiré was not attempted as only part of a specimen could be inspected with this technique. This was due to the limited size of the available gratings. Out of 9 specimens reported in Table 3, five seemed to provide good correlation between eddy current and D Sight. In two specimens, the eddy current initially gave weak indication of corrosion than D Sight but with increase in time of exposure to accelerated corrosion, eddy current indications became stronger. This was the first indication that D Sight is more sensitive to lap splice corrosion than eddy current.

D Sight inspections of 39 specimens from the general specimen population and from the accelerated corrosion study were compared with their respective eddy current scan results. These correlations have been tabulated into four categories with total numbers of specimens in each category given in Table 4. These numbers can be further reduced to note that good correlation between D Sight and eddy current was obtained in 24 out of the total of 39 specimens (62%). The fact that a correlation was not observed in 15 specimens can be attributed to several factors:

- Greater sensitivity of D Sight (corrosion was confirmed by shadow moiré in four accelerated corrosion specimens in this category).
- D Sight is equally sensitive to the first and the second layer corrosion. Eddy current was used for first layer corrosion detection only since it can be expected to detect corrosion in the second layer of 20% or higher.

- Reworked lap splices with excessively thick sealant may appear similar to a corroded joint and produce D Sight false calls.
- When attempting to detect a low level of corrosion (2 to 3%) using D Sight an inspector may pick up some surface anomalies which were produced during assembly.
- Two eddy current indications in the fourth category were false calls caused by paint patches on the specimen surface (specimens were not stripped for eddy current).

Based on the first three categories in Table 4, the D Sight results indicate that the population of specimens was well balanced between non-corroded, corroded and lightly corroded specimens (11:13:12). The fourth category in Table 4 contained non-corroded or lightly corroded specimens and do not affect this balance (14:13:12). The final observation which can be made is that by adding the four (shadow moiré confirmed) corroded specimens from the third category to the second category (13+4) and adding the first and second category the total correct D Sight indication number was (14+13+4=31). This translates to a nearly 80% (31/39) success rate for the D Sight corrosion inspections supported by other NDT methods. The remaining 20% of specimens either contain a low level of corrosion or second layer corrosion both undetectable by eddy current or represent D Sight or eddy current false calls.

It is suggested that with the increase in the number of specimens subjected to accelerated corrosion and periodic moiré inspections, the uncertainty regarding the number of D Sight calls which could not be confirmed will be reduced substantially. Also improved eddy current probes with 5% corrosion resolution should reduce the uncertainty. Tear down of this group of specimens would also help resolve the issue. It is felt, however, that the number of destructive tests should be kept at a minimum, as the corroded specimens should be retained for future evaluations of improved D Sight and other NDT systems. An example of an in-service corroded specimen which was subjected to tear down subsequent to a D Sight inspection is shown in Figure 6. The D Sight inspection indicated light to moderate corrosion. Thickness loss measured ultrasonically was found to vary from 4% to 12%.

Excessive sealant application was mentioned as a possible cause of D Sight false corrosion indication. Most aeroplane operators can provide maintenance records which could help resolve such ambiguity. Removal of corrosion prior to application of sealing material and riveting reduces the original thickness of the skin. This is a general problem for all NDT techniques that measure thinning or bulging as an indication of corrosion. If maintenance records are not available these methods are not capable of differentiating between corrosion thickness loss and prior maintenance activity. Through a study, it may be possible to find differences in D Sight signatures caused by corrosion or excessive sealant application.

4. MODELLING OF PILLOWING DUE TO CORROSION - D SIGHT IMAGE SIMULATION.

The object of the model is to predict the extent of corrosion within the joint in terms of thickness loss at the internal surfaces of the lap splice skins from the amplitude of the pillowing in the outer skin. Also, the model can be used to generate simulated D Sight images of corroded lap splices for calibration of DAIS indications. An analytical model was first stage in the development used to determine the degree of corrosion pillowing in a plate that was fixed at the four corners. Finite Element Methods (FEM) in conjunction with the analytical model were then used to determine the amplitude of the pillowing in a lap

splice.

4.1. Analytical Model

An analytical model of the pillowing in fuselage joints has been developed on the premise that after the lap splice disbands, assuming the surfaces were initially bonded, the aircraft skin between the rivets deforms perpendicularly to the lap splice surface creating space within the joint to accommodate the additional volume required by the corrosion product.

The model initially assumes that the product of corrosion is distributed within the joint such that a uniform lateral pressure is exerted on the fuselage skins. It was also assumed that the joint was symmetrical about its mid-plane. Thus, only the outer skin of the lap splice was modelled. The closed-form classical plate theory of Timoshenko and Krieger [17] was used to calculate the deformation of the outer skin supported by equidistant rivets and subjected to a uniform lateral pressure. As a first approximation, the dimensions of the rivets are taken to be small, that is, they offer only point supports. The plate segment bounded by four rivets is considered to be pinned at its four corners and subjected to a uniform pressure. Symmetrical boundary conditions were applied to all four edges of the plate [15].

Results obtained from this model indicate that the amount of pillowing is independent of the thickness of the skin (given constant lap skin thickness ratio). In a lap splice with equidistant rivets the maximum deflection (in the centre of the modelled plate) is nearly four times the thickness of the skin material lost to corrosion. This helps to explain D Sight's high sensitivity to lap splice corrosion.

4.2 FEM Model

An actual lap splice can contain free edges and stiffeners which cannot be modelled using the closed-form solution. Therefore, finite element techniques were required to develop a model of an aeroplane lap splice. Two finite element models were generated, to determine the accuracy of the 3D general shell and 3D brick elements to model the out-of-plane displacements. The mesh size was refined to determine the effect that element size has on the accuracy of the results. From this study, it was concluded that the 3D general shell elements could not accurately model the pillowing effect. Upon refining the mesh, the 3D general shell elements produced results that were, at best, 7% higher than the closed-form solution while the 3D brick elements were within 2% [15].

The 3D brick elements were used to model a typical Boeing slice with a hat stiffener. Pillowing deformations were calculated first for 10% corrosion on each faying surface. The deformed surface was used to generate a D Sight image using ray tracing software. The resultant simulated image compares favourably with a D Sight image of a heavily corroded lap splice (Figure 7). Thus a capability to provide a D Sight inspector with a collection of calibration images for a particular aircraft type was demonstrated and will be the subject of further refinement.

5. DAIS FIELD TRIALS

5.1 USAF corrosion NDT evaluations

Valuable experience with D Sight based equipment was first obtained under a Canadian Department of Defence funded project. These tests involved inspections of CF-18 composite structures and lead to the development of a composites inspection head (DAIS 500). Later the same equipment was used during the two

stages of corrosion NDT equipment evaluations carried out by ARINC on behalf of USAF in Oklahoma City. The second of these trials led to a very structured study during which the corrosion findings in selected areas of a KC135 aircraft were correlated with tear down and x-ray based thinning measurement investigations. DAIS 500 (optimized for composites) was rated as excellent for its corrosion detection ability, while the false call rate and human factors associated with the use of the equipment were rated acceptable [18]. It should be added that the Oklahoma City trials took place before and during early stages of DAIS 250C corrosion equipment development. Based on their findings, ARINC has acquired a DAIS 250C system for rapid scanning of aircraft and two eddy current systems for local verification.

5.2 B-737-200 inspection

The authors evaluated the DAIS 250C in the field for the first time at the Federal Aviation Administration (FAA) Aging Aircraft NDT validation Center (AANC) operated by Sandia National Laboratories in New Mexico. The AANC has acquired one of the early Boeing 737-200 models for the purpose of providing a NDT test bed. The DAIS inspection followed two service bulletin calling for inspection of all longitudinal and circumferential lap splices from BS 259.5 to BS 1016. Over 85% of the inspection area was covered. The remaining 15% could not be inspected at the time due to the unavailability of suitable staging equipment at AANC. Time required to complete the inspections according to the service bulletin is 278 person-hours. After factoring the 15% of the fuselage which was not inspected, the DAIS inspection, including interpretation and documentation, took 36 person-hours. The result of the inspection was presented on a 'turtle' diagram and in detail on printed D Sight images. It should be mentioned that for this inspection, a 50% overlap was chosen for the DAIS head placement effectively doubling the number of D Sight images acquired.

The baselining effort (detailed inspection using standard NDT technologies) for the AANC aircraft has only been carried out recently and the results are not yet available, however during the last 10 months since the DAIS inspection several other NDT methods were evaluated on smaller sections of the aircraft. The Double Spring Hopping Probe method sensitive to disbonding, has shown at least 90% agreement with DAIS 250C results [19] (B737 splices are bonded).

5.3 Air Canada Maintenance Facility

A field trip to the Air Canada maintenance facility in Winnipeg, Manitoba, provided an opportunity to operate DAIS equipment on aircraft which were subjected to regular airline maintenance. Sections of a DC-9 undergoing a D2 check and an A-320 undergoing a C1 check were inspected without interference with other activities. A section of a Continental Airlines Boeing 727 aft belly skin was also inspected and was later removed and shipped to NRC in an attempt to correlate DAIS 250C findings with close visual inspection of the removed skin.

The skin is a section of the aircraft belly from BS 1010 to BS 1183 from S26L to S26R. It contains one circumferential butt splice at BS 1060. Several areas were repaired using riveted patches. All of the doublers, triplers and repair patches were included in the shipment. The substructure (stringers and frames) were not shipped with the skin sections (except for stringer 30). This presents some difficulty in correlating D Sight findings with close visual inspection (Figure 8) as it is very likely that in some locations it was the substructure which was corroding and not the skin as was the case in a few areas where corrosion affected the

doubler or stringer 30 but not the external skin. Because of this limitation some D Sight findings could not be confirmed by a close visual inspection of the skin at NRC. However, the opposite appears to be true - all close visual corrosion findings were confirmed by D Sight. The corroded areas under the repair patches where the corrosion product had been removed prior to patch application, as expected, did not produce D Sight corrosion signatures.

The field trials have provided a valuable experience in the use of DAIS equipment on large transport aeroplanes. Based on this experience, the production equipment currently under construction will be lighter, will provide a method of easy referencing of D Sight images to the specific location on the aeroplane and the inspection will be driven through a computer based plan. The image interpretation and reporting will be facilitated through the use of CAD software.

6. CONCLUSIONS AND RECOMMENDATIONS

Accelerated corrosion testing of lap splices should continue with the aim of reducing the uncertainty regarding D Sight corrosion detections at low levels of corrosion. The testing concentrated on DC9 and B727 lap splices should also be expanded to other aeroplane lap splice constructions.

Corrosion modelling and D Sight image simulation should be expanded to include a range of corrosion levels and other lap splice designs.

Both the modelling and accelerated corrosion testing should include corrosion in second and third faying surfaces as D Sight may have a distinct advantage over other NDT methods in these areas.

A study attempting to delineate differences between D Sight signatures for corrosion and excessive sealant application should be undertaken.

Certain lap splice designs are not amenable to unaided visual and eddy current inspections for corrosion.

DAIS 250C has a demonstrated rapid scan capability with high sensitivity for lap splice corrosion.

A library containing over 150 lap splice specimens has been established at the NRC for the purpose of developing corrosion detection NDT methods.

7. ACKNOWLEDGEMENTS

The authors wish to thank:

- FAA Technical Center, Transport Canada Transportation Development Centre, NRC and Diffracto Ltd. for the project funding.
- USAF, DND for additional financial support.
- D.L. Simpson (NRC) for his thoughtful guidance at the inception of the project.
- T. Marincak (NRC) and R. Reynolds (Diffracto) and numerous other colleagues from NRC and Diffracto Ltd. for their contributions.
- Air Canada, Continental Airlines and AANC for making their facilities and aircraft available for inspections.

8. REFERENCES

- [1] Goold, I. "Still Flying at Forty", Flight International, 26 May - 1 June, 1993, pp 33-44

- [2] Alcott, J. "An Investigation of Non-destructive Inspection Equipment: Detecting Hidden Corrosion on USAF Aircraft", Materials Evaluation, January 1994, pp 64-73.
- [3] U.S. Department of Transportation, Proc. of the International Conference on Aging Airplanes, June 1-3, 1988, DOT-TSC-FA890-88-26.
- [4] Komorowski, J.P., Gould, R.W., Pastorius, W.J. "A Technique for Rapid Inspection of Composite Aircraft Structure for Impact Damage" in "The Impact of Emerging NDI Methods on Aircraft Design, Manufacture and Maintenance," AGARD CP-462, May 1990, paper 11.
- [5] U.S. Patent #4,629,319, Dec. 16, 1986 - held by Diffracto Ltd. (D Sight™).
- [6] Komorowski, J.P., Simpson, D.L., Gould, R.W., "Enhanced Visual Technique for Rapid Inspection of Aircraft Structures", Materials Evaluation, December 1991, pp 1486-1490.
- [7] Keicher, J.A., and Roach, D., "FAA Sample Defect Library", Aging Aircraft NDI Validation Center, Sandia National Laboratories, Albuquerque, NM, June 1994
- [8] Krishnakumar, S., Komorowski, J.P. and Sproule, I., "Chemical Characterization of Corrosion Products in Fuselage Lap Joints", Rept. No. LTR-ST-1952, Institute for Aerospace Research, National Research Council of Canada, November 1993.
- [9] Uhlig, H.H., Revie, R.W., "Corrosion and Corrosion Control", John Wiley and Sons, New York, 1971.
- [10] Godard, R.W., Jepson, W.B., Bothwell, W.B. and Kane, W.B., "The Corrosion of Light Metals", John Wiley and Sons, New York, 1967.
- [11] Evans, W.B., "The Corrosion and Oxidation of Metals: Scientific Principles and Practical Applications", Edward Arnold (Publishers) Ltd., London, 1960.
- [12] Deltombe, E. and Pourbaix, M., "Corrosion", Vol.14, pp.496, 1958.
- [13] Hart, R.K., Trans. Faraday Soc., Vol.53, pp.1020, 1957.
- [14] Shipko, F.J. and Haag, R.M., Report KAPL-1740, General Electric Co., Knolls Atomic Power Laboratory, July 1957.
- [15] Bellinger, N.C., Krishnakumar, S., Komorowski, J.P., "Modelling of Pillowing Due to Corrosion in Fuselage Lap Joints", Journal of CASI, Sept., 1994.
- [16] Eddy Current Inspection, Detection of Corrosion Manual, page 42, paragraph 2.1.6, McDonnell Douglas.
- [17] Timoshenko, S., and Woinowsky-Krieger, S., "Theory of Plates and Shells", Second Edition, McGraw-Hill Book Company, 1959.
- [18] Alcott, J. et al., "Results of On-Aircraft Demonstration of Nondestructive Inspection Equipment to Detect Hidden Corrosion on USAF Aircraft", Prepared for OC-ALC/TIES Tinker AFB, ARINC Research Corporation, April 1994.
- [19] Rose, J.L., Rajana, K.M., Hansch, T.M., "A Report on a Field Trip to Sandia National Laboratories, AANC", Pennsylvania State University, Feb 11, 1994.

Serial number	Specimen number	Aircraft ID	Joint Type	Condition	Surface Treated	Period of Exposure
1	51L2	B727	Lap	Original		1104 hrs
2	43L6	B727	Lap	Original		1104 hrs
3	43L7R	B727	Lap	Rebuilt	1	1104 hrs
4	46L3A	B727	Lap	Rebuilt	1+2	1104 hrs
5	46L3C	B727	Lap	Rebuilt	1+2	1104 hrs
6	46L3E	B727	Lap	Rebuilt	1+2	1007 hrs
7	46L4A	B727	Lap	Rebuilt	1	1104 hrs
8	46L4C	B727	Lap	Rebuilt	2	1104 hrs
9	47-5	B727	Lap	Rebuilt	2	1007 hrs
10	56T1A	DC-9	Lap	Rebuilt	1	1007 hrs
11	56T1B	DC-9	Lap	Rebuilt	2	1007 hrs
12	56T1C	DC-9	Lap	Rebuilt	6	1007 hrs
13	56T21A	DC-9	Lap	Rebuilt	1+2	1104 hrs
14	56T10A	DC-9	Butt	Rebuilt	3+4	695 hrs
15	56T10B	DC-9	Butt	Rebuilt	5	695 hrs
16	56T10C	DC-9	Butt	Rebuilt	3+4	695 hrs
17	56T19A	DC-9	Butt	Rebuilt	3+5	1104 hrs
18	56T19D	DC-9	Butt	Rebuilt	3+4	1007 hrs
19	WA7A	DC-10	Butt	Rebuilt	3+4	695 hrs
20	WA7B	DC-10	Butt	Rebuilt	3+4	695 hrs

Table 1. List of specimens exposed to accelerated corrosion.

	Formula	Molecular Weight (gms/mole)	Density (gms/cc)	Molecular Weight Ratio	Molecular Volume Ratio Vmr
Pure Aluminum	Al	26.98	2.702	1	1
Aluminum Oxide	Al ₂ O ₃	101.96	3.965	3.779	2.575
Aluminum Oxide Monohydrate	Al ₂ O ₃ .H ₂ O	119.96	3.014	4.446	3.986
Aluminum Oxide Trihydrate	Al ₂ O ₃ .3H ₂ O	155.96	2.42	5.78	6.454

Table 2. Molecular Volume Ratio of Aluminum Oxides

Specimen	D Sight result	Shadow Moiré	Eddy Current
56T21A	light corrosion	light corrosion	rivets too close for complete inspection
46L3E	mostly middle row but also light corrosion in top and bottom	mostly middle row (0.33 mm)	no indication
43L6	all corroded	all corroded but less in top row (0.18 mm)	all corroded
51L2	bottom, middle and top rows corroded	bottom, middle but less in the top row (0.13 mm)	weak indication in all rows
46L4C	top, middle and bottom but not everywhere	top, middle and bottom but not everywhere (0.25 mm)	some corrosion indication
46L4A	all corroded	all but light (0.13 mm)	some areas mostly middle row
46L3C	all corroded	all corroded (0.18 mm)	most areas corroded
46L3A	middle and top row light corrosion	middle and top light corrosion (0.09 mm)	no indication
43L7R	all corroded	all corroded (0.18 mm)	little corrosion

Table 3. Comparison of D Sight with Shadow Moiré and Eddy Current.

Good correlation between D Sight and eddy current maps		No correlation	
No corrosion found by either method	Corrosion found by both methods	D Sight found corrosion but no eddy current indication	Eddy current indication but no D Sight confirmation
11	13	12	3

Table 4. Number of specimens in each inspection result category.

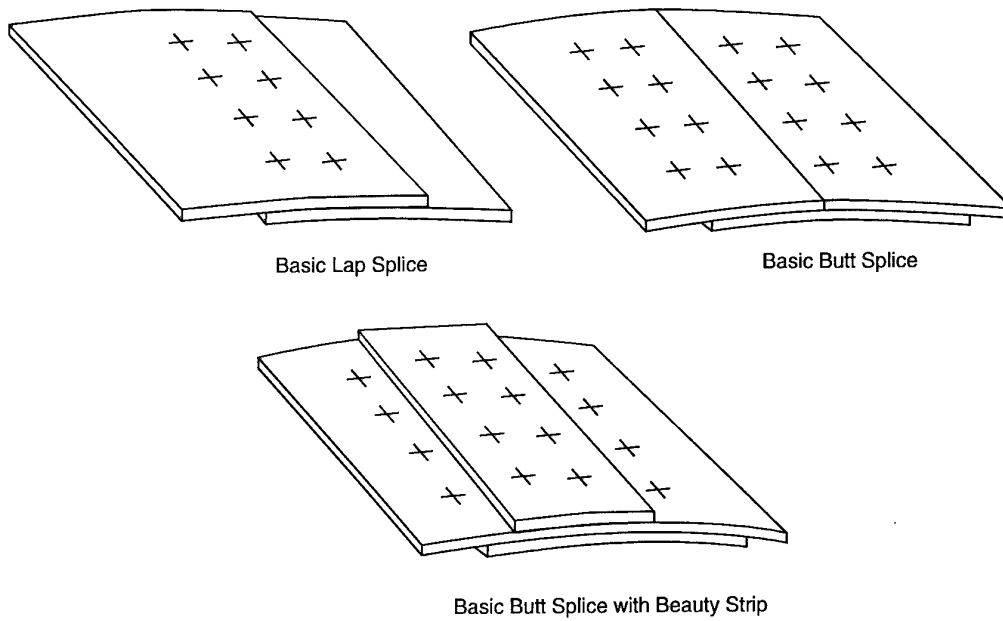


Figure 1. Basic aircraft fuselage lap splice designs.

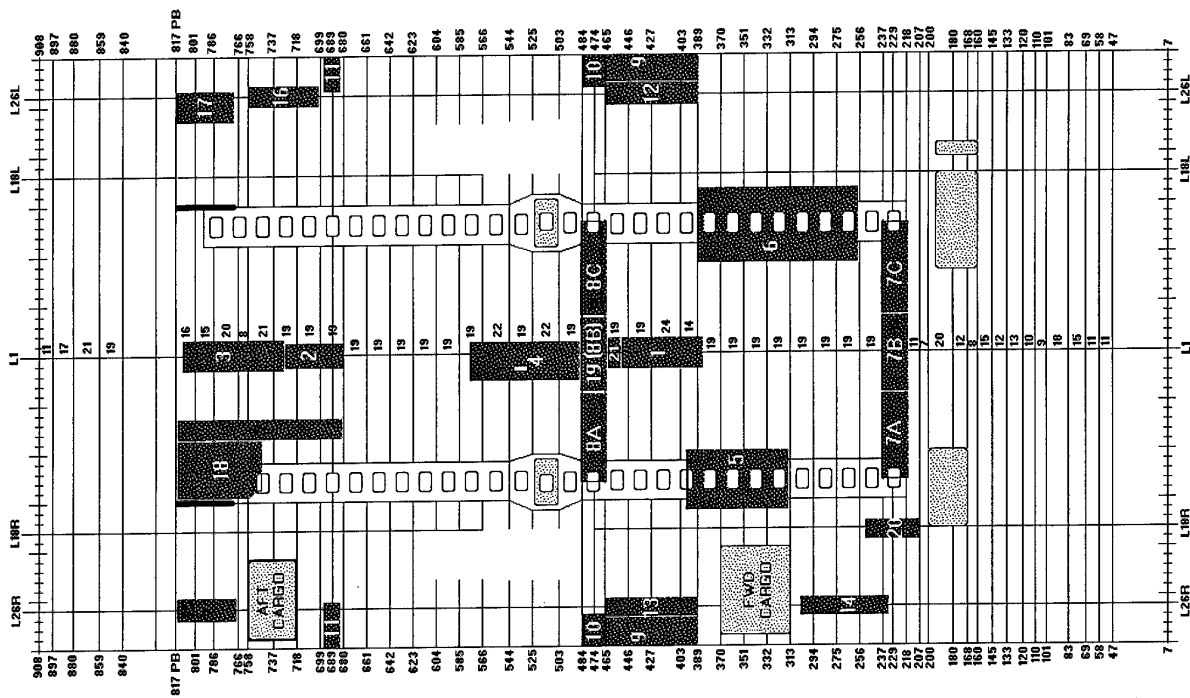


Figure 2 Specimens retrieved from DC9-14.

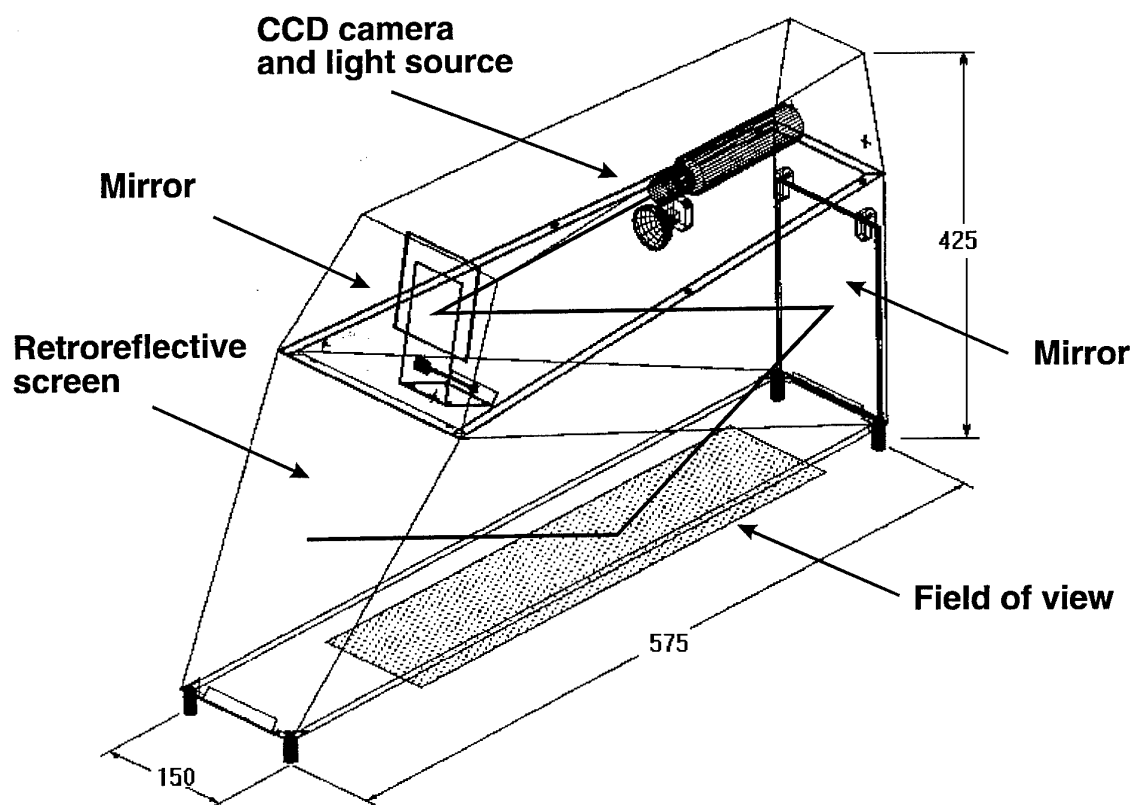
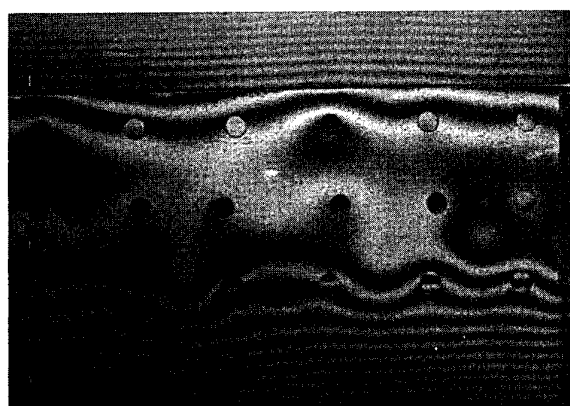
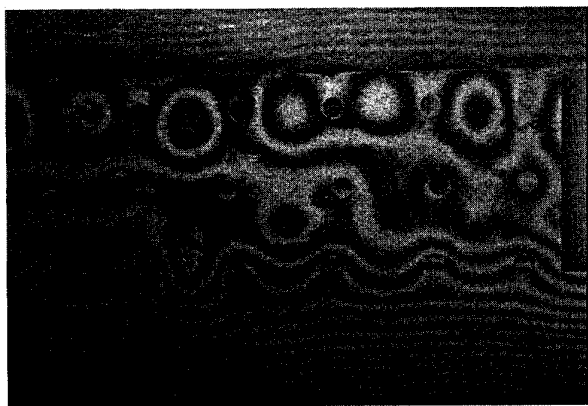


Figure 3. Schematic diagram of DAIS 250C inspection head

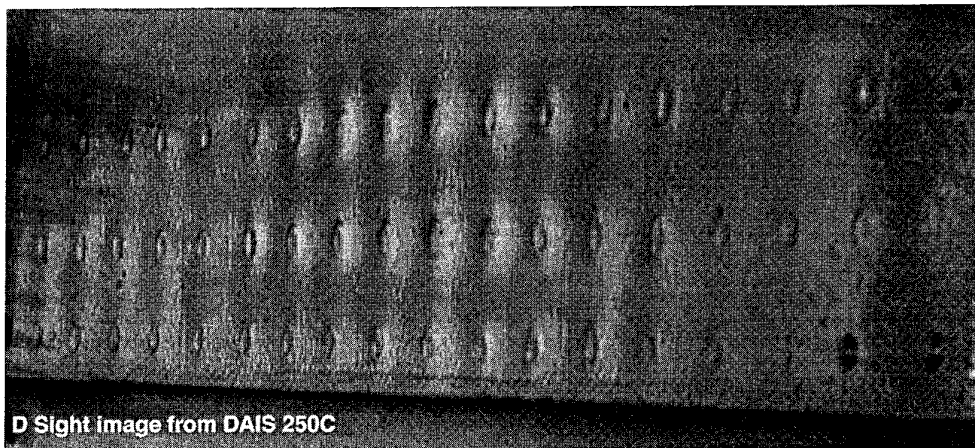


409 hours

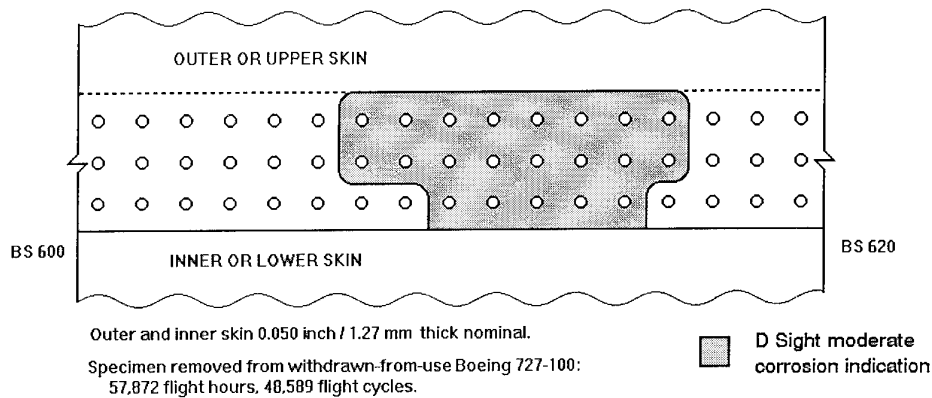


629 hours

Figure 4. Shadow Moiré of specimen 43L6 at two corrosion exposure times

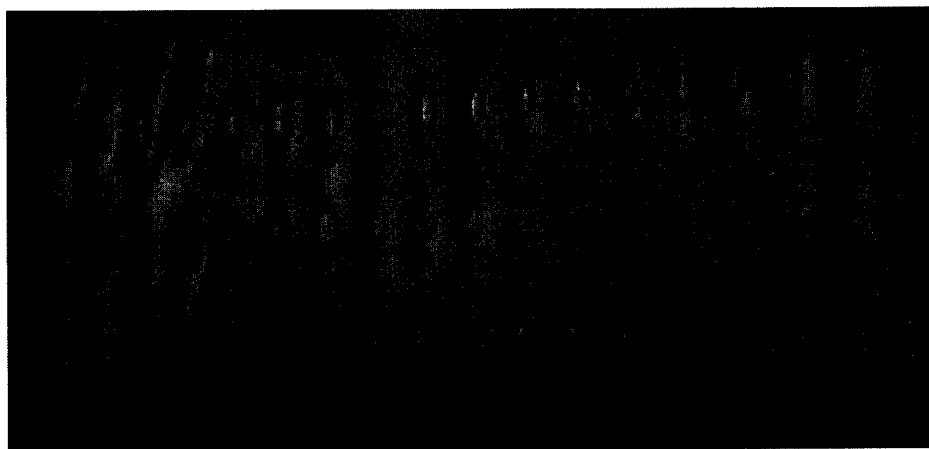


NRCC / CNRC DEFECT LIBRARY SPECIMEN 46L2
 DIFFRACTO LIMITED D SIGHT CORROSION INSPECTION
 STRINGER 19 LEFT (BS 600-620)

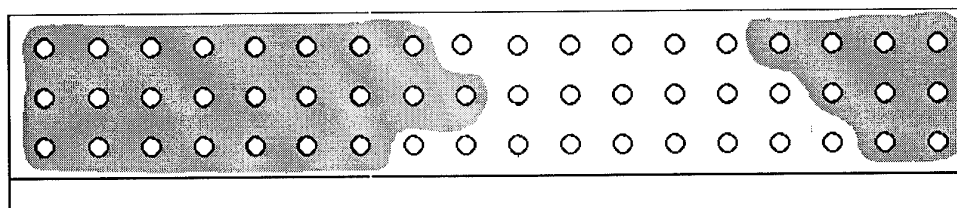


Eddy Current Inspection scan

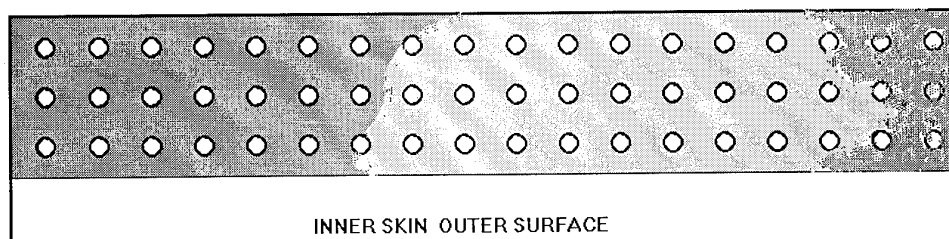
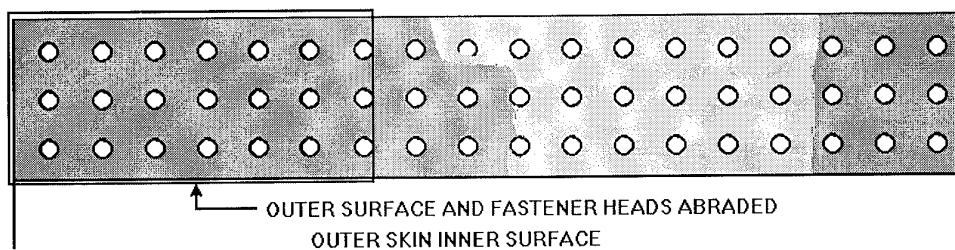
Figure 5. D Sight image, D Sight corrosion interpretation and eddy current scan showing corrosion.





D Sight image



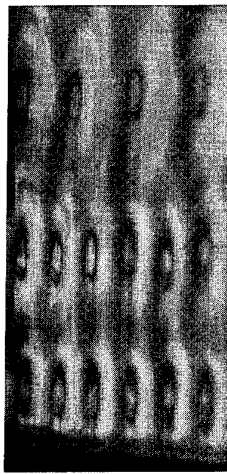
D Sight corrosion map



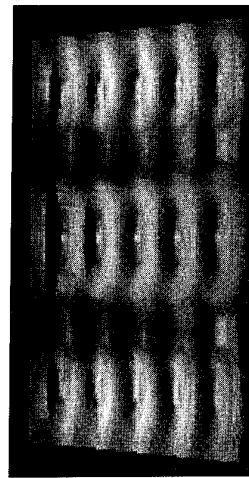
 CORROSION
 NO CORROSION

TEARDOWN INSPECTION OF SPECIMEN B727 51L1

Figure 6. Specimen 51L1 D Sight and teardown maps of corrosion



DAIS 250C image of a heavily corroded lap splice (two lower rivet rows).



D Sight image of 20% corrosion (10% in each faying surface) generated using ray tracing software based on FEM deformation computation.

Figure 7. Comparison of a DAIS 250C and simulated D Sight images.

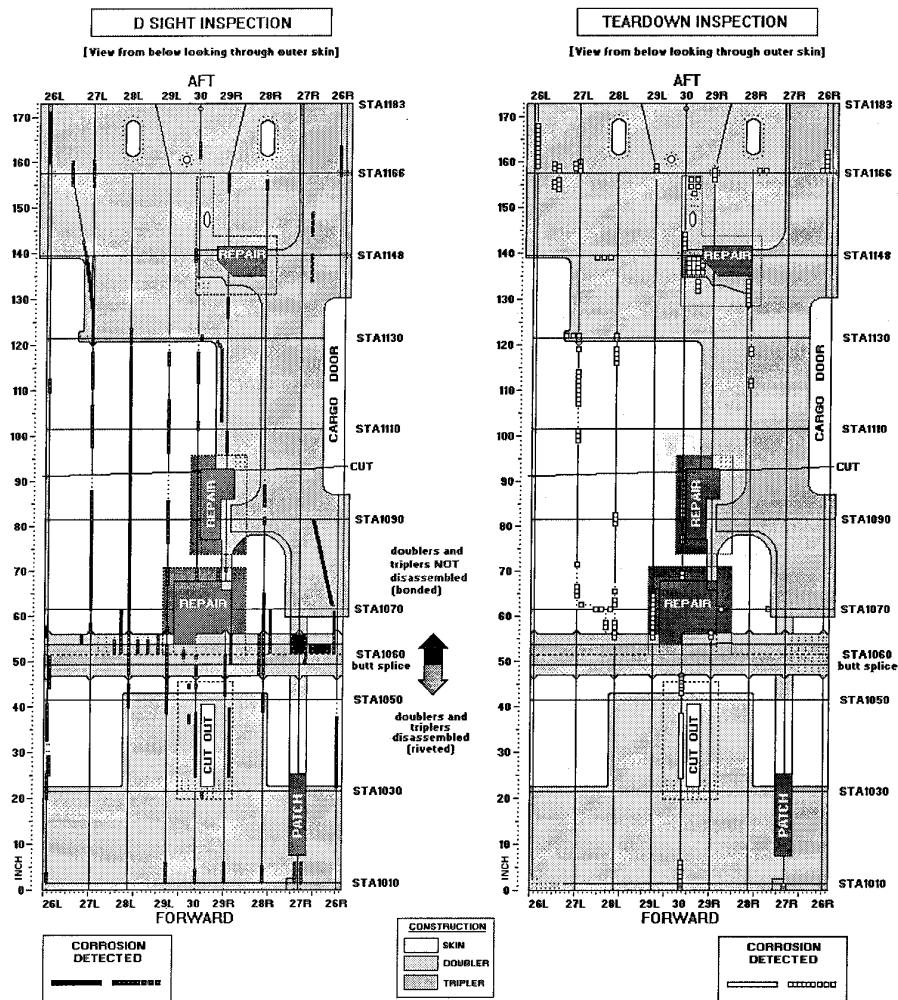


Figure 8. B-727 aft belly skin. Comparison of DAIS 250C and tear down inspections.

THE USE OF ELECTROCHEMICAL IMPEDANCE SPECTROSCOPY TO PREDICT THE CORROSION OF ALUMINUM-LITHIUM ALLOYS IN MARINE ENVIRONMENTS

D. R. Lenard and J. G. Moores
Defence Research Establishment Pacific
FMO Victoria, B.C., Canada VOS 1B0

P. R. Roberge and E. Halliop
Royal Military College of Canada
Kingston, ON, Canada K7L 2W3

SUMMARY

In order to acquire some experience with the behaviour of aluminum-lithium alloys in the marine environment, the Defence Research Establishment Pacific compared panels made from Aluminum Alloy (AA) 2090 and 8090 sheet with the conventional alloys AA 7075 and 2024, respectively, in several tests involving long term exposure to sea water fog and full or partial immersion in sea water. The results of these tests were then compared with the results of a new technique, developed by the Royal Military College of Canada for the analysis of electrochemical impedance measurements, that was performed on these alloys in simulated sea water. The long term exposure tests indicated that corrosion problems could occur with aluminum-lithium alloys in the marine environment. The 8090 alloy was found to suffer from severe localized attack, including intergranular cracking, along edges that were immersed in sea water. The 2090 alloy, however, appeared to offer some advantages over its 7075-T6 counterpart, as it was more resistant to corrosion at its edges, even though it suffered as much or more corrosion on the rolled surfaces. On some 2090 panels, the corrosion resistance of the edges was found to be enhanced by cold work associated with shearing. Polarization resistance measurements were generally consistent with the results of the long term exposure tests, although they predicted corrosion rates for the rolled surfaces of the 8090 and 7075 alloys that were apparently too high. The angle of depression of the Nyquist plots appeared to correlate with the number of corrosion sites within a given area and was in good agreement with visual observations of the long term exposure panels.

INTRODUCTION

Aircraft designers, manufacturers and operators are continually seeking new materials for aircraft structures that have higher strength-to-weight ratios in order to achieve significant weight reductions. A lighter airframe can result in lower fuel consumption, longer range, higher acceleration and/or heavier payloads. This search has led to heightened interest in the development and use of aluminum-lithium alloys. These alloys offer the promise of lower density, higher elastic modulus, higher strength and improved thermal stability when compared to conventional aluminum alloys^{1,2}.

Historically, improvements in mechanical properties with new alloys have often resulted in increases in susceptibility to corrosion that were not adequately studied prior to the specification of these alloys in aircraft structures. For example, aircraft designers were quick to specify the T6 temper of AA 7075 because of its high modulus and strength. It was subsequently discovered to be highly susceptible to stress corrosion and exfoliation in marine environments at great cost to aircraft operators³. As a result of this history and because elemental lithium is extremely reactive, there has been considerable interest in the corrosion susceptibility of aluminum-lithium alloys. A variety of accelerated corrosion tests⁴ and standard electrochemical techniques^{5,6} have been used to study the corrosion behaviour of Al-Li. No consistent picture of the corrosion resistance of these alloys has yet emerged. Although there is general agreement that localized corrosion can occur in these alloys, there are differences of opinion about the relative susceptibilities between different Al-Li alloys and with respect to conventional alloys⁷⁻¹⁰.

The Canadian Department of National Defence had been planning to acquire a new helicopter to replace its existing Sea King and Labrador fleets. The manufacturer of this helicopter favoured the extensive use of Al-Li sheet, extruded profiles and forgings. In order to acquire some first hand experience with the behaviour of these alloys in the marine environment, the Defence Research Establishment Pacific (DREP) subjected panels made from AA 2090 and 8090 sheet, along with 2024 and 7075 sheet, to several tests involving exposure to sea water fog and full or part immersion in sea water. The results of these tests were then compared with the results of a new technique developed and performed by the Royal Military College of Canada for the analysis of electrochemical impedance measurements on these alloys in simulated sea water.

ELECTROCHEMICAL IMPEDANCE SPECTROSCOPY

In recent years, electrochemical impedance spectroscopy (EIS) has found increasing use in the investigation of the mechanisms and rates of corroding systems. The nondestructive nature of the test, the short time needed to attain reproducible results and the need for electrochemical monitoring of corrosion processes in situ have all contributed to the growing acceptance of this method.

EIS data can be obtained by applying a small sinusoidal

current signal to a specimen and measuring the amplitude and phase shift of the resulting voltage. For many corroding interfaces, EIS measurements taken over a wide range of frequencies show a circular arc in the complex impedance plane when the real and imaginary components are plotted against each other in a Nyquist plot^{11,12}. By examining the impedance at appropriate frequencies, accurate values of the polarization resistance can be determined. Using the Stern-Geary equation, corrosion rates can be obtained as an inverse function of the polarization resistance¹³. In many systems of practical interest, analysis of EIS data is complicated by the fact that the Nyquist plots exhibit depression below the real axis, and by low corrosion rates which make it difficult to obtain reproducible results at all frequencies. Roberge and co-workers¹⁴⁻¹⁶ have recently developed statistical and geometric analysis techniques that have overcome these difficulties. Their procedure yields reliable values for both the polarization resistance and the angle of depression. In a recent study of mild steel specimens in inhibited sodium chloride solutions, they were able to obtain overall corrosion rates from the polarization resistance and to show a correlation between the angle of depression and the extent of localized corrosion (pitting)¹⁷.

EXPERIMENTAL PROCEDURE

The 76 x 76 mm panels used in the exposure tests were sheared from sheets made of Aluminum Alloys 2024-T3, 2090-T8, 7075-T6 and 8090-T851. Specimens made from AA 6061-T6, an alloy commonly used in marine applications, were included in the exposure tests and appear in some photographs but were not part of the comparison with electrochemical experiments. The nominal compositions of these alloys are shown in Table 1. Both surfaces of each panel were sanded with 120 grit silicon carbide abrasive paper and each panel was then fitted with two ceramic multiple-crevice washers (designed according to ASTM G78) that were held in place with a #12 stainless steel nut and bolt assembly that passed through a 6.3 mm central hole. Each bolt was fitted through plastic tubing to prevent contact with the aluminum panel. Each washer provided twelve separate sites for initiation of crevice corrosion. Each panel was suspended by way of a plastic-coated wire that was passed through a 3 mm hole that had been drilled in one corner of the specimen.

One set of specimens was exposed to a sea water fog at 35°C for four months in an Atlas SF850 Corrosive Fog Exposure System. The exposure was conducted according to ASTM B117 with the exception that natural sea water was used to generate the fog instead of the standard sodium chloride solution.

The remaining specimens were suspended in sea water that was drawn from the Strait of Juan de Fuca and directed through a tank measuring 16 X 62 x 177 cm. The sea water flowed past any specimen immersed in it at a rate of 1 cm/sec and was then returned to the Strait 40 m from the

intake. The water temperature in this location is within the range 7-11°C throughout the year. One set was suspended in a single row perpendicular to the direction of flow so that one half of the specimen was under water. A second set was suspended in a single row 1 m downstream from the first so that the entire specimen was immersed.

All specimens were removed after an exposure time of four months. After the specimens were dismantled the aluminum panels were cleaned by immersion in concentrated nitric acid. They were then rinsed with distilled water and allowed to dry after a final rinse with ethanol. Sections were cut from the panels and set in epoxy according to standard metallographic techniques in an effort to determine the depth of corrosion that had been initiated at the edges of the specimens.

The EIS specimens were cut to appropriate sizes for mounting in epoxy. The samples were mounted in a manner that would expose only one of each of three orthogonal planes that were parallel and/or perpendicular to the rolling direction of the sheet. Henceforth, these exposed planes will be called the rolled surface, the long transverse edge (perpendicular to the rolled surface and containing the rolling direction) and the short transverse edge (perpendicular to both the rolled surface and the rolling direction), respectively. Prior to mounting, provisions were made for electrical connection to the unexposed back of the samples and the unexposed edges were coated with an aluminum-vinyl anticorrosive paint to prevent crevice corrosion between the epoxy mount and the aluminum electrodes. After mounting, the specimens were polished (using 240, 400 and finally 600 grit papers) and cleaned with dichloromethane and acetone.

For each experiment, a pair of identical aluminum specimens (same alloy and same exposed face) were immersed in a 2 l beaker containing a solution of 3% sodium chloride for 14 days. Each cell was equipped with an air purge and a saturated calomel reference electrode brought into close proximity with one electrode by a Luggin probe. The mounted specimens were separated by 2.5 mm and kept in a stable parallel position with plastic holders.

Electrochemical impedance measurements were performed with a commercial generator/analyzer (Solartron Model 1255) at the corrosion potential and always taken in the direction of decreasing frequency. A potentiostat was not used in these measurements. The alternating current was applied between the two aluminum electrodes and kept at a value which would not cause more than 10 mV difference (peak to peak) across the cell. The reference electrode served only to measure electrochemical potential noise, which was independently monitored between EIS measurements. A custom-made multiplexer directed the inputs from each technique. The measurements could be performed automatically for up to eight cells in any order and in time intervals specified by the user. Polarization resistance values (R_p) were determined automatically during

experiments and the data were analyzed for their deviations from the semi-circle of a Nyquist representation.

At the completion of these experiments, the specimens were removed and examined with both optical and scanning electron microscopy to observe any differences in corrosion morphologies.

Finally, two new sets of 2090 panels were subjected to full immersion in sea water for three months. One set was prepared with sheared edges like those used in the earlier long term exposure tests while the edges of the other set were polished using progressively finer grit papers ranging from 80 to 600 grit. This procedure resulted in the removal of approximately 0.4 mm of material from each edge and produced a surface similar to that used in the EIS experiments.

RESULTS AND DISCUSSION

Long Term Exposures

A summary of the results of the long term exposures is shown in Table 2. After the exposure to the sea water fog, crevice corrosion had initiated under one site on the 8090 alloy. Some minor corrosion was also observed along rolling marks that became visible after the exposure. Deep pits were observed on the surface of the 2024 alloy, which also suffered crevice corrosion under six of the twenty-four initiation sites, with three of these sites showing substantial penetration. Deep pits were also observed on the surface of the 2090 alloy but crevice corrosion had not been initiated. Pitting had occurred on the surface of the 7075 alloy as well, but the depth of attack was not as severe as that which occurred on either the 2090 or 2024 alloy. This observation was consistent with the higher copper concentration present in the 2000-series alloys. Crevice corrosion was observed under one initiation site on the 7075 alloy.

In all cases, the specimens that were completely immersed in sea water showed a reduction in the intensity (depth of penetration) of corrosion, if any, in the crevices from that observed in the sea water fog exposures. This suggests that the corrosion that occurred in the crevices in the fog exposures was more a result of moisture retention in the crevices than a result of mechanisms such as differential aeration that are normally associated with crevice corrosion. The rolled surface of the 8090 sheet showed selective corrosion, without deep pits, that etched the surface in a manner which served to highlight the rolling direction of the sheet without causing much metal loss. Corrosion of the surface of the 2024 alloy was characterized by a large number of deep pits. Corrosion of the 2090 alloy occurred in the form of a smaller number of broad pits that were scattered over the surface. The number and severity of these pits increased near the edges of the panel. The surface of the 7075 alloy was characterized by a larger number of pits than the 2090, with the average pit on the

7075 having a smaller surface area.

The partial immersion test presented the toughest challenge to the alloys because the air/water interface created the possibility of differential aeration cells resulting from changing oxygen concentrations as a function of distance from the interface. In all cases, the interface was near the central hole. The rolled surface of the 8090 sheet suffered the least corrosion under these circumstances. In addition to the corrosion of the immersed surface described previously, several isolated but deep pits were observed at the air/water interface, as shown in Figure 1. Corrosion of the wetted area of the 2024 sheet was as severe as previously described but no additional corrosion was attributed to the presence of the air/water interface (Figure 2). The 2090 alloy surface appeared as before, with the addition of extensive corrosion at and just above the air/water interface (Figure 3). In this case the corrosion products produced at the interface crept up the panel, bringing along sea water by capillary action. The resulting "poultice" produced an excellent environment for the corrosion that ensued. A similar phenomenon was observed on the 7075 sheet (Figure 4).

The extent and type of corrosion on the edges of the exposed panels were often quite different than those found on the rolled surfaces. The 8090 panel exhibited one large pit on one of the edges but was essentially unattacked elsewhere. The edges of the 2024 panel exhibited two pits, one of which had initiated on the edge while the other was associated with a pit on the rolled surface. Large cracks were observed on the edges of the 7075 panel. These cracks are consistent with the development of intergranular cracking, to which 7075 is known to be susceptible. The edges of the 2090 and 6061 panels were essentially unaffected by the fog exposure.

The 8090 panel that was completely immersed in sea water exhibited only superficial corrosion on the rolled surfaces, while being severely attacked on the edges in a manner consistent with the selective corrosion often associated with intergranular cracking. This observation was confirmed by metallographic examination, which showed extensive intergranular cracking associated with the corrosion that had been initiated on the edge. The 2024 panel was severely corroded along the edges, with a combination of pitting of the edge and selective attack. No evidence of intergranular cracks associated with this corrosion could be found.

The 6061 panel showed some pitting along both edges. Although 6061 is known to be susceptible to shallow pitting in sea water, the observed intensity of attack was somewhat surprising. This was attributed to copper ions which plated out of the sea water after being introduced into it from the corroding 2000-series alloys in the partial immersion test that was conducted 1 m upstream. This hypothesis is supported by the lack of pitting observed on the 6061 panel in the partial immersion test. In this case the copper ions released from the 2000-series alloys were carried

downstream before they could affect the 6061 panel.

Metal loss on the edges of the 2090 panel was primarily associated with pits that occurred on the rolled surfaces. Several pits that appeared to have been formed in the centre of an edge were actually found to be part of a larger pit that had initiated on the rolled surface and then undercut the surface until they became visible again at an edge. One "crack" was found which did appear to have been initiated at the edge of the specimen. Metallographic examination revealed intergranular cracks at the base of the pit that resulted from the corrosion at this site. The 7075 panel showed virtually no corrosion along one edge and severe selective attack along each of the other three edges. The lack of corrosion of the one edge was considered to be anomalous as 7075 is known to be susceptible to corrosion in sea water¹⁸. This conclusion was supported by the observation of corrosion on all four edges of the salt fog specimens, which were exposed to a less aggressive environment than full immersion. Evidence of extensive intergranular cracking was also found on this specimen.

Figure 5 shows one of the edges of the panels that were partially immersed in sea water. The edge shown in this photograph was completely immersed in the sea water and, except for the observation that the 7075 panel showed selective attack along both immersed edges and the absence of corrosion on the 6061 panel as discussed previously, appeared similar to those of the specimens that had been completely immersed. One of the edges of the 7075 panel showing selective attack was the corresponding edge to the one which did not corrode in the full immersion exposure, adding support to our treatment of the edge that did not corrode as anomalous.

The effects of shearing or polishing the edges of the AA 2090-T8 panels after immersion in sea water for 4 months are shown in Figure 6. These effects are discussed in more detail in the section on the results of EIS.

Electrochemical Impedance Spectroscopy

The average corrosion rates, determined from the polarization resistance measurements, and the average depression angles for each face of each alloy are shown in Table 3. According to the polarization resistance data, the 8090 alloy showed roughly equal corrosion rates for all three faces. With the assumption that the angle of depression increases with increased pitting, the EIS data indicated that the rolled surface of the 8090 had the lowest pitting rate, followed by the long transverse edge and the short transverse edge, which had the highest rate. Examination of the surfaces of the EIS specimens with optical and scanning electron microscopy suggested that the correlation between angle of depression and pitting rate involved the number of pits formed in any given area (pit density) rather than the pit depth (Figure 7). The low pitting rate suggested by EIS for the rolled surface was consistent with visual observation of the long term exposure

panels. However, the approximate equivalence of the corrosion rates for all three faces was not. If the interpretation of the EIS data is correct, the corrosion of the rolled surface must occur at this high rate during the initial 14 days in which EIS data was collected, but then fall to a very low value over the longer term. The polarization resistance data for the 2024-T3 alloy showed a pronounced difference in overall corrosion rate between its rolled surface and its edges, with the edges having consistently higher rates. A similar trend was observed for the angle of depression, the average of which would fall to about 13° without the data points collected in the first 50 hours. These results are consistent with observations made on the long term exposure panels, which were characterized by a higher density of localized corrosion sites on the edges.

On the basis of the EIS data, the conclusion would be reached that the edges of the 8090-T851 alloy had lower overall corrosion rates and were less prone to pitting than their 2024-T3 counterparts. The edges of the 8090 long term exposure panels had substantial areas where no visible corrosion occurred. This could be consistent with the lower overall corrosion rates and lower pitting density suggested by EIS in comparison with 2024. However, the depth of attack within each pit was as large or larger than a corresponding pit on 2024. Thus the rate of corrosion within a pit was as least as severe for 8090 as for 2024. EIS alone gave no indication of this phenomenon, which was also observed on the EIS specimens when they were examined after they were removed from the electrochemical cell. The polarization resistance values for the rolled surfaces of the 8090 and 2024 were approximately equal. This result does not correlate with the appearance of the long term exposure panels. As discussed previously, corrosion of the rolled surface of the 8090 must initially occur at a high rate, but then fall to a much lower value over the longer term. The lower pitting density suggested by EIS for the rolled surface of the 8090 was, however, consistent with visual comparison of the long term exposure panels.

According to the polarization resistance data, the rolled surface of the 2090-T8 specimens had a lower overall corrosion rate than either of the long transverse or short transverse edges, which were themselves corroding at roughly equal rates. The rolled surface also had a lower angle of depression than either of the edges throughout the duration of the experiment. As with the 8090 alloy, the angle of depression corresponds well with the number of pits found on these surfaces at the end of the experiment. This does not, however, correlate with the corrosion observed on the long term exposure panels. As previously discussed, most of the corrosion of the edges of these panels was associated with pits that had developed on the rolled surfaces. We postulated that this inconsistency between EIS and long term exposure experiments could be caused by the different methods of preparation of the edges. The exposed surfaces of the EIS specimens were cut and then polished whereas the original long term exposure

panels had been sheared. The edges of these panels did not receive any subsequent preparation. The appearance of the edges of the two sets of 2090 specimens that were fully immersed in sea water for three months support this hypothesis. The polished edges showed pitting that had been initiated on the edges while most of the corrosion of the sheared edges was associated with pits that had developed on the rolled surfaces (Figure 6). Furthermore, the greatest depth of corrosion attack on the rolled surfaces of the panels with sheared edges occurred immediately adjacent to those edges. A similar phenomenon was not observed on the specimens with polished edges. Thus the cold work associated with shearing appeared to reduce the initiation of corrosion on the edges. This conclusion was supported by the corrosion observed around the identifying numbers that had been scratched into the rolled surfaces. The numbers themselves suffered no corrosion while the surrounding surfaces had been preferentially corroded to the extent that the depressions created by the scratches became higher than the adjacent material. Slife⁶ also postulated that cold work could have an effect on the corrosion rate of AA 2090.

The corrosion rate determined by polarization resistance for the rolled surface of the 7075 was higher than that measured for the edges. This was not consistent with the appearance of the long term panels, which suffered more metal loss along the edges than the rolled surface. The angle of depression data indicated that the rolled surface of the 7075 had the lowest pitting density, while the long transverse and short transverse edges had higher rates. These results did correlate very well with the long term exposure tests, in which the edges did indeed suffer much worse localized attack.

According to the polarization resistance data, the rolled surface of the 2090 alloy had a consistently lower corrosion rate than the same surface of the 7075. This did not appear to be consistent with the long term exposure tests, in which corrosion damage seemed to be more extensive on the surface of the 2090 alloy. On the other hand, the polarization resistance data suggested that the edges of the 2090 were only slightly more corrosion resistant than the 7075 edges. Once again, this did not appear to be consistent with visual observation of the long term exposure panels. In this case, the edges of the 2090 panels, whether sheared or polished, suffered noticeably less corrosion than their 7075 counterparts. The angle of depression data indicated that the pit density should be lower on the rolled surface of the 2090 than the 7075 and that the pit density should be much lower on the edges of the 2090 than the 7075. These results are completely consistent with the appearance of the long term exposure panels. As was the case for the comparison between the 8090 and 2024 alloys, the angle of depression data for the 2090 and 7075 alloys provided a better correlation with the long term exposure tests than the polarization resistance measurements. However, as in the case of the 8090 alloy, the correlation involved only the pit density, not the rate of attack within

each pit (Figure 8).

CONCLUSIONS

The long term exposure tests indicated that the rolled surfaces of the 8090-T851 sheet were more resistant to corrosion than the conventional 2024-T3 sheet. Except for some pits which developed at an air/water interface, these surfaces suffered only minor corrosion which highlighted rolling marks in the 8090 sheet. Although this material did suffer corrosion under one crevice in the exposure to sea water fog, the attack was less severe than that observed on the 2024. However, the 8090 experienced severe localized attack along edges that were immersed in sea water. A smaller proportion of the surface area of the 8090 edges was attacked than of the 2024, but the depth of attack within a corroding area was at least as severe as for 2024.

The corrosion rate determined by polarization resistance for the rolled surface of 8090 appeared to be much higher, in relation to the edges and to the rolled surface of the 2024, than that observed on the long term exposure panels. Examination of the EIS specimens with optical and scanning electron microscopy suggested that a correlation existed between the angle of depression and the number of pits in a given area. Conclusions drawn from the angle of depression data were consistent with the appearance of the long term specimens.

Evidence of intergranular corrosion was not found on the 2024 specimens. Severe intergranular cracking was found to be associated with the pitting initiated at the edges of the 8090 alloy. Unless care is taken to seal the edges of components made from 8090-T851 and to deny access of sea water to crevices, then corrosion failures can be expected to occur even though exposed surfaces of the alloy may appear undamaged.

The long term exposure tests indicated that the rolled surfaces of the 2090-T8 sheet suffered as much or more corrosion damage than their counterparts on the 7075-T6 sheet. Some fairly deep pits occurred on the rolled surfaces of the 2090, even in the exposure to sea water fog. This result was not surprising, given the higher copper concentration in the 2090 alloy. However, increased corrosion was not observed under the crevice initiation sites and localized corrosion was substantially reduced along the edges. Both alloys showed extensive corrosion under a poultice of corrosion products at the air/water interface in the partial immersion test. Intergranular cracking was observed at the base of a pit on the edge of a 2090 panel, while extensive intergranular cracking was found on the 7075 panels. Such cracking can, of course lead to structural weakness without much visible corrosion. Thus, the 2090 alloy does appear to offer some advantages over 7075-T6 sheet. Corrosion initiated at edges, whether pitting or intergranular cracking, is very difficult to detect on an aircraft structure. The 2090 sheet appears to be more resistant to corrosion at the edges than the 7075. Corrosion

of the rolled surfaces of the 2090 sheet can easily be controlled by the proper application of protective coatings.

The angle of depression data was found to correlate well with the pit density observed on the rolled surface and edges of the 2090 EIS specimens, but not with the long term exposure panels. Additional tests suggested that the corrosion resistance of the edges of the long term panels was due, in part, to cold work associated with shearing. Nonetheless, even the edges of cut and polished specimens of 2090 showed much less corrosion than their 7075 counterparts. As was the case for the 8090 alloy, the polarization resistance data suggested a higher corrosion rate for the rolled surface of the 7075 than that observed in the long term exposure tests. However, the angle of depression data correlated very well with the appearance of the long term panels. Furthermore, conclusions drawn from the angle of depression data on the comparative behaviour of the 2090 and 7075 alloys were completely consistent with those drawn from the appearance of the long term panels.

Because the polarization resistance measurements resulted in corrosion rates for the rolled surfaces of 8090 and 7075 that were too high in relation to their edges and to the alloys against which they were compared, the angle of depression of the Nyquist plots provided a better correlation with visual observations of the long term exposure panels. However, the EIS measurements were apparently insensitive to the existence of intergranular cracking and to the rate of corrosion within a pit. Thus, EIS can be a useful technique for rapidly assessing the relative corrosion resistance of different aluminum alloys but cannot be used in isolation to completely characterize the corrosion resistance of an alloy.

REFERENCES

1. W. E. Quist and G. H. Narayanan, "Aluminum-Lithium Alloys" in "Treatise on Materials Science and Technology", edited by A. K. Vasudevan and R. D. Doherty, Vol. 31, pp. 219-250 (1989)
2. R. J. H. Wanhill, L. Schra and W. G. J. Hart, International Conference AIM/ASM on Evolution of Advanced Materials, Milano, Italy, 31 May-2 June 1989
3. S. J. Ketcham and J. J. de Luccia in "Aircraft Corrosion", AGARD Conf. Proc. No. 315 (1981)
4. C. J. E. Smith, J. A. Gray, L. Schra and J. A. M. Boogers in "New Light Alloys", AGARD Conf. Proc. No. 444
5. R. G. Buchheit Jr., J. P. Moran and G. E. Stoner, Corrosion, Vol. 46, pp. 610-617 (1990)
6. R. I. Slife, Corrosion 88 Conf., St. Louis, Paper No. 385, NACE
7. B. B. Bavarian and M. Zamanzadeh, Corrosion 88 Conf., St. Louis Paper No. 386, NACE
8. J. P. Moran, E. A. Starke Jr., G. E. Stoner and G. L. Cahen Jr., Corrosion, Vol. 43, pp. 374-382 (1987)
9. T. Sheppard and N. C. Parson, Mat. Science and Tech., Vol. 3, pp. 345-352 (1987)
10. R. T. Holt, Canadian Aeronautics and Space J., Vol 35, pp. 128-137 (1989)
11. K. Hladky, L.M. Callow and J.L. Dawson, Br. Corros. J., Vol. 15, pp 20-25 (1980)
12. M.W. Kendig, E.M. Meyer and G. Lindberg, Corros. Sc., Vol. 23, pp. 1007-1015 (1983)
13. D.C. Silverman and J.E. Carrico, Corrosion, Vol. 45, pp. 280-287 (1988)
14. P.R. Roberge and R. Beaudoin, J. Appl. Electrochem., Vol. 18, pp. 38-42 (1988)
15. P.R. Roberge and R. Beaudoin, J. Appl. Electrochem., Vol. 18, pp. 601-607 (1988)
16. P.R. Roberge, E. Halliop, M. Asplund and S.V. Sastri, J. Appl. Electrochem., Vol 20, pp. 1004-1008 (1990)
17. P.R. Roberge, V.S. Sastri and V. Maxwell, Corrosion, Vol. 48, p. 333 (1992)
18. Godard, H.P., Jepson, W.B., Bothwell, M.R. and Kane, R.L., "The Corrosion of Light Metals", Wiley and Sons, New York, p. 140, (1967)

Table 1. Nominal composition of alloys tested, wt-%

Alloy	Li	Cu	Mg	Si	Fe	Mn	Zn	Zr
2024	-	3.8-4.9	1.2-1.8	0.5	0.5	0.3-0.9	0.25	-
2090	1.9-2.6	2.4-3.0	0.25	0.1	0.12	0.05	0.1	0.08-0.15
6061	-	0.15-0.40	0.8-1.2	0.4-0.8	0.7	0.15	0.25	-
7075	-	1.2-2.0	2.1-2.9	0.4	0.5	0.3	5.1-6.1	-
8090*	2.35	1.23	0.67	0.02	0.03	0.001	0.02	0.11

Note a: Actual heat analysis for the material supplied by ALCAN

Table 2. Results of long term exposure tests.

Alloy	Salt Fog		Total Immersion		Partial Immersion (air/water interf.)
	rolled surface	minor	rolled surface	minor selective corr.	a few deep pits
8090-T851	edges	1 pit	edges	severe selective attack (cracking)	
	crevices	1 site			
	rolled surface	many deep pits	rolled surface	many deep pits	no additional corrosion
2024-T3	edges	2 pits	edges	severe pitting and selective attack	
	crevices	6 sites			
	rolled surface	deep pits	rolled surface	broad pits	extensive "poultice" corrosion
2090-T8	edges	no attack	edges	pits initiated on rolled surface	
	crevices	none			
	rolled surface	shallow pits	rolled surface	many small pits	extensive "poultice" corrosion
7075-T6	edges	large cracks	edges	severe selective attack	
	crevices	1 site			

Table 3. Average corrosion rates from polarization resistance measurements and average depression angles during 14 days of exposure.

Alloy	Face	Corrosion Rate (mm/y)	Angle of Depression (degrees)
8090-T851	Rolled Surface	0.05	6
	Long Transverse	0.04	12
	Short Transverse	0.03	17
2024-T3	Rolled Surface	0.05	17
	Long Transverse	0.16	21
	Short Transverse	0.22	23
2090-T8	Rolled Surface	0.06	10
	Long Transverse	0.08	16
	Short Transverse	0.09	19
7075-T6	Rolled Surface	0.14	12
	Long Transverse	0.11	33
	Short Transverse	0.12	29

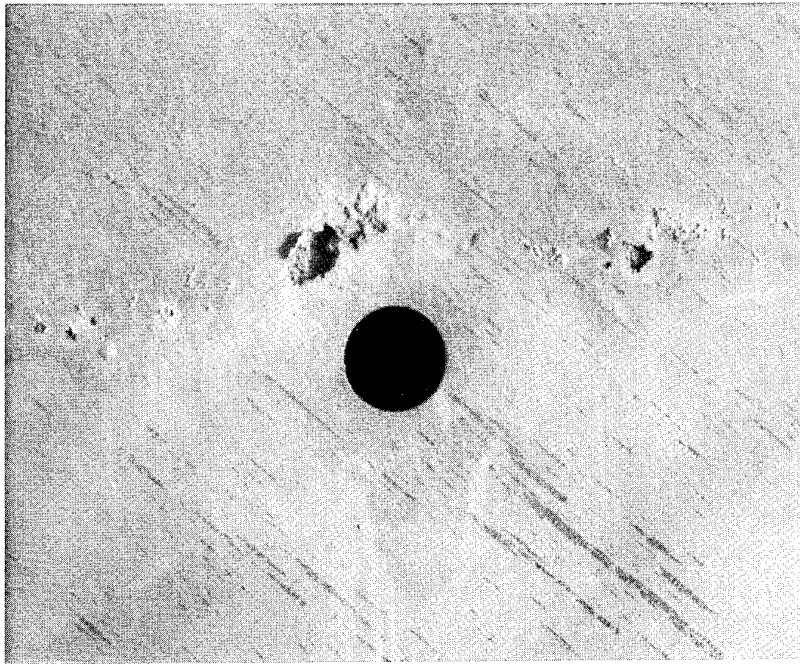


Figure 1. Appearance of AA 8090-T851 panel after partial immersion in sea water for four months. The air/water interface was near the top of the central hole.

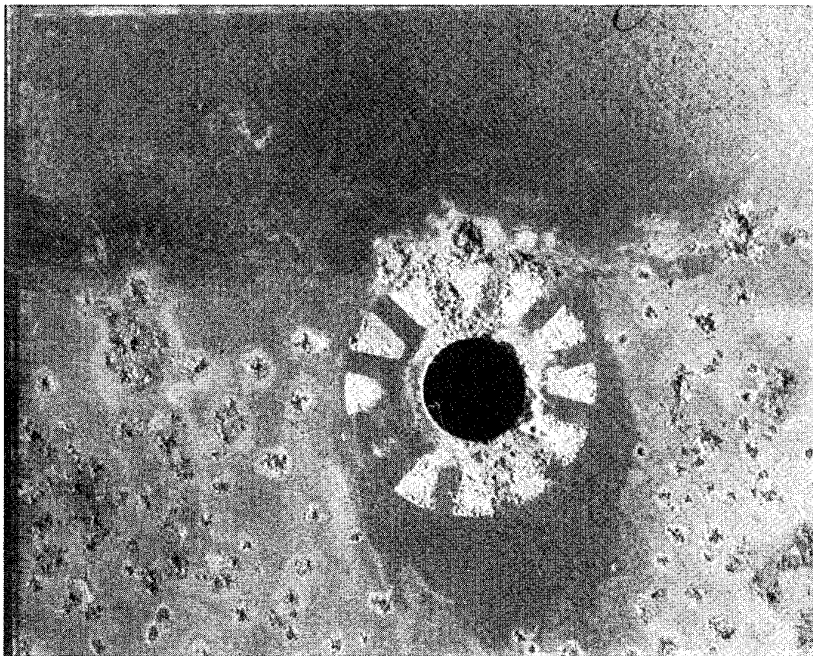


Figure 2. Appearance of AA 2024-T3 panel after partial immersion in sea water for four months. The air/water interface was near the top of the central hole.

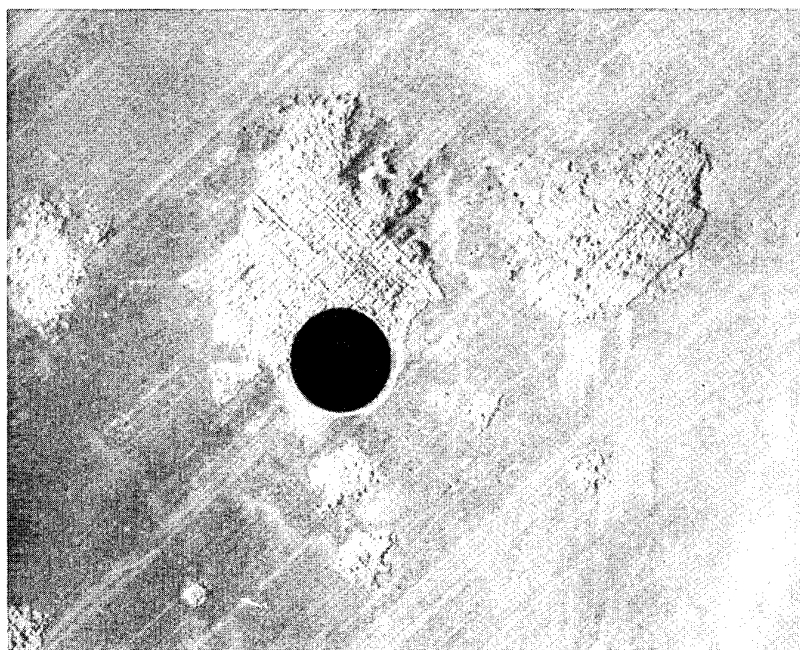


Figure 3. Appearance of AA 2090-T8 panel after partial immersion in sea water for four months. The air/water interface was near the top of the central hole.

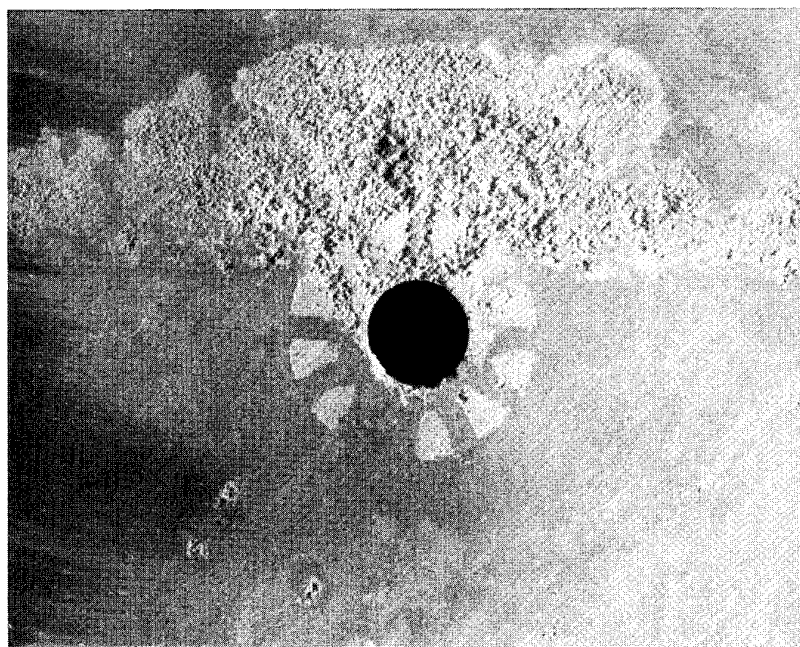


Figure 4. Appearance of AA 7075-T6 panel after partial immersion in sea water for four months. The air/water interface was near the top of the central hole.

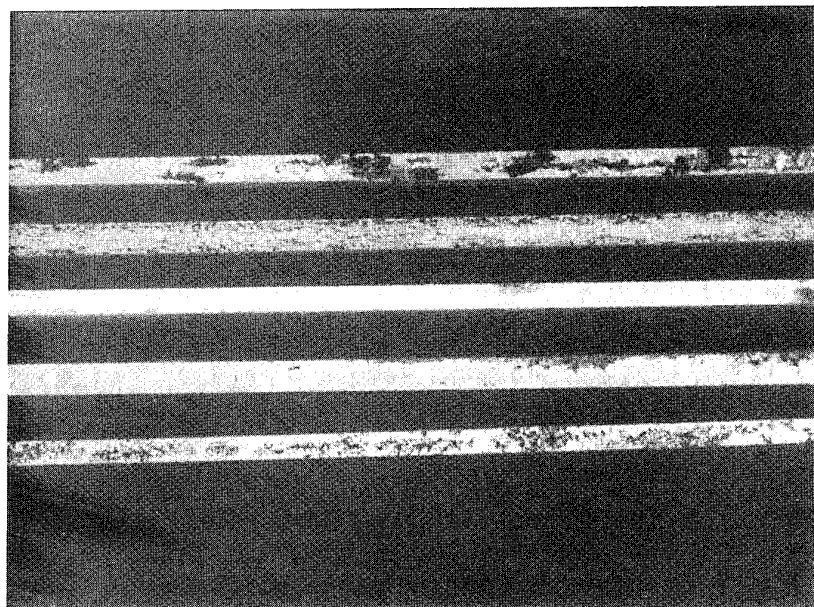


Figure 5. Appearance of the edges of the aluminum panels partially immersed in sea water for four months. These edges were completely immersed throughout the test. From top to bottom: (i) 8090-T851, (ii) 7075-T6, (iii) 6061-T6, (iv) 2090-T8 and (v) 2024-T3.

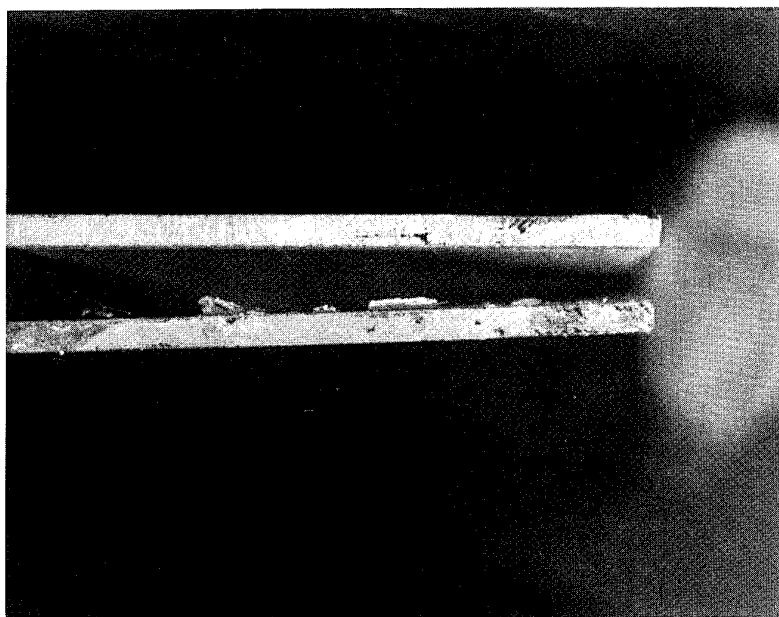
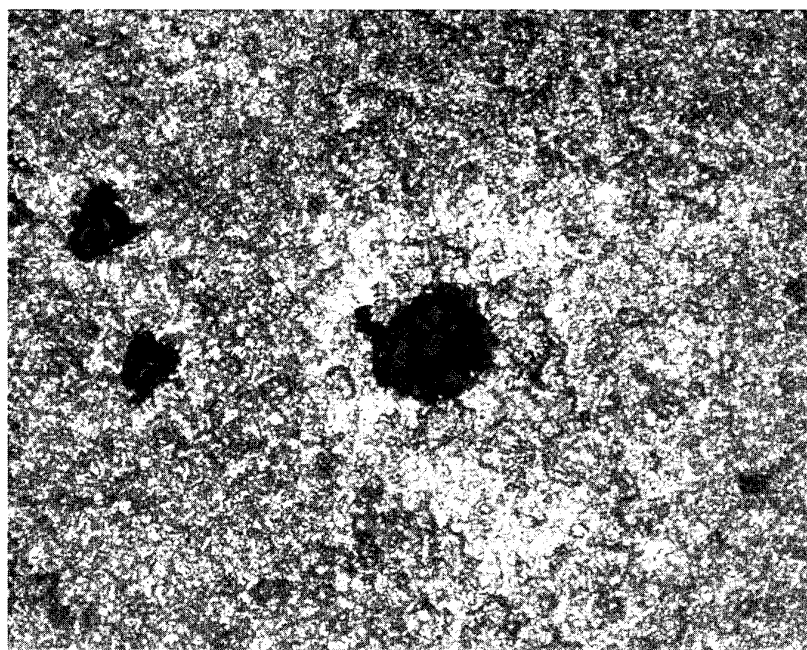


Figure 6. Appearance of the edges of the AA 2090-T8 panels after immersion in sea water for four months. The top panel has sheared edges while the edges of the lower panel were polished.

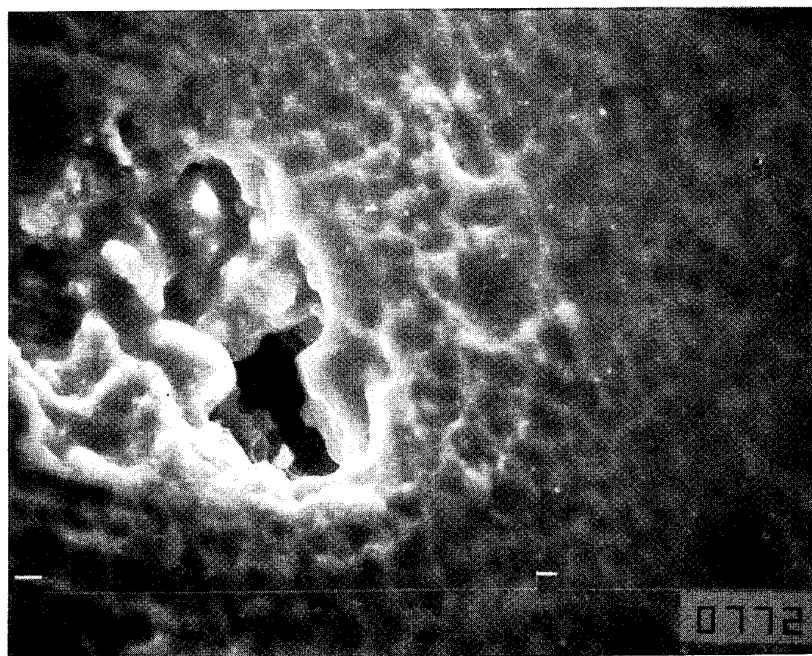


(a)

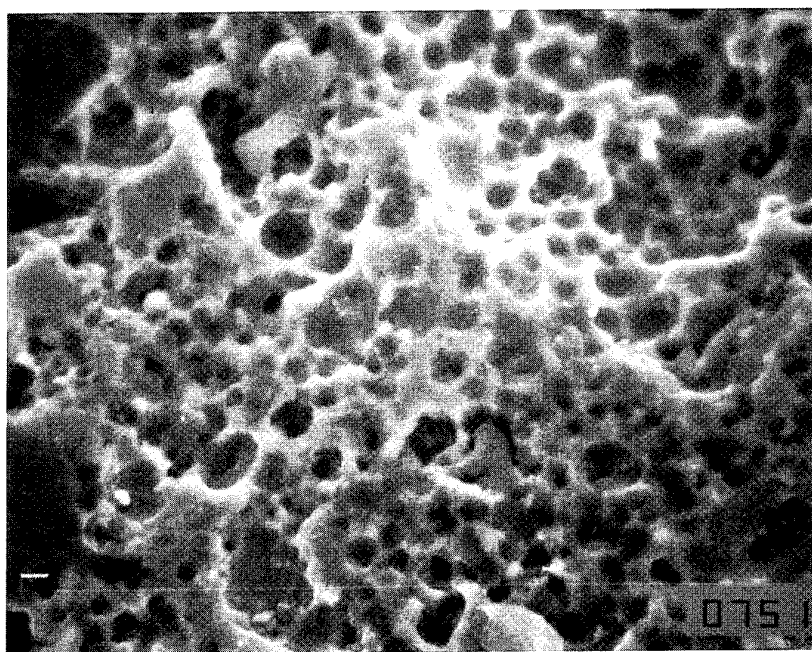


(b)

Figure 7. Micrographs of two surfaces of AA 8090-T851 at the end of the EIS experiments. (a) Rolled surface. (b) Long transverse edge. 100x.



(a)



(b)

Figure 8. Scanning electron micrographs of short transverse edges after EIS experiments for: (a) 2090-T8 (b) 7075-T6. 700x.

Non-Destructive Detection of Corrosion for Life Management

David A Bruce
Structural Materials Centre
Defence Research Agency
Farnborough, Hampshire,
GU14 6TD, UK

© British Crown Copyright 1994 /DRA

Published with the permission of the Controller
of Her Britannic Majesty's Stationery Office

1 SUMMARY

In recent years, aircraft operators have been driven to increased use of Non-Destructive Evaluation (NDE) to ensure airworthiness during life extensions for ageing aircraft or as an integral part of a damage tolerant lifting philosophy. Major airframe static and fatigue tests are routinely used to highlight problem areas on airframes where design limitations or changes of usage may lead to early failures. The results of such tests become progressively less reliable as the age of the airframe increases and the operating conditions diverge from those under which the tests were conducted. Increased inspection, whether by visual or other means is usually the only alternative to wholesale refurbishment or replacement of aircraft or components. Almost all of the development to date of NDE techniques for corrosion detection and characterisation has been concentrated on existing airframe materials, principally Aluminium alloys and steels. The current capabilities of corrosion detection techniques will be reviewed and current research aimed at areas where there is a requirement for improved detection capability will be described. New materials, such as Polymer Matrix Composites, will experience different types of "corrosive" deterioration. The capability of NDE methods to detect material degradation in new composite materials will be discussed. Finally, reliance on NDE, choice of NDE technique and optimal scheduling of inspections all require an assessment of the reliability of NDE methods. It will be shown that a range of NDE techniques with differing capabilities and characteristics will be required to ensure compatibility with maintenance schedules if full use is to be made of NDE for life management of structures which may be subject to corrosion.

2 INTRODUCTION

During the 1950s and 60s when many of the aircraft which are currently in service were initially designed, corrosion was not viewed as a serious life-limiting factor. During this period most aircraft were replaced in service due to technical obsolescence. A few types had to be prematurely retired when design limitations led to unexpected fatigue problems.

The last 20 years or so have seen a change in this picture. In both the civil and military fields, technical improvements to airframes has slowed down, becoming evolutionary rather than revolutionary. Existing airframes are retained in service on economic grounds. The cost of renovating the airframe, replacing and modernising engines and avionics, is substantially less than the investment required to replace the aircraft, while incurring only a limited performance penalty.

In recent years, aircraft operators have been driven to increased use of Non-Destructive Evaluation (NDE) to ensure airworthiness during life extensions for ageing aircraft or as an integral part of a damage tolerant lifting philosophy. Major airframe static and fatigue tests are routinely used to highlight problem areas on airframes where design limitations or changes of usage may lead to early failures. The results of such tests become progressively less reliable as the age of the airframe increases and the operating conditions diverge from those under which the tests were conducted. It has not been possible to incorporate the environmental effects which lead to corrosion into major airframe fatigue tests. Clearly this represents a major limitation in the use of fatigue tests to predict damage in ageing aircraft. Increased inspection, whether by visual or other means is usually the only alternative to wholesale refurbishment or replacement of aircraft or components.

Almost all of the development to date of NDE techniques for corrosion detection and characterisation has been concentrated on existing airframe materials, principally Aluminium alloys and steels¹. In section 2, current capabilities of corrosion detection techniques will be discussed along with ongoing research aimed at areas where there is a requirement for improved detection capability.

New materials, such as Polymer Matrix Composites, are coming into service on the most recent types of civil and military aircraft. These materials do not undergo the same corrosion processes which affect metals, nevertheless it is possible that they will experience different types of "corrosive" deterioration. The capability of NDE methods to detect material

degradation in such composite materials will be discussed in section 3. Finally, reliance on NDE, choice of NDE technique and optimal scheduling of inspections all require an assessment of the reliability of NDE methods. In section 4 the effect of the reliability of NDE methods on inspection intervals will be discussed briefly. It will be shown that a range of NDE techniques with differing capabilities and characteristics will be required to ensure compatibility with maintenance schedules if full use is to be made of NDE for life management of structures which may be subject to corrosion.

3 CORROSION DETECTION IN TRADITIONAL AIRCRAFT MATERIALS

3.1 Corrosion problems in aircraft

Corrosion causes problems for many industries, particularly power generation, oil and gas drilling and chemical engineering. NDE methods have been developed and are in regular use for corrosion detection in many situations. Various techniques are also used for monitoring corrosion rates as a guide to repair and maintenance scheduling^{2,3}.

The aircraft industry poses several unique problems in corrosion detection. The most pressing problems have been highlighted, since the Aloha incident in 1988, as the occurrence of corrosion in multi-layer structures such as lap joints. The NDE techniques which can be used to detect corrosion in such structures are constrained by the need to be able to distinguish between indications due to the presence of corrosion and effects due to the complex structure. In other industries, it is usually sufficient to detect corrosion at a fairly advanced stage when there has been a considerable loss of material. In the case of aircraft lap joints, and many other aircraft corrosion problems, the principal concern is that the presence of corrosion will promote other types of damage. This means that the corrosion must be detected when it is at a very early stage, before the loss of material becomes significant.

The two features which distinguish the corrosion detection requirements for aircraft from those of other industries are the need to detect corrosion at an early stage and the complexity of the structures which have to be inspected. These effects rule out many of the simpler methods which have proved effective in cases where it is only necessary to detect gross corrosion in simple structures.

3.2 Visual inspection as a search tool

Although visual inspection is not always counted as an NDE technique, it is one of the primary methods for identifying problem areas on aircraft. This is especially relevant for the case of corrosion where there is no

analogue of the major fatigue test to highlight problem areas. Visual inspection, aided by the use of suitable light sources to highlight surface unevenness is used extensively as a large area search tool to detect corrosion damage around fasteners. When corrosion occurs within an aluminium structure, the corrosion products expand to approximately three times the volume of the original material. The presence of entrapped corrosion products between thin layers of the structure causes deformation of the skin giving rise to a characteristic "quilting" or "pillowing" effect around the fasteners. In extreme cases this is readily identifiable but at an earlier stage it may be ambiguous and the inspection then depends on the judgement of the inspector. In many situations by the time that quilting becomes apparent it is already too late to effect an economical repair.

In current practice NDE techniques other than visual inspection are only employed to inspect suspect areas which have been highlighted by either visual inspection or fleet experience on other aircraft.

3.3 NDE techniques for detection and characterisation

Most of the standard NDE methods have been used to detect corrosion under some set of circumstances^{1,4}. Since aerospace offers a wide range of corrosion problems, almost all NDE techniques can find an application. The most important corrosion detection problems all require early detection of corrosion at or around complicated structural elements and considerations of structural effects and required sensitivity are the major limitation to the techniques which can be employed.

In simple situations where the corrosion occurs in a readily accessible layer of the structure, for example in the outside skin, the most direct measurement of the corrosion damage can be obtained by pulse-echo ultrasonic measurements. In cases of severe attack, ultrasonic thickness measurements can give a quantitative picture of the remaining material⁵. Where the corrosion is at a very early stage, the loss of material may not be measurable, but nevertheless a reduction in the reflected amplitude may be detectable. Ultrasonic amplitude measurements are difficult to perform accurately and repeatably. Again this is not a problem if the corrosion is severe, but it limits the sensitivity of the technique when attempting to distinguish corrosion in its early stages. Research is currently underway to examine the best way of interpreting the ultrasonic amplitude information to develop robust algorithms for corrosion measurement while improving the sensitivity.

Ultrasonic methods are severely hampered by the presence of interfaces within the structure as these partially reflect the incident ultrasonic signal. In

adhesively bonded aluminium structure it is impractical to inspect beyond the second metal layer and even measurements of the second layer properties suffer from reduced sensitivity. The main alternative technique which can be used on multi-layer structure is eddy current inspection. Eddy current methods do not give a direct measure of the depth of corrosion damage. They are sensitive to the presence of any conducting material and are therefore affected by the presence of structural elements which can cause severe complications in interpretation. The use of an imaging system can help to distinguish between structural effects and damage. Detection of corrosion in a single layer is straightforward. The sensitivity depends primarily on the layer thickness which determines the frequency which must be used. Eddy current inspection of multi-layer systems is complicated by the need to distinguish between variations in thickness of the metal layers due to corrosion, and variations in the thickness of the intervening adhesive or sealant layers. Although the latter perturb the eddy current signals they are of no structural significance.

In relatively simple two-layer systems the effect of inter-layer spacing variations can be minimised by a careful choice of frequency⁵. For more complicated systems it is necessary to use a more sophisticated technique, either combining the data at several frequencies^{6,7,8,9} or using pulsed excitation¹⁰. Current research programs are looking at the possibilities of using these advanced techniques, but as yet they are complicated to apply and little use has been made of them in the field.

Radiography has been used for corrosion detection for many years. The two types of radiography which may be used for corrosion detection are X radiography and neutron radiography. These are sensitive to different effects and have quite distinct merits and limitations.

X rays are attenuated by matter at a rate which is approximately proportional to the density of the material. X radiography is therefore sensitive to the total areal density of the material through which the X rays propagate. Where there has been appreciable material loss there will be lower attenuation of the X rays and this is not difficult to image. The highest sensitivity is obtained by using the lowest energy of X rays which will propagate through the thickness of metal to be inspected. Since higher energies are required for thicker structure, the sensitivity decreases as the thickness of the structure increases. The technique does not give a quantitative measure of the material loss, although it would be possible to provide this if required. The principal problem for the use of X radiography in aircraft corrosion problems is that where the corrosion takes place between layers of the structure the corrosion products may be retained in place. Unlike the case of material loss, retained corrosion products cause an increase in the attenuation of X rays. This can be

imaged⁵, but there can be ambiguities due to the presence of other materials and this limits the sensitivity of the technique.

Unlike X rays, beams of neutrons are very weakly attenuated by the metals commonly used in aircraft structure, particularly aluminium. Neutrons are, however, strongly absorbed and scattered by hydrogen. Since corrosion products contain a large proportion of hydrogen, a neutron radiograph gives an image of the corrosion products^{5,11}. Since the neutron beam is barely attenuated by the aluminium, it is possible to penetrate thick pieces of structure without a significant loss of sensitivity. Unfortunately the neutrons are sensitive only to the presence of particular elements, not to the compounds in which they are contained. Any source of hydrogen will therefore show up on the neutron radiograph. This severely restricts the usefulness of neutron radiography for inspection of aircraft. There are many other sources of hydrogen including moisture, fuel and oil residues, sealants, adhesives, paint and even dirt. These can all cause indications on neutron radiographs which can obscure the presence of corrosion. The difficulty in distinguishing corrosion products from other hydrogenous materials has largely prevented the use of neutron radiography for corrosion detection, although it has been used with success to detect water ingress. A second limiting factor is the high cost of providing the specialised facilities required.

Various other techniques, including thermography^{12,13,14,15}, optical methods and acoustic emission^{16,17} have been proposed and in some cases demonstrated. While they may be usable in specialised applications these techniques do not appear to present any real improvement over the methods described above, except perhaps in speed of inspection (see §4.3).

3.4 Detection of secondary effects

The techniques described above provide a range of capabilities for detecting and characterising corrosion. Ongoing research programmes seek to improve the sensitivity and practicality of the techniques particularly the ability to discriminate between corrosion and other effects. A major limitation in applying all of these techniques is the time, and hence the cost of using them. The attention of the aircraft operator must be drawn to the suspect area by some other reason before the technique can be applied. In the absence of an effective large area search technique there may be occasions when, rather than trying to detect the corrosion itself, it is more economical to detect a secondary form of damage which has been promoted by the corrosion. If this can be detected quickly a more sensitive corrosion detection technique can be performed later to check for the presence of corrosion in the suspect areas, if required. The use of

visual inspection to detect suspected areas of quilting is the simplest example of this approach.

Other secondary approaches which have been applied include the detection of disbonding or sealant failures by ultrasonics and the detection of cracking around fasteners by eddy currents.

With the ultrasonic detection of disbands there is a need for a follow-up inspection to determine whether the area of disbond actually contains corrosion. This inspection could also use an ultrasonic technique but would probably be performed using a higher frequency to maximise sensitivity, it would therefore be more time consuming.

The detection of cracking around overstressed fasteners or emanating from corrosion pits in fastener holes would not necessarily require further inspection to determine if the crack was corrosion related. It might still be advantageous to check for corrosion using an appropriate inspection technique to aid decisions about severity and repair. Conventional eddy current crack detection thresholds are such that detection of cracking around countersunk fasteners would probably be too late to give adequate warning of corrosion. Advanced instruments optimised for fastener inspection are now available¹⁸ and these might, under suitable circumstances, provide an adequate detection capability for corrosion and related cracking.

4 DETECTION OF DETERIORATION IN ADVANCED MATERIALS

4.1 Corrosion of advanced materials

The materials which are either in use or are contemplated for use in airframe primary structures fall, from an NDE viewpoint, into two categories. These may be loosely regarded as advanced metal alloys and composites.

Development of advanced metal alloys such as aluminium-lithium may give rise to slightly different corrosion problems than those of the current materials described above. However, from the point of view of detecting the occurrence of corrosion or characterising the corrosive attack in some way, it is unlikely that the advanced materials will differ in any substantial way from the current materials. The same NDE methods would be applied with only minor developments to optimise techniques for particular materials.

The development of composite materials might cause completely different inspection problems. Interpreting corrosion in its widest sense as deterioration due to ageing rather than fatigue there are possible mechanisms for corrosion which do not exist for a conventional metal.

The most extensively used composite materials at the present time are carbon-fibre reinforced organic matrix materials (CFRP). These materials exhibit a number of ageing mechanisms. The dry composite may age by a slow accumulation of microcracks which eventually nucleate a critical delamination¹⁹. The process can be accelerated by moisture ingress^{20,21} and thermal spiking²². Moisture can also attack the fibre-matrix interface leading to disbonding^{23,24}, cause plasticisation of the resin matrix²¹ and leech out some of the lighter molecules in the resin^{25,26}. The fibres themselves may be subject to attack by moisture, especially in areas where dissimilar materials are in contact and some concern has been expressed over the possibility of long term chemical changes in the matrices due to ultraviolet rays.

Other composite materials may suffer from similar degradation mechanisms. Ceramic matrix composites have been developed to provide a tougher material than the monolithic ceramic. In the early life of such a material, crack propagation is arrested by the reinforcement. Ultimately this may cause a sufficient build-up of microcracks to adversely affect material performance. Metal matrix composites and hybrid materials containing metal and organic layers may suffer from corrosion caused by chemical reactions between the component materials and possibly water.

All of these degradation mechanisms are, of course, allowed for in the airframe design to the extent that they should not adversely affect the performance of the materials during their service life. If the airframes were to be replaced at the end of this life, corrosion problems would only affect systems where there had been some marked change in circumstances, unforeseen at the design stage. The economic pressures to extend airframe life are likely to intensify in the future, however, and this may lead to the composite airframes remaining in service until material degradation sets in and renders their further use uneconomic. This situation already appears to have been reached with metallic structure in civil airliners.

4.2 NDE for material degradation in advanced materials

The discussion of current NDE techniques for corrosion detection in §2 concentrated on the detection of discrete defects, either areas of material loss, corrosion product or secondary defects associated with areas of corrosion. Some of the degradation processes mentioned in §3.1 may also lead to discrete defects which are large enough to be detected individually by current techniques. Although the inhomogeneity of composite materials reduces the sensitivity which can be attained, it may be expected that development of existing methods will provide techniques for the detection and characterisation of this type of degradation.

The other mechanisms, those which may lead to either a weakening of the material without the occurrence of discrete flaws, or to the formation of large numbers of microscopic defects, will have to be detected by measuring changes in the material properties. A number of NDE techniques are already used for material property assessment. The most widely used methods for inspection of organic matrix composites use measurements of ultrasonic attenuation. This is effective for the detection of porosity caused by problems during manufacture. It should also be effective as a means of detecting degradation mechanisms which led to the creation of microscopic voids in the material. It has been shown, for example, that the damage caused by thermal spiking of a moist composite produces an increase in ultrasonic attenuation²². Measurements of ultrasonic velocity can be used to monitor cure processes and to determine reinforcement density. An adaptation of the technique ought to be capable of detecting areas where the elastic modulus of the composite has been affected by plasticisation or by the build-up of a significant defect concentration. Further research will be required to ascertain the level of deterioration which would be detectable using these techniques.

Eddy current methods provide a complementary range of capabilities since they probe only conducting structure. They may be expected to be able to detect deterioration of metal matrix composites if this results in a reduction in the electrical conductivity. Similarly they will be sensitive to changes in metal layered hybrid materials where interpretation of the eddy current signals will be the main challenge. Eddy current methods are more difficult to apply to CFRP as inhomogeneities in the material can mask conductivity changes due to damage. In principle, however, eddy currents give the most direct method for detecting damage to the conducting fibres and may therefore be usable to detect degradation of the fibres themselves or of the fibre/matrix interface. The application of eddy current inspection to composite materials is at a very early stage of development and considerable further work will be required to assess the full potential of the technique, however it has been shown to be effective for the detection of fibre breakage caused by impact damage or cracking.

4.3 Large area techniques

The NDE techniques referred to in the above section share the limitation noted in §2 that they are capable of detailed characterisation of a small area of structure but are slow to apply over a large area. If the justification for extending the life of airframes until corrosion problems appear is economic, it would be highly desirable if not essential to have a rapid search tool which could inspect large areas.

In areas where degradation of the material leads to deformation, such as composite swelling on moisture absorption or quilting around mechanical fasteners, it may be possible to rely on visual inspection, possibly using aids such as the D-sight technique^{27,28}, for large area coverage.

Material degradation effects might also be detectable from the thermal or mechanical properties of the system. Already it is routine to use thermal imaging for the detection of entrapped water in honeycomb. Thermal imaging or pulsed thermography may be useful also for detection of changes in matrix properties of CFRP and similar composites. Optical techniques to measure surface distortion under applied stress or vibration and various low frequency acoustic or mechanical impedance techniques also offer some potential for detecting gross deterioration but probably do not currently have sufficient sensitivity to detect the more subtle changes which may be expected with systems in current use.

5 THE USE OF NDE FOR LIFE MANAGEMENT

5.1 NDE and Airworthiness philosophies

Aircraft may be operated under a damage tolerant, safe life or fail safe approach to airworthiness. NDE is explicitly relied upon only in the damage tolerance methodology, where the structure is inspected periodically in order to ensure that it is free from harmful defects and may be cleared for a further period of operation. Military types operated under safe life policies and civil aircraft which use a fail safe approach are cleared for operation to a nominal airframe life, although they do rely upon inspection within that life to some extent.

If economic pressures dictate that the aircraft be kept in service after the end of its safe life, an alternative method must be employed to ensure continued safe operation. Many structural elements and components can be replaced or refurbished. Others, after inspection to ensure their continued fitness for purpose, may be returned to service for a further life. This further life is calculated using the damage tolerance principle of allowing for the presence of undetectably small defects²⁹. The choice between replacement and inspection will be made primarily on economic grounds.

The relationship between airworthiness and NDE capabilities involves several elements. These are, the way in which NDE reliability is specified, the procedures by which the reliability must be verified and the inspection intervals which result from the demonstrated NDE reliability and the required safety level. Inefficiency in any of these elements can greatly

reduce the potential savings offered by optimal use of NDE.

5.2 Specification and Verification of NDE Reliability

NDE can only be relied upon to ensure safety once it has been demonstrated to be effective. In many instances, a simplistic view is taken of the capabilities of NDE and it is assumed that all defects above a certain size will be detected. There is in practice no size above which a defect can be detected with complete certainty. Restricting NDE to look for defects only of a sufficiently large size that the detection is virtually certain inevitably leads to conservative estimates of this critical defect size. The resulting estimate of the largest defect which could be missed, however infrequently, is often unacceptably large and NDE is therefore not used.

There has been considerable interest in the assessment or verification of NDE reliability^{30,31,32}. This is usually expressed as a "probability of detection" (POD) curve, showing the probability of detecting a defect as a function of defect size. Current research is aimed largely at developing more efficient methods for incorporating the results of NDE reliability trials into the overall airworthiness methodology³³. Providing the reliability can be assessed, however, optimal scheduling of inspections can be achieved to provide stipulated safety levels.

One of the major considerations when assessing the viability of an inspection strategy is the trade-off between the reliability required and the resulting inspection interval. In general, achieving a high reliability requires a time-consuming and hence relatively expensive inspection technique. An improved understanding of the link between reliability and inspection frequency may allow the use of lower-reliability and hence less expensive techniques as large area search tools for routine inspection.

A sensible compromise must be reached when specifying NDE requirements between needlessly high sensitivity and the desire for rapid inspections. The standard introduced by the USAF some years ago²⁹ as part of its damage tolerance procedures has since been widely adopted. This requires a POD of 90% to be demonstrated at the 95% confidence level at the desired detection threshold.

In practice, imposing this arbitrary standard to all inspection tasks has resulted in several difficulties. Many inspection techniques do not have a high enough reliability to enable the "90/95" criterion to be demonstrated economically. Some techniques do not even approach a POD of 90%³⁴. Such techniques may provide the most cost-effective inspection scheme if appropriate scheduling of inspections can be arranged.

5.3 NDE Reliability for life management

There are two types of defect which can be expected to predominate in ageing aircraft, fatigue cracks and corrosion. A considerable amount of work has already been done on the reliability of NDE techniques for crack detection, although much of this is of limited applicability to real inspection situations^{32,34}. There is no comparable information on the reliability of corrosion detection methods. Verifying the reliability of an NDE technique for the detection of corrosion defects in airframes could be an expensive and time consuming undertaking in which the number of specimens which could be provided would necessarily be small.

The NDE specification and verification process can be tailored to optimise NDE utilisation in two different ways depending on the type of inspection planned and its relationship to the aircraft maintenance schedule.

For inspections which involve little or no preparation and which can conveniently be carried out during normal aircraft operations, the NDE reliability can be used to calculate inspection intervals directly to achieve a given safety level. Comparison of the overall cost of different inspection strategies can be based on inspection costs alone or can take likely repair costs into account. In planning a verification exercise to demonstrate the required POD the cost of this should be considered when minimising the overall cost of inspection.

Inspections which involve extensive aircraft preparation are practicable only if they can be carried out during planned major servicing. Since the inspection interval is determined by the maintenance programme, this becomes the determining factor for the required NDE reliability. Optimising the NDE requirement then becomes merely selecting the technique which most economically or conveniently provides the required reliability.

Although the small size of such a verification experiment will inevitably result in a low value for the POD at a high confidence level, this need not result in an unacceptably short inspection interval. A current rule of thumb used in setting inspection intervals is that a defect should be inspected at least three times during its growth to the critical size. For any given confidence level which will be used to define the POD estimate, it is possible to predict the number of inspections which will be required during the defect life. The number of inspections depends on both the true probability of the technique finding a defect and the number of trials used to verify the POD. Table 1 shows the result for the 95% confidence level

It can be seen that using a considerably less reliable inspection technique imposes only a slight burden in terms of increasing the number of inspections

True Proba bility	No. of inspections for verification				
p_i /%	20	50	100	200	∞
95	5	4	4	3	3
85	6	6	5	5	4

Table I: Expected number of inspections required to obtain overall safety level of 1 in 1000.

required. Similarly, reducing the size of the verification exercise results in only a modest increase in the number of inspections required. If the inspection interval is fixed by the maintenance schedule for the aircraft there may be no gain in using the higher reliability technique or in requiring a large and costly verification programme.

By choosing a technique with suitable reliability and planning the verification of this appropriately, any desired safety level can be ensured at minimum overall cost.

6 CONCLUSIONS

Corrosion and corrosion related defects have become a major life limiting factor in the operation of aircraft. The extension of airframe life often presents a choice between inspection and replacement to ensure airworthiness. The choice will usually be made on economic grounds.

NDE techniques exist to detect corrosion in many circumstances. Gross corrosion in simple structures is not difficult to detect. The requirements of the aerospace industry include the detection of corrosion at an early stage, the ability to distinguish indications due to corrosion from structural effects in complicated structures. Current research aims to improve the capabilities of current detection methods in both of these respects.

In current practice NDE techniques other than visual inspection are only employed to inspect suspect areas which have been highlighted by either visual inspection or fleet experience on other aircraft. The provision of rapid techniques for the inspection of large areas would be very valuable. Such techniques could be used as a routine search tool, backed up by the more sensitive characterisation and measurement methods.

Corrosion or degradation processes affecting new, advanced materials can be grouped into two classes from an NDE point of view. Corrosion of novel alloys,

along with similar processes involving loss of material in composite materials can be detected by existing techniques, suitably optimised for the material in question. Novel deterioration processes which might affect composite materials require alternative techniques. Ultrasonic and eddy current methods which are currently used for determination of material properties offer a basis for the solution of some of these problems.

Whenever NDE is required to ensure that critical components or structures are free from defects, the reliability of the NDE technique becomes an important factor in determining the overall safety level. Reliance on NDE to detect corrosion implies that the reliability of the detection techniques should be established. Little information is currently available on this.

7 REFERENCES

- 1 A useful review is given in "Nondestructive Evaluation methods for characterisation of corrosion" Beissner R E and Birring A S NTIAC-88-1 (1988)
- 2 Hobin T P Brit J NDT **20** 284 1978
- 3 Constantinis D A "Corrosion condition monitoring, state of the art" in NDT 86 ed Farley J M and Hanstead P D 61 EMAS 1987
- 4 Hagemeyer D J, Wendelbro A H and Bar-Cohen Y, Mat Eval **43** 426 1985
- 5 Smith R A "Non destructive evaluation for corrosion in ageing aircraft" DRA Technical Report DRA/SMC/TR941004 1994
- 6 Deeds W E and Dodd C V Int Adv NDT **8** 317 1981 also Dodd C V and Deeds W E Rev Prog Quant NDE **6** 849 1987
- 7 Hayford D T and Brown S D "Feasibility evaluation of advanced multifrequency technology for use in naval air maintenance environment" Naval Air Engineering Center (NAEC) report NAEC-92-143 1980
- 8 Hagemeyer D J Mat Eval **40** 682 1982
- 9 Thomson J G Mat Eval **51** 1398 1993
- 10 Bowler L R and Harrison D J Rev Prog Quant NDE **11A** 241 1992
- 11 Mast H U and Schultz R "Neutron radiography - applications and systems" in AGARD conference proceedings no 462 "Impact of emerging NDE-NDI methods on

- aircraft design, manufacture and maintenance" paper 14 1989
- 12 Hobbs C and Temple A Brit J NDT **35** 1993
- 13 Birring A S Rowland S N and Burkhardt "Detection of corrosion in Aluminum aircraft structures" Report 17-9366 SW Research Inst. (San Antonio TX) 1984
- 14 Cielo P Maldague X, Deom A A and Lewak R Mat Eval **45** 452 1987
- 15 Heath D M, Welch C S, Winfree W P, Heyman J S and Miller W E Rev Prog Quant NDE **5b** pp 1125 and 1133 1987
- 16 Scott I G "Acoustic emission and corrosion" Ninth world conference in NDT paper 4J-5 1980
- 17 Pollock A A "Acoustic emission capabilities and applications in monitoring corrosion" in "Corrosion monitoring in industrial plants using nondestructive testing electrochemical methods" ASTM STP 908 ed Moran G C and Labine (Philadelphia PA) p30 1986
- 18 Harrison D J "Progress in the detection of cracks under fasteners using eddy currents" DRA Technical report 91024 1991
- 19 Prinz R "Growth of delaminations under fatigue loading" in "Characterisation, analysis and significance of defects in composite materials" AGARD-CP-355 paper 5 1983
- 20 Scanabel W "Polymer Degradation : Principles and Practical Applications" Hansa International, Germany 1981
- 21 Delasi R and Whiteside J B "Effect of moisture on epoxy resins and composites" Advanced Composite Materials - Environmental Effects ASTM STP 658, ed J R Vinson p2 1978
- 22 Collings T A and Stone D E W "Hygrothermal effects in CFC laminates Part II Damaging effects of temperature, moisture and thermal spiking" RAE Tech Report 84003 1984
- 23 Ashbee K H G and Wyatt R C Proc Roy Soc A **312** 553 1969
- 24 Kaelble D H, Dynes P J, Crane L W and Maus L J Adhesion **7** 25 1975
- 25 Ashbee K H G and Farrar N "Detection and Identification of Changes in the Physical Properties of Fibre/Matrix interface" Proc 1975
- Int Conf on Composite Materials AIME p771 1975
- 26 Morgan R J and O'Neal J E "The durability of Epoxies" Polym-Plast Technol Eng **10** 49 1978
- 27 Hageniers O L "Diffractosight - A new form of surface analysis" SPIE **814** Photomechanics and speckle metrology p193 1987
- 28 Komorowski J P, Gould R W and Pastoris W J "A technique for rapid inspection of composite aircraft structure for impact damage" in AGARD conference proceedings no 462 "Impact of emerging NDE-NDI methods on aircraft design, manufacture and maintenance" paper 4 1989
- 29 USAF Mil Spec "Aeroplane damage tolerance requirements" MIL-A-83444 1974
- 30 Packman P F, Klima S J, Davies R L, Malpani J, Moyzis J, Walker W, Yee B G W, and Johnson D P "Reliability of Flaw Detection by Nondestructive Inspection" in AMS Metals Handbook Vol 11 NDI and Quality Control.
- 31 Rummel W D Mat Eval **40** 922 (1982)
- 32 Rummel W D "Assessment and demonstration of the capabilities of NDI processes, equipment and personnel" in "Impact of emerging NDE-NDI methods on aircraft design, manufacture and maintenance" AGARD-CP-462 paper 4 1989
- 33 Bruce D A "Inspection Reliability" in "Impact of Emerging NDE-NDI Methods on Aircraft Design, Manufacture and Maintenance" AGARD-CP-462 paper 5 1989
- 34 Lewis W H, Dodd B D, Sproat W H and Hamilton J M "Reliability of Nondestructive Inspections" Lockheed Georgia Company report SA-ALC/MME 76-6-38-1 1976

HEALTH AND USAGE MONITORING SYSTEMS - CORROSION SURVEILLANCE

J D Smart

Engineering Test Facilities
AVRO International Aerospace
Chester Road, Woodford
Cheshire SK7 1QR, England

D C Weetman

Real Time Corrosion Management Limited (CML)
Bainbridge House, Granby Row
Manchester M1 2PW, England

1. SUMMARY

A predictive method of determining the inspection requirements for specific areas of individual aircraft could offer major advantages in terms of safety and maintenance and repair costs. An approach such as Health and Usage Monitoring in Service, in which the condition of components is monitored whilst in operation, would allow inspection requirements to be minimised and maintenance to be carried out as it becomes necessary.

To use such an approach on aircraft would require very sensitive monitoring techniques. Modern electrochemical corrosion instrumentation could offer the required levels of sensitivity for detecting and characterising the corrosion processes which precede the development of observable damage.

This paper details a programme carried out to assess the suitability of such electrochemical monitoring instrumentation for aerospace applications and to assess the feasibility of producing an aircraft system on which a predictive corrosion monitoring system could be based.

2. INTRODUCTION

Corrosion presents a major threat to the structural integrity of both military and commercial aircraft and may significantly affect the viability of extending the life of particular aircraft types. Many aerospace materials are inherently reactive and can be degraded very rapidly if inadequately protected against their operational environment. As the length of time in service increases, there is also a

greater probability that corrosion will be associated with other forms of damage, such as fatigue cracking. It is therefore critical that any areas affected by corrosion are identified and corrective action is taken well before structural integrity has been compromised. Ideally, corrosion should be identified in its early stages, before extensive rectification work is required.

The conventional approach for dealing with corrosion is by routine inspection, repair and maintenance. Detailed inspections are usually carried out during periodic overhauls when there is the opportunity to remove protective treatments, panels and insulation to allow for visual or more specialised examination of the structure. The frequency of these inspections is usually based on the age of the aircraft and on general service experience.

This approach has certain disadvantages due to the large variation in the corrosion problems which can be experienced even with identical aircraft types. This variation may be attributable to the different operating roles and environments in which the aircraft are employed, to variations in the aircraft specification or to differences in the maintenance procedures used by various operators. Even with individual aircraft, changes in operational usage can result in a dramatic change in the rate of corrosion degradation. It is therefore possible that only a small number of aircraft in a fleet may be badly affected by corrosion in particular areas.

Experience has shown that the corrosion problems associated with aircraft tend to be underestimated rather than overestimated. For many aircraft types, it has been reported that detailed inspections have revealed more widespread and severe attack than had been expected⁽¹⁾. This may be due in part to the variable nature of the problem and also to the failure of the inspection methods to detect minor corrosion damage at the onset of attack. For whatever reason, a delay in detecting corrosion until it has become established or reached a level at which another failure mechanism has become active, will usually prove to be costly because the repairs required will then be more difficult, time-consuming and expensive.

Conversely, the frequency of routine inspection that is specified may be higher than required for certain areas of some aircraft. This also will result in cost penalties because the inspections are expensive to carry out and require the aircraft to be taken out of service.

A more accurate method of determining the inspection requirements for specific areas of individual aircraft would therefore offer major advantages in terms of safety and maintenance and repair costs.

The shortcomings in the conventional approach to maintaining aircraft serviceability have created interest in the development of approaches better suited to modern operational requirements. Health and Usage Monitoring in Service (HUMS) and Structural Usage Monitoring in Service (SUMS) are two such initiatives which are used for helicopters⁽²⁾. Their principal objective is to predict and neutralise attack before significant damage is sustained. They employ an approach whereby the condition of components is monitored whilst in operation and not just assessed intermittently at routine inspections. This minimises inspection requirements yet ensures that maintenance is carried out as it becomes necessary. In concept, the approach is akin to "just in time" manufacture, with similar benefits of close control and cost reduction.

Recognition of the advantage to be gained from predictive management of corrosion is becoming more widespread

in the aerospace industry, following such development in the nuclear, chemical and offshore oil production industries. It has been shown that significant cost savings can be achieved, equivalent to approximately half the cost of using the conventional maintenance approach (Figure 1)⁽³⁾.

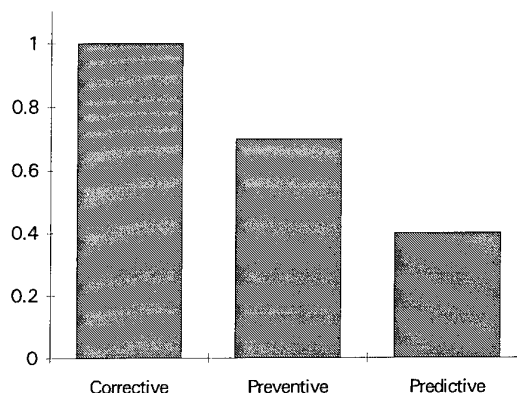


Fig. 1 Relative Costs of Different Approaches to Maintenance

To use such an approach on aircraft would require very sensitive monitoring techniques which could detect and identify some or all of the corrosion processes which precede the development of observable damage. Such processes would include the degradation of protective treatments, pitting, stress corrosion cracking, crevice attack or uniform attack.

3. ELECTROCHEMICAL CORROSION MONITORING

Modern electrochemical corrosion instrumentation could offer the required levels of sensitivity for detecting and characterising corrosion processes at their initiation stages. It can be used to monitor the electrochemical signals which are generated spontaneously by changes in the electrochemical conditions at corroding surfaces.

Such instrumentation was initially developed more than ten years ago for the power generation industry to appraise corrosion behaviour under corrosive condensate films. The technology is now also used in oil and gas production, as well as the nuclear, chemical, petrochemical and refining industries.

As part of the Brite-Euram project BE-3355 "New Accelerated Corrosion Test Methods"⁽⁴⁾, a programme has been carried out to assess the suitability of such electrochemical monitoring instrumentation for aerospace applications.

The programme involved the simultaneous application of a number of separate but complementary electrochemical monitoring techniques. These included :

Electrochemical Potential Noise (EPN)

Electrochemical Current Noise (ECN)

Electrochemical Impedance Measurement (EIM)

Zero Resistance Ammetry (ZRA)

3.1 Electrochemical Noise (EPN/ECN)

Electrochemical Potential Noise (EPN)^(5,6,7,8,9) is a generic term used to describe the spontaneous fluctuations or transients observed in the current or potential time record of an electrochemical reaction⁽¹⁰⁾. These originate as a result of stochastic processes occurring on the electrode surfaces. The fluctuations are usually of low amplitude (less than 1 mV) and of low frequency (in the range 1Hz and below). The electrochemical noise technique relies solely on the measurement of these spontaneous fluctuations of the free corrosion potential of the test electrode. No external perturbations are required.

The instrumentation effectively measures the rms value of the amplitude of the electrochemical noise over a narrow band of frequencies. The output is proportional to the logarithm of the rms value of the amplitude of the electrochemical noise in the measured frequency range, spanning a range of amplitudes from 1 μ V to 10mV.

Electrochemical Current Noise (ECN)^(5,6,7,8,9) is similar to EPN, except that fluctuations in current flow between two similar electrodes, typically less than 1 μ A, are monitored

The main advantages of the noise techniques lie in their capability of detecting localised corrosion ie pitting or crevice attack. It has

been found that such forms of attack give unique "signatures" and experience has shown that data obtained can be related in real time to the degree of localised attack. Thus, electrochemical noise gives useful information at the onset of attack and during continued pitting or crevice corrosion.

3.2 Electrochemical Impedance Measurement (EIM)

Electrochemical Impedance describes the response of an electrochemical interface, such as that between a corroding electrode and the surrounding environment, to an externally- applied, alternating, electrical perturbation⁽⁵⁾. For example, a small amplitude (about 20 mV) sinewave voltage applied between a pair of corroding electrodes causes the flow of a sinusoidally varying (a.c.) current with a phase shift dependent on the cell parameters. The electrochemical impedance of the cell can then be determined at the measurement frequency as the ratio of the applied voltage to the resultant current.

In reality, the electrochemical interface behaves as a combination of resistance, capacitance and other elements, causing a phase shift between the applied voltage perturbation and the observed current. A high frequency perturbation applied to the test electrode enables measurement to be made of the electrolyte (or solution) resistance. Measurements made at very low frequencies allow the sum of the electrolyte resistance and the charge transfer resistance to be obtained. Experience has shown that measurements should be taken over a frequency range of some 7 decades, namely 10kHz to 1 mHz, depending on the particular system being studied⁽¹¹⁾. In practice, complications due to concentration (diffusion) effects are usually present, but analysis of the impedance data can allow an estimation of the charge transfer resistance of the system under test. This can then provide a measure of the corrosion rate using the Stern-Geary relationship :

$$I_{corr} = B/R_p$$

where B is the Stern-Geary constant and R_p is the polarisation resistance.

3.3 Zero Resistance Ammetry (ZRA)

Zero Resistance Ammetry measures the galvanic current between two electrodes whilst imposing essentially zero resistance to the flow. It is usually employed with dissimilar metals, but may be used with certain advantages to monitor the current between two nominally "identical" electrodes⁽⁹⁾.

In theory, two such electrodes should maintain the same free-corrosion potential, hence no current should flow. In practice, their potentials differ slightly and fluctuate. When coupled through a ZRA they are maintained at a common potential and the resulting mean current, together with any fluctuations, is manifested as a current flow.

The instrument output is proportional to the logarithm of the rms value of the ZRA current and may be used to identify patterns of fluctuations corresponding to localised corrosion attack. Experimental evidence indicates that in many systems, the D.C. value of the current during active corrosion is proportional to the corrosion current.

The techniques described above were used for :

Electrochemical monitoring of specimens representing different aerospace alloys and protective treatments after exposure to various test environments. The tests included long-term exposure - attached to an aircraft or placed in an industrial environment - and accelerated corrosion tests such as salt spray and alternate immersion.

Electrochemical monitoring in real-time of untreated specimens immersed in various test solutions during slow strain rate or constant load tests.

Installation of prototype corrosion monitoring equipment and sensors on board an aircraft in order to monitor the variations in environmental corrosivity experienced during flight.

The aircraft system was also later modified to allow monitoring of different types of sensor in order to assess the feasibility of producing an aircraft system on which a predictive corrosion monitoring system could be based.

4. RESULTS

4.1 Laboratory tests - Electrochemical Noise

It was demonstrated that individual cracking events could be detected and identified as they occurred by electrochemical noise monitoring.

Figures 2 to 4 show the electrochemical noise data obtained during slow strain rate and constant load tests⁽¹²⁾.

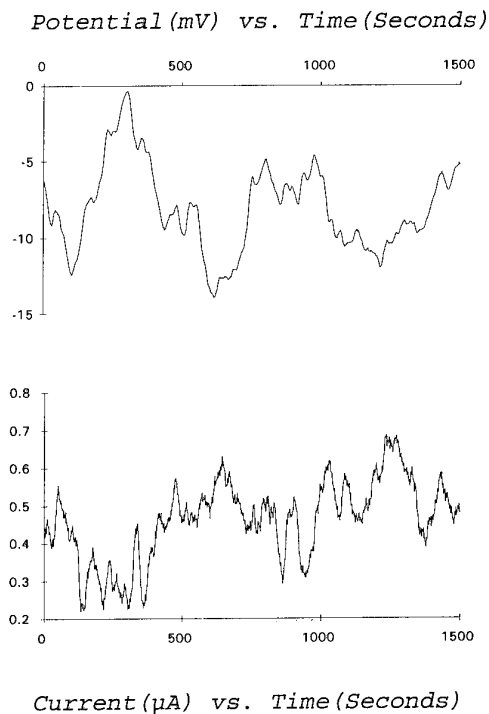
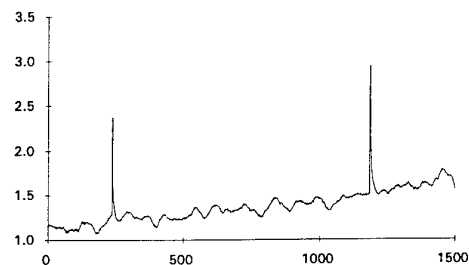
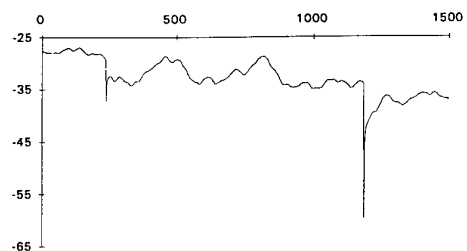


Fig. 2 Electrochemical Noise Data
8090.C - SSR Test - 45 minutes

Figure 2 shows the response of alloy 8090-T8171 during a slow strain rate test ($2.8 \times 10^{-6} \text{ s}^{-1}$) in Substitute Ocean Water at 25°C . The data was acquired approximately 45 minutes into the test and the response is indicative of micro-pitting. The first anodic dissolution transients, typical of stress corrosion cracking, appeared approximately 2 hours into the test (Figure 3). All of the large noise transients observed throughout the test were found to correspond to transients in the stress-strain curve, confirming that they were related to significant cracking events.

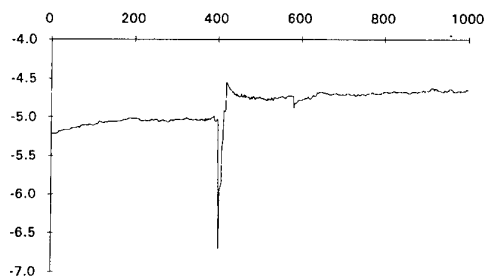
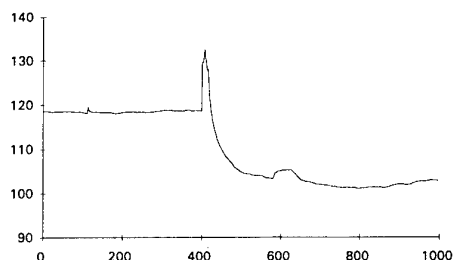
Potential (mV) vs. Time (Seconds)



Current (μA) vs. Time (seconds)

Fig. 3 Electrochemical Noise Data
8090.C - SSR Test - 120 Mins

Potential (mV) vs. Time (Seconds)



Current (μA) vs. Time (seconds)

Fig. 4 Electrochemical Noise Data
L95 - Constant Load (428MPa)

A different response was monitored during tests on alloy 7075-T651 subjected to a constant load test at 428 MPa in S.O.W. at 40°C. Figure 4 shows a cathodic potential transient and corresponding cathodic current transient. These are associated with the generation of nascent hydrogen. The cathodic transients are immediately followed by an shift in the potential in the anodic direction, with an associated anodic shift in the current. The response was therefore indicative of hydrogen-induced crack propagation, rapidly followed by anodic dissolution associated with re-filming of the exposed crack surfaces. This would be a step-wise mechanism, with the anodic dissolution resulting in generation of more nascent hydrogen and subsequent further hydrogen-induced crack propagation.

It was shown that electrochemical noise and impedance monitoring could provide information concerning the degradation of coated specimens⁽¹³⁾. The electrochemical noise data could be utilised in its raw form or analysed statistically to provide information on overall trends.

Figure 5 shows the variation in electrochemical current noise rms on 7075-T651 specimens installed in an aircraft for up to 12 months. This indicates clear differences in the protection conferred by the various treatments. Activity was greatest on the untreated (T1) specimens. The effect of applying a typical in-situ protective treatment ie chromate conversion plus PX32 wax-based protective (T4) was shown to have resulted in an immediate improvement in corrosion performance, to similar levels as those specimens with the standard protective treatment (T2 - anodise plus epoxy primer). However, the data showed that this treatment lost its effectiveness after about 9 months without replenishment. Treatment T3 - chromate conversion plus epoxy primer - showed no loss in performance but appeared to be less protective than treatment T2.

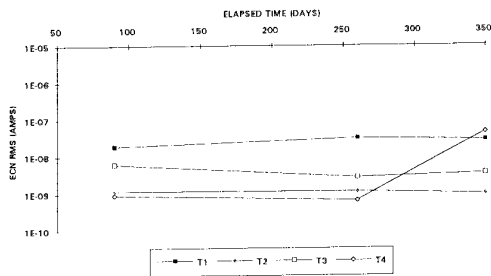


Fig. 5 Variation in Current Noise RMS Long Term Exposure In Aircraft

Similar results were obtained on specimens exposed to an industrial environment for up to 15 months (Figure 6). Degradation of the treatment T4 was again apparent, and treatment T2 was again shown to offer the highest level of protection.

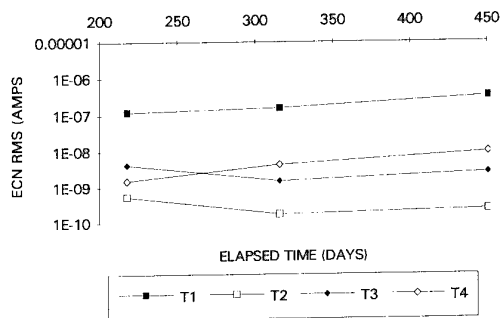


Fig. 6 Variation in Current Noise RMS Long Term Exposure In Industrial Environment

Alternate immersion testing in 3.5% NaCl solution was shown to be a very aggressive test, resulting in a rapid degradation of treatments T3 and T4 (Figure 7). An increase in activity was apparent after only 120 cycles (5 days) for these treatments, with the level of activity approaching that of the untreated specimens after 480 cycles.

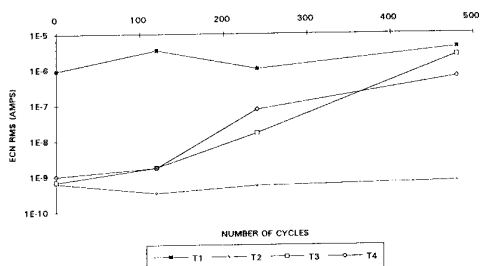


Fig. 7 Variation in Current Noise RMS Alternate Immersion Testing

NB For all of the tests, the monitoring was carried out before corrosion was visible on any of the treated specimens. The only visible degradation was a lightening in colour of the epoxy primer.

4.2 Laboratory Tests - Electrochemical Impedance

There was found to be a good correlation between the electrochemical noise and impedance data⁽¹³⁾. The impedance results confirmed that treatment T5 provided a high level of protection at the initial stages of the in-flight exposure tests, with a charge transfer resistance (R_{ct}) of approximately 50 kOhm.cm² (Figure 8).

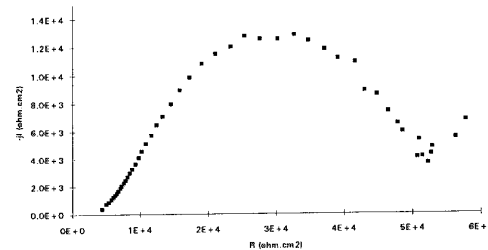


Fig. 8 Electrochemical Impedance Data Treatment T5 After 90 Days Exposure In Aircraft

After 350 days - when the noise response indicated that corrosion activity had increased - impedance data showed the R_{ct} to have fallen to approximately 20 kOhm.cm² (Figure 9).

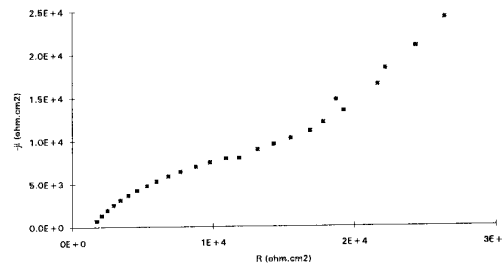


Fig. 9 Electrochemical Impedance Data Treatment T5 After 350 Days Exposure In Aircraft

In contrast, R_{ct} for treatment T4 remained reasonably constant at approximately $500 \text{ k}\Omega\text{cm}^2$ during the in-flight exposure tests (Figure 10).

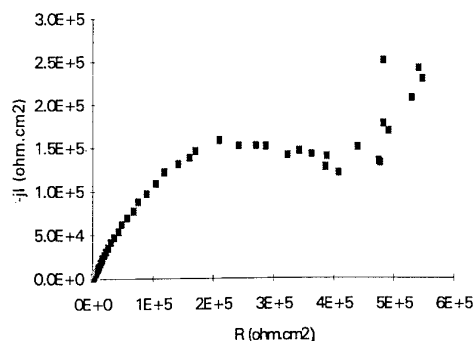


Fig.10 Electrochemical Impedance Data Treatment T4 After 350 Days Exposure In Aircraft

After 240 cycles of the alternate immersion test, however, when the noise data registered a greatly increased level of activity associated with treatment T4, the impedance response shown in Figure 11 was obtained, indicating an R_{ct} of approximately $10 \text{ k}\Omega\text{cm}^2$.

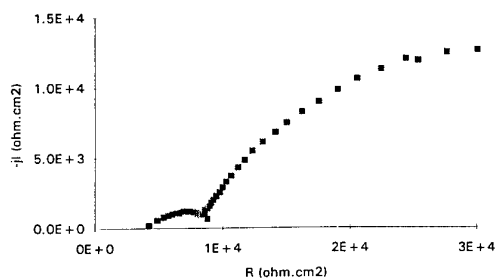


Fig.11 Electrochemical Impedance Data Treatment T4 After 240 Cycles Alternate Immersion Test

4.3 Corrosion Surveillance on Board an Aircraft

The prototype aircraft corrosion monitoring system consisted of a multiplexed analogue electrochemical noise system. This was installed in a pressurised section of a large maritime reconnaissance aircraft and was connected to corrosion sensors, platinum-resistance thermometers and a pressure sensor installed in the wing locations shown in Figure 12.

These locations were chosen because they were known to be particularly susceptible to corrosion attack.

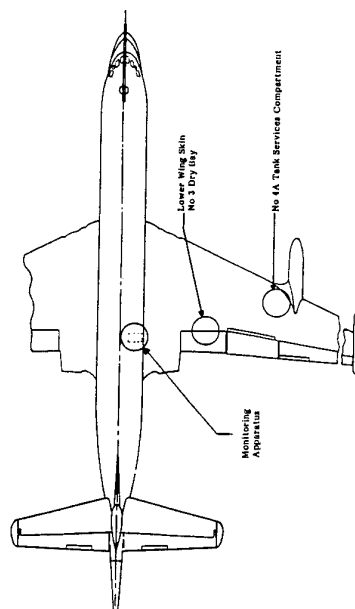


Fig. 12 Location of Aircraft Corrosion Monitoring System and Sensors

The environmental corrosivity sensors were installed in holders which allowed the sensors to be flush-mounted and to be thermally bonded to the aircraft lower skin. They were manufactured from a similar material to that of the aircraft lower skin panels and were designed to monitor corrosion due to condensation and moisture run-off. The corrosion surveillance sensors were bonded directly to the aircraft structure and were over-painted with a thinned coat of epoxy primer (approximately 50% thinner than that normally applied).

Data was recorded over a period of about 30 months, with the monitoring unit being switched on shortly before each flight. The unit interrogated each sensor in turn, and received an input every 15 seconds of one of the variables being monitored. The data was logged continuously on a portable computer which had sufficient capacity for several weeks operation.

For most sets of data, the onset of corrosion correlated exactly with activities such as take-off, with a correspondingly rapid decrease in observed activity on landing. Fluctuations in the data seemed to indicate that corrosion activity increased during periods when an aqueous film was likely to form on the sensor surfaces. This could be due to condensation of entrapped moist air as the aircraft ascended, by melting of ice particles or condensation onto cold surfaces as the aircraft descended or on passing through weather fronts or the cloud base^(14,15,16).

Typical data recorded during flights is shown in Figures 13 to 15.

Figure 13 shows data recorded during a flight. The rapid reduction in pressure and the more gradual decrease in temperature as the aircraft took off and gained altitude led to a noticeable increase in corrosion activity, indicated by the large fluctuations in electrochemical potential and current noise. Small changes in altitude and temperature, approximately one hour into the flight also produced fluctuations in the noise data. Approximately 3 hours into the flight, the activity once again increased, continuing at this level until the aircraft descended when the activity practically ceased.

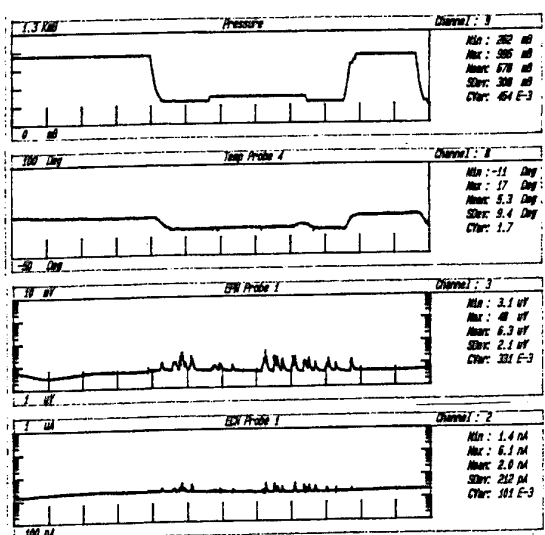


Fig. 13 Data Recorded During Flight

A different pattern of behaviour was recorded during the same flight from the sensors installed in the bay open to the atmosphere (Figure 14).

It appeared that the de-icing system had been activated shortly before take-off, allowing warm air to pass through the bay and resulting in a small amount of corrosion activity.

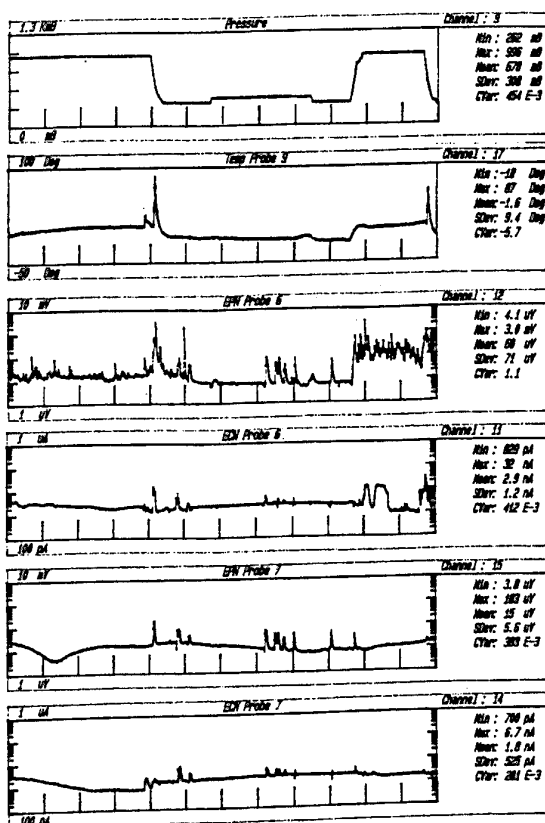


Fig. 14 Data Recorded During Flight

During take-off there was a sharp increase in temperature and also in corrosion activity. The next noise fluctuations, approximately one hour and three hours into the flight, corresponded to those recorded in the enclosed bay. The activity then increased as the aircraft descended and this activity was sustained for about forty minutes, as indicated by the ECN traces for probe 6. Corresponding periods of activity were also recorded from the coated sensor, but the activity was at a lower level than that on the environmental sensor.

Analysis of all the data collected^(14,15) indicated that corrosion activity was generally higher in the open bay than in the enclosed bay. As would be expected, in both areas there was a lower level of activity on the coated sensors compared with the uncoated environmental sensors.

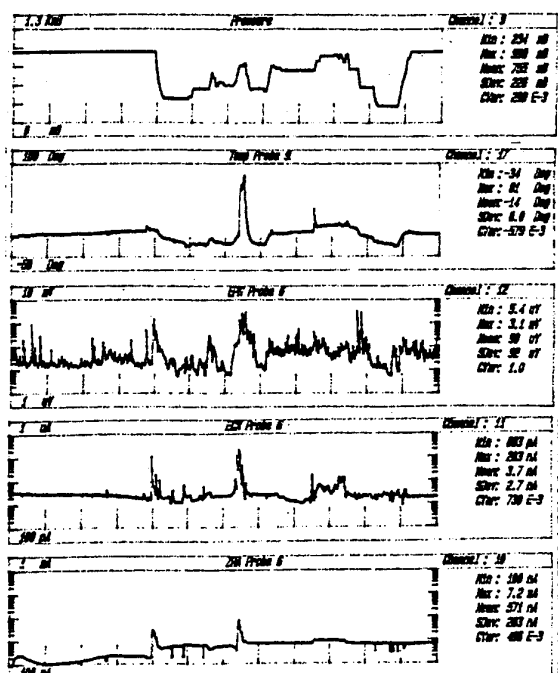


Fig. 15 Data Recorded During Flight

Data from another flight is shown in Figure 15. An increase in activity was observed immediately upon take-off, with further significant fluctuations corresponding to changes in altitude. The effect of a large increase in temperature from the de-icing system approximately 150 minutes into the flight was to dry out the probes. As the probes dried out and the electrolytes became more concentrated there was a large increase in corrosion activity, but this soon reduced as the drying out continued. A similar, but smaller event was also evident after a further two hours and there was then a reduced level of corrosion activity corresponding to the ascent, cruise and landing at the end of the flight. Over the period monitored, the data indicated that corrosion activity on the aircraft was generally very low, but there were rapid increases in activity on take-off and a correspondingly rapid decrease in activity on landing. Corrosion activity increased during periods when an aqueous film was likely to form on the aircraft surfaces and so flights with a more varied flight pattern tended to exhibit a higher level of corrosion activity. The corrosion activity was relatively insignificant when the aircraft was on the ground.

Statistical analysis of the current noise data showed evidence of seasonal fluctuations, with activity generally more active during Winter and early Spring compared with the Summer months (see Figure 16). The degree of localisation of the corrosion, measured as the ratio of the electrochemical current noise to the ZRA current, indicated that the attack was initially fairly uniform but had become more localised over the monitoring period (see Figure 17). Based on the long-term data, it was estimated that the general corrosion rate of the environmental sensors was of the order of 20 microns per annum, but with localised penetration probably becoming more significant.

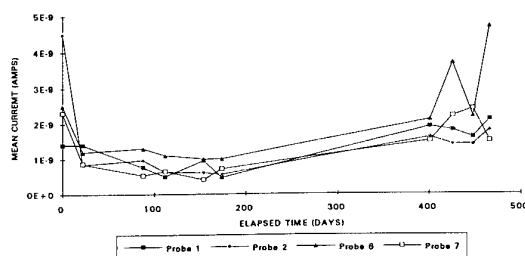


Fig. 16 Long-Term Trend In Electrochemical Current Noise Data

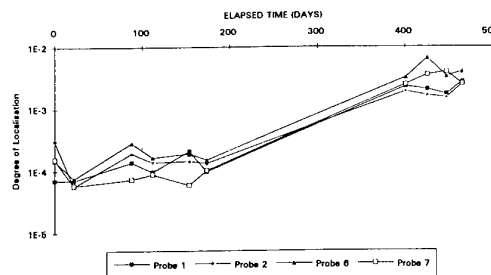


Fig. 17 Long-Term Trend In Electrochemical Current Noise Data

5. CONCLUSIONS

Laboratory trials have shown that electrochemical noise and impedance monitoring techniques can be used for the detection and characterisation of corrosion processes, including those which precede the development of observable damage. These processes include the degradation of protective treatments and corrosion activities such as uniform attack, stress corrosion cracking, pitting and crevice corrosion. Individual cracking events can be detected and identified as they occur by electrochemical noise monitoring, or the data can be analysed statistically to provide information on overall trends.

Installation of a prototype monitoring system in an aircraft has demonstrated that such techniques can be used to continuously monitor the localised corrosion activity occurring in specific areas. Particular incidences of high corrosion activity, related to operational activities, can be identified and estimates of the degree of corrosion can be made, based on long-term trends. The techniques could therefore form the basis for a predictive corrosion monitoring system for aircraft, which would offer major advantages in terms of safety and maintenance and repair costs.

6. REFERENCES

1. Houlihan, G.J., "Corrosion Control for an Aging Fleet" Aerospace Corrosion Control Symposium Proceedings, Amsterdam, March 1992, Paper 3.
2. Extracts from the Publicity Library, Stewart Hughes Ltd.
3. "Power Plant Diagnostics Go On-Line", Mechanical Engineering, December 1989.
4. Technical Annex, BE-3355 "New Accelerated Corrosion Test Methods", May 1990
5. Fitzgerald, B.J., Meredith, J.O. and King, R.P., "On-Line Corrosion Monitoring: A Case History".
6. Rothwell, A.N. and Eden, D.A., "Electrochemical Noise Techniques for Determining Corrosion Rates and Mechanisms", NACE Corrosion '92, Nashville, Tennessee, 26 April-1 May 1992.
7. Eden, D.A. and Rothwell, A.N., "Electrochemical Noise Data: Analysis, Interpretation & Presentation", NACE Corrosion '92, Nashville, Tennessee, 26 April-1 May 1992.
8. Eden, D.A., "ASTM Electrochemical Noise Workshop", Atlanta, 5 May 1993.
9. Dawson, J.L., Farrell, D.M., Aylott, P.J. and Hladky, K., "Corrosion Monitoring Using Electrochemical Noise Measurements", Corrosion '89, New Orleans, April 1989, Paper 31.
10. Dawson, J.L., "Electrochemical Corrosion Monitoring, An Overview: Fundamentals & Applications".
11. Hladky, K., Callow, L.M. and Dawson, J.L., "Corrosion Rates from Impedance Measurements: An Introduction", British Corrosion Journal,, 1980, Vol.15, No.1.
12. Smart, J.D., Eden, D.A., Weetman, D.C., Quirk, G.P. and Ryder, J.C., "Final Report, Brite-Euram Project BE-3355 - New Advanced & Accelerated Corrosion Tests", CML Report 201-2, June 1993.
13. Smart, J.D., "Brite-Euram Project 3355, Contract No., BREU-0176-C(MB), British Aerospace Contribution to Part I - Electrochemistry", ADE-EFM-R-RES-CR-0292, December 1993.
14. Smart, J.D., "The Evaluation of a Prototype Corrosion Monitoring System, First Progress Report", ADE-EFM-R-801-CR-0135, April 1992.

15. Eden, D.A. and Weetman, D.C.,
"Second Progress Report on the
British Aerospace Divisional
Technology Project ST/SI/8/M02
- The Evaluation of a Prototype
Corrosion Monitoring System",
CML Report DCW07A54.REP,
July 1992.
16. Whyte, S.M., Quirk, G.P.,
Ryder, J.C., Weetman, D.C.,
Rothwell, A.N. and Cox, W.M.,
"Progress Report on the
British Aerospace Advanced
Corrosion Monitoring and
Surveillance Initiative", CML
Report 201-1,
January 1992.

EDDY CURRENT DETECTION OF PITTING CORROSION AROUND FASTENER HOLES

J.H. Heida and W.G.J. 't Hart

National Aerospace Laboratory NLR

P.O. Box 90502, 1006 BM Amsterdam

The Netherlands

1. SUMMARY

An evaluation of the eddy current technique for the detection and depth assessment of corrosion around fastener holes in F-16 lower wing skins is described. The corrosion type in this structure is pitting corrosion at the countersink edge of the fastener holes. Due to a corrosion clean-up limit of only 1.5 - 2.5 %, a maximum thickness reduction in the range of 0.08 - 0.32 mm is allowed (depending on local skin thickness). This specifies the needed sensitivity for in-service corrosion inspection.

In the evaluation use was made of specimens cut out of the F-16 lower wing skin structure. In total twelve specimens were exposed to an accelerated corrosion test (EXCO-test). Eddy current inspection of the specimens with installed fasteners was performed with a standard eddyscope and four different eddy current probes. After the eddy current inspection cross-sections of the twelve specimens were made to determine the extent of pitting corrosion at the countersink edges.

After evaluation of the inspection results the following conclusions can be drawn:

- For in-service detection of countersink edge corrosion standard visual inspection is the preferred technique regarding the simplicity, sensitivity and reliability of inspection.
- For the purpose of depth assessment the eddy current technique is capable of detecting countersink edge corrosion with a depth from about 0.1 mm. Due to the corrosion clean-up limit of only 1.5 - 2.5 % (0.08 - 0.32 mm), however, the eddy current technique is considered not applicable for in-service depth assessment of countersink edge corrosion in F-16 lower wing skins.

2. INTRODUCTION

F-16 aircraft are operational in the Netherlands since 1979. The aircraft are exposed to natural environmental conditions such as rain, seawater, high humidity and (acid) pollutants. Exposure to these rather aggressive conditions results in corrosion if the corrosion protection system on the aircraft is breached and unable to provide adequate protection. Although high performance organic coatings are applied on F-16 aircraft (a chromate containing epoxy primer and a high-flexible polyurethane topcoat), corrosion attack was already observed after a few years of service. Two specific regions, namely the lower wing skin and the air intake inner skin, suffer from premature corrosion attack. Especially the occurrence of corrosion in the lower wing skin is serious, since the corrosion clean-up limit for this structure is only

1.5 - 2.5 % of the local skin thickness. Besides, a special investigation showed that corrosion can have an effect on fatigue crack initiation. Therefore it is essential to detect early corrosion and to take corrosion-preventive measures.

This paper describes an evaluation of the eddy current technique for the in-service detection and depth assessment of corrosion around fastener holes in the aluminium lower wing skins. The evaluation makes use of specimens cut out of the F-16 lower wing structure. Advantages and limitations of the inspection technique are described. The paper concludes with a guide-line for the in-service corrosion inspection of F-16 lower wing skins.

3. CORROSION OF F-16 LOWER WING SKIN

Lower wing skin corrosion occurs preferentially around fasteners when the paint system has been cracked. Paint cracking around fasteners was already observed in an RNLA F-16 aircraft with a service life of 1½ years. It was found that cracks in the paint occurred on either side of the fasteners in the spanwise direction (Fig. 1). This can be attributed to fastener tilting due to shear load transfer. Corrosion attack may initiate after paint cracking, resulting in paint blistering, degradation of the aluminium countersink edge and rusting of the fastener head if the cadmium plating has previously been damaged (Fig. 2).

The aluminium alloy used for the lower wing skin is chromic-acid anodized 7475-T7351. The T7351 heat treatment (overaged condition) makes the alloy resistant to exfoliation corrosion, a type of corrosion that gave many corrosion problems in e.g. the 7075-T6 lower wing skins of NF-5 aircraft. However, 7475-T7351 is prone to pitting corrosion and the corrosion process is possibly promoted by galvanic coupling with the fastener. This is an interference fit steel fastener with a cadmium coating. Figure 3 shows a cross-section with corrosion attack (pitting) at the countersink edge. This concerns in-service corrosion after an operational life of 1½ years. More details about the occurrence of F-16 lower wing skin corrosion are given in references 1 and 2.

The NLR experience so far with in-service corrosion and laboratory corrosion tests on specimens from the F-16 lower wing skin is that corrosion attack under a cracked paint system is exclusively restricted to countersink edge corrosion. This confirms the effectiveness of wet installation of fasteners in preventing corrosion attack in the countersink and the cylindrical hole. This information is important for establishing suitable inspection techniques.

The occurrence of corrosion in the F-16 lower wing skin is especially serious since the corrosion clean-up limit is only 1.5 - 2.5 % of the local skin thickness (maximum depth of damage after rework). When this limit has been exceeded after rework, the engineering department should be consulted for further action. According to the manufacturer this limit is based on both the static strength and fatigue limits of the aircraft structure. The thickness of the F-16 lower wing skin at the relevant fastener locations varies from 0.2 inch (5.1 mm) at the tip to 0.5 inch (12.7 mm) at the wing root. A corrosion clean-up limit of 1.5 - 2.5 % results then in a maximum thickness reduction in the range of 0.003 inch to 0.0125 inch (0.08 - 0.32 mm). This specifies the needed performance of the inspection technique for the lower wing skin concerning reliability and accuracy.

Besides the corrosion clean-up limit, another point of concern is that countersink edge corrosion can have an effect on fatigue crack initiation. In a special investigation this effect was determined for F-16 lower wing skin joint specimens under manoeuvre loading (Ref. 3). The specimens in this investigation were Double Dogbone low load transfer joint specimens made of 7475-T7351 aluminium of thickness 6.3 and 9.6 mm and containing two C9570-8 (¼ inch) blind countersink fasteners. The specimens were corroded to corrosion depths of 0.15, 0.3 and 0.5 mm at the countersink edge. For a specimen thickness of 9.6 mm no effect of corrosion attack on fatigue life was observed. However, for the specimens of 6.3 mm thickness a fatigue life reduction occurred for all mentioned corrosion depths. For the corroded specimens all fatigue cracks initiated on the corroded countersink, while the uncorroded specimens showed fatigue crack initiation in the cylindrical part of the countersink hole. Examples of fracture surfaces are shown in figure 4. These observations, together with the low corrosion clean-up limit, emphasizes the need to detect early corrosion and to take corrosion-preventive measures.

4. NON-DESTRUCTIVE INSPECTION

For the detection and characterization (sizing and depth assessment) of corrosion around fastener holes a number of non-destructive inspection (NDI) techniques can be used (Refs. 4-6). As mentioned before, the type of corrosion attack in the F-16 lower wing skin is pitting corrosion at the countersink edge. Based on this specific corrosion type, the following recommendations for in-service corrosion inspection can be given:

a) Corrosion detection.

Detection of countersink edge corrosion is preferably done by simple, visual inspection. The occurrence of corrosion is in general accompanied by paint-blistering, so visual inspection can also include the monitoring of the paint system condition. Visual inspection has to be performed after aircraft washing and with adequate lighting. Inspection must lead to the indication of areas worthy of closer attention, and to provide a general statement of yes-or-no acceptance.

b) Corrosion characterization.

Characterization of countersink edge corrosion will include close inspection of defined areas with more sensitive NDI-equipment. The inspection must be capable to detect, size and assess the depth of the corrosion. For this purpose the eddy current technique is considered to be the most suitable NDI-technique.

Other NDI-techniques currently in use by the RNLAf (e.g. penetrant, radiographic and ultrasonic inspection) are not considered applicable or suitable for this specific corrosion inspection.

5. EDDY CURRENT INVESTIGATION

The applicability of the eddy current technique for the detection and depth assessment of corrosion around fastener holes in F-16 lower wing skins was evaluated. Details of the investigation are given in reference 7.

5.1 Specimens

Twelve representative specimens were cut out of an F-16 lower wing skin (Fig. 5). The specimen material is chromic-acid anodized aluminium alloy 7475-T7351. All specimens contained one interference fit steel fastener NAS 4452 with cadmium coating. Six specimens with the original F-16 paint system and six specimens with removed paint system (removed with TURCO-stripper 5469) were exposed with different duration to an accelerated corrosion test (EXCO-test conform to ASTM G34-79). The exposure times are given in table 1. A previous investigation (Ref. 1) showed that this test gives corrosion attack comparable to the corrosion damage around fasteners observed in service. The six specimens with the original F-16 paint system were exposed with installed fasteners. Along the countersink edge the paint system was mechanically removed to promote corrosion attack. The specimens without paint system were exposed without fasteners. To prevent severe overall corrosion the specimens were sealed with wax except for an area of about 1 mm from the countersink edge in the direction of both the countersink and the skin surface.

5.2 Eddy current inspection

In the evaluation of the eddy current technique for the purpose of in-service corrosion inspection, the following conditions were made:

- Use of standard equipment. Therefore only manual inspection with commercially available probes, and no automated in-situ C-scanning technique, was considered.
- Local inspection with high sensitivity of the aluminium-fastener area. Therefore only small diameter probes and no probes that view a larger area, such as sliding probes and rotating surface probes, were considered.

In view of these conditions, eddy current inspection was carried out with a standard phase analysis eddyscope (NORTEC-19e^{II} of Staveley Instruments Inc.) and the following four eddy current probes:

- NORTEC 3551 F (Staveley Instruments Inc.).
This is a standard absolute shielded pencil-probe with a frequency range of 100 kHz - 500 kHz. The probe outer diameter is 3.5 mm; the shielded coil has an effective sensitive area approximately 2 mm in diameter.
- NORTEC PR/1 kHz - 100 kHz/A (Staveley Instruments Inc.).
This is a reflection absolute shielded pencil-probe with a frequency range of 1 kHz - 100 kHz. The probe outer diameter is 6.3 mm; the shielded coil has an effective sensitive area approximately 2 mm in diameter.
- AN05-3 (EMA-Elektronik).
This is an absolute shielded probe with a frequency range of 10 kHz - 2 MHz. The probe outer diameter is 7 mm; the shielded coil has an effective sensitive area of approximately 0.8 x 1 mm².

- AN16-2 (EMA-Elektronik).

This is an absolute shielded probe with a frequency range of 10 kHz - 1 MHz. The probe outer diameter is 7 mm; the shielded coil has an effective sensitive area of approximately $1 \times 2 \text{ mm}^2$.

The first two probes are standard probes comparable with those currently used by the RNLAf. Eddy current probes AN05-3 and AN16-2 are special probes developed for quantitative assessment of surface corrosion (Ref. 8). The design of these probes is so that there is no area with reduced sensitivity at the probe centre (so-called blind spot in the flux distribution).

In the investigation the probes were scanned along the line of cross-sections A, as indicated in figure 6. During the eddy current inspection also the specimens corroded without installed fasteners were provided with fasteners. The eddy current responses of the aluminium-fastener transition were subsequently compared for the different specimens. For all inspections also the eddy current responses of lift-off and edge-effect were observed. To optimize the eddy current response for corrosion detection different test frequencies in the range of 100 kHz - 2 MHz have been applied. For aluminium alloy 7475-T7351 (conductivity 42 % IACS) these frequencies result in a standard depth of penetration δ of 0.07 mm (at frequency 2 MHz) to 0.32 mm (at frequency 100 kHz). In general the effective depth of penetration will be about three times these values.

5.3 Inspection results

Twelve specimens were exposed with different duration to an EXCO-solution (Tab. 1). After the EXCO-test the specimens were photographed, see for example figure 6 for specimens 1A, 3A, 4A and 6A. Figure 6 shows a corrosion attack comparable to the corrosion damage around fasteners

observed in service. Visual inspection of all specimens showed corrosion attack for an exposure time from 4 hours (specimen 3A) for the specimens with paint system, and corrosion attack for an exposure time from 2 hours (specimen 2) for the specimens with removed paint system.

After visual inspection the twelve specimens were inspected with four eddy current probes according to the procedure given in section 5.2. A detailed description of the inspection results is given in reference 7. In summary we can say that the standard absolute shielded pencil-probe NORTEC 3551 F shows the best capability for the detection of corrosion around the steel fasteners in the F-16 aluminium lower wing skin structure. The optimum frequency for corrosion detection with this probe is approximately 200 kHz. At this frequency clearly different eddy current responses of the aluminium-fastener transition, indicating the presence of countersink edge corrosion, are observed for specimens 4 A (with paint system) and specimen 2 (paint system removed). For specimens with longer EXCO exposure times the difference in fastener response is increasing. Figure 7 gives some examples of the eddy current responses observed for the standard probe NORTEC 3551 F.

The special probes AN05-3 and AN16-2 show some capability for corrosion detection. Of the two probes the AN05-3 probe working at a frequency of approximately 1000 kHz has the best performance. In comparison with the standard probe NORTEC 3551 F, however, the applicability for corrosion detection is less promising.

After the eddy current inspection cross-sections of the twelve specimens were made along the line A-B as indicated in figure 6. The cross-sections show pitting corrosion (no indication of exfoliation corrosion) at the countersink edges.

Table 1 Corrosion attack as determined from cross-sections

SPECIMEN NUMBER	PROTECTION	EXCO EXPOSURE TIME (HOURS)	CORROSION ATTACK (MM)					
			SIDE A			SIDE B		
			1	2	3	1	2	3
1 1A	S FP	0 0	0.0 0.0	0.0 0.0	0.0 0.0	0.0 0.0	0.0 0.0	0.0 0.0
2 2A	S FP	2 2	0.12 0.06	0.73 0.14	0.0 0.12	0.08 0.0	0.21 0.0	0.03 0.12
3 3A	S FP	4 4	0.18 0.15	0.63 0.14	0.22 0.14	0.11 0.22	0.32 0.34	0.08 0.24
4 4A	S FP	8 8	0.36 0.31	1.88 0.52	0.38 0.32	0.32 0.22	1.50 0.36	0.30 0.22
5 5A	S FP	16 16	0.56 0.44	1.64 0.56	0.56 0.42	0.54 0.34	2.32 0.80	0.60 0.30
6 6A	S FP	32 32	1.05 0.66	2.40 0.61	1.20 0.74	1.16 0.74	2.04 1.12	1.28 0.58

S Sealant on anodised surface and in countersink

FP Fastener + Paint system

For both the specimens with and without the F-16 paint system there is corrosion attack for an EXCO exposure time from 2 hours (specimens 2A and 2). For longer EXCO exposure times the degree of corrosion attack is clearly increasing. The cross-sections of the type A specimens further show that the corrosion attack is restricted to the countersink edges, indicating an optimum sealing of the countersink by the wet installation of the fasteners.

To enable a more quantitative comparison of the corrosion attack for the different specimens, the extent of corrosion attack was measured at the countersink sides A and B in the cross-sections. More specifically, the radial length of the corrosion attack along the skin surface and the depths of the corrosion attack in the skin surface and in the countersink surface were measured (Tab. 1). The values in table 1 clearly show the increasing degree of corrosion attack for increasing exposure times to the EXCO-solution. This increase can be observed for all three length and depth measures, and for both the specimens with and without the F-16 paint system.

5.4 Discussion

Evaluation of the inspection techniques for the purpose of corrosion detection shows that visual inspection is more sensitive than eddy current inspection. With visual inspection only the corrosion attack of the painted specimen with an EXCO exposure time of 2 hours was not detected. Besides the higher sensitivity visual inspection is also easier to perform, takes less inspection time and probably has higher reliability for in-service corrosion detection than the eddy current inspection technique.

For the purpose of corrosion characterization, and especially for depth assessment, visual inspection is not suited. For this purpose the eddy current technique is considered to be the most suitable NDI-technique. As mentioned before, evaluation of different eddy current probes resulted in an optimum corrosion detection capability for the standard absolute shielded pencil-probe at a test frequency of about 200 kHz. To quantify these inspection results the deviation in the eddy current response of the aluminium-fastener transition has been plotted against the corrosion depth (Tab. 1, side A, measure 1) in figure 8. The deviation (D), defined as the distance between the lines of fastener response for specimens with and without corrosion, is expressed in arbitrary units.

Figure 8 shows that there is a reasonable correlation between the deviation in the eddy current response and the corrosion depth. Further, the corrosion detection capability is best, as expected, for the specimens 1 to 6 with removed paint system. To provide an estimate of the sensitivity of the eddy current technique for corrosion depth assessment, the sensitivity is set to correspond to a deviation D equal to 0.5. The graphs in figure 8 then show that this sensitivity is roughly 0.2 mm for specimens with paint system and roughly 0.1 mm for specimens with removed paint system.

We can conclude that the eddy current technique has a high sensitivity for corrosion depth assessment. However, if we regard a conservative value of 0.08 mm for the corrosion clean-up limit in the thin sections of the F-16 lower wing skin, then the sensitivity of the eddy current technique is considered not sufficient.

6. IN-SERVICE CORROSION INSPECTION

Summarizing the results of the eddy current investigation

we can say that for in-service detection of countersink edge corrosion around the fastener holes in the F-16 lower wing skin, standard visual inspection is the preferred technique. Further, despite the high sensitivity of the eddy current technique, the corrosion clean-up limit of only 1.5 - 2.5 % is the main reason that the eddy current technique is considered not applicable for in-service depth assessment of countersink edge corrosion in F-16 lower wing skins. For the same reason also other NDI-techniques are considered not applicable. This leaves few alternatives for in-service corrosion inspection. The following guide-lines can hence be given:

- Visual inspection around fastener holes.
- Local removal of paint system after visual detection of corrosion.
- Mechanical removal of all corrosion presence in view of the clean-up limit of only 1.5 - 2.5 %.
- Measurement of remaining skin thickness to check whether the corrosion clean-up limit has been exceeded or not. Thickness gauging can be done e.g. with a high-precision ultrasonic contact pencil transducer or more simply with a dial-indicating depth micrometer.
- Consultation of the engineering department in case of local exceedance of the corrosion clean-up limit.

7. CONCLUSIONS

Based on an investigation into the applicability of the eddy current technique for the detection and depth assessment of corrosion around fastener holes in F-16 lower wing skins, the following conclusions are reached:

1. The corrosion type in F-16 lower wing skins is pitting corrosion at the countersink edge of fastener holes.
2. The corrosion clean-up limit of 1.5 - 2.5 % for F-16 lower wing skins results in a maximum thickness reduction in the range of 0.08 - 0.32 mm, depending on local skin thickness. This specifies the needed sensitivity for in-service corrosion inspection.
3. For in-service detection of countersink edge corrosion standard visual inspection is the preferred technique regarding the simplicity, sensitivity and reliability of inspection.
4. For in-service characterization (especially depth assessment) of countersink edge corrosion by means of eddy current inspection the optimum performance was demonstrated by a standard absolute shielded pencil-probe at a test frequency of about 200 kHz. This probe is capable of detecting countersink edge corrosion with a depth from about 0.2 mm for specimens with paint system and about 0.1 mm for specimens with removed paint system. The inspection results of this probe show a reasonable correlation between the deviation in the eddy current response of the aluminium-fastener transition and the corrosion depth.
5. Despite the high sensitivity of the eddy current technique the corrosion clean-up limit of only 1.5 - 2.5 % (0.08 - 0.32 mm) is the main reason that the eddy current technique is considered not applicable for in-service depth assessment of countersink edge corrosion in F-16 lower wing skins.

8. ACKNOWLEDGEMENT

The authors would like to acknowledge the support of the Scientific Research Division of the Directorate of Materiel, Royal Netherlands Air Force.

9. REFERENCES

1. Bonnee, W.J.A., "Corrosion and corrosion removal on F-16 aircraft", NLR TR 88089 C, 1988.
2. Hart, W.G.J. 't and Boogers, J.A.M., "Corrosion protection systems for F-16 aircraft", NLR TR 89171 C, 1989.
3. Hart, W.G.J. 't and Boogers, J.A.M., "Effect of countersink edge corrosion on fatigue crack initiation, to be published.
4. Bunce, H.G., "Corrosion and non-destructive testing", Aircraft Engineering, Vol. 61, No. 4, 1989, pp. 2-8.
5. Alcott, J., "An investigation of nondestructive inspection equipment: detecting hidden corrosion on USAF aircraft", Materials Evaluation, Vol. 52, No. 1, 1994, pp. 64-73.
6. Hagemaijer, D.J. and Nguyen, K., "Automated eddy current scanning of aircraft for corrosion detection", Materials Evaluation, Vol. 52, No. 1, 1994, pp. 91-95.
7. Heida, J.H. and Hart, W.G.J. 't, "Eddy current detection of corrosion around fastener holes in F-16 lower wing skins", NLR CR 94057 L, 1994.
8. Thomas, H.M., "Bildverarbeitung unterstützt Wirbelstromprüfung", Materialprüfung, Vol. 34, No. 5, 1992, pp. 135-138.

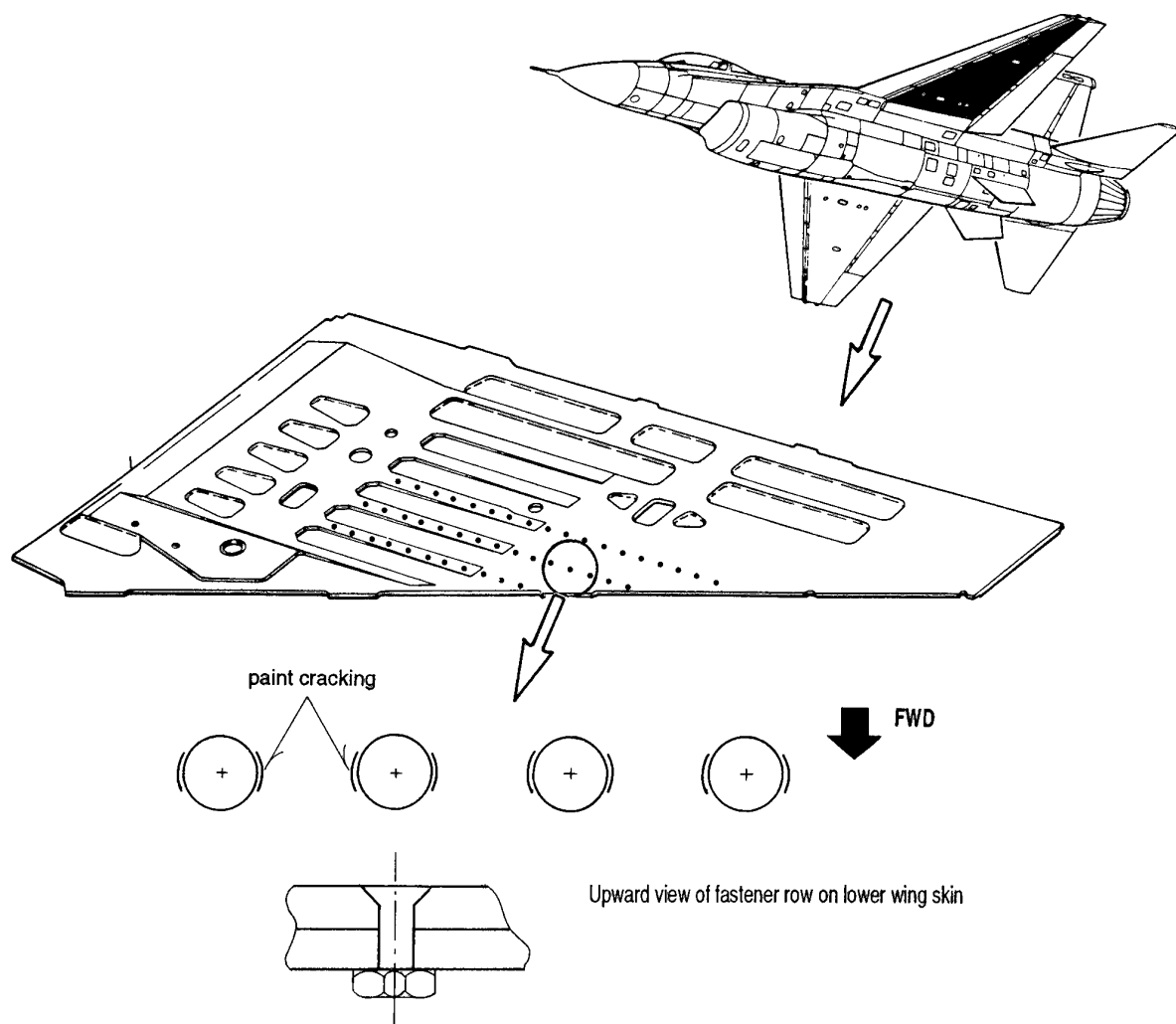


Fig. 1 Paint cracking in highly loaded components attributed to tilting of the fasteners due to shear load transfer

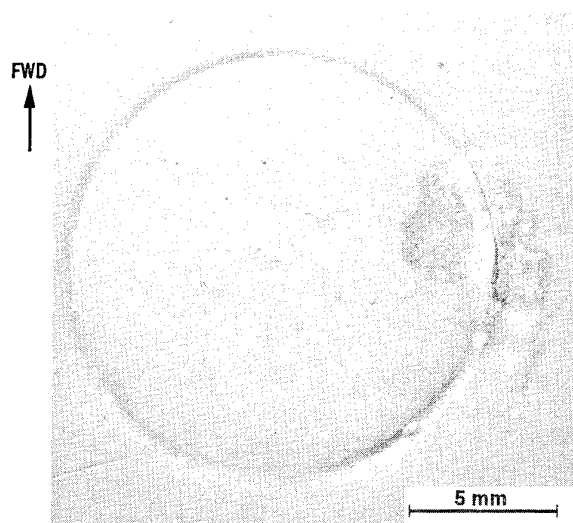


Fig. 2 Start of in-service corrosion at locations where the paint-system is cracked

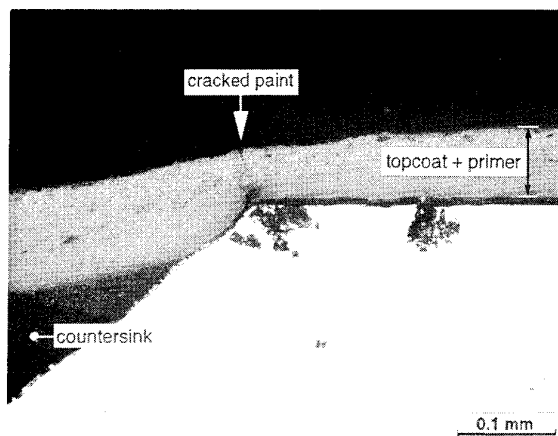
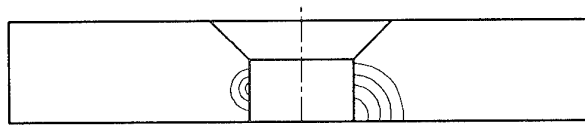
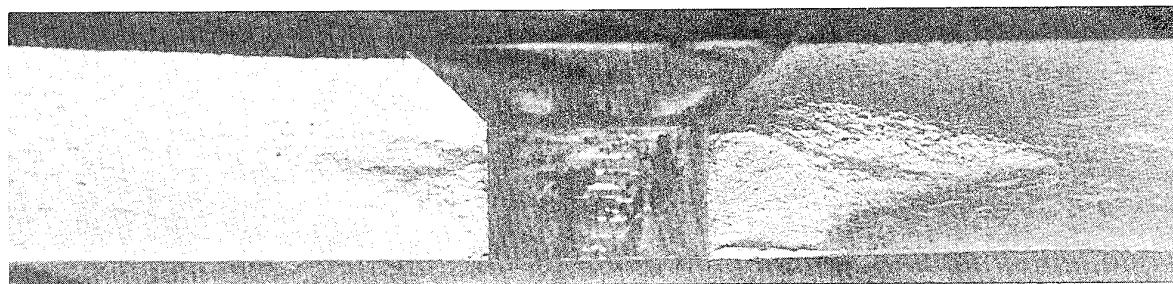


Fig. 3 Corrosion attack in countersink edge under cracked paint system



a) No corrosion

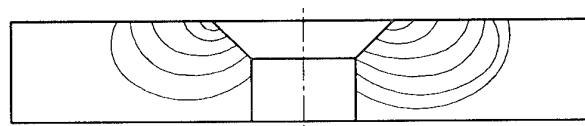
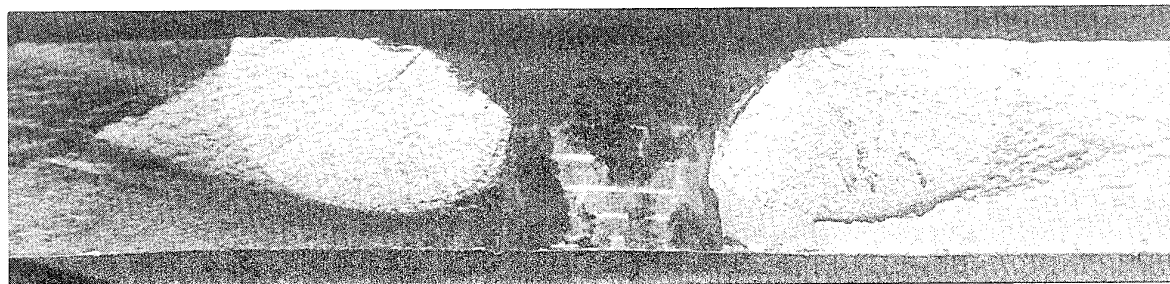
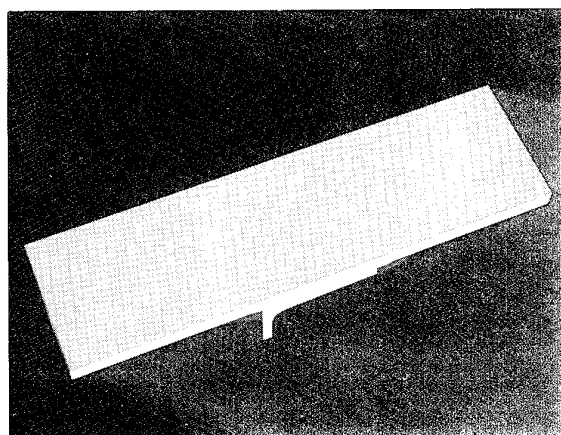
b) Countersink edge corrosion.
Corrosion depth 0.3 mm

Fig. 4 Examples of fatigue crack initiation in uncorroded and corroded joint specimens (half specimen thickness 6.3 mm). [Figure 12 from Ref. 3]



- Aluminium alloy : 7475-T7351
- Surface pre-treatment: Chromic-acid anodized;
per MIL-A-8625, Type I
- Primer : Epoxy primer S15/76 of ADAF;
per FMS 3027, MIL-P-23377
- Top coat : High-flexible, polyurethane
Aerodur HF A132 of ADAF;
per MIL-C-83286
- Fastener : NAS 4452 H-type, Interference
fit steel fastener with cadmium coating,
90° countersink surface;
1/4 inch or 5/16 inch diameter hole
- EXCO test : Conform to ASTM G34-79

Fig. 5 Test specimen from F-16 lower wing skin

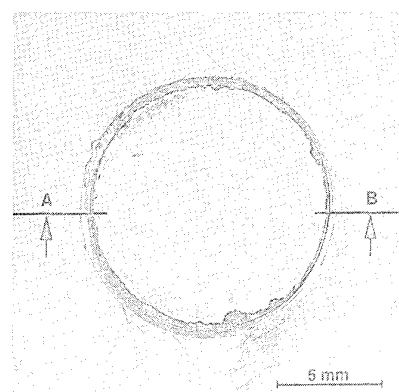
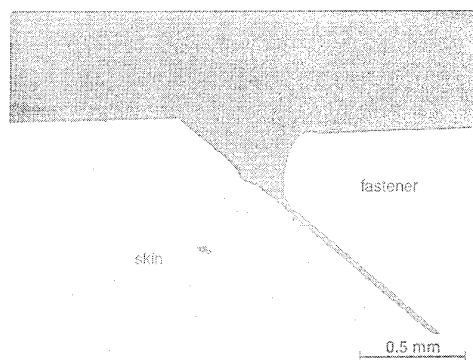
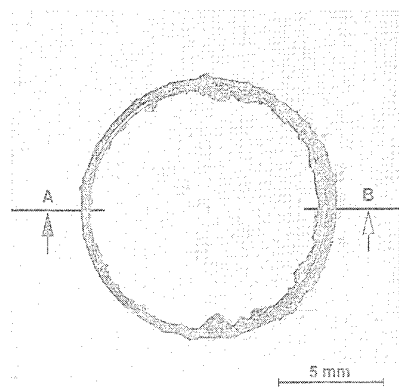
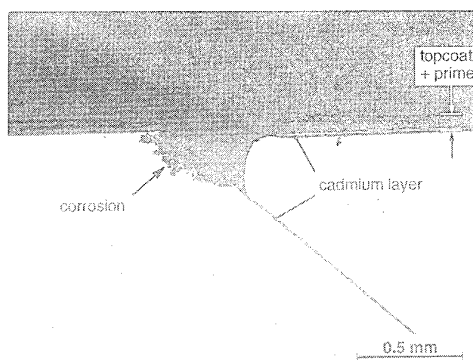
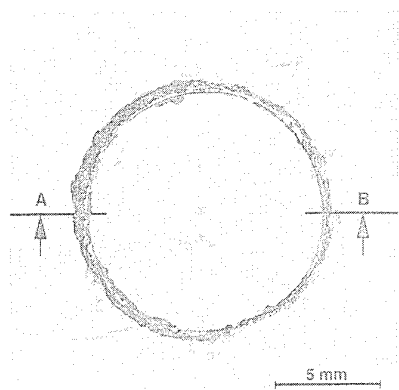
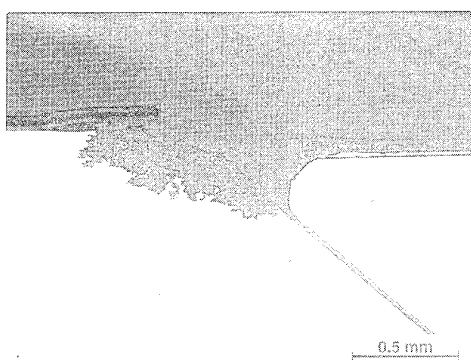
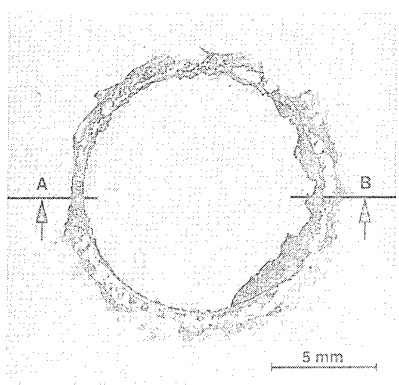
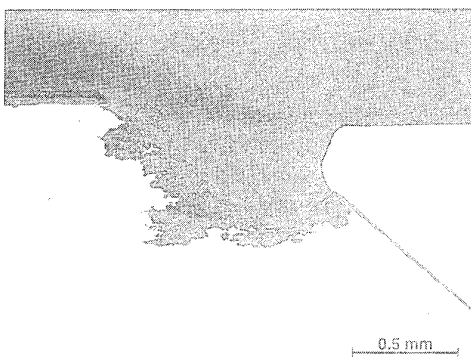
**Specimen 1A**0 hours in
EXCO-solution**cross-section A****Specimen 3A**4 hours in
EXCO-solution**cross-section A****Specimen 4A**8 hours in
EXCO-solution**cross-section A****Specimen 6A**32 hours in
EXCO-solution**cross-section A**

Fig. 6 Corrosion attack in F-16 lower wing skin specimens (with paint system) after exposure to an EXCO-solution (conform to ASTM G34-79)

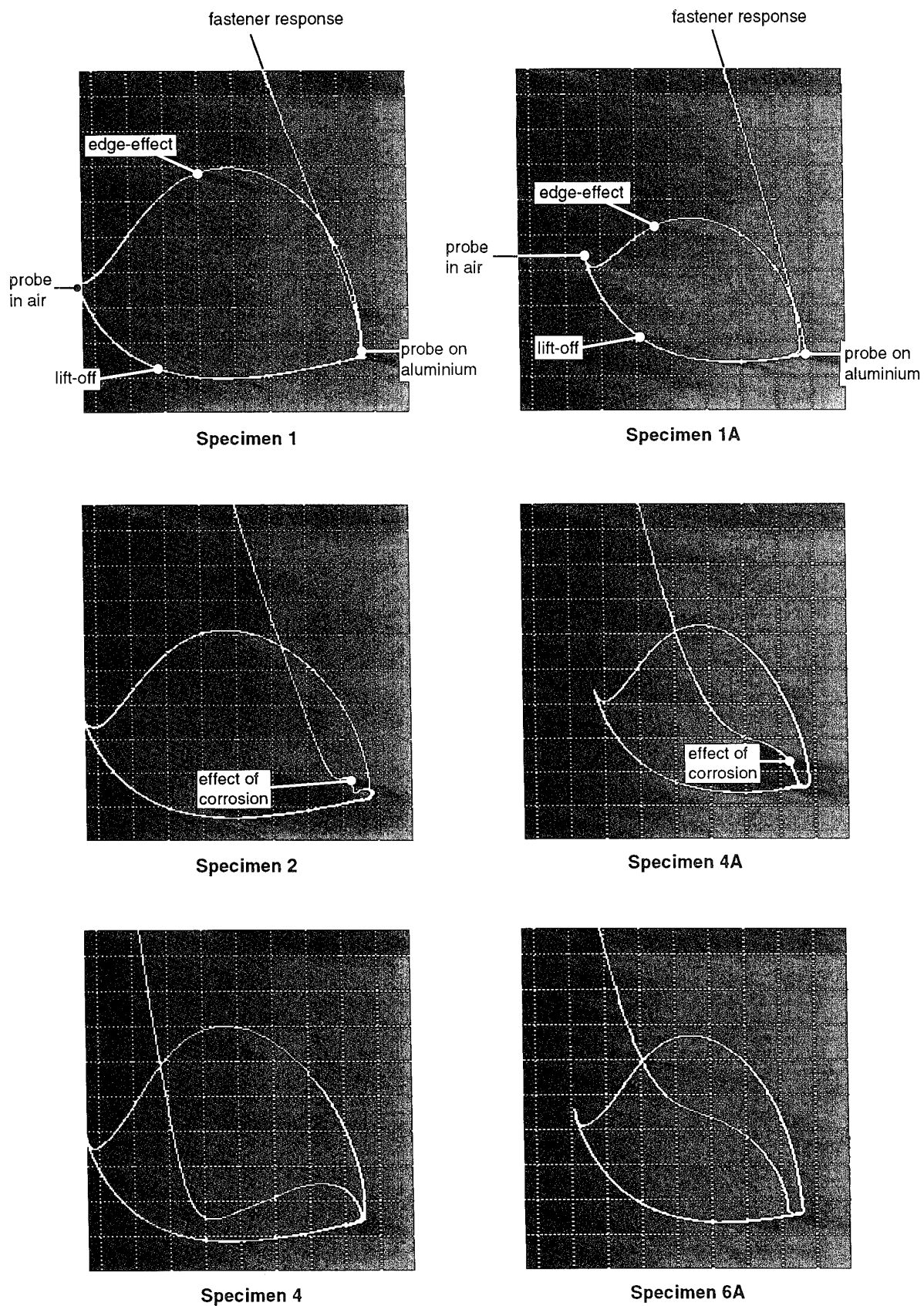
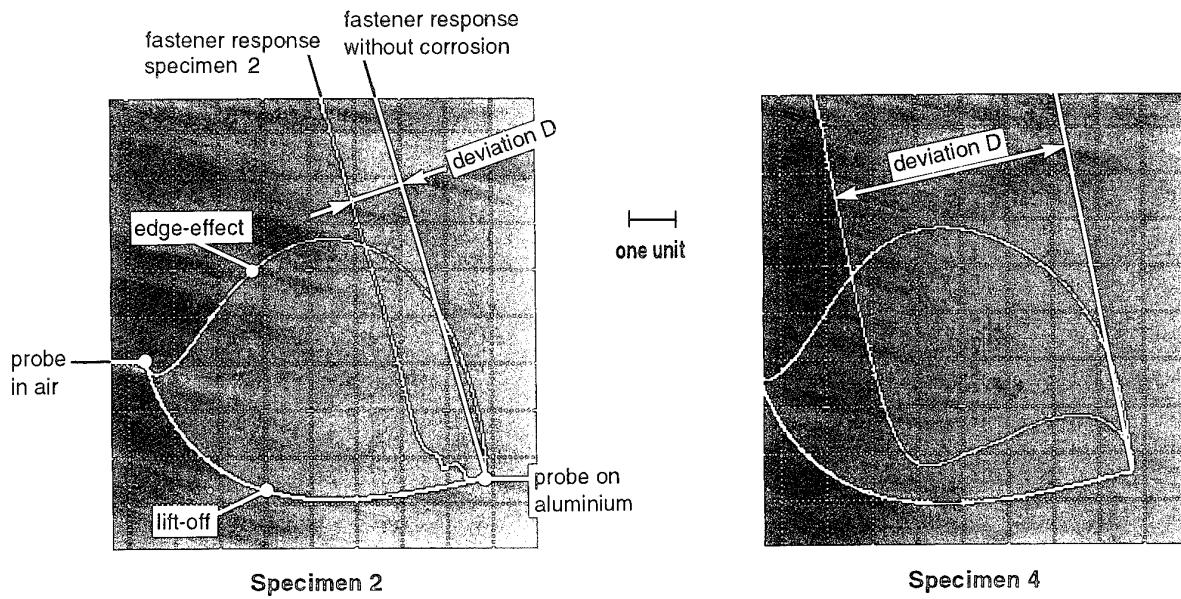


Fig. 7 Examples of eddy current response of the aluminium-fastener transition.
 Specimens 1A, 4A, 6A (with paint system) and 1, 2, 4 (paint system removed).
 Eddy current probe NORTEC 3551F, test frequency 200 kHz



Eddy-current responses at a test frequency of 200 kHz for specimens 2 and 4, paint system removed

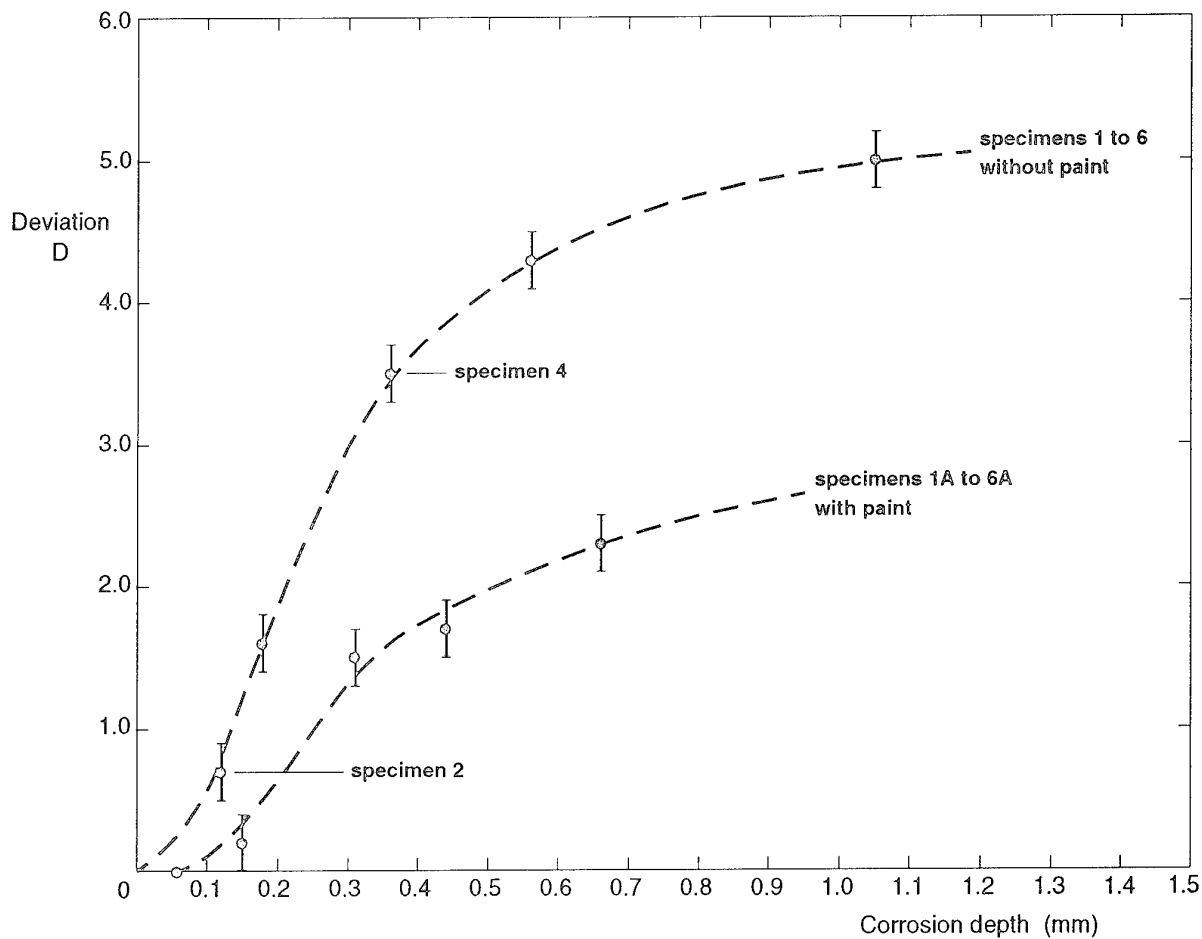


Fig. 8 Deviation D in the eddy current response of the aluminium-fastener transition (EC probe NORTEC 3551F, test frequency 200 kHz) versus the countersink edge corrosion depth (table 1, side A, measure 1). Specimens 1A to 6A (with paint system) and specimens 1 to 6 (without paint system)

IN-SITU DETECTION OF SURFACE PASSIVATION OR ACTIVATION AND OF LOCALIZED CORROSION: EXPERIENCES AND PROSPECTIVES IN AIRCRAFT

A. Pourbaix

CEBELCOR, Belgian Center for Corrosion Study
Avenue Paul Héger, grille 2, B 1050 Brussels

SUMMARY

The surveillance of the actual conditions of materials in aircrafts and the analysis of the influence of flight or standby conditions require detection methods that give quantitative and instantaneous results and that are related to the real degradation process. Electrochemical methods derived from methods used in laboratory have proven to be of interest. The scientific concepts and the instrumentation are generally easily applicable to field conditions; some effort is necessary to develop relevant sensors. The first example applies to the phosphating of carbon steels before painting. The characterization of surface passivation or reactivity can be of interest before and during the surface conversion processes. The second example applies to the detection of crevice corrosion, as may occur in riveted joints.

1. INTRODUCTION

1.1 Quality control of surface preparation before anticorrosive protection is important. Surface conversion and coating with paints are classical operations but still, this is a recognized need for reliable methods to describe the quality of the surface.

One example will be presented, on the surface preparation of carbon steel before phosphating.

1.2 The surveillance of on-going corrosion processes in aircrafts and the analysis of the influence of flight or standby conditions require detection methods that give quantitative and instantaneous results and that are related to the real degradation process.

Electrochemical methods derived from techniques used in laboratory have proven to be of interest for crevice corrosion, as may occur at riveted joints. An example will be given, taken from an on-line application in the chemical industry.

2. ASSESSMENT OF SURFACE REACTIVITY BEFORE SURFACE CONVERSION

2.1 Field of application:

The method was originally proposed for assessing the surface reactivity of cold rolled steel sheets before phosphatizing. The method is useful to assess differences of

surface reactivity which may result from carbonaceous residues, from surface segregation of iron oxides or manganese oxides, from alloying elements (P, Nb, N) and from different annealing treatments, storage conditions, surface contaminations and degreasing treatments. Surface reactivity is considered here as a capability for a surface to react at the same rate and after the same incubation time at all place.

2.2 Scientific base

The phosphating process starts with a dissolution of the oxides, then of the base metal. During the dissolution of the metal, hydrogen is evolved and the pH increases near the surface. This results in the precipitation of zinc phosphates or, in cases, also of iron and manganese phosphates. For a good quality of the phosphated products, it is important that the dissolution of the steel and the subsequent formation of the phosphate layer take place everywhere at the same time and at the same rate. Otherwise, active spots coexist with small areas already covered with phosphate, and this counteracts the beneficial effect of the oxidizing additives present in most phosphating solutions.

Attempts were made to use electrochemical impedance spectroscopy and scanning potential mapping to describe the reactivity at every point of the surface, but at the time of this study, it was found easier and cheaper to develop a method based on more classical electrochemical techniques.

In the method eventually developed, the zero-current potential measurement is used to indicate the dissolution of surface oxides and the beginning of the dissolution of the base metal, and polarization resistance measurements indicate the amount and the distribution of the surfaces concerned with

this dissolution and the coverage given by the phosphate layer.

2.3 Materials and method

The measurements were made in a standard phosphatizing solution (zinc phosphate, pH 2.75, free acidity 12.5 ml NaOH 1N for 100 ml and total acidity 22 ml NaOH 1N for 100 ml, with nitrites and nitrates as accelerators. Reference: Granodine 164-Cebelcor).

The method was tested on a series of 20 different steels of different compositions or annealed in different atmospheres (DX gas: $\text{CH}_4 + \text{CO} + \text{CO}_2 + \text{H}_2 + \text{N}_2$ or HNX gas: $\text{H}_2 + \text{N}_2$) (1,2). The responses to the electrochemical tests were compared with the results of salt spray tests on phosphated, painted and scratched panels, as is usually done for the evaluation of phosphate coatings.

Polarization resistance is measured under galvanostatic control, to allow for the free potential changes that occur inevitably during the phosphatation reactions. The polarization cycle used was 0.5 Hz and the potential increment ΔE was limited to 10 mV. A cell attached to the steel sheet with magnets is convenient for control on car assembly lines.

2.4 Results

Figure 1 shows, on the left part, the results for a steel with an heterogeneous surface with a low reactivity: it takes some time for the oxide to be dissolved and for the potential to drop, and the final phosphate layer coverage, measured by the polarization resistance, is rather poor.

The right-hand side of figure 1 shows the results for a very reactive steel: the oxides are quickly dissolved, as indicated by the immediate drop of the potential, and the final coverage is good, as indicated by the high value of the polarization resistance.

It was interesting to observe the large difference in reactivation time for the 20 steels tested: from 1 to 200 s. Among the 20 different coils tested, the worst steel in terms of surface reactivity was also the first to fail in the salt spray test.

The selectivity of the electrochemical reactivity test was much better than that of the salt spray test. It is thought that the electrochemical reactivity tests deals exactly with the phosphating process and that, as such, it is a sound test to appraise the quality of the surface preparation.

2.5 Application to aircrafts

Similar methods may be used to control pickling and other surface preparation. The preparation of aluminium before painting by solutions containing chromic or phosphoric acid produce a complex layer of small thickness (1-5 μm) that has a significant effect on the performances of the coating, but which is difficult to describe by physical or chemical methods. An electrochemical method such as described for the phosphating of steel could be a valid tool to evaluate the quality of this conversion layer.

3. DETECTION OF CREVICE CORROSION

3.1 Field of application

Crevice corrosion is of special concern in riveted joints of aircrafts

3.2 Scientific base

The mechanism of crevice corrosion in restricted geometries such as rivets, gaskets or deposits is well known: the access of oxygen is limited locally and, on passive metals, the absence of oxygen favours

depassivation and may initiate crevice corrosion. Once this process has started, it is sustained by the coupling between passive areas (outside the crevice) and active areas (inside the crevice), by the formation and the hydrolysis of metal ions and by the diffusion of anions towards the crevice, to balance the production of positive ions. These anions are mostly chlorides, which in turn increase the depassivation effect. As a result, a specific environment builds up in the crevice, with a low pH and a high chloride content and a low electrode potential, whereas the potential outside the crevice may be much higher. The coupling current between the crevice area and the surrounding surfaces is an indication of the activity of crevice corrosion.

3.3 Materials and methods

Systems for the detection of crevice corrosion have been developed where an artificial crevice is connected to a large cathode through a zero-resistance ammeter. Systems where the cathode is the actual surface of the real structure are particularly relevant to the real situation. The geometry of the artificial crevice should of course be similar to the real situation; this may sometimes be the difficult part of the development.

One interesting application was in a plant for the bioproduction of amino acids. Different raw products were used: sugar beat molasses or starch. Severe crevice corrosion occurred in the crevice areas of multiple effects concentrators. Apparently, crevice corrosion was more severe when the cheaper raw product, with a higher chloride content, was used. To verify this, a crevice corrosion monitoring cell was installed on-line. The output of the monitoring cell was the electrode potential in the crevice, the electrode potential of the cathode and the coupling current (figure 2). This system showed not only the influence of the chloride

content of the raw product, but also the influence of specific operating conditions such as cooling periods and cleaning operations: during cooling periods, the amount of dissolved oxygen increases and this increases the electrode potential of the cathode and the coupling current. Cleaning was obviously made with oxidizing disinfectants, and this had the same but stronger effect.

3.4 Application to aircrafts

Localized corrosion is a problem at riveted joints. The metal to metal crevice at riveted joints can be reproduced; only the opening of the crevice should be exposed to the environment, the rest of the anode being masked by epoxy. This anode is then installed in the middle of a large cathode, electrically isolated from it, except for the connection to the zero-resistance ammeter. In conditions of exposures to atmospheres, a thin film of condensation, rain or brine wets both the crevice and the cathode and allows for a coupling current to flow when crevice corrosion is active.

This detection system can deliver instantaneous data; it may be useful to

indicate the periods of flights that are critical for crevice corrosion: flights in sea-brine, remanence period of earlier flights in brine, effects of rinsing.

REFERENCES

1. P.CARPENTIER, A.POURBAIX, X.Z.YANG, G.MILANESE. "Une méthode d'évaluation de la réactivité de surfaces d'aciers destinés à la phosphatation", *Rapports Techniques CEBELCOR*, vol.145, RT.267 (1983).
2. G.MILANESE, A.POURBAIX, M.MEMMI "Studi del compartamento alla fosfatazione ed alla corrosione di laminati a freddo ad alta resistenza", *Rapporto finale, convenzione CECA 7210-KB/408*, (1982)
3. A.POURBAIX, J.KISSEL, I.COUZET "Electrochemical Corrosion Monitoring and Corrosion Prevention Methods", *Proceedings of an International Symposium on Corrosion Science and Engineering*. Vol.2, ed. Cebelcor, Brussels March 12-15, 1989, *Rapports Techniques CEBELCOR*, vol.158, RT.298 (1989)

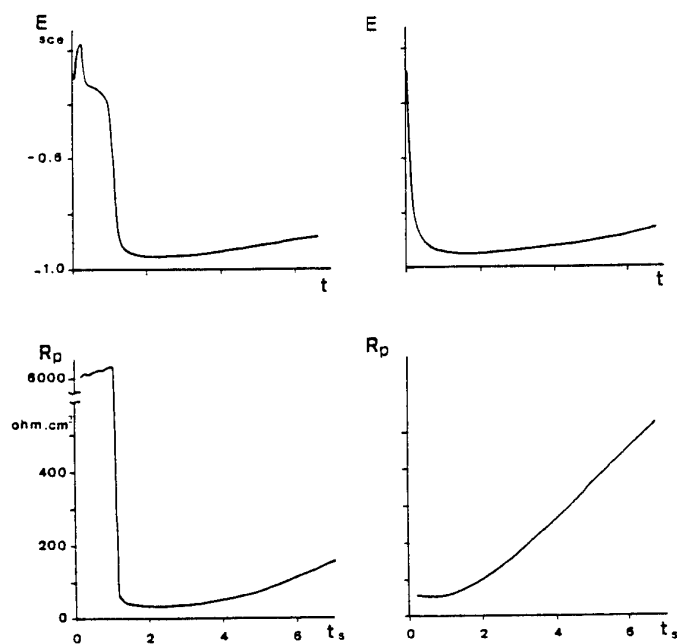


Figure 1: Results of electrochemical tests for surface reactivity of carbon steel before phosphating
left: heterogeneous surface with low reactivity - right: highly reactive surface

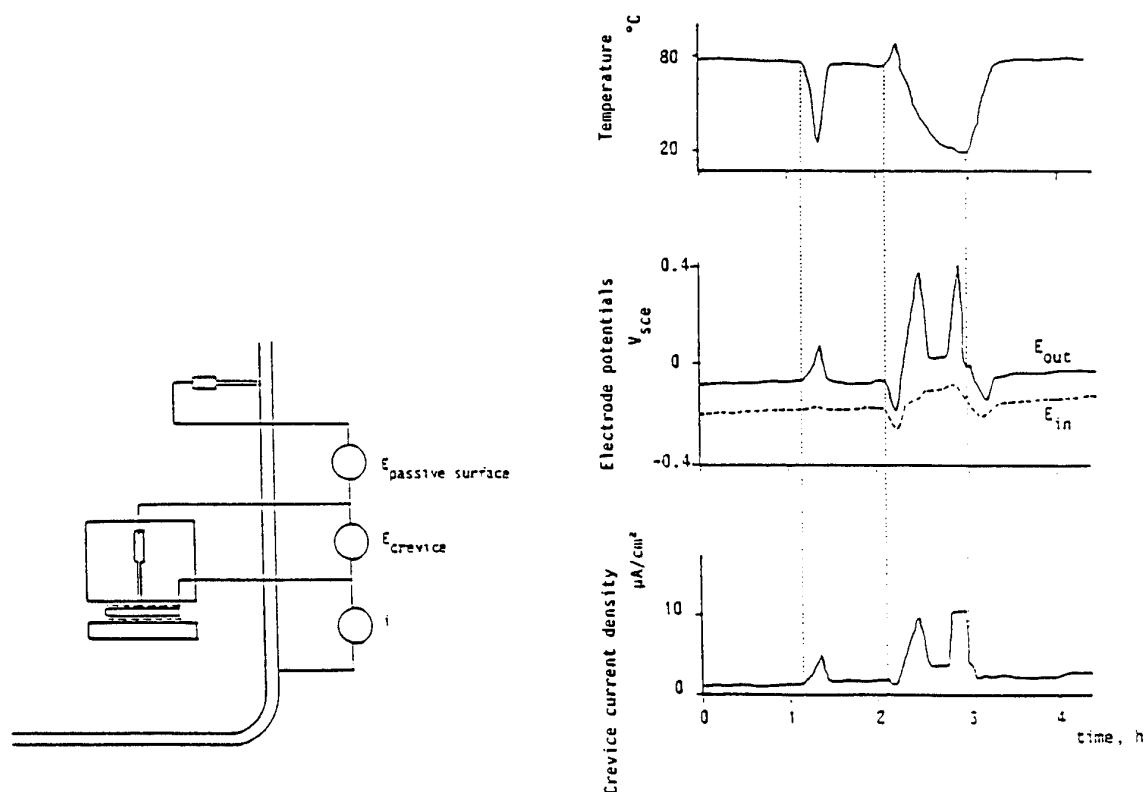


Figure 2: On-line cell for monitoring crevice corrosion, and example of results showing the occurrence of crevice corrosion during cooling and cleaning periods

TEST METHOD AND TEST RESULTS FOR ENVIRONMENTAL ASSESSMENT OF AIRCRAFT MATERIALS

A. Pourbaix
CEBELCOR, Belgian Center for Corrosion Study
Avenue Paul Héger, grille 2, B 1050 Brussels

SUMMARY

A study was conducted to identify whether life prediction of high strength aluminium alloys for aircrafts can be determined from short term accelerated atmospheric corrosion tests. The method used is a wet and dry method with electrochemical measurements to characterize the formation or destruction of passive layers. The materials tested include high strength steel 4130, precipitation hardening 15-7 Mo-PH steel and aluminium alloys 6061, 7075 and 2024 with different heat treatments and surface conditions. It appears that the ranking of different Al alloys depends on the type of atmosphere (chloride, acid). The method also clearly showed the detrimental effect of chromated cadmium plating on the hydrogen embrittlement of high strength steel. Corrosion processes of aluminium and high strength steels were clearly identified and useful recommendations could be derived from such tests.

1. AIM OF THE WORK

A study was conducted to identify whether life prediction of high strength aluminium alloys for aircrafts can be determined from

short term accelerated atmospheric corrosion tests.

2. MATERIALS AND METHODS

The method used is a wet and dry method with electrochemical measurements to characterize the formation or destruction of passive layers (figure 1) (1). The test solutions are:

- distilled water exposed to air (pH around 5.7) to simulate non polluted land (rural) atmospheres
- NaHSO_3 10^{-4}M and 10^{-3}M solutions with different pH (adjusted with H_2SO_4) to simulate industrial atmospheres and acid rains, with pH around 4.0, 3.5 and 3.2
- artificial sea water diluted 100 times, to simulate marine atmospheres
- sea water diluted 100 times + NaHSO_3 10^{-3}M adjusted to pH 3.2, to simulate mixed marine-industrial atmospheres.

The cycle duration was 60 min, with 15 or 40 min immersion and 45 or 20 min emersion, and a drying temperature of 40 to 60°C. The test solution is aerated and continuously renewed at a low flow rate.

The materials tested include aluminium and aluminium alloys 6061, 7075 and 2024 with different heat treatments and surface

conditions, and high strength steel 4130 and precipitation hardening 15-7 Mo-PH steel.

The results of the tests are given as changes of electrode potential during immersion with time, the aspect of corrosion (pits, depths, intergranular...) and the weight losses.

3. RESULTS

Interesting results are summarized as follows:

- the absence of corrosion is indicated by high potentials throughout the test (example: figure 2, for Al-Mn alloy 3103-H24 in clean atmosphere)
- general corrosion is indicated by potential lower than the hydrogen/water equilibrium potential (example: figure 3, for Al-Mn alloy 3103-H24 in industrial atmosphere)
- pitting corrosion is also indicated by low potentials (example: figure 4, for Al-Mn alloy 3103-H24 in marine atmosphere)
- Al-Zn alloys 7075-T6 is known to suffer occasionally from exfoliation, and this is not the case for the same alloy in the T73 temper. A clear difference appeared between these two tempers: the 7075-T6 alloy shows potentials lower than the hydrogen/water equilibrium potential, whereas the alloy 7075-T73 showed potentials higher than the hydrogen/water potential (figures 5 and 6).
- the interpretation of electrode potentials for the case of Al-Cu alloys is more complex: local redeposition of copper produces high potentials which may be confused with an indication of no-corrosion, although these alloys are highly susceptible to pitting corrosion (and to intergranular corrosion at the bottom of pits).
- in spite of the chromatation treatment, the cadmium coating on 4130 and 15-7 Mo-PH high strength steels lowers the potential below the hydrogen potential, and this may be dangerous for the hydrogen embrittlement of the 4130 steel (figures 7 and 8). In mixed

marine + industrial atmosphere, the chromated coating has been completely dissolved after about 12 days of test, as shown in figure 8. This raises questions on the justification for this surface treatment on high strength steels.

More results are described in (2).

4. PROSPECTIVE FOR AIRCRAFT APPLICATIONS

The method is useful and fast for the selection of materials and for the study of different environmental conditions. The results confirmed the well-known advantage of 7073-T73 over 7973-76 for resistance to intergranular and exfoliation corrosion, but it seems that this advantage is more pronounced in acid rains than in marine conditions. The ranking of different high-strength Al alloys depends on the type of atmosphere (chloride or acid). The accelerated method described is convenient to study the influence of the many factors that influence corrosion resistance. The method also clearly showed the detrimental effect of chromated cadmium plating on the hydrogen embrittlement of high strength steel.

ACKNOWLEDGMENT

This work was supported by the United State Army Research Development and Standardization Group USARDG, London, under contracts DAJA 45-83-C-0011 and DAJA 45-84-0041.

REFERENCES

1. M. POURBAIX, J. VAN MUYLDER, A. POURBAIX, J. KISSEL. "Applications of an electrochemical wet and dry method for

atmospheric corrosion testing", Rapports
Techniques Cebelcor, vol.139, RT.259 (1980)
2. "Understanding and laboratory prediction of
the atmospheric corrosion behaviour of steels

and non-ferrous metals and alloys". Final
report to contract DAJA-45-84-0041 for
USARDSG, London. Cebelcor, 31.1.87.

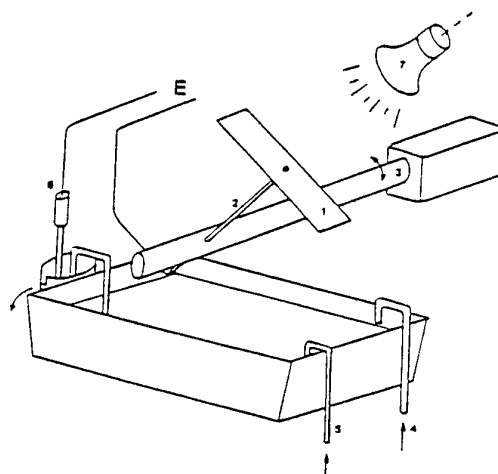


Figure 1: Detail of an individual cell of the accelerated test unit for atmospheric corrosion
1. sample 4: test solution 5: air 6: reference electrode

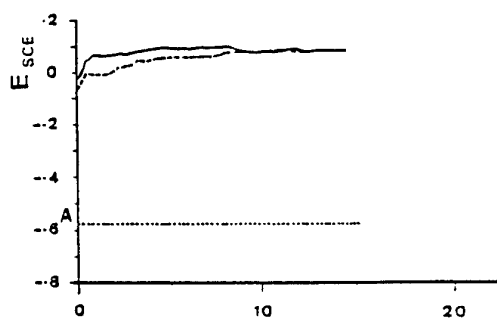


Figure 2: E-t curve for 3103-H24
in rural atmosphere

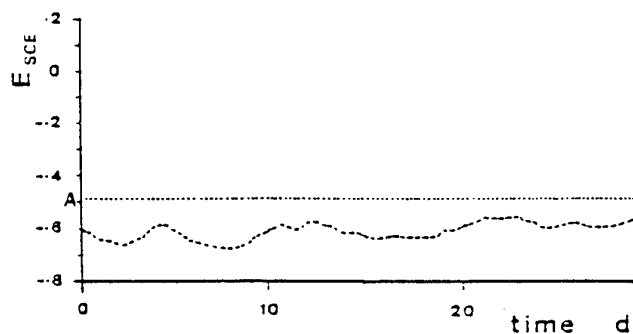


Figure 3: E-t curve for 3103-H24
in industrial atmosphere

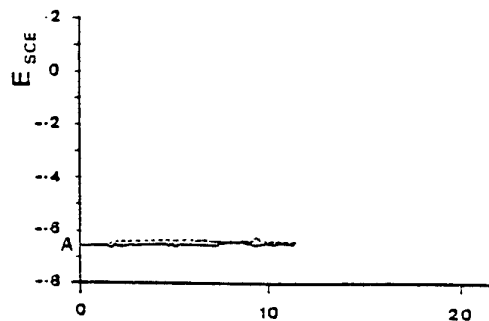


Figure 4: E-t curve for 3103-H24
in marine atmosphere

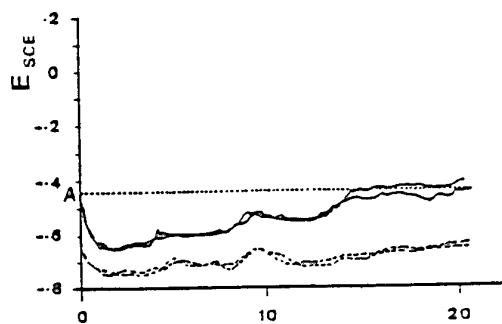


Figure 5: E-t curves for 7075-T6
in industrial atmosphere

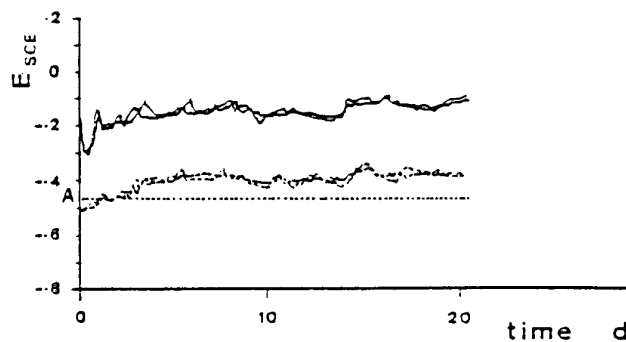


Figure 6: E-t curve for 7075-T73
in industrial atmosphere

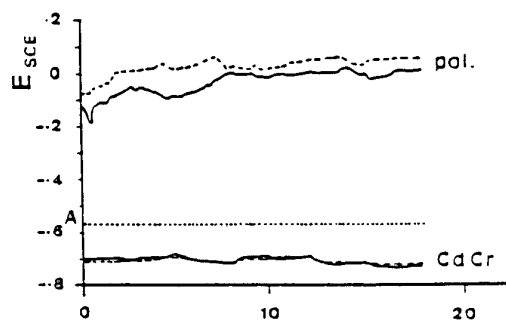


Figure 7: E-t curves for cadmium coated
and for polished 15-7 Mo-PH
in rural atmosphere

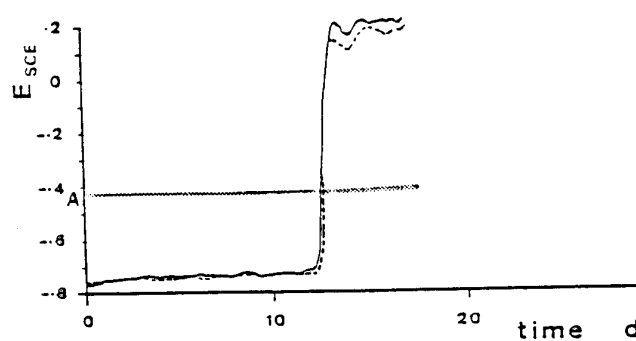


Figure 8: E-t curve for cadmium coated
15-7 Mo-PH steel in industrial
atmosphere

CORROSION PROTECTION MEASURES FOR CFC/METAL JOINTS OF FUEL INTEGRAL TANK STRUCTURES OF ADVANCED MILITARY AIRCRAFT

by

Claus D. Hamm

Deutsche Aerospace AG, Military Aircraft

D-81663 München POSTFACH 801160

Germany

0. SUMMARY

Assembly of carbon fibre composites (CFC) and aluminium structures shall be avoided in unprotected conditions. The more noble CFC could cause fatal galvanic corrosion on the aluminium part. Adequate protection methods for electrical isolation of these dissimilar materials shall be adopted.

Adhesion of the coatings on both the CFC and aluminium substrate during exposure to the simulated fuel tank environment is an essential requirement for corrosion protection and fuel tightness of the joint.

In a sequence of material and functional tests for selection of adequate coatings and associated materials as well as galvanic corrosion and integral tank aspects have been taken into account. Additional to the static panel tests for paint adhesion corrosion tests under dynamic loading and corrosive environment were performed.

Based on the experience of these investigations the selected combinations of coatings, sealants and associated materials were applied on structural tank box for final evaluation. This test article represented the section of a fuselage integral fuel tank structure. For simulation of the complete in-service spectrum, during the life of an aircraft structure, static and dynamic loads were induced.

The internal tank environment was simulated by water as fuel replacement and by pressurisation of the compartment. Resistance of the CFC/aluminium joint to galvanic corrosion and liquid tightness of

the selected integral tank concept proved excellent under simulated conditions.

1. INTRODUCTION

The airframe of high performance military aircraft is built by a variety of dissimilar materials with different electrochemical potential. Weight saving aspects, which are based on operational requirements, cause the airframe manufacture to use light materials with high stiffness. Materials which are able to meet this aspects are carbon fibre composites (CFC) and aluminium alloys. Especially for integral tank structures the application of larger integrated components with a reduced amount of fasteners is preferable. Composite materials, as CFC, are suitable for realisation this design philosophy.

One problem in complex airframe structures is, that most of the CFC structure have interfaces to other materials which are susceptible to galvanic corrosion in contact with the composite. As aluminium alloys are extensively used on airframe structures the contact with CFC can not be avoided.

Isolation methods on the aluminium part as well as on the CFC laminate shall be applied to prevent galvanic corrosion.

Dielectric coatings and materials which are resistant to fuel and a fuel/water mixture which is present at the tank floor area

were tested for application in this joints. Besides of the corrosion preventive properties of these coatings and materials the applicability for sealing of a integral tank structure was an important criteria.

The problem is not only caused by fuel, but by a more aggressive fluid fuel/water/mixture. For simulation of this fluid under laboratory conditions for panel tests a fuel/salt water mixture is used. The presence of this corrosive environment at relative high fuel temperature was the requirement for selection of adequate coating materials and protection methods. Static and dynamic corrosion tests were performed on coupons using several materials and coatings. Verification of the selected isolation methods and the sealing concept on a structural test article have been performed and qualified for application on aircraft.

This presentation gives a comprehensive report on the activities which were conducted to investigate applicable methods.

2. REQUIREMENTS FOR A FUEL INTEGRAL TANK STRUCTURE

In this evaluation program for a high performance aircraft the fuel content is used for cooling of other aircraft systems. After the heat exchangers the fuel temperature may reach about 95°C in certain locations of the tank.

For consideration of all environmental aspects existing in the tank area a fuel/water mixture has been used for a series of tests. This extremely aggressive fluid was simulated for tests by a mixture consisting of equal parts of a 3,5 % salt solution and jet fuel.

Since aircraft structures are subjected by dynamic loads and shall withstand a structural life of about 6000 flight hours

this aspect has been considered essential for simulation of fuel tank relevant joints in test. Taking into account this operational aspect isolation and sealing methods were evaluated to the criteria.

3. ELECTROCHEMICAL COMPATIBILITY OF CFC AND ALUMINIUM

A material immersed in an electrolyte gets a certain electrochemical potential when the oxidation-reduction equilibrium is adjusted. This potential is characteristic for the material and the electrolyte. Materials having higher potentials are considered to be more noble, whereas material with lower potentials are said to be more active. The more noble material acts as the cathode and the more active as the anode (see Fig.1).

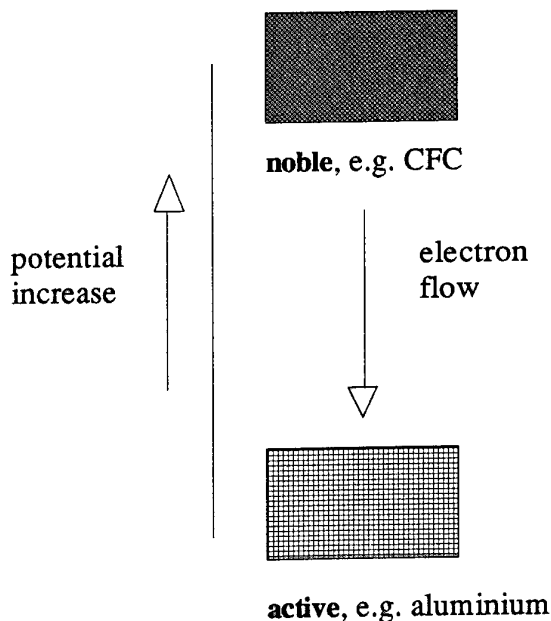


Fig.1 Electrochemical potential of CFC and aluminium

Galvanic corrosion is an electrochemical process involving electrical conducting materials with dissimilar potentials, on which an oxidation-reduction process occurs. The more active material is being dissolved. This effect is known as corrosion.

CFC behaves electrochemically like a very noble material. It does not corrode, but it can cause corrosion on other materials when in direct contact. When CFC is coupled to a less noble joining partner, e.g. aluminium, in a wet environment, and the latter is the anode and may undergo anodic dissolution.

In case of the integral fuel tank the aluminium structure may act as the anode and, attached to CFC, may undergo galvanic corrosion if not adequately protected.

4. CFC/ALUMINIUM STRUCTURE OF AN ADVANCED FUEL INTEGRAL TANK

The design goal for an integral fuel tank structure is the reduction of potential leakage. Extensive use of fasteners increases the threat of the occurrence of such a failure. Therefore, in case of the selected tank structure the amount of fasteners has been drastically reduced by adoption of large integral stiffened CFC components. Figure 2 shows an integral fuel tank structure consisting of an external CFC skin with integral stiffeners, and CFC and aluminium frames.

Assembly of the CFC skin to the substructure restricted the application of state of the art sealants. Pot life aspects of sealants and possible displacement of the CFC skin during mating operations excluded the use of pasty materials in the joining area.

Therefore non adhesive sealing tapes have been adopted for application on faying

surfaces of larger CFC/aluminium joints. In concert with sealing tapes and compounds, corrosion protective coatings and dielectric materials the electrochemical isolation between these dissimilar materials have been assured. Verification of the combined protective methods were performed in a detailed test program.

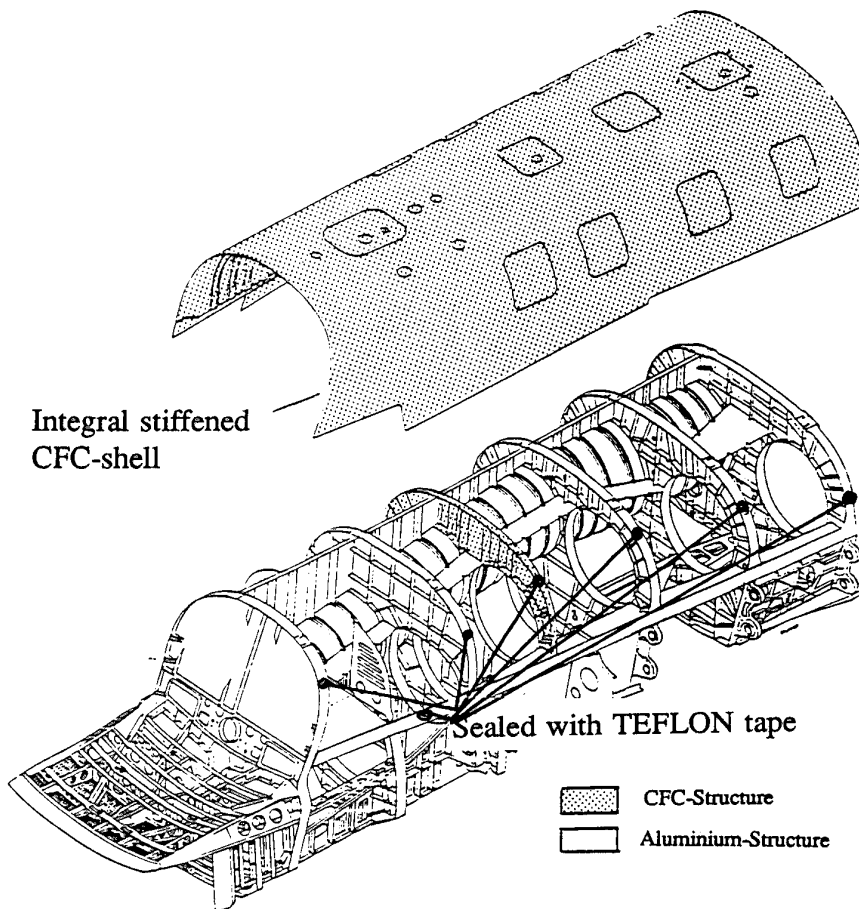


Fig. 2 Centre fuselage fuel integral tank structure with a high degree of CFC structural parts

5. REALISTIC SIMULATION OF THE CONDITIONS IN THE CONTACT AREA CFC/ALUMINIUM

5.1 Selection of coatings on panel tests and investigations with the sealing tape

5.1.1 Selection of coatings

In a series of static panel tests the adhesion and corrosion preventive properties of several coatings were evaluated in the environment as shown in para. 2. Substrate materials involved were the aluminium alloy 2024T3 unclad and the CFC prepreg with BMI matrix resin.

The aluminium sheets were pretreated by Chromic Acid Anodising (CAA), the CFC specimen were coated after removal the peel ply. The applied coatings were of

polyurethane primer, designated PR1560, and a zinc chromate loaded epoxy primer. After immersion of the specimens for 1000 hours at 95°C in a salt water/fuel mixture and jet fuel containing 30 % aromatics (toluene) for reference, the polyurethane primer PR1560 showed the best properties at these test conditions.

Epoxy primers experienced good resistance to this fluids. No loss of adhesion and no signs of any corrosion occurred on the test panels.

Further tests for determination the adhesion behaviour of polysulfide sealants on both coatings showed reduced adhesion properties on the epoxy primer. Depending on these results the polyurethane primer has been selected for application on the fuselage integral tank structure.

5.1.2 Investigation of the sealing tape

For the sealing tape TEFLON in expanded condition has been adopted. Tests for evaluation of the galvanic corrosion preventive properties were performed on test coupons representing the dissimilar materials and the protection coating according to para. 5.1.1.

The coupon consisted of a CFC and aluminium part with the sealing tape as interface material. The two halves of the coupon were fastened with titanium HI-LOKs. To allow penetration of the test fluid to the joining area no edge sealing were applied. Static exposure of the coupons take place in fuel tank environment, as shown in para. 5.1.1.

After finishing these tests no sign of corrosion was found on the faying surface of the aluminium part.

5.2 Preparation of coupons for corrosion tests under dynamic loading

5.2.1 Coupon design and associated materials

The coupon consisted of a CFC and an aluminium part and represented a single shear specimen. The two parts of the coupon were assembled by HI-LOK countersink head fasteners. This fastener type was used to evaluate the influence of the environment to the countersink on the aluminium side. On the CFC part a steel washer was placed under the collar to prevent delamination. Although incompatible with the steel washer aluminium collars were used due to supply problems.

Figure 3 shows the design of the test coupon.

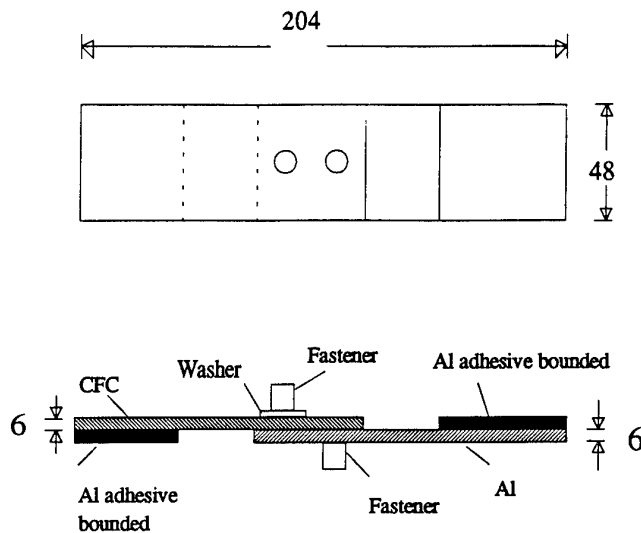


Fig. 3 Coupon for corrosion tests

For production of the coupons the following materials and standard parts were used:

Materials:

CFC with BMI resin matrix

Number of plies: 51

AL sheet: 7075/7351

Standard parts:

Fastener: HI-LOK, countersink head,
titanium alloy, 6 mm diameter,
14 mm grip length

Collar: Aluminium alloy, SAA treated

Washer: Corrosion resistant steel,
passivated

5.2.2 Variation of surface treatment for the coupons

Instead of the polyurethane primer which has revealed the best sealant adhesion in

the test program as stated in para. 5.1 the epoxy primer was used in these tests. Because of comparable resistance properties to the polyurethane primer in the test fluid the achieved results should also be transferable to general structure applications.

Although inadequate for integral fuel tank structure, untreated coupons were exposed to the test environment for reference to show the fatal corrosion attacks on the aluminium structure, when unprotected in contact with CFC.

A summary of the surface preparation of the CFC and the aluminium part of the coupon is shown in Table 1.

HI-LOK collars and washers remained in as received condition, that means no additional protection has been applied.

5.2.3 Test Conditions

Due to safety aspects the test fluid to simulate the integral tank environment could not be used. Instead of a fuel/salt water mixture the coupons were exposed to a neutral salt water solution of 3,5 % NaCl and 35 °C. The lower test temperature was adopted due to heating restrictions of the salt spray chamber.

In the first step all variants of test coupons shown in Table 1 were exposed in a salt fog cabinet for 500 hours. Subsequent to this static exposure to the salt environment, dynamic loads were applied to the coupons in a constant amplitude loading sequence in tension only. The frequency selected was 5 Hz and the total number of cycles at max. load level of 4 KN were 10^6 .

Table 2 shows an overview on the achieved test results.

Table 1: Variants of surface protective treatments applied on the faying surface of the test coupons

Number of Test Variants	Surface Protective Treatment		Application of Sealant and/or Scrim on the Faying Surface	Assembly of Fastener
	CFC	Aluminium		
1	none	none	none	dry
2	Epoxy Primer	CAA plus Epoxy Primer	none	dry
3	none	CAA plus Epoxy Primer	Polysulfide Sealant PR1750	Polysulfide Sealant PR1750
4	Epoxy Primer	CAA plus Epoxy Primer	1 Ply Scrim plus Polysulfide Sealant PR1750	Polysulfide Sealant PR1750
5	Epoxy Primer	CAA plus Epoxy Primer	Polysulfide Sealant PR1750	Polysulfide Sealant PR1750

Table 2: Evaluation of test results

Number of Test Variants	Test Sequence and Evaluation of the experienced galvanic Corrosion Defect on the Aluminium Part and Location on the Test Coupon			
	500h static Salt Fog Test	Dynamic Loading with alternate Salt Fog Test	500h static Salt Fog Test	Location of Defect on Test Coupon (see Fig. 4)
1	Extensive corrosion attack	Extensive corrosion attack	Additional corrosion found on edges	I, II, III, IV
2	No corrosion found	No corrosion found	No corrosion found	III, IV
3	No corrosion found	No corrosion found	Corrosion found on edges	II,
4	No corrosion found	No corrosion found	No corrosion found	
5	No corrosion found	No corrosion found	No corrosion found	

As already expressed in para. 5.2.1 an inadequate fastener, collar, washer combination was used, so that corrosion between aluminum collar/ titanium HI-LOK and steel washer/aluminium collar was unavoidable.

During the dynamic load tests an alternate immersion procedure was applied in the test rig by exposure of the coupons to neutral salt solution as mentioned above with immersion and drying cycles in the proportion of 10 min to 50 min. This procedure was applied over a period of appr. 55 hours.

After finishing this procedure the coupons were again statically exposed to the salt fog cabinet for 500 hours. The idea behind this additional exposure was, to recognise the corrosive influence of dynamic loading with respect to possible micro cracks.

5.2.4 Evaluation of the test results

As expected the unprotected coupon from test variant 1 in Table 1 experienced extensive galvanic corrosion in the contact area of the aluminium part. An improved behaviour against contact corrosion was shown by coupons of test variant 2, on which no attack were found on edges and faying surfaces of the aluminium parts.

Although the aluminium parts were protected, corrosion attacks were detected on coupons of variant 3. These were caused by the uncoated CFC parts and the movement under loading, which obviously resulted in partial damage of the coating.

Comparable to variant 2, specimens of variants 4 and 5 experienced no corrosion on the aluminium part in contact with CFC.

Table 2 summarizes the evaluation results, and Figure 4 shows the typical locations of corrosion on the test coupon.

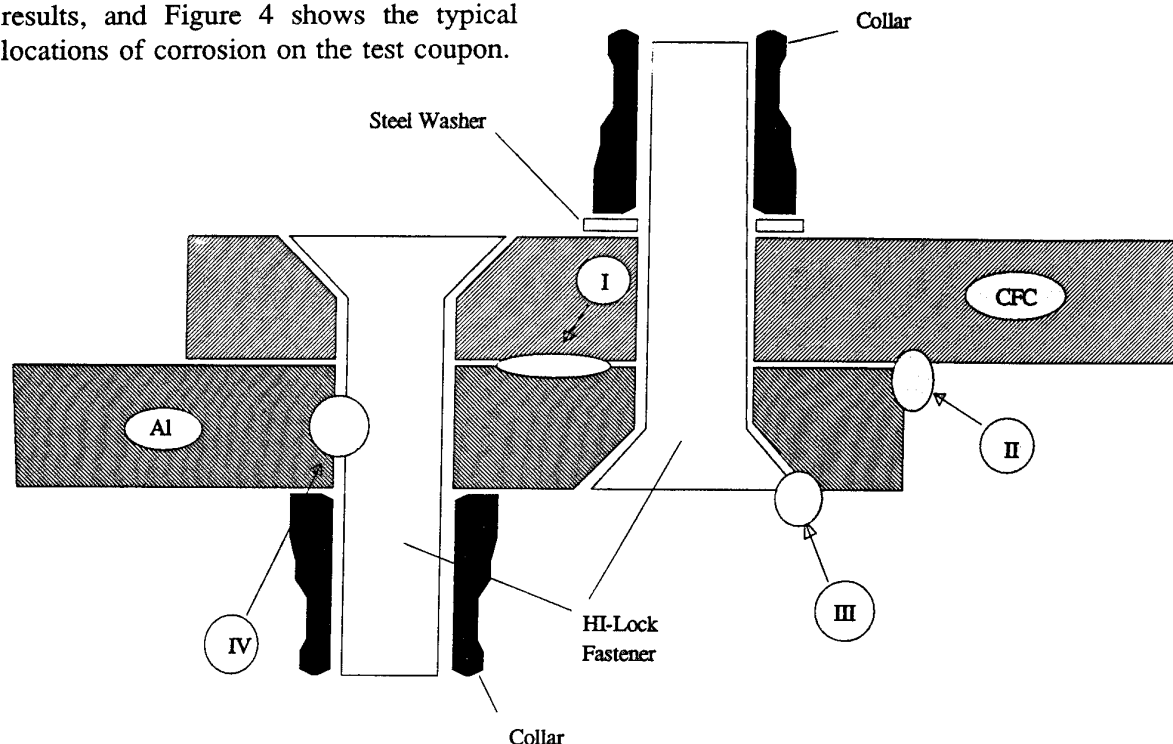


Fig. 4 Location of corrosion attacks on the test coupon

5.2.5 Conclusion of the corrosion coupon test under dynamic loading

The test results show that only painting of both the CFC part and the aluminium sheet leads to an effective protection against galvanic corrosion. Wet assembly of the joint with polysulfide sealant show further improvement in prevention of penetration of corrosive media. Improved protection for the aluminium is achieved by application of 1 ply of glass fibre scrim to the CFC contact surface.

HI-LOK fasteners which were dry installed caused contact corrosion on the aluminium part, especially in the hole/shaft interface and in the countersink, as shown in Fig. 4. This has not been an adequate installation and was finally adopted to see an possible effect to the CFC/aluminium contact area

if the electrolyte penetrates along the fastener. This expected effect did not occur .

5.2.6 Consequence of these test results to the fuselage fuel tank structure

Analogical to the results achieved by these corrosion tests, isolation methods for the integral fuel tank structure were derived. Because the fuel and especially the fuel/salt water environment, with significant higher temperatures, the polyurethane primer PR1560 was selected for fuel tank application because of improved adhesion of sealants, which is essential for fuel tightness.

In consequence of the above test results it was proposed to implement the barrier

system in a full size structural component (see para. 6), for verification of the complete experience extracted from these testing. The idea behind this project was the simulation of both, the adopted sealing system and the capability of these coatings, seals and sealant compounds, to prevent galvanic corrosion on the aluminium structure in contact with CFC components.

6. VERIFICATION OF THE INTEGRAL FUEL TANK SEALING CONCEPT WITH A STRUCTURAL TANK BOX

6.1 Concept for a structural tank box

The integral tank box represented a segment of a real fuselage integral tank structure for a high performance aircraft. Associated constructions, structural materials, surface protective treatments, barrier systems for prevention of galvanic corrosion and the sealing system were comparable to those of a integral tank structure.

Dynamic loads simulated to the expected flight spectra were induced to the structure. Pressure and heat for simulation of the tank environment were applied in defined cycles (see Fig. 7).

For safety aspects water has been used for simulation of the fuel. Figure 5 shows the fuselage integral tank box.

6.2 Applied protection systems

With respect to the results achieved by the corrosion test under dynamic and the integral fuel tank specific sealing materials and methods the following protection scheme was applied:

Aluminium structure:

CAA plus polyurethane primer PR1560

CFC structure:

1 ply glass fibre scrim plus polyurethane primer PR1560. The scrim was applied in the contact area only.

Polysulfide sealant PR1750 was used for fuel tight sealing of the faying joint. In view of the large CFC skin component (see Fig. 2) non adhesive sealing tapes were applied.

A thixotropic variant of the sealant PR1750 were used for filleting all structure seams.

The fasteners were wet installed with oversealing of the collars.

Figure 6 shows in principle the variants of adopted protection and sealing systems.

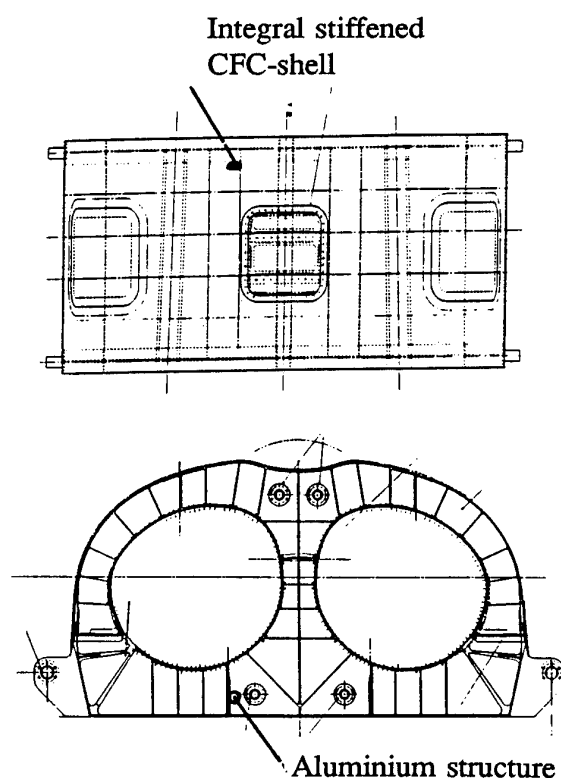


Fig.5 Test box for simulation the fuselage integral tank concept

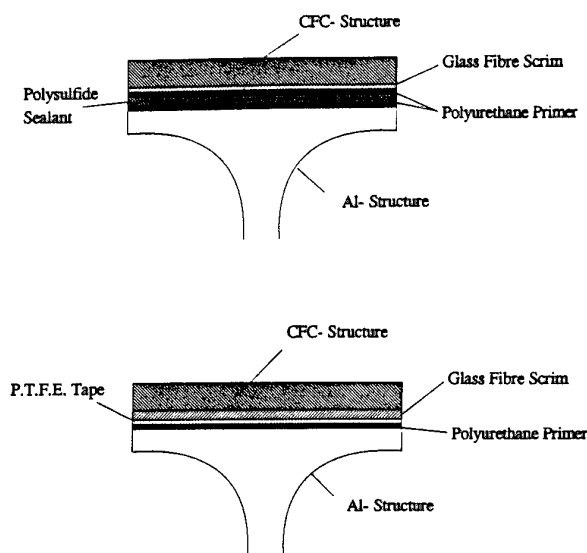


Fig. 6 Schematic view of the protection and sealing system without edge sealing

6.3 Test conditions

6.3.1 Simulation of the integral tank environment

As already expressed in para. 6.1 water has been used for simulation of the fuel. This was necessary in view of safety aspects, as for realistic simulation of the tank environment the water has to be heated up to 90°C which would have caused a safety hazard in case that fuel would have been used. For the galvanic corrosion aspect water represented an adequate liquid to evaluate the influence on the joint CFC/aluminium because of the long duration of the test sequence.

6.3.2 Loading and test cycles

Static and dynamic loads were induced in

the tank box structure representing the spectra of an advanced fighter aircraft. Wing bending moment and fuselage torsion were simulated.

The fuel tank pressure and temperature varied within a cycle of 200 flights as shown in Fig. 7. A total of 18.000 flight hours (SFH) were simulated, applying a defined fatigue spectra.

Additionally pressure was applied inside the air intake ducts.

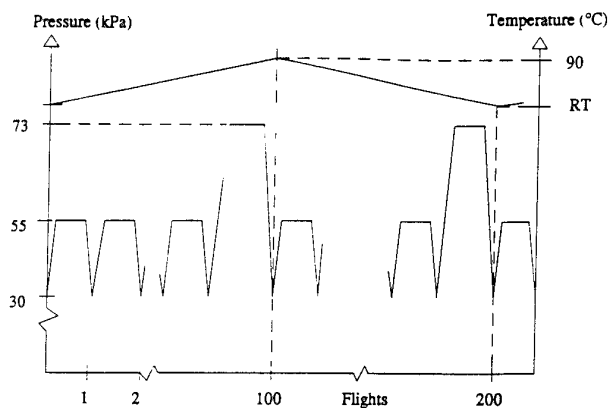


Fig. 7 Variations of temperature and pressure within a 200 SFH cycle

6.3.3 Exposure time to water

The number of 18.000 flights represented an exposure time of about 2.700 hours in water and under loading.

6.4 Discussion of test results

This structural test was performed with a simulated flight spectrum under extreme loading conditions. Exposure of the associated materials to water and under load for a period of approximately 2700 hours represented more than worst case condition.

The main goal of this test program, the leakage tightness of the integral fuel tank sealing concept, has been achieved. No leakage has been experienced during the test period. The second aspect of this program the avoidance of galvanic corrosion on the interfaces of CFC and aluminium was examined after dismantling the adequate joints.

Independent of the sealing method, whether non adhesive tapes or pasty sealing materials were used, no signs of any corrosion have been found on the aluminium surface of the CFC /aluminium joints. This excellent result confirms the overall combined leakage tight and corrosion prove integral fuel tank concept for a high performance aircraft.

7. CONCLUSION

Weight saving aspects for operational reasons and the requirement for minimisation of the number of fasteners underlines the adoption of materials, allowing manufacturing of highly integrated components. Carbon fibre reinforced composites are most suitable for this application due to its high stiffness and low density. But in combination with an aluminium structure galvanic corrosion on this less noble material may occur, if not adequate protected.

In view of the assembly situation in the integral fuel tank structure a sequence of tests was performed for qualification of material for dual application. Goals in this program have been twofold, the prevention

of galvanic corrosion on the aluminium part and fuel tightness of the tank structure.

The result of this investigation was, that a combination of glass fibre scrim and polyurethane primer on the CFC side, and an equivalent primer coating on the aluminium part, wet assembled with sealant or sealed with a non-adhesive tape provides excellent protection against galvanic corrosion in the integral fuel tanks.

In principle these results are transferable to any general airframe structure consisting of these dissimilar materials.

REFERENCES

The content of this paper is based on the following MBB/DASA internal experiences and reports:

- * Investigation of the corrosion behaviour of CFC/aluminium joints in corrosive environment under dynamic loading.
Author: E. Bilgram
- * Investigation of the corrosion behaviour of CFC/aluminium joints exposed to the alternate immersion test under static loading.
Author: M. Steinert
- * Testing of a centre fuselage integral tank structure (tank box) sealing configuration.
Author: Bayerl
- * Investigation of physical properties of polymeric materials for application on fuselage integral tank structures.
Author: C. Hamm

CORROSION PREVENTION WITH ENVIRONMENTALLY COMPLIANT MATERIALS - A DESIGN CHALLENGE

C. W. Matz
Deutsche Aerospace Airbus GmbH
Hünefeldstr. 1-5, 28183 Bremen, Germany

Summary

In order to eliminate hazardous properties many well proven materials and processes for corrosion prevention have to be replaced. Examples are Chromates in primers, sealants and pretreatment processes, Cadmium as plating material and solvents, which usage shall be significantly reduced.

The replacement materials often do meet the usual requirements completely.

Examples are given how the deficit in performance can be overcome by design changes and supplemental measures.

1. Introduction

Besides occupational health and safety aspects environmentally driven investigations on flows and balances of materials have uncovered new reasons to eliminate hazardous compounds. Within the production of the aircraft industry specially the materials and processes for corrosion prevention are of major concern, because the state of the art technology contributes to many environmental problems. Examples are the usage of CFC's (ozone depleting properties in the upper atmosphere) for cleaning purposes, VOC's in organic coatings (creating ozone/smog in the lower atmosphere), toxic heavy metals emitted with the waste water of galvanic shops and hazardous solid residues from treatment and coating facilities, for which alternatives instead of disposal have to be found.

Besides legal obligations to replace hazardous compounds (e.g. Montreal protocol 1987/CFC's) also the economic motivation is increasing because the handling with hazardous compounds needs more and more work force to fulfill monitoring, supervising and proving activities. In the following some fundamental considerations and examples - gained by experience are presented in order to replace hazardous materials.

2. General Approach

First task is to determine the occurrence of hazardous materials. Today this is done on a routine basis by the mandatory procedure that, before any purchase of new material, the relevant Material Safety Data Sheet (MSDS) is evaluated by the responsible persons for health, safety, environment, and the materials and processes department. Most helpful is the new MSDS format of the EU (see directive 91/155/EEC), which generally covers all aspects in the necessary extent and detail. If hazardous compounds are identified a decision tree has to be worked off (see Fig. 1). In some cases the consequences were easy to carry out like the selection of paints with less harmful (i.e. non teratogenic) solvents or the sealing of anodised Aluminium workpieces with hot water instead of Chromate solutions. The remaining problems were prioritised against the general targets of

- avoiding halogenated solvents
- replacing cancerogenic, mutagenic teratogenic compounds
- and minimizing volatile organic compounds (VOC's) respectively hazardous air pollutants (HAP's).

If no obvious 1 : 1 replacement solutions are available, in depth investigations are necessary including a careful examination of specifications with respect to realistic and relevant requirements.

In order to open the problem to solutions as far as possible such basic specifications shall contain only performance criteria dividing in indispensable and "nice to have" items. Care must be taken that the remaining catalogue is complete and apparent self-evident properties are included. An example is that most material and process specification for CFC's did not mention their inflammability but, on the other hand, this property was needed for operating the state of the art equipment. As result of such investigations and inspite of lengthy development efforts the result may be materials and processes, which meet only part of the original technical requirements. This is the scenario where flexibility and creativity of design departments are challenged in order to introduce environmentally compliant materials.

3. Example : Cadmium replacement

Cadmium is cancerogenic, ecotoxic and enriched in biologic organisms (e.g. mushrooms). In aircraft applications plated Cd-layers fulfill several functions:

- galvanic corrosion protection of rusting steels
- galvanic corrosion protection of dissimilar metal assemblies with Al structures.
- suitable sliding and lubrication properties (see joining of fasteners)
- good ductility
- electric conductivity
- solderability

Additionally Cd possesses useful practical aspects:

- Cd-plating can be applied in exactly determined thicknesses
- The coatings are free of pores
- Cd itself is rather corrosion insensitive
- In case of sacrificial anodic dissolution of Cd the corrosion products are of such kind that fasteners can be loosened without major difficulties
- Paints adhere well on Cd-layers
- During service Cd-plated steels do not suffer from additional Hydrogen embrittlement

This combination of properties turns out to be rather unique. Any alternative material/process has therefore only limited potential to replace Cadmium.

Coatings of Aluminium for instance have the disadvantage that in case of galvanic corrosion the Al-layer itself has a

tendency to repassivate, thereby losing the protection activity for the substrate material. Also the corrosion products stuck fasteners to such an extent that they usually have to be drilled out.

Developments to overcome these problems by use of Al-alloy coatings are currently evaluated.

Another alternative for Cd-plating is the application of a double layer system consisting of an Al-flake filled ceramic and a PTFE pigmented PU coat, the first taking care of the cathodic protection and the second guaranteeing tribological properties. Compared to Cd this coat system is isolating and thickness control is not as good. Furtheron painting of such treated parts should not be required because of lack of adherence.

Currently it is planned to introduce this coating system on clipnuts because corrosion tests with typical assemblies showed that this configuration is even better performing than the Cd treated material of today.

A major progress in replacing Cd also in other applications is expected from the activities of the GARTEUR Action Group No. 17, which will finish their investigation efforts on alternatives for Cadmium by July 1996.

4. Example : Chromate Free Corrosion Inhibiting Primers (CFCIP)

Chromates are hazardous materials. Any exposure to them is of toxicologic concern. The worst effect is due to the inhalation of dust containing soluble Chromates, which results in a high risk of getting bronchial cancer. Main sources of such dusts in our industry are the spray application of wash primer (containing Zinc Chromate), the same process with basic primers for corrosion protection (containing Zn and/or SrCrO_4), and removing of such coats from surfaces for repair and maintenance purposes. On the other hand the aircraft industry relies since decades upon the unique corrosion inhibiting properties of chromates. The protection of aluminium alloys, inclusive the safeguarded integrity of load carrying primary structures built out of Al, is not only demonstrated in laboratory tests, but also well proven by in service experience. The need to replace soluble Chromates from the corrosion inhibiting primers might therefore affect the principal concepts of corrosion protection and maintenance schedules with all their economical and safety implications. This alone requires a thorough and complete evaluation of replacements before any risks are taken.

For the investigations approved paint manufacturers were asked to supply their latest technology chromate free corrosion inhibiting primers together with compatible top coats, suited for interior structural application. The tests according to current specifications showed, that with exception of the corrosion inhibiting properties, the CFCIP's are at least equivalent to their chromated counterparts. This lack of equivalence can be clearly seen from filiform corrosion test on Chromic Sulfuric Acid etched substrate (see Fig. 2). Does this result stop any application of the CFCIP's? How this difference in quality is to be valued?

One has to take into account that most state of the art corrosion test are mainly done for comparison reasons, but not well suited to predict in service behaviour.

The clear message of this result was to develop improved corrosion tests which utilise

- materials and processes of the today production
- realistic exposure conditions
- simulate well known damage scenarios and

- creates meaningful results with low scatter and good reproducibility.

The in service experience generally shows following weak points of the Al-structure:

- Corrosion starting from local accidental damage (by scratches or impacts)
- Corrosion starting from edges with insufficient protection (coverage of coatings, probability of damage)
- Crevice corrosion

The scenarios of accidental damage and insufficient edge protection are covered satisfactorily by the well known test specimen because they are exposed with artificially produced scratches. For crevice corrosion testing purposes a new specimen design was created (Fig. 3).

This specimen is exposed by an alternative immersion procedure according to EN 3212.

Comparative exposure tests with corrosive electrolytes confirmed that the buffered sodium chloride solution (30 g/l NaCl; 1,25 g/l Boric acid; 0,10 g/l NaH_2PO_4 + Na_2CO_3 solution (100g/l) to make pH 8) is also in this crevice situation rather aggressive.

This test procedure creates damage pictures similar to failures in reality.

As key corrosion tests the best compromise up till now is, according to our experience, the combination of this new "crevice corrosion test" and the filiform corrosion test (EN 3665), reflecting interior and exterior corrosion events. The result obtained with such tests adopting the today surface treatment (Chromic Acid Anodizing) is shown in Fig. 4 + 5.

The filiform corrosion of the tested Chromate free paints is well within the current requirements (2 mm) and about the same as with chromated primer.

Within the crevice corrosion test the results were very remarkable by the fact that the chromate free primers show, compared to chromated ones, about twice the generally rather low extension rate, when clad material is examined. With bare substrates all specimens showed about the same performance. We suppose that this is due to the fact that with the clad substrate the galvanic element is stronger and in this case the superior inhibition properties of chromates are dominating.

Thus it is shown again that CFCIP's are not completely equivalent to chromated primers in their corrosion inhibition properties. On the other hand the overall protection level seems to be sufficient together with an optimized substrate surface pretreatment (e.g. chromic acid anodizing)

In order to evaluate this remaining risk, we started an in service evaluation program with specimen flying in the bilge area of an A320 aircraft, but meaningful results are not yet available. Presently additional aircrafts join this program in order to achieve some statistical significance. A major problem is also the time that is needed for a sound result. Parallel to this activity we looked for alternatives to improve the today situation. Part of the target may be reached by introduction of low chromated primers, where several possibilities can be considered. One of them is the reduction of amount of soluble Chromates, another the replacement of Sr and ZnCrO_4 by less soluble species like BaCrO_4 , which are not yet suspected to be cancerogenic. Based on a Chromate free formulation we tested several materials modified in the above mentioned manner (see Table 1). The result of a filiform test (see Fig. 6) showed that these modified

primers perform like Chromate free formulations. Additionally it is known that in some transport aircrafts primers containing only small amounts of BaCrO_4 (about 2 %) are applied since decades with good in service experience, especially on anodised surfaces. Comparison tests (filiform corrosion, alternate immersion test) with Chromate free primers indicated again performance level of the CFCIP's.

The overall conclusion is that Chromate free corrosion inhibiting primers can be introduced on anodized substrates. Their actual implementation however needs the willingness of design authorities and customers to tolerate a change in current specifications.

5. Conclusion

As shown by some examples a successful introduction of environmentally compliant materials needs the support of design departments, because material and process development can not offer in every case a simple 1 to 1 replacement. Additionally modification of well proven standards and procedures might be necessary, which needs the acceptance of customers and certification authorities.

Variation	SrCrO_4 [%]	BaCrO_4 [%]
A	1	0
B	2	0
C	0	7,5
D	1	7,5

Table 1: Low Chromated primers, Chromate content of base material

Determination of actions in order to replace hazardous materials

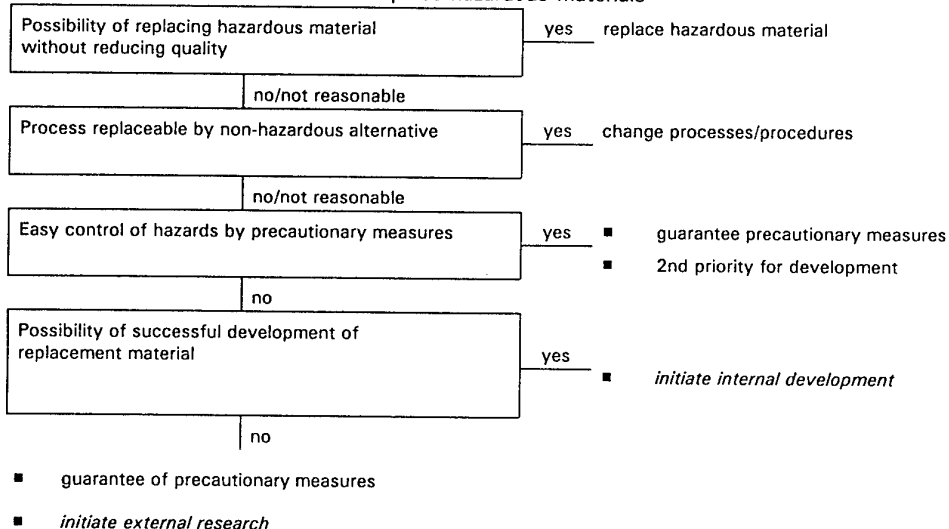


Figure 1: Matrix of decisions

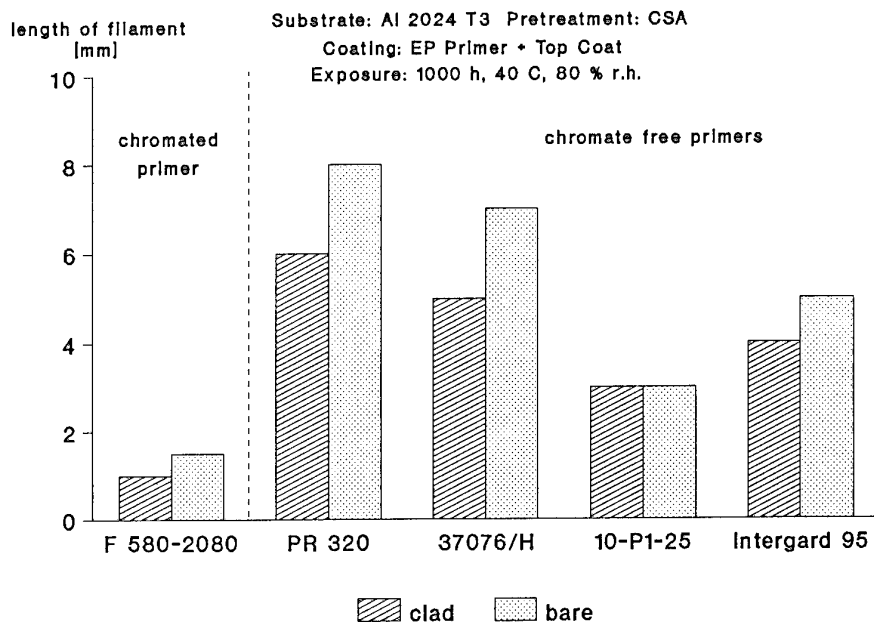


Figure 2: Filiformcorrosion test

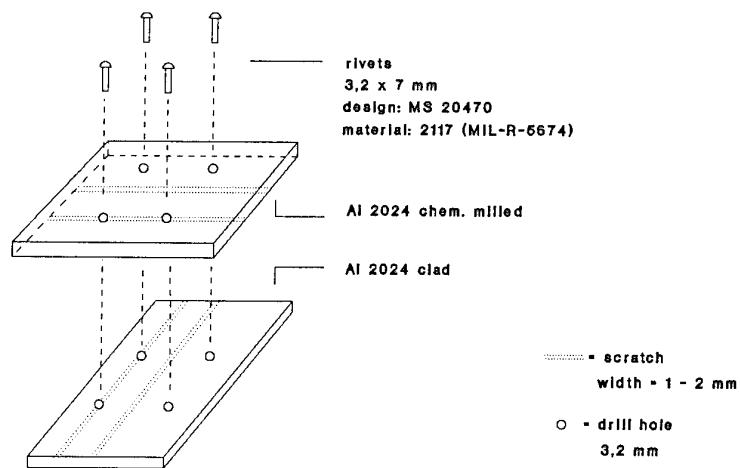


Figure 3: Test specimen for Crevice Corrosion Test

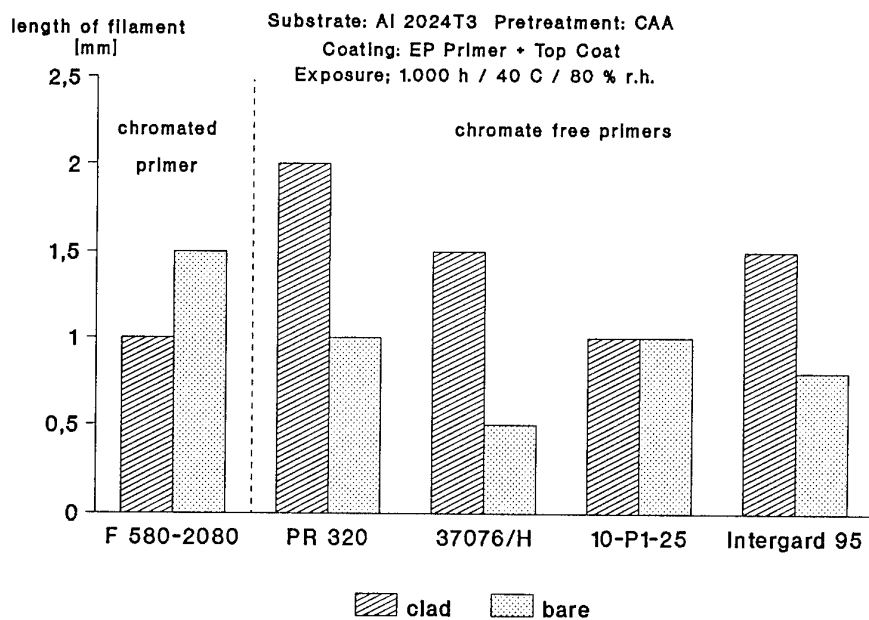


Figure 4: Filiformcorrosion test

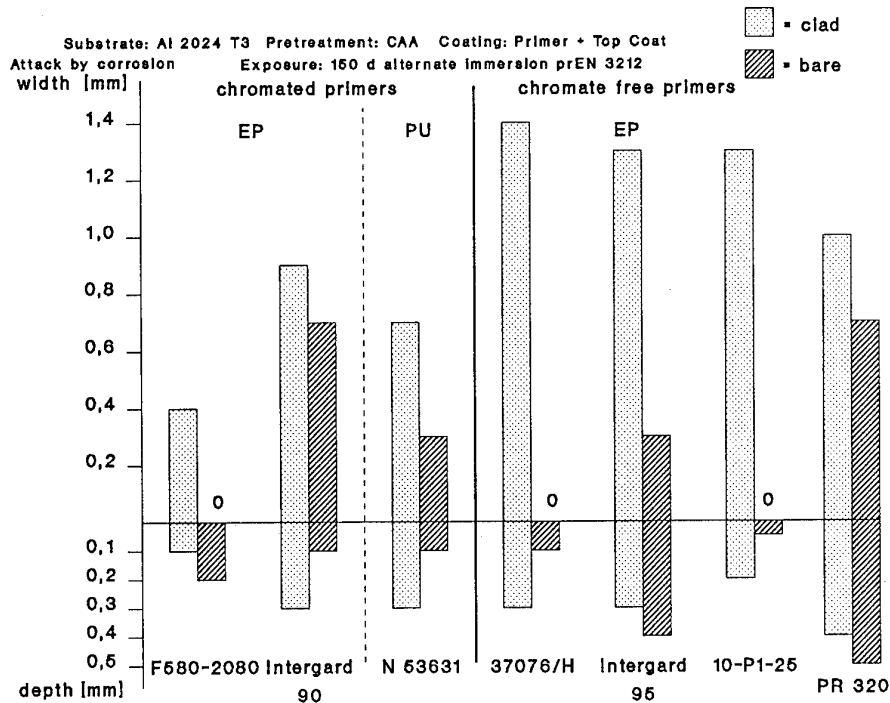


Figure 5: Crevice Corrosion test

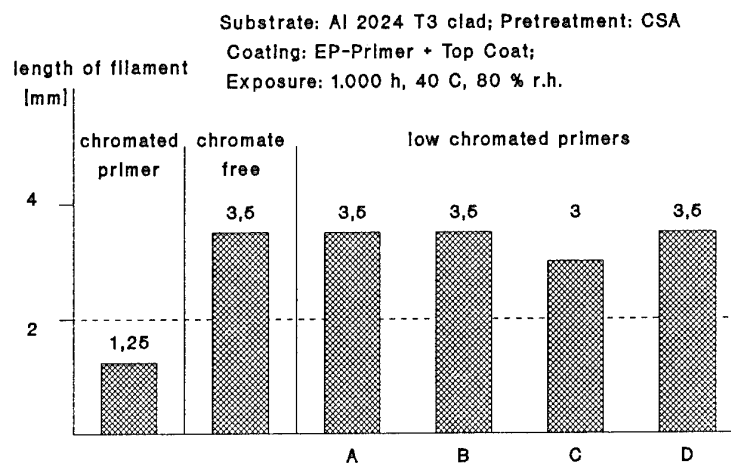


Figure 6: Filiformcorrosion test

New Nondestructive Techniques for the Detection and Quantification of Corrosion in Aircraft Structures

W.P. Winfree
K.E. Cramer
P.H. Johnston
M. Namkung
Nondestructive Evaluation Sciences Branch
NASA Langley Research Center
MAIL STOP 231
23681-0001

SUMMARY

An overview is presented of several techniques under development at NASA Langley Research Center for detection and quantification of corrosion in aircraft structures. The techniques have been developed as part of the NASA Airframe Structural Integrity Program. The techniques focus on the detection of subsurface corrosion in thin laminated structures. Results are presented on specimens with both manufactured defects, for calibration of the techniques, and on specimens removed from aircraft.

1 INTRODUCTION

The NASA Airframe Structural Integrity Program was initiated in October, 1990 with the objective of developing improved technology to support the safe and economical operation of commercial aircraft. The program has three principle focuses; Structural Mechanics, Fracture Mechanics and Quantitative Nondestructive Evaluation (NDE). The Quantitative Nondestructive Evaluation Program has concentrated on the development of area inspection techniques for the detection of cracks, disbonds and corrosion in the fuselage with particular emphasis on the lap joints and tear straps. These techniques offer more economical operations by reducing the man hours required for performing the inspection without reducing its safety or reliability.

Four techniques are being developed for the detection of corrosion in the airframes. They are based on eddy current, ultrasonic, thermal and x-ray stimuli of the structure. Eddy current techniques are currently the most often employed technique for inspection of commercial aircraft. The eddy current technique being developed is based on a new probe design which has an output that is easily interpreted and has a reduced sensitivity to lift off error. It has been shown to be able to determine the material loss in first and second layers. The ultrasonic system is a pulse echo based technique which accurately quantifies the material loss in the first layer of the structure. It has been integrated into a portable scanner to enable rapid imaging of the corrosion area. The thermal technique is a large area technique capable of locating regions with 10% or more material loss. Finally the x-ray system is based on a novel x-ray concept called "reverse geometry x-rays" which enables the detection throughout the full thickness of the structure.

Each of the techniques complements the other techniques being developed. The thermal system allows for a quick survey of the structure to locate suspect regions. The ultrasonic technique quantifies the corrosion in the outer layer to a high degree of accuracy. The eddy current technique can accurately quantify the material loss in the first and second layer and with the complementary ultrasonic data determine the extent of material loss in the second layer as

compared to the first layer. Finally x-ray radiation penetrates deep into the structure enabling detection and quantification of corrosion which is to far from the surface of the structure to be detected by other techniques.

2 EDDY CURRENT SELF-NULLING PROBE

Eddy current techniques are commonly used for detection of cracks and corrosion in commercial aircraft structures. Recently a new probe was developed at NASA Langley Research Center for performing eddy current inspections (Ref. 1). The probe has two concentric coils which are separated radially and at one end by a electromagnetic shield. At the open end, the shielding stops which allows for electromagnetic coupling between the two coils when the probe is held in the air. When a high frequency voltage is applied to the outer coil, a voltage is induced in the inner coil, which is easily detected. When the open end of the probe is placed against a highly conductive material, the electro-magnetic coupling is significantly reduced and the induced voltage in the inner coil is reduced to approximately zero. Therefore the probe is referred to as a self-nulling probe.

If the voltage applied to the outer coil is kept constant, then the amplitude of the induced voltage in the inner coil is a monotonically increasing function of the coupling between the two coils. The coupling is a function of the conductance of the structure at the open end of the probe, which changes in the presence of cracks, corrosion and other structural defects. Therefore by measuring the amplitude of the voltage of the inner coil, it is possible to determine the extent of coupling between the two coils. Therefore the advantage of the probe is the simplicity of this measurement compared to traditional eddy current measurements which require a measurement of the impedance of the coil.

Eddy current techniques detect variations in the substrate's ability to generate an eddy current in the presence of a time varying magnetic field. Therefore eddy current techniques are sensitive to any changes in the material which affects the conductance of the material such as cracks or variations in thickness. For a conductive material, the penetration of a periodically varying magnetic field perpendicular to the surface of the layer decreases exponentially away from the surface and can be expressed as

$$B_z = B_0 e^{-z/\delta} \quad (1)$$

where B_0 is the magnetic field at the surface, z is the distance from the surface and δ is the skin depth of the material. The skin depth is given by the expression

$$\delta = \frac{c}{\sqrt{2\pi\mu\omega\sigma}} \quad (2)$$

where c is the speed of light, ω is the angular frequency of

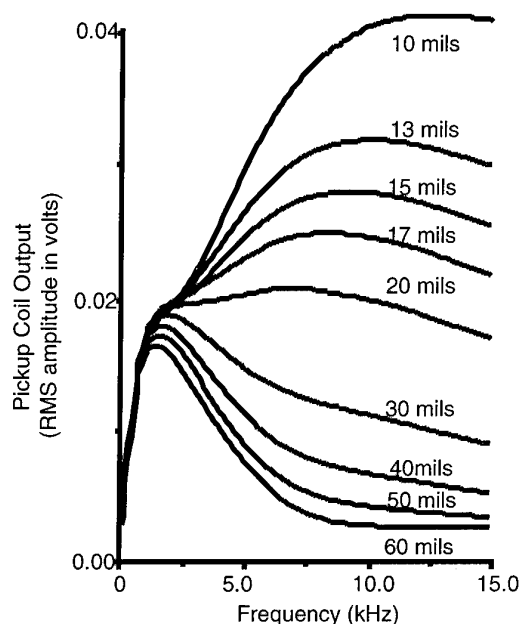
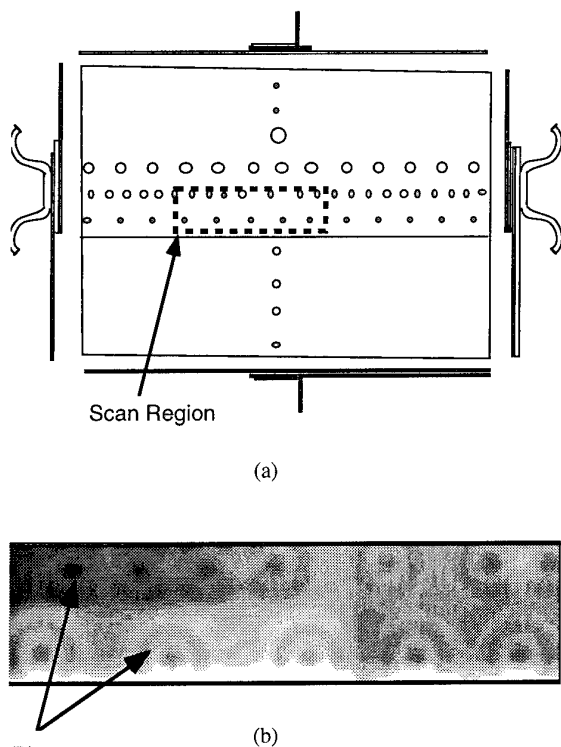


Figure 1. Amplitude of voltage on inner coil versus frequency for several different thicknesses of 2024 aluminum.

the periodically varying field and μ and σ are the permeability and conductivity of the material.

For aluminum the two important variables in this equation are frequency of the excitation and the conductivity. The



Rivets

Figure 2. Image of amplitude of induced voltage on inner coil of self-nulling probe as it is scanned over specimen.

- (a) Schematic of specimen
(b) Image of output voltage of self-nulling probe instrument as function of position.

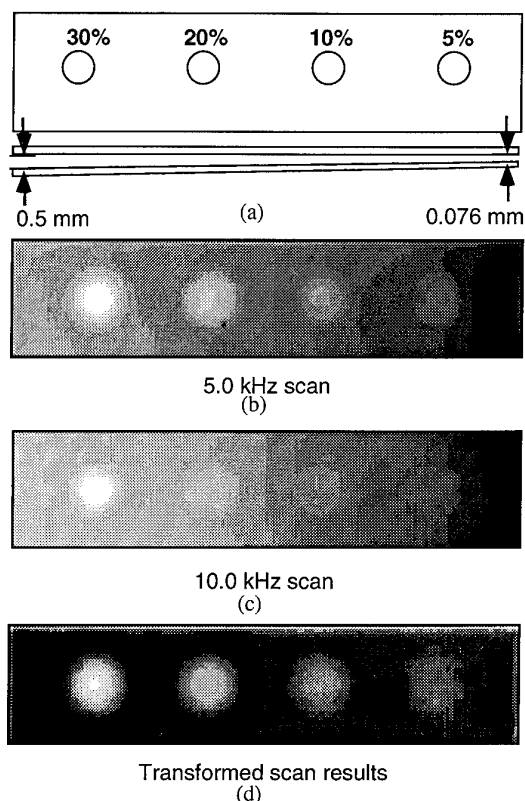


Figure 3. Separation of gap spacing effects from material loss effects.

- (a) Specimen configuration
(b) Image of output of self-nulling probe instrument as a function of position for 5 kHz drive frequency.
(c) Image of output of self-nulling probe instrument as a function of position for 10 kHz drive frequency.
(d) Image following data reduction technique which combines information from both frequencies to eliminate affect variable gap between layers.

electrical conductivity of aluminum is relatively high and does not tend to vary significantly within a sheet. The excitation frequency is a tunable parameter which can be optimized for given thickness of material. For layer thicknesses much greater than the skin depth of the material (high frequencies), the magnetic field does not penetrate through the layer, therefore there is no change in the effective conductance as a function of thickness. However for thickness of the layer less than the skin depth, the alternating magnetic field penetrates through the layer and the effective conductance depends on the thickness of the layer. For the self-nulling probe the result is a leakage of magnetic field from the outer coil to the inner coil and an induced voltage on the inner coil. The induced voltage as a function of frequency for several different thicknesses of aluminum is shown in Figure 1. As can be seen from the figure there is a strong dependence both the frequency and thickness. This dependence is a result of both the change in effective conductance and the frequency response of the probe. It is apparent for this probe that the response is dominated by the probe design at frequencies below approximately 2.5 kHz. At frequencies above 5 kHz there is a strong dependence on the

thickness of the material which can be used to calibrate the system, enabling subsequent gauging of layers of the same material.

The probe can be used as the sensor of a mechanical scanner for imaging variation in the thickness of a layer. For a multilayer structure, such as an aircraft fuselage, the induced voltage is a function of the thickness of all the layers the magnetic field is able to penetrate. The results of a single frequency scan of a lap joint specimens with corrosion is shown in Figure 2. As can be seen from the image there is a clear indication of the region of corrosion in the lap joint. Determination of the thickness of the top layer of the lap joint from this single measurement is not possible, since the response of the layer depends on the thickness of the top layer, thickness of the bottom layer and the separation of the two layer. However measurements at several different frequencies enables independent characterization of these parameters.

The advantage of measurements at just two frequencies can be seen when examining the two plates with a variable separation between the plates (Ref. 2). Measurements at a single frequency have a combined effect from both the variation in the separation of the two plates and the variation of the thicknesses of the plates as can be seen in Figure 3b and 3c. Inputting the measurements at the two different frequencies into an appropriate inversion algorithm yields a measurement of the thickness variation in the bottom plate independent of the gap spacing. The results of such an inversion are shown in Figure 3d. Inversion algorithms are currently being developed for independent characterization of two layers with a variable gap spacing from measurements at multiple frequencies. Such techniques offer a powerful tool for corrosion assessment in real structures.

3 ULTRASONIC INSPECTION SYSTEM

Ultrasonic techniques for nondestructive evaluation of structures are based on the propagation of high frequency sound in the structure. A discontinuity in the acoustic properties of the structure results in a reflection of the sound in the media. For a single plate if the propagation direction is perpendicular to the surface the round trip time in the plate is given by

$$\Delta t = \frac{2l}{v} \quad (3)$$

where l is the thickness of the layer and v is the velocity of sound in the layer. Ultrasonic thickness gauges utilize this relationship by propagating a sound wave in the layer, measuring the first arrival time of the ultrasonic echo back to the transducer. The thickness of the layer is then calculated by multiplying the delay time times the velocity, which is assumed to be a known quantity. For this technique to be effective the response of the transducer following excitation must be near zero before the arrival of this echo. For thin gauge aluminum such as typical found in aircraft fuselages, this condition is often difficult to meet.

A second technique for characterization of the thickness from ultrasonic measurements is based on the ultrasonic resonance of the layer (Ref. 3). Resonance frequencies of the layer are given by

$$f_n = \frac{n}{\Delta t} = \frac{nv}{2l} \quad (4)$$

where n is an integer and represents the order of the

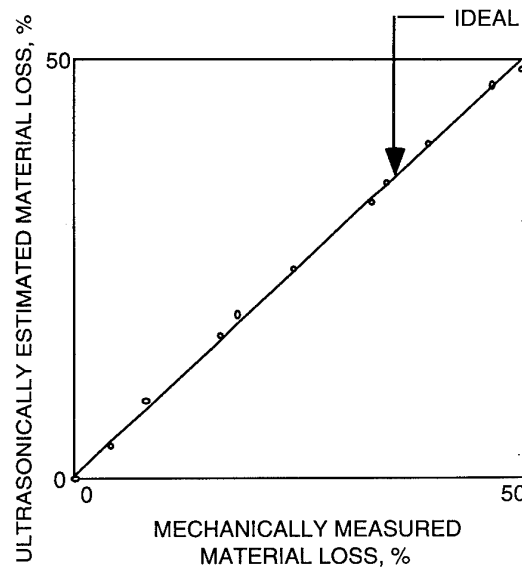


Figure 4. Comparison of mechanical measurements of material loss in samples with ultrasonic measurements from fourier transform of pulse echo.

resonance. By measuring the resonance frequency of the layer the thickness can be calculated from $nv/2f_n$ assuming the order of the resonances is known. One advantage of this technique is that it only requires the Q of the layer be greater than the Q of the transducer to separate the transducer response from the layer response. Since the transducer is acoustically damped and the layer is not, this condition is easily met.

For aluminum thicknesses typically used as skins in aircraft the fundamental frequency ($n=1$) is on the order of 2-4 MHz, therefore a 3.5 MHz damped transducer is used to excite the layer. Since this is considerably less than the 20 MHz transducers required for pulse echo measurement, there are other advantages to this technique. One is that phase cancellation caused by surfaces which are not perfectly flat and parallel is significantly less at 3 MHz than 20 MHz. A second advantage is the effect of variations in the coupling layer between the transducer and structure are less significant at lower frequencies.

Measurements were performed on a series of samples of known thickness. A comparison of mechanical measurements and ultrasonic measurements of the thickness are shown in Figure 4. As can be seen from the figure the agreement between the two is excellent. From this measurements, it was determined the technique is capable of measuring the thickness of the upper layer to within 3%.

This technique has been integrated into a portable hand scanner which can image the defects in a aircraft structure. The ultrasonic response of the structure is first reduced by a neural network (Ref. 3) to determine if the structure is bonded or disbonded. If the lap joint is disbonded, the resonance frequency of the top layer is determined from a fourier transform of the response. The thickness of the layer calculated from the resonance frequency is displayed on a color monitor as a color coded pixel. The process is real time, all the processing being performed in a time insignificant to the time require to move the transducer to a new position. The result is a real time image of the extent of disbonding and corrosion in the lap joint. A typical image is shown in

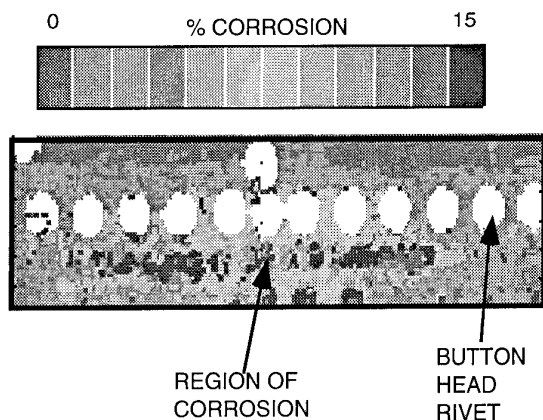


Figure 5. Image of corrosion in lap joint as measured with ultrasonic system.

Figure 5. The specimen is the same panel inspected with the self-nulling probe. As can be seen from the figure, the agreement between the two techniques as to the extent of corrosion is very good.

4 THERMOGRAPHIC INSPECTION SYSTEM

Thermographic imaging is a relatively new technique for inspection of aerospace structures. Thermographic imaging has a significant advantage over other techniques in that it does not require physical contact between the inspection system and the aircraft. Infrared thermography is performed with an infrared imager capable of scanning large areas in a fraction of a second. Recent technological developments have enhanced thermographic inspections, significantly increasing the reliability of the technique. In particular, the development of inexpensive image processors and high speed computers have permitted precise timing of the application of heat, an increased signal to noise ratio for the thermographic images and enabled the development of post processing procedures.

Thermographic inspection involves the application of heat to the surface of a structure and subsequent measurement of the surface temperatures as a function of time. For aircraft lap joint inspections, flash lamps or quartz lamps are used to apply heat to the exterior surface of the aircraft and the temperature of the exterior surface temperature is measured with an infrared camera. In a relatively short period of time, heating the surface creates a temperature differentials where there are variations in the local heat flow characteristics of the structure. The presence of corrosion reduces the heat flow from the upper to lower layers of the structure. This reduction of heat flow is reflected in an increase in temperature over the corroded region which can be used to identify these regions.

The surface temperature as a function of time is measured with an infrared imager consisting of a single liquid nitrogen cooled HgCdTe detector (8 - 12 μm). By scanning the focus of the detector over the field of view, the infrared radiation from the surface is measured. For a surface emissivity of 1, this radiation is a function of the temperature of the surface. For emissivity of the surface less than 1, the radiation from the surface is a function of the surface temperature plus a reflection of background infrared radiation. Bare aluminum surfaces have emissivities of less the 0.1, therefore infrared

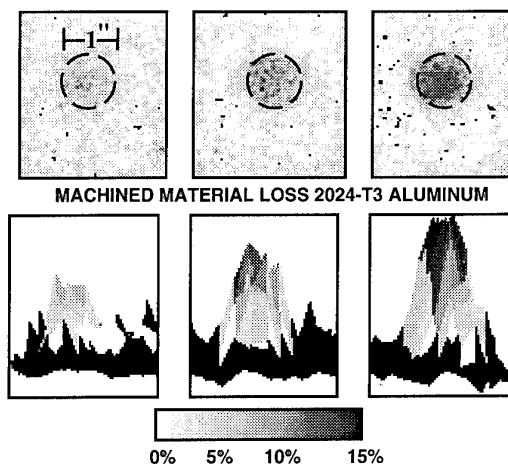


Figure 6. Thermographic quantification of corrosion in single layer of aluminum. (Ref. 4)

images of bare surfaces represent the background infrared fields rather than the surface temperature.

To perform measurements on aluminum, a thin layer of high emissivity material must be applied to the surface. Paint is typically an excellent emissivity coating, with a high emissivity independent of the color in the 8-12 μm region. Therefore aircraft which are painted typically require no special treatment before inspection. An unpainted aircraft can be coated with commercially available water washable coatings to increase the surface emissivity.

For quantitative measurements synchronization is required between the heating and data acquisition. The precise timing is provided by synchronizing the data acquisition and the application of heat with a small microcomputer. The microcomputer also allows processing of the data to enhance the contrast between corroded and noncorroded regions and perform quantitative measurements.

For a single thin aluminum layer, 1mm in thickness, the temperature following flash heating of the surface achieves a through the thickness equilibrium in less than 30 msec. Since this is faster than the typical scan rate of the infrared imager, the first image obtained is of the equalized state where the change in temperature is given by

$$\Delta T(x, y) = \frac{H(x, y)}{\rho c l(x, y)} \quad (5),$$

where $H(x, y)$ is the heat deposited by the flash as a function of position, ρ is the density, c is the specific heat and $l(x, y)$ is the thickness as a function of position. For the region of interest, $H(x, y)$ is either constant or slowly varying function which can be independently determined (Ref. 4). For this case, the thickness as a function of position can be determined by inverting equation 5 to give

$$l(x, y) = \frac{H(x, y)}{\rho c \Delta T(x, y)} \quad (6).$$

Images on material loss in a single layer of aluminum is shown in Figure 6. As can be seen from this image there is good agreement between the material loss as estimated from this technique and mechanical measurements. This relationship is only accurate while there is not significant

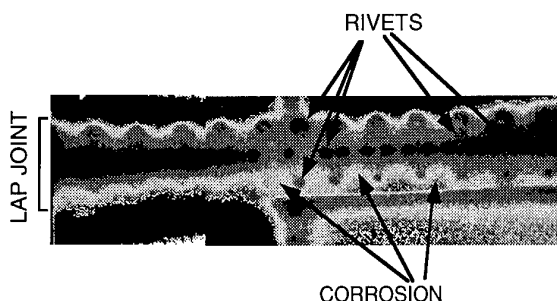


Figure 7. Image of corrosion in lap joint specimen obtained from thermographic technique.

lateral heat flow in the layer. For longer times, lateral heat flow reduces the contrast between corroded and noncorroded regions.

A similar relationship to equation 6 can be determined for step heating of the layer, where the flash heating is replaced by a constant flux. For this case, the inversion has the form

$$I(x, y) = \frac{F(x, y)}{\rho c \frac{dT(x, y)}{dt}} \quad (7),$$

where $F(x, y)$ is the flux applied to the surface. This can be applied to data taken with quartz lamps, however, with these systems the flux is not typically a step function in time and the time derivative requires acquisition of temperature at several different times allowing lateral heat flow during the measurement. As a result quantitative measurements with quartz lamps is more difficult.

Quantitative measurements in multilayered structures is also difficult, requiring separation of the thermal response of the aluminum layers from layers of corrosion products, adhesive materials and air gaps. This is possible if the initial time dependence of the temperature is known (Ref. 5), but this measurement is difficult with infrared imagers. However the infrared technique is still an excellent technique for detection of corroded regions. Results have indicated corrosion with material loss of 10% or more is easily detected with this technique. A thermographic inspection of a lap joint specimen with corrosion is shown in Figure 7. As can be seen from the figure there is good agreement between this technique and previously discussed techniques.

5 REVERSE GEOMETRY X-RAY

Radiographic inspection is different from other techniques in its ability to perform full volume inspections. Its major disadvantage is safe application which limits access to the aircraft during the inspection. However, for some inspections, x-rays are capable of detecting flaws which are inaccessible with other techniques. A recent development in x-ray radiography called "Reverse Geometry X-rays"¹ offers significant advantages over conventional radiographic techniques.

The principle difference between "Reverse Geometry X-ray"[®] imaging and conventional radiography is the source. For conventional radiography the source is a point source,

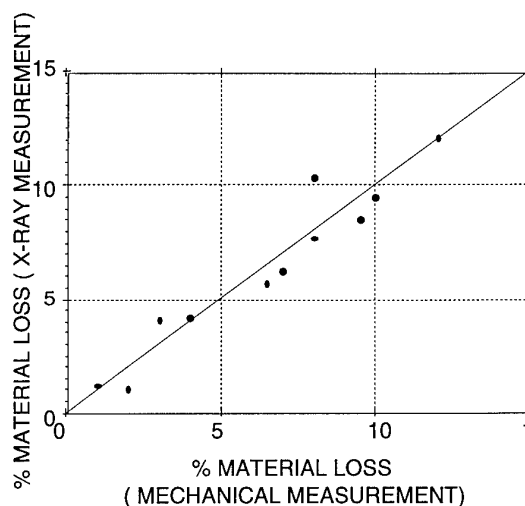


Figure 8. Comparison of mechanical measurement of material loss and material loss calculated from x-ray attenuation in specimens. (Ref. 6)

from which x-rays are emitted. The structure to be inspected is placed a sufficient distance from the source to illuminate the region of interest. For "Reverse Geometry X-rays"[®] the source is a scanned source which is placed near the structure. In contrast to conventional radiography where an area detector is typically used, the radiation intensity for "Reverse Geometry X-rays"[®] is measured with a point detector. By synchronization of the detector output with the position of the x-ray source, an x-ray image of the structure being inspected is generated.

There are several advantages in scanning the source. One is that the detector can be designed to reduce the amount of received scattered radiation, which causes a blurring in the image. Another is that point detectors can be made which are much smaller than conventional x-ray sources. The detector can be remotely positioned inside a structure to improve the interpretability of the images. Finally more than one point detector can be used at a time to yield structural depth information.

If scattered x-rays are unable to reach the detector, the detected x-ray intensity at energy E , $I(E)$, transmitted through a single homogeneous material is given by

$$I(E) = I_0(E) e^{-\mu(E)l} \quad (8)$$

where $I_0(E)$ is the original x-ray beam intensity, l the material thickness transversed and $\mu(E)$ the material's linear attenuation coefficient. The linear attenuation coefficient for aluminum is strongly dependent on the x-ray energy at low energies (<40 keV), while less dependent on energy at higher energies. To first order, for a thin layer of material, the energy spectrum does not change as it passes through the layer and $\mu(E)$ is assumed to be a constant. Using this assumption, the natural logarithms of the ratio of transmitted to original intensity is directly proportional to the material thickness transversed. This ratio can be obtained from the normalized image for an uncorroded and corroded region of the sample and hence the percentage material loss can be calculated.

The results of measurements performed on a series of specimens is shown in figure 8 (Ref. 6). As can be seen from

1. "Reverse Geometry X-ray" is a registered trademark of Digiray Corporation, San Ramon, CA

the figure there is generally good agreement between mechanical measurements and measurements from the "Reverse Geometry X-ray[®]" system. While the overall agreement is within 2% of the mechanically measured value, several points have a large deviation from the mechanical measurements. This may be a result of corrosion products being packed into the corroded area. If the corroded area is packed with corrosion products, the attenuation in the x-rays, as they passed through the corrosion products, will result in an apparent increase in the thickness of the layer. Other efforts have shown it is possible to eliminate this error by performing measurement as several different x-ray energies.

7 CONCLUSION

New techniques are currently being developed for the detection and quantification of corrosion. The four techniques presented here are eddy current, ultrasonic, thermographic and x-ray technologies. Each of the techniques complement each other by filling a inspection requirement. The thermographic technique performs rapid surveys of the structure to locate corroded regions. The ultrasonic technique accurately determines the thickness of the top layer. The eddy current is able to quantify the material loss in one than more layer. Finally the x-ray technique is able to detect corrosion in built up structures.

REFERENCES

1. Wincheski,B., Fulton,J., Nath,S. and Namkung,M. "New Eddy Current Probe for Thickness Gauging of Conductive Materials", *in* "Review of Progress in Quantitative Nondestructive Evaluation", *13B*, 1994, pp1939-1946.
2. Fulton,J.P., Wincheski,B., Nath,S. and Namkung,M. "Corrosion Detection in Airframes Using a New Flux-Focusing Eddy Current Probe", *in* "ASNT 1994 Spring Conference", 1994, pp34-36.
3. Prabhu,D.R.,Abedin,M.N. and Johnston,P.H., *in* "Review of Progress in Quantitative Nondestructive Evaluation", *13B*, 1994, pp1919-1926.
4. Syed, H.I, Winfree,W.P., Cramer,K.E. and Howell,P.A., "Thermographic Detection of Corrosion in Aircraft Skin" *in* "Review of Progress in Quantitative Nondestructive Evaluation", *12B*, 1993, pp2035-2041.
5. Emeric,P.R. and Winfree,W.P., "Thermal Characterization of Multilayer Structures from Transient Thermal Tesponse" *in* "Review of Progress in Quantitative Nondestructive Evaluation", *to be published*.
6. Birt,E.A., Parker,F.R. and Winfree, W.P., "Quantification of Corrosion Damage in Aircraft Skin Using a Novel X-ray Radiography System", *in* "Review of Progress in Quantitative Nondestructive Evaluation", *13B*, 1994, pp1963-1970.

ORGANIC COATING TECHNOLOGY FOR THE PROTECTION OF AIRCRAFT AGAINST CORROSION

Charles R. Hegedus,
Stephen J. Spadafora*, and Anthony T. Eng*

Air Products and Chemicals Inc.
Allentown, PA (USA) 18195

*Naval Air Warfare Center
Aircraft Division
P.O. Box 5152
Warminster, PA (USA) 18974-0591

ABSTRACT

Coating systems on military and commercial aircraft perform a variety of functions. Clearly, the most critical of these is the protection of aircraft structures from environmental degradation. Protective coatings serve as the primary defense against corrosion of aircraft metallic alloys, as well as degradation of other materials such as polymeric composites. Traditional coatings for aircraft include epoxy primers and polyurethane topcoats. Primers normally contain high concentrations of corrosion inhibitors, such as chromates, and they are designed to provide superior adhesion and corrosion protection. Polyurethane topcoats are formulated to enhance protection and durability; they also provide desired optical effects (i.e., aesthetics or camouflage). More recently, alternative coatings have been developed, such as self-priming topcoats, flexible primers, temporary and multi-functional coatings. These new developments reflect trends in protective coatings technology, changes in aircraft operational requirements/capabilities, and, most dramatically, concerns over environmental protection and worker safety. This issue has created a drive toward coatings with low (possibly zero) concentrations of volatile organic compounds (VOCs) and non-toxic corrosion inhibitors. In turn, these changes have led to concerns over long-term performance, especially protection against corrosion. This paper reviews current organic coatings technology for the protection of aircraft structures and discusses future needs and trends based on advancing technology, environmental concerns, and operational requirements.

INTRODUCTION

Coating systems on military and commercial aircraft perform a wide variety of functions; they provide desired optical effects (i.e., aesthetics, camouflage), corrosion prevention, erosion control, markings, electrical grounding, electromagnetic shielding, as well as other specialized properties. Clearly, their most critical contribution is the protection of materials and structures from corrosion and other forms of environmental degradation. A United States Air Force study (1) has concluded, "The rate controlling parameter for the corrosion of aircraft alloys, excluding the mechanical damage factor, is the degradation time of the protective coating system." It must be emphasized that coatings protect not only metallic alloys from corrosion, but also plastics and polymeric composites from various degradation mechanisms (2).

Careful consideration of aircraft materials deterioration is essential, due to the high cost of these aircraft in addition to the severe environmental and conditions in which they operate. For example, many military aircraft are deployed at coastal land bases or on board aircraft carriers. The continuous proximity to salt water and high humidity combined with atmospheric impurities cause one of the most corrosive natural environments. Another example is the frequency of cabin pressurization/de-pressurization with commercial flights. Multiple daily flights over long periods of time cause fatigue, which combined with corrosion, can cause rapid catastrophic damage. In addition, many operational and maintenance chemicals commonly used or found on aircraft, such as paint strippers, battery acid, de-icing fluids, and cleaners, are corrosive. These effects are exaggerated even more so with aging commercial and military aircraft fleets.

Because of the performance benefits provided by coatings, and the high cost of aerospace systems, only the most protective and durable paints have been developed and used on aircraft. They must meet demanding criteria, including:

- (i) room temperature cure (high temperature and ultraviolet cure are currently impractical except for small parts),
- (ii) long-term corrosion protection and excellent adhesion to a wide variety of substrates,
- (iii) resistance to aggressive operational and environmental chemicals (hydraulic fluids, engine oils, fuels, sea spray, etc.), and
- (iv) superior long term exterior durability with minimal change in optical or physical properties.

In many cases, the coating systems used over the past 25 years consisted of epoxy primers and polyurethane topcoats. These materials have met the aforementioned aerospace demands and have provided superior corrosion protection, especially when combined with diligent maintenance practices.

Recently, alternative coatings have been developed, such as self-priming topcoats, flexible primers, temporary and multi-functional coatings. Other changes in coating composition and application procedures have occurred because of concerns for environmental protection and worker safety. Many of these coatings have contained high levels of volatile organic compounds (VOCs) as solvents and plasticizers, and heavy metal compounds as corrosion inhibitors and colorants. These ingredients are being severely regulated and coating formulations are being drastically changed accordingly. Nonetheless, corrosion protection remains a primary requirement and therefore these changes have led to justified concerns over long term performance. These issues are all at the forefront of coatings technology.

This paper is a general review of: mechanisms by which coatings protect aircraft, standard coatings (i.e., primers and topcoats) and coating systems, specialty coatings (i.e., fuel tank, high temperature, rain erosion), environmentally compliant coatings issues, and future trends in aircraft coatings technology.

CORROSION CONTROL BY ORGANIC COATINGS

Modern aircraft are complex structures which are manufactured from a large variety of materials. Although aluminum alloys are most common on aircraft due to their high specific strength. There are also numerous alloys of steel, titanium, and magnesium, all of which can be treated with a myriad of inorganic or metallic coatings prior to painting. The use of polymeric composites, which may contain highly cathodic carbon fibers (3), and engineering plastics, which may be partially conductive, increases the complexity of corrosion control. Nonetheless, coatings are designed to protect all of these surfaces from degradation. Since aluminum is the most common material, the corrosion mechanisms most common with its alloys are frequently observed on aircraft structures. These include intergranular, exfoliation, galvanic, pitting, and filiform corrosion. Reference (4) provides an excellent documentation of aircraft corrosion causes and case histories. References (5) & (6) describe guidelines and specifications for aircraft corrosion control.

Corrosion of painted aircraft structures can occur underneath the coating or, more commonly, at defects in the coating or discontinuities in the substrate (i.e., fasteners, rivets, corners, joined or faying surfaces, etc.). In fact, one of the most common locations for corrosion to occur is around fastener heads, which attach the aircraft skin to the frame. Low temperature (-65°C) flexing and vibration during flight causes paint around the fastener heads to crack, thereby exposing the underlying bare metal. Complicating this issue is the dissimilar metals between the fastener and aircraft skin, which can lead to galvanic corrosion. The coating system on aircraft must prevent these types of degradation from occurring.

Regardless of the type of corrosion, the process requires the presence of water, anions, cations and oxygen (7,8). In addition, although most corrosion processes are thermodynamically preferred, the rate of corrosion must be substantial enough to be significant during the lifetime of the substrate/coating system. Aircraft coating systems are designed to prevent several of these conditions from occurring. One approach is having the coating system form a physical barrier between the substrate and the surrounding environment. The traditional coating system of an epoxy primer and polyurethane topcoat provides a very good barrier. When combined, they have a relatively low water absorption and vapor transmission rate (9) which effectively minimizes oxygen, moisture, and ions from reaching the substrate. This is provided by both the crosslinked epoxy and polyurethane binders, and the pigments, which reinforce the barrier effect. In fact some lamellar (plate-like) fillers such as talc and mica

are incorporated into the primer so that when the coating is applied, they will align parallel to the substrate (similar to roof tiles), forming a more resistant environmental barrier.

Although these coatings are designed to minimize the transport of foreign species, especially those which will promote the corrosion process, inevitably contaminants will reach the substrate. When this occurs, it is of utmost importance that they do not disrupt the coating-substrate adhesion. If this were to occur, it is likely that the corrosion inhibiting capabilities of the coating will be severely diminished. This is especially true of water which is notorious for causing disbonding of coatings by preferentially interacting with the substrate (10,11). Therefore, aircraft coatings must also be capable of maintaining their adhesive strength when exposed to high concentrations of water. Coating adhesion is caused by both mechanical and chemical interactions between the coating and the substrate. Mechanical contributions are caused by the coating hanging on to microscopic ridges or teeth on the substrate, and this effect is promoted by the use of a high tensile strength coating such as an epoxy primer. In addition, inorganic surface pretreatments can increase the surface roughness and chemical interactions to enhance this effect. Chemical contributions to adhesion are created by molecular interactions between the coating and the substrate. In many cases these interactions result in the formation of secondary bonds. However, it has been shown that primary bonding between the coating and substrate can occur, and this mechanism is more likely to prevent disbonding due to water (12). Therefore, aircraft coatings must not only delay the diffusion of foreign species to the substrate, but they must also resist the effects if these species reach the coating-substrate interface.

As mentioned above, another area where corrosive media can reach a substrate is at discontinuities in the structure where paint can crack and chip. One classic example is around fastener heads. Epoxy primers used on aircraft are brittle, especially at low temperatures, which are experienced at high altitudes. When the aircraft vibrates and flexes during flight, the coating system can crack. In order to prevent this mode of coating failure, elastomeric primers (i.e., polyurethanes, toughened epoxy, or polysulfides) can be used. It has been shown that use of these coatings will enhance the flexibility and toughness of the coating system, thus preventing these failures and susceptibility to corrosion (13).

The above cases describe how coatings prevent corrosion by maintaining an effective barrier between the substrate and the corrosive environment. Another important mechanism by which coatings protect aircraft structures is the incorporation and use of chemically active corrosion inhibiting pigments. They perform at sites where bare metal is exposed by making the corrosion mechanism thermodynamics unfavorable and/or by slowing the corrosion reaction kinetics to a minimal rate. Traditionally, strontium, barium, zinc, and lead chromates have been used in aircraft primers for this purpose. Chromates are oxidizing inhibitors which adsorb onto the metal surface, repair the passivating oxide film, and effectively inhibit the corrosion process (14-16). This mechanism has been termed precipitation inhibition and it is

highly dependent upon the solubility of the pigment in water and the diffusion (leaching) rate of the chromate ion out of the coating to susceptible areas. Simply stated, the inhibitor ions leach out of the coating at defects and actively inhibit corrosion of the exposed metal. If the leaching rate is too slow, not enough chromate ion will be available to prevent corrosion. If the rate is too high, the coating system will prematurely become deficient of inhibitors, causing long term corrosion problems. The rate of this transport is highly dependent upon temperature, pH, and interactions between the pigment and binder system. Therefore, each coating must be specifically developed to perform in the intended application.

Until recently, chromates were virtually the sole source for active corrosion inhibition in aircraft coatings. This was due to their outstanding performance in protecting nearly all metals in a large range of environments. However, chromates have been shown to be carcinogenic, and their use and disposal are being severely restricted. (See section on COMPLIANT COATINGS ISSUES.) This has led to much research and development of non-toxic inhibitors for use in coatings, including those for aircraft. Pigments which have been investigated as alternatives include phosphates, borates, molybdates, nitrates, and silicates. The mechanisms by which these inhibitors perform have not been thoroughly defined. Proposed mechanisms for zinc phosphate include the adsorption of ammonium ions, complex formation on the exposed surface, passivation through a phosphating process, and anodic/cathodic polarization. Phosphates, borates, and silicates are generally regarded as anodic passivators which reduce the rate of corrosion by increasing anodic polarization. Molybdates also have been classified as anodic inhibitors and especially effective at inhibiting propagation of pits. At high concentrations, the oxidizing action of molybdates is the main factor behind its corrosion inhibiting ability. Molybdate ions migrate into anodic areas and accumulates there, especially in pitted areas.

Although these pigments individually provide some level of corrosion inhibition, in general, one for one substitution for chromates has not resulted in coatings with equivalent corrosion prevention capabilities. However, a number of researchers have found that combinations of inhibitors provide nearly equivalent or superior properties as chromates (17-19). In some cases, synergistic effects/performance have been reported. For example a series of primers and self-priming topcoats which contain inhibitor pigmentation mixtures have been developed for aircraft applications (18,20). In another example, although not investigated specifically for aircraft coatings, Hare and Fernald have reported good corrosion inhibition with manganese tetroxide combined with calcium borosilicate (21). Also, alkaline extenders, such as wollastonite, have displayed a synergistic effect with inhibitive pigments as described in reference (22). These results have been displayed in accelerated laboratory exposures, electrochemical analysis, and, most importantly, real world applications. A direct cause and effect relationship for these results has not been definitively proven. However, it has been postulated that combinations of inhibitors provide a variety of inhibition mechanisms which may prevent the

aforementioned types of corrosion by affecting the thermodynamics and/or kinetics of the corrosion process. In addition, interactions may occur between inhibitors, causing the noted synergistic effects.

STANDARD FINISHING SYSTEM

The most common organic coating system applied to the exterior surfaces of military and commercial aircraft consists of a solvent-borne epoxy primer and a solvent-borne polyurethane topcoat. In addition to this primer and topcoat paint system, other technologies have been introduced such as water-borne epoxy primers, self-priming topcoats, and flexible primers. These organic coatings are applied over inorganic surface treatments to further enhance their performance properties. All of these coating systems have protected aircraft structures from the frequently harsh operational environment due to their exceptional corrosion inhibition, adhesion, and durability characteristics. The practical lifetime of these coatings on military and commercial aircraft exterior surfaces is 4 to 8 years, after which the coating system is chemically removed via methylene chloride based materials or ablatively removed using focused mechanical and/or intense light energy methods (i.e. plastic media, waterjet, wheat starch, carbon dioxide, flashlamp, and/or laser). The aircraft exterior surface is subsequently cleaned, pretreated, and repainted. A general description of the finishing system used on aircraft is outlined in references (6,23-26).

In general, the coating materials, processes, and specification requirements used by the military and the commercial sector are very similar. However, there are slight differences between commercial and military coatings in that the specific needs of the user activity are addressed. For instance, the commercial sector requires more strict operational fluid resistance properties and places more emphasis on aesthetics, whereas the military requires increased corrosion resistance and minimized detectability. The critical properties of commercial and military coatings are listed in Table 1.

SURFACE PREPAINT TREATMENTS AND COATINGS

The primary goal of surface preparation and pretreatment processes is the enhancement of the corrosion resistance and adhesion properties of subsequent organic coatings. Proper surface preparation is an important step in the protective treatment of aluminum, and is accomplished by using materials such as alkaline cleaners, etchants and deoxidizers. These materials remove organic contamination along with the existing surface oxide layer of the aluminum to prepare it for subsequent chemical pretreatments. These protective pretreatments are used because of their enhancement of the overall protective finishing system. For example, the U.S. Navy specifies the MIL-S-5002 "Surface Treatments and Inorganic Coatings for Metal Surfaces of Weapon Systems" Military Specification for surface preparation and pretreating of virtually every aircraft and weapon system they use. The two primary surface pretreatments for aircraft are chromate conversion coatings and anodic films. Chromate conversion coatings (CCC) are excellent surface pretreatments for

aluminum alloys. These materials chemically form a surface oxide film (typically 40-60 mg/ft²), which enhances the overall adhesion and corrosion prevention properties of the protective finishing system applied over them. Anodize processes form a thicker oxide film (200+ mg/ft²) by electrochemical means which provides more protection against degradation than chemical conversion coatings.

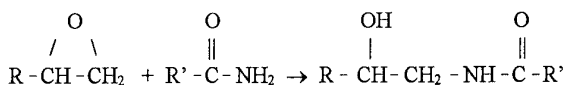
One of the main environmental thrusts in the pretreatment area is the total elimination of hexavalent chromium. This toxic material has been used widely in the aforementioned processes because of its outstanding performance as a corrosion inhibitor for aluminum. This property is of particular importance to the aerospace industry due to the extensive use of aluminum in aircraft and aerospace systems. Chromium VI is a known carcinogen, however, and regulatory agencies have recently enacted rules which limit or prohibit the use of this material. This has resulted in a need for alternative materials to be developed.

Non-chromated alkaline cleaners and non-chromated deoxidizers have been identified as acceptable alternatives to the current chromated processes, and are being implemented by most of the U.S. aerospace industry. These materials have provided satisfactory performance in these surface preparation operations and in some cases they have been more cost effective than their chromated predecessors. Typical CCC film performance requirements are covered by MIL-C-5541 "Chemical Conversion Coatings on Aluminum and Aluminum Alloys" and CCC material properties are described in MIL-C-81706 "Chemical Conversion Materials for Coating Aluminum and Aluminum Alloys." Numerous non-chromated surface pretreatment materials have been investigated as replacements for the CCC. A summary of one such investigation is described in Reference (27). While there have been some promising alternatives based on performance, these alternatives have had either process or performance deficiencies that limit their use as across the board replacements. Chromic acid anodizing (CAA) has been widely used in aerospace production and maintenance operations. Typical performance requirements for this type of film are described in MIL-A-8625 Type I "Anodic Coatings, for Aluminum and Al Alloys." However, due to the increasing restrictions on hexavalent chromium, several potential alternatives have been identified and incorporated into the MIL-A-8625F specification. These alternatives are: sulfuric/boric acid anodize (Type IC), sulfuric acid anodizing (Type II), and thin film sulfuric acid anodizing (Type IIB). Information on these processes can be obtained from References (28-31).

PRIMER

Epoxy resins are commonly used as binders in high performance primers due to their exceptional adhesion and chemical resistance properties. The solvent-borne epoxy primer is manufactured and packaged as a two component epoxy/polyamide system. One component contains an epoxy resin which is the product of a condensation reaction between epichlorohydrin and bisphenol A. The second component is a solution of a multi-functional polyamide resin in a solvent

blend. Upon mixing the two components, which is done just prior to application of the primer, reaction of epoxide and amide groups within the resins ensues:



The product of this reaction is a highly crosslinked polymer which forms the matrix of the primer film. The chemical and mechanical properties of the epoxy matrix cause the primer to be adherent, chemically resistant, and durable. Hydroxyl groups on the solid epoxy are usually given credit for the excellent adhesion of these coatings. References (32) and (33) provide detailed discussions of epoxy resin chemistry for coatings.

The epoxide component of the primer contains various pigments, including titanium dioxide, strontium chromate, and extender pigments. Strontium chromate is the most critical of these pigments since it is well known as an exceptional corrosion inhibitor, especially for aluminum. Titanium dioxide in the primer enhances durability, chemical resistance, and opacity of the applied coating. The extender pigments can be silicas, silicates, carbonates, or sulfates. The extenders are normally inexpensive and provide a cost effective component which "fills" the coating and reduces gloss of the applied film. The surface irregularities which cause gloss reduction also act as anchors for a topcoat, thus enhancing inter-coat adhesion by improving the mechanical attachment. References (24) & (25) provide a comprehensive review of epoxy primer technology for aircraft applications.

Upon mixing the two components of the epoxy/polyamide primer, the curing reaction begins. At this stage, the coating is suitable for spray application. After application of the coating to a dry film thickness of 13 to 38 microns (0.5 to 1.5 mils), the coating is tack-free within 1 to 5 hours and dry hard within 6 to 8 hours. If a topcoat is to be applied, it is usually accomplished within the tack-free to dry hard time period to ensure proper adhesion. The primer attains sufficient dry film properties within 7 days of application.

Since water is a primary factor in reducing adhesion of paint films and causing cathodic disbondment, adhesion is considered a critical paint performance property. Adhesion of the primer is characterized by a tape test after a 24 hour immersion exposure period in distilled water (34). The required performance is no coating removal from the substrate. Adhesion is also characterized by a method which quantifies the force required to scrape the primer from the substrate (35). Typically scrape adhesion values of at least 3 kg is considered acceptable. Other adhesion tests primarily employed in the research and development laboratories are the tensile adhesion and Hesiometer knife-cutting adhesion tests (36). These sophisticated laboratory adhesion tests yield quantitative data but require more training and expertise to perform the tests and to analyze data compared to the tape and scrape adhesion tests.

Corrosion resistance is evaluated by applying the primer to a chromate conversion coated aluminum substrates such as 2024

T3. After curing for 7 days, the primer is scribed with an "X" so that the substrate is exposed. Resistance to 5% NaCl salt fog exposure is required such that no substrate corrosion or coating defects are produced after 2000 hours of exposure (see Figure 1). Note for Figure 1: MIL-P-23377 is a strontium chromate-containing primer which is commonly used in military aerospace applications. Resistance to filiform corrosion after exposure to hydrochloric acid for one hour followed by exposure to high humidity for 1000 hours, is required for primers. Generally, specimens should not exhibit filiform growth from the scribe greater than 3.175 mm (0.125 in). In addition to the salt fog and filiform tests, the U.S. military also requires the corrosion resistance of primed and then scribed aluminum/graphite epoxy specimens. This forms a galvanic couple which must withstand 5% NaCl salt fog exposure for 500 hours such that pitting greater than 1 mm (0.039 in) is not produced. SO_2 /salt fog exposure and electrochemical impedance spectroscopy have also been used to evaluate the corrosion resistance properties of coating systems.

WATERBORNE PRIMER

The high performance waterborne epoxy primer that is currently used on exterior surfaces of many military aircraft was developed (37) and implemented into the U.S. aerospace community in the late 1970's to mid 1980's. (Although this technology is currently used only on interior surfaces of commercial aircraft (38), it is expected to be implemented on exterior commercial aircraft surfaces in the near future.) This primer is supplied as a 2 component epoxy/amide or epoxy/amine system. The resin systems are water-reducible and film formation occurs via coalescence of resin particles and crosslinking of the epoxy/polyamide reactive groups. The pigments used are similar to those used in the solvent-borne primer system. For example, strontium chromate pigment is used as the primary active corrosion inhibitor in many waterborne primers. Organic co-solvents and surface active agents are also used to enhance formulation and processing properties such as water miscibility and dispersion stability, as well as film formation and quality.

FLEXIBLE PRIMER

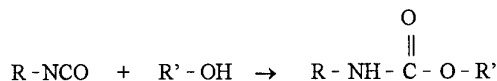
The epoxy primer is brittle, especially at low temperatures (-51°C), which can potentially result in extensive cracking of the paint system in highly flexed areas of the aircraft. Sealants, which are sometimes spray applied between the primer and topcoat in aircraft finishing systems, to increase overall coating system flexibility, are soft, easily deformed, and difficult to apply and remove. An alternative is an organic coating that possesses the adhesion of a primer and the flexibility of a sealant, thus eliminating the logistical and application problems inherent in stocking and applying two materials instead of one. An elastomeric primer which provides these benefits has been characterized and implemented on Navy aircraft. This material is based on polyurethane resin technology and a pigment system which contains strontium chromate for corrosion inhibition and extender pigments for gloss control. Most of the requirements for this flexible primer are similar to those in the current

epoxy primer specifications, with the exception of film flexibility, which is significantly more stringent than those exhibited by the current epoxy primers: 80% versus 10% room temperature elongation, respectively. One of the major coating failure mechanisms on aircraft is cracking around fasteners, thus exposing bare metal. Application of this coating to numerous U.S. Navy and Air Force aircraft has resulted in less coating system failures due to cracking and chipping.

TOPCOAT

A high performance topcoat is applied to aircraft in order to enhance protection against the operational environment and to provide desired optical properties. Aliphatic polyurethane coatings are ideal for this application due to their superior weather and chemical resistance, durability, and flexibility. It is interesting to note that although polyurethane topcoats have become increasingly popular over the last twenty-five years, initial versions of these materials were applied to German aircraft during World War II.

Polyurethanes are a huge class of polymers with a wide variety of chemical and physical properties. Most urethanes used in aircraft coatings are two component, reactive materials. One component of the coating is a polyisocyanate resin or an isocyanate terminated prepolymer based on hexamethylene diisocyanate (HDI). The second component contains a hydroxylated polyester. Upon mixing, the isocyanate groups react with the hydroxyl groups of the polyester:



The resulting polymer is flexible yet extremely durable and chemical resistant. Aliphatic isocyanates and polyesters are used in topcoats because they provide outstanding weather resistance compared to aromatics, which degrade when exposed to ultraviolet light. References (39-42) provide more detailed discussions about polyurethane chemistry.

When the two components are combined and the polyurethane reaction begins, the coating is ready for application (i.e. no induction time is required). This coating is normally spray applied to a dry film thickness of 50.8 ± 7.6 microns (2.0 ± 0.3 mils). The typical topcoat is set-to-touch and dry hard (when cured at room temperature) within 2 and 6 hours, respectively. Although the painted surface can be handled after 6 hours without damage to the coating, full performance properties are normally not obtained until approximately 7 days.

The performance properties required in current specifications are listed in Table I. The most critical requirements are weather resistance, chemical resistance, and flexibility. Weather resistance is evaluated by laboratory exposure in an accelerated weathering chamber (43) for 500 hours. This chamber is a continuous cycle of high intensity ultraviolet light (zenon arc) and water spray. Although studies have shown that there is no precise correlation with outdoor exposure (44-46), the accelerated exposure does indicate if the coating is susceptible to ultraviolet and/or water degradation. These results are used in conjunction with actual outdoor exposure

for 1 year. Both accelerated and real-time weathering conditions cause only minimal changes in the color, gloss, and flexibility of high performance aircraft topcoats.

Chemical stability is evaluated by exposure of the applied topcoats to various operational fluids such as lubricating oil, hydraulic fluid, and jet fuel at elevated temperatures and/or extended durations. Aerospace topcoats are also subjected to a dry heat of 121°C (250°F) for 4 hours. Suitable topcoats show no defects other than slight discoloration after exposure to these conditions.

Flexibility requirements for polyurethane topcoats include impact and mandrel bend tests. For high gloss colors, a 60% elongation of the coating after impact at room temperature and a 180° bend around a 0.95 cm (0.375 in) cylindrical mandrel at -51°C (-60°F) are required without cracking of the film. Flexibility requirements for low gloss colors are less stringent since it is difficult to formulate flexible low gloss coatings due to high pigment concentrations, which normally embrittle the film.

SELF-PRIMING TOPCOAT

The self-priming topcoat (SPT) is a VOC compliant, non-lead, non-chrome high-solids polyurethane coating that was designed to replace the current primer and topcoat paint system used on aircraft (18). The SPT possesses the adhesion and corrosion inhibition properties of a primer as well as the durability and optical properties of a topcoat. See Table I and Figure 1 for a list of typical properties and salt spray corrosion resistance, respectively. The SPT effectively eliminates the need for a primer and thus eliminates the application manpower, time, and materials. In addition, the hazardous emissions and toxic wastes that are associated with current aerospace primers are eliminated. To this date, SPT's have been successfully applied to over 350 U.S. Navy and Air Force aircraft during their scheduled depot-level maintenance period.

SPECIALTY COATINGS

In addition to the current primers, topcoats, and self-priming topcoats which are used as the primary protective coating system for the bulk of the exterior surfaces of military aircraft, other specialized coatings are utilized to address specific concerns. This section will review several coating materials which address these concerns.

SEALANTS

Although the current epoxy primers provide excellent adhesion and corrosion inhibition, they are brittle. This lack of ductility may result in cracking of the paint system on highly flexed areas of the aircraft. In order to improve the overall flexibility of the epoxy primer polyurethane topcoat coating system, sealants are frequently incorporated into aircraft finishing systems. These sprayable materials are applied between the primer and the topcoat at thicknesses up to 203 microns (8 mils) and are primarily formulated from polysulfide, polyurethane, and polythioether binders. Their elastic nature minimizes cracking of the paint system. Critical

requirements in these specifications are low-temperature flexibility (mandrel bend tests), chemical resistance (fluid immersion at elevated temperatures), and corrosion resistance (5% NaCl salt spray tests). Although these sealants provide corrosion protection by the formation of a relatively impermeable barrier, some sealants also contain strontium chromate for chemical corrosion inhibition. An in depth discussion of the specific chemistry and application properties of sealants is beyond the scope of this paper and will not be addressed here. However, a detailed discussion of this technology is provided in references (47,48).

RAIN EROSION COATINGS

In addition to their harsh environment, aircraft must also endure seemingly harmless natural conditions that can deteriorate the performance of coatings and their underlying structures. One example of this phenomenon occurs when airborne debris, such as sand or rain droplets, impact aircraft leading edges and radomes during flight. The force of impact from these particles can erode the coating system and adversely affect the underlying substrate. The current primer and topcoat, and SPT paint systems do not provide adequate protection against this condition. Even when applied at two to three times its normal thickness, the coating system erodes prematurely.

The rain erosion resistant coating used on U.S. Navy aircraft is a two component polyurethane material. One component consists of a pigmented high molecular weight polyether type polyurethane. The other component contains a clear ketimine (blocked diamine) resin that acts as both a crosslinking agent and a chain extender. When combined, the two components form an elastomeric coating which can absorb and dissipate the energy of impacting rain droplets, thus preventing failure. Flexibility is characterized by a 0.635 cm (0.25 in) mandrel bend at -51°C (-60°F) and tensile elongation of 450 %, whereas the standard topcoat only requires a 0.95 cm (0.375") or 1.27 cm (0.5") mandrel and elongation of 20 or 60 %. However, in order to exhibit this high elasticity, the polymer crosslink density is decreased causing reduced chemical resistance and weathering properties. In order to improve the finishing system durability, these materials are normally overcoated with the standard topcoat.

Although elastomeric coatings offer increased resistance to rain erosion, the optimum protection for Navy aircraft is provided by elastomeric tapes. These materials can be clear or pigmented, polyurethane based films and are supplied with or without an adhesive backing. Unlike coatings, these tapes are bonded to the surface and do not require a drying time. Early versions of these materials were clear aromatic type polyurethanes. Although durable, these aromatic materials had poor weatherability. The latest versions of these materials, however, are aliphatic. These new materials are extremely durable and have excellent weatherability.

HIGH TEMPERATURE RESISTANT COATING

Various areas of U.S. Navy aircraft are routinely subjected to elevated temperatures during operation. The standard paint system was only designed to resist thermal exposures up to

176°C (350°F) for short durations. Therefore, two types of materials are employed for application in these areas: ceramic coatings and high temperature resistant silicone based coatings. Since ceramic coatings are beyond the scope of this review, they will not be discussed. Typical high temperature silicone based coatings use aluminum pigment and are designed to withstand temperatures up to 650°C (1200°F). It can be applied by conventional air spray and is cured by heating to 204°C (400°F) for 1 hour or upon elevated temperature exposure under component operation. During the curing period, the binder system for this coating will oxidize, leaving a barrier layer of silicone oxide/aluminum to protect the underlying substrate from adverse conditions. Although this material provides adequate barrier protection in the high temperature range, the performance diminishes dramatically in the mid-temperature range (260 to 370°C, 500 to 700°F) or when damaged.

FUEL TANK COATINGS

Certain internal areas of aircraft are exposed to selective environments which pose unique problems. One example is fuel tanks. Aviation fuels contain additives which may be corrosive. If left unprotected, fuel tanks would corrode and leak. In order to protect these areas, epoxy or polyurethane fuel tank coatings are used. These highly cross-linked, chemically resistant coatings are two component materials designed for application to non-ferrous surfaces. The fluid resistance requirements for this material are significantly more severe than those of the standard primer and topcoat. The conventional topcoat must withstand 24 hour immersion on unscribed panels without degradation, whereas the fuel tank coating specification requires 14 days immersion of specimens with scribes through the coating. This high degree of chemical resistance is necessary because the coating is not only subjected to the various chemicals contained in aviation fuels, but it is also exposed to aircraft operational chemicals, salt water and dilute acidic solutions (49).

COMPLIANT COATINGS ISSUES

ENVIRONMENTAL REGULATIONS AND HAZARDOUS MATERIALS

As the environmental consciousness of the world continues to increase, more efforts are being devoted to finding safe, compliant solutions to past, current, and future environmental problems. One major factor affecting the United States in recent years, has been the Clean Air Act Amendment (CAAA) of 1990. This law significantly effects the type of materials and processes which will be approved for use in the future. In response to this situation, the U.S. aerospace industry has expanded its efforts to reduce the amounts of hazardous materials generated from the cleaning, pretreating, plating, painting and paint removal processes used in both production and maintenance operations. The materials associated with these processes have been identified as major sources of hazardous waste by the U.S. Environmental Protection Agency (50). Specifically, numerous research and development efforts have been established to address the environmental concerns

with organic coatings. These environmental efforts can be described by two main thrusts: the development of low volatile organic compound (VOC) coatings, and the development of non-toxic inhibited coatings. The efforts in low VOC are aimed at reducing the volatile organic compound content of aircraft coatings to meet environmental regulations, especially the State of California's Air Quality Management Districts (AQMD) rules and the CAAA Control Techniques Guideline (CTG) for the aerospace industry (one of 174 source categories). The development of non-toxic inhibited coatings is concerned with eliminating toxic heavy metal pigments, such as lead, chromates and cadmium used in protective primers and topcoats.

Low VOC versions of the standard military aircraft primers and topcoats have already been developed to comply with the CAAA Aerospace CTG. These materials are based on water-borne, high solids and exempt solvents technology.

WATER-BORNE TECHNOLOGY

Water has long been used as a carrier for organic coatings. The polymers for these coatings are usually modified with hydrophilic groups and dispersed in water to form either solutions or emulsions. Most latex paints are based on thermoplastic resins which are suspended in water to form spherical particles. These particles, whether pigmented or neat, are usually covered with a thin layer of emulsifier to maintain a stable dispersion. When applied to a surface, these spheres coalesce into a continuous film as the water of the emulsion coating evaporates. This film formation mechanism tends to lead to longer drying times in high humidity environments. Other effects of using water as the diluent include: smoother surface finishes due to greater flow times, less overspray when using air application equipment (due to the higher density of water), and easier clean up (usually accomplished with soap and water). Unfortunately, these coatings have some disadvantages. For example, they are more sensitive to surface contamination, like oils and greases. Also, these films tend to be porous and their high affinity for water can lead to poor resistance in moisture environments resulting in coating blistering when wet, or exposed to high humidity conditions.

Most polymers used in high performance coatings are not readily soluble in water. For this reason, co-solvents are used to stabilize the dispersions and improve particle coalescence and film formation. One of the first high performance water-borne coatings was an epoxy/polyamide aircraft primer. The epoxy liquid resin usually contains some aliphatic epoxy monomer, which lowers the viscosity and aids in the coalescence of the two primary resins. The polyamide part usually contains some additives, such as high-boiling aromatic and water miscible co-solvents, that assist in the formation of the final film.

Polyurethane coatings are another area where high performance water-borne coatings have been investigated. One-component polyurethane dispersions have been in existence for some time and generally consist of fully reacted polyurethane resins which are predominately thermoplastic. Since urethanes are not readily compatible with water, these

systems are modified ionically and non-ionically with hydrophilic groups to aid in the stability of the dispersions. After application, these films form by the coalescence of the long chain urethanes. Although some work has been performed to investigate ways of crosslinking these systems, they tend to have lower crosslink densities and are not as chemically resistant as their solvent-borne counterparts.

Recently, resin manufacturers have shown signs of success in working with two component water based polyurethane resins for high performance coatings. One example of this type of material is based on an aliphatic polyol prepolymer and a polyisocyanate. The polyols are prereacted with a diisocyanate and emulsifying agents to form a linear hydroxy-terminated prepolymer. The hydroxy-functional groups aid in the stabilization of the polyurethane dispersion. In addition, a water dispersible polyisocyanate has been synthesized which has a preferential affinity for the polyol over the water competitor. The two components are mixed with an excess of isocyanate to form the final high performance polyurethane product. Other variations on water based urethane chemistry are being investigated by the U.S. commercial resin industry, and coating's manufacturers have begun to formulate finished products from this technology.

HIGH SOLIDS TECHNOLOGY

Another method to attaining a lower VOC coating is through the use of high solids technology. Several paths to increase coating solids are possible. The first and most obvious reduction comes from simply lowering the solvent concentration. While this approach reduces the VOC content, it shortens the pot life and significantly increases the resin viscosity when traditional raw materials are used. Also, the surface finish tends to be rougher from decreased flow characteristics. Using low molecular weight resins can produce a high solids coating with lower viscosity and better flow properties. However, these materials tend to have shorter workable pot lives and lower flexibility when cured with traditional polyisocyanates. This lower flexibility is related to the increase in crosslink density resulting from the smaller backbone structures between functional groups. Using narrow molecular weight distribution isocyanate terminated prepolymers as the isocyanate source produces low VOC coatings with good performance and processing characteristics. These prepolymers yield coatings with lower viscosity, shorter drying time, and longer pot life.

A third approach is to use blocked polymers which yield a longer pot life, but they tend to be less mobile with slower reaction rates. Their decreased reactivity leads to long drying times, which is not desirable. Finally, high-boiling solvents can be used to replace convention solvents. By incorporating these materials, the applied films retain the solvent longer giving smoother surface finishes. However, this solvent retention leads to longer drying times and can allow the coating to continue to flow. This characteristic has produced a new phenomenon where sharp edges can be exposed with time. Finally, solvent retention can result in eventual porosity in the film, decreasing chemical resistance properties.

In summary, each individual approach has identified deficiencies which present a challenging problem to resin companies. However, a combination of these technologies appears to have the greatest potential for success and is being pursued by numerous U.S. manufacturers. Several aerospace coating specifications have been developed based on this technology.

EXEMPT SOLVENT TECHNOLOGY

A final alternative to high VOC coatings can be attained by the use of non-photochemically reactive solvents such as 1,1,1-trichloroethane (TCA) and methylene chloride. Since these solvents don't contribute to the formation of smog, many U.S. federal and state environmental agencies have exempted them from VOC regulations. At first, this was the most popular and easiest approach to solving the VOC problem, since only minor formulation modifications were necessary for incorporating TCA and the coatings had virtually the same application and drying properties. These changes were readily implemented by the U.S. aerospace industry. However, there were limitations on the use of TCA. TCA is reactive with aluminum and can not be applied with spray equipment containing any aluminum parts. Also, retained chloride ions in the film could cause stress corrosion cracking in high strength structural alloys under high temperature conditions. More recently, chlorinated solvents have come under attack due to their ozone depleting potential, which further complicates the use of these solvents. This approach best served as an interim solution to the VOC problem, while resin manufacturers developed the necessary technology to solve the long term problem.

LOW VOC TECHNOLOGY STATUS

Numerous military and commercial specifications have been written to cover materials based on these technologies. However, in light of the proposed CTG and the ozone depleting substances problem, these material specifications are currently being modified to eliminate the type allowing exempt solvents and all other non-compliant versions. This will authorize only low VOC materials for use. High performance VOC compliant primers, topcoats, and self-priming topcoats are required to have a maximum VOC content of 340, 420, and 420 g/l.

NON-TOXIC INHIBITIVE PRIMER

Chromates have been the workhorse corrosion inhibitor for commercial and military aerospace primers. Unfortunately, these toxic heavy metal chromate pigments are being regulated by the EPA. Therefore, non-toxic alternatives have begun to be developed and many Government and industry efforts are involved in the development of non-toxic inhibited, low VOC aircraft coatings. Current available primers are based on 2-component high solids or water-borne epoxy systems and corrosion inhibitors such as molybdates, nitrites, borates, silicates, and/or phosphates as well as a variety of metal cation systems. These primers have shown promise in general corrosion resistance and adhesion tests. To-date, however, all of these primer have had problems providing adequate filiform corrosion resistance. In addition, many of these experimental

coatings have exhibited flexibility, strippability, viscosity and storage stability deficiencies. Further investigation of these materials is being conducted to alleviate these problems. Finally, a better understanding of the corrosion inhibiting mechanisms associated with these non-toxic inhibitors, both individually and as multiple inhibitor systems, needs to be attained to formulate corrosion preventive primers more effectively and efficiently.

PAINT APPLICATION EQUIPMENT

As part of the CAAA Aerospace CTG, conventional air spray application equipment will no longer be authorized for applying paints. Conventional air spray equipment has a transfer efficiency of approximately 28%. The types of paint application equipment authorized for these materials will be similar to those specified by the State of California's AQMD Regulations which require minimum transfer efficiencies of 60% to 85% and maximum gun tip air pressures of 10 psi. A number of alternative technologies have been proposed to meet this requirement. The only two spray application techniques authorized will be electrostatic and high-volume low-pressure (HVLP) spray guns. Both of these techniques have improved transfer efficiencies over conventional air spray. Roller, brush, dip and other non-spray methods are also acceptable. Each of these techniques has its own unique capabilities and limitations. Some methods can be used in combination (i.e. plural component, air-assisted airless with electrostatic) to yield even higher efficiencies.

The method of cleaning spray equipment is also being regulated under the CTG. The old solvent wash method, which generated large quantities of hazardous waste and was time consuming, is being prohibited. Some type of enclosed cleaning method, which captures the majority of the cleaning solvent, has to be used. Paint gun washers that meet this requirement have been identified. In addition to drastically reducing the solvent emissions, these enclosed cleaning operations take approximately one fourth of the working time as compared to the old method.

FUTURE TRENDS IN AEROSPACE COATINGS

Research and development of organic coatings for aerospace applications is a continuous, dynamic process which is caused by:

- (i) implementation of stringent legislation on and regulation of material usage, emissions, and disposal,
- (ii) advances in raw material chemistry, along with desires to improve coating performance and address environmental regulations, and
- (iii) changes in aircraft design, materials, and performance.

Although innovative technologies such as corrosion sensor, pressure sensitive, and preferentially strippable coatings are beneficial to the industry, it appears that the biggest driver in coatings research and development is the continuous implementation of more stringent environmental regulations which limit the types and amounts of materials used in coatings formulation and application processes. These mainly affect volatile organic compounds and heavy metals, although

other types of chemicals are also under scrutiny. These regulations are causing dramatic changes in how coatings are formulated as well as the raw material from which they are derived. It is expected that research and development of low VOC polymer systems (i.e., high solids, waterborne, powder coatings, etc.) and non-heavy metal compounds will continue well into the next century and the advances from these fundamental efforts will be translated to changes in coatings technology. In addition, the approach to improve aircraft finishing system performance will be attained through investigation and utilization of high performance polymers, pigments, and additives.

REFERENCES

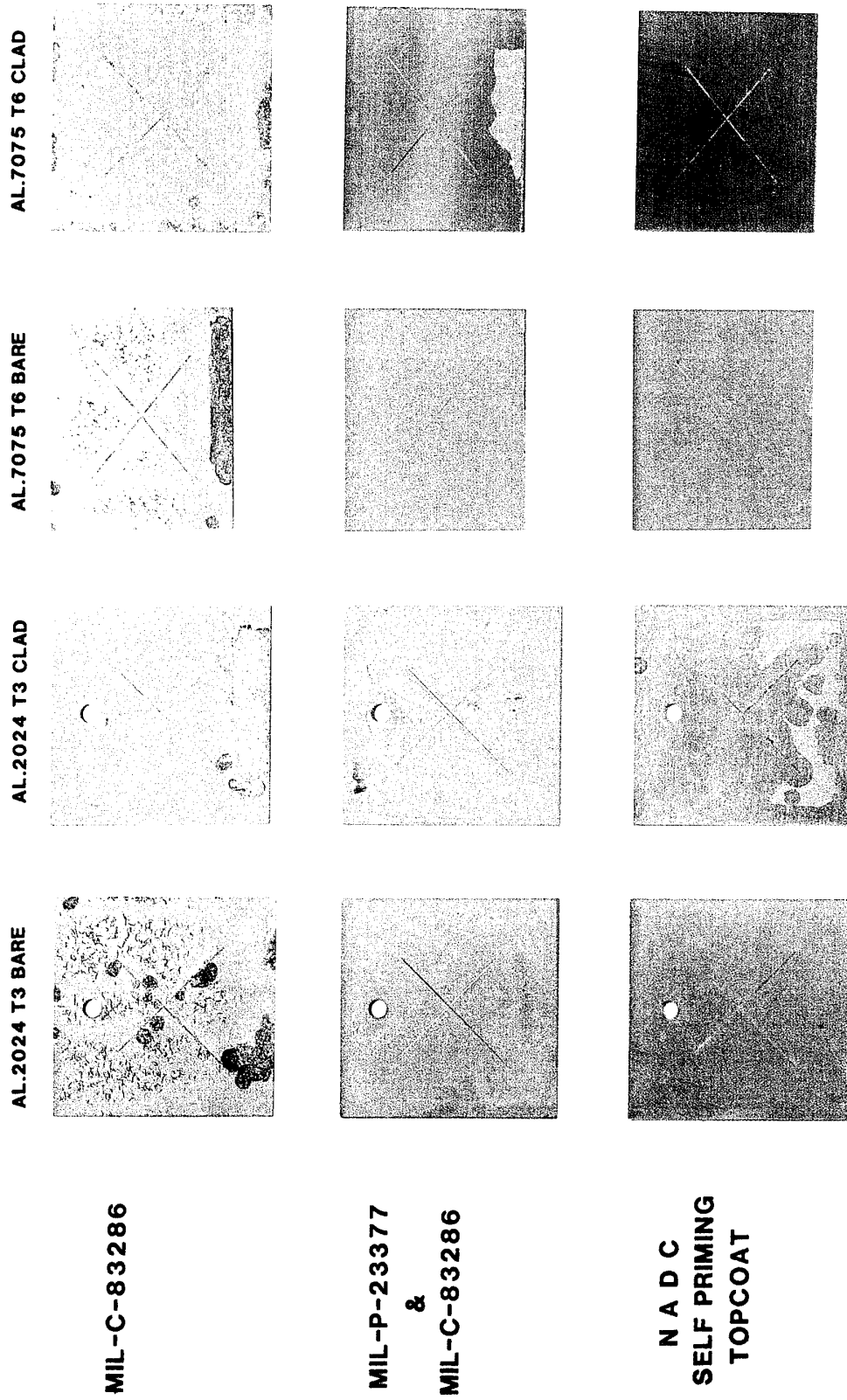
1. Miller, R.N., "Predictive Corrosion Modeling Phase I/Task II Summary Report," Air Force Wright Aeronautical Laboratories Report AFWAL-TR-87- 4069, Wright-Patterson Air Force Base, OH, August 1987.
2. Cochran, R.C., et al., 73rd AGARD Panel/Specialists Meeting on Aerodynamics and Aeroelasticity, North Atlantic Treaty Organization, AGARD Report 785, Oct 1991.
3. Fisher, P. and De Luccia, J.J., Naval Air Development Center Report NADC-75031-30, Warminster, PA, April 1975.
4. Wallace, W., et al., AGARD Corrosion Handbook Volume 1, Aircraft Corrosion: Causes and Case Histories, North Atlantic Treaty Organization, AGARD-AG-278 (1985).
5. De Luccia, J.J., et al., AGARD Corrosion Handbook Volume 2, Aircraft Corrosion Control Documents: A Descriptive Catalogue," North Atlantic Treaty Organization, AGARD-AG-278 (1987).
6. Ketcham, S.J., "A Handbook of Protective Coatings For Military and Aerospace Equipment," TPC Publication 10, National Association of Corrosion Engineers (1983).
7. Lambourne, R. (Ed.), Paint and Surface Coatings: Theory and Practice, John Wiley, New York (1987).
8. Fontana, M.G. and Greene, N.D., Corrosion Engineering, 2nd Ed., McGraw-Hill, (1978).
9. Beck, T.R. and Rugieri, R.T., Contract No. N62269-82-C-0261, Naval Air Development Center Report NADC-84107-60, Warminster, PA, April 1984.
10. Spadafora, S.J. and Leidheiser, H., Jr., J. Oil and Colour Chem. Assoc., 71, 9 (1988).
11. Leidheiser, H., Jr. and Funke, W., J. Oil and Colour Chem. Assoc., 70, 5 (1987).
12. Walker, P., J. Paint Tech., 31, 9 (1967).
13. Pulley, D.F. and Spadafora, S.J., "Elastomeric Primers and Sealants," Naval Air Development Center Report NADC-83140-60, Warminster, PA, November 1983.
14. Pryor, M.J., Z. Elektrochem., 62, 782 (1958).
15. Heine, M.A. and Pryor, M.J., J. Electrochem. Soc., 114, 1001 (1967).

16. Leidheiser, H., Jr., Paint Research Institute, FSCT, Paint Research Institute, Proc./No. 145.
17. Foster, T., et al., J. Coat. Tech., 63, 801, October 1991.
18. Hegedus, C.R., et al., UNICOAT Program Summary, Naval Air Development Center, Warminster, PA, March 1990.
19. Carlson, E.J. and Martin, J.F., "Environmentally Acceptable Corrosion Inhibitors: Coorelation of Electrochemical Evaluation and Accelerated Test Methods, Federation of Societies for Coatings Technology 71st Annual Meeting and Paint Industries' Show, Atlanta, GA, October 1993.
20. Hegedus, C.R. and Green, W.J., U.S. Patent No. 4,885,324, December 1989.
21. Hare, C.H. and Fernald, M.G., Mod. Paint and Coat., April 1984.
22. Hare, C.H., J. Prot. Coat. and Linings, September 1989.
23. Military Specification, MIL-F-7179, "Finishes, Coatings, and Sealants For The Protection Of Aerospace Weapons Systems," December 1991.
24. Lewin, J.B., "Aircraft Finishes," Treatise on Coatings Volume 4, Formulations Part I, Myers, R.R. and Long, J.S. (Eds.), Marcel Dekker (1975).
25. Chattopadhyay, A.K. and Zentner, M.R., "Aerospace and Aircraft Coatings", Monograph Publication, Federation of Societies for Coatings Technology, Blue Bell, PA, May 1990.
26. Wernick, S. and Pinner, R., The Surface Treatment and Finishing of Aluminum and Its Alloys, 4th Ed., Robert Draper, Ltd (1972).
27. Spadafora, S.J., Naval Air Warfare Center Aircraft Division Warminster Report # NAWCADWAR-92077-60, 18 August 1992, Warminster, PA.
28. Chang, T.C., McDonnell Douglas Report No. MDC-K5784, January 28, 1991.
29. Moji, Y., Boeing Aerospace Co., Report No. D6-55313TN, February 6, 1990.
30. Cochran, W.C., Electroplating Engineering Handbook, L. J. Durney-Ed., Van Nostrand Reinhold Co., 1984.
31. Howard, M., Rohr Industries Report No. RHR-90-194, December, 1990.
32. Martens, C.R. (Ed.), Technology of Paints, Varnishes, and Lacquers, Reinhold Book Corp., New York (1968).
33. Boxall, J. and von Fraunhofer, J.A., Concise Paint Technology, Chemical Publishing, New York (1977).
34. American Society for Testing and Materials, Designation: D3359, "Standard Test Methods for Measuring Adhesion by Tape Test," Phila, PA, September 1987.
35. American Society for Testing and Materials, Designation: D2197, "Standard Test Method for Adhesion of Organic Coatings by Scrape Adhesion," Phila, PA, October 1986.
36. Asbeck, W.K., "Measuring the Adhesion of Coatings," J. Paint Tech., 43, 556, May 1971.
37. Albers, R.A., U.S. Patent 4,352,898, October 1982.
38. Forrest-Woodard, M.A., et al., Design and Technology Times, August 1994.
39. Saunders and Frisch, Polyurethanes: Chemistry and Technology, John Wiley, New York (1962)
40. Oertel, G. (Ed.), Polyurethane Handbook, MacMillan Publishing, New York (1985).
41. Potter, T.A. and Williams, J.L., J. Coat. Tech., 59, 749, p. 63-72 (1987).
42. van der Ven, L.G.J., et al., "The Curing of Polyurethane Coatings; Chemical and Physical Information Processed in a Mathematical Model," Proceedings of the American Chemical Society Division of Polymeric Materials: Science and Engineering, Toronto, Canada (1988).
43. American Society for Testing and Materials, Designation: G26, "Standard Practice for Operating Light-Exposure Apparatus (Xenon-Arc Type) With and Without Water for Exposure of Nonmetallic Materials," Phila, PA, September 1988.
44. Scott, J.L., J. Coat. Tech., 49, 633, p. 27-36 (1977).
45. Simms, J.A., J. Coat. Tech., 59, 748, p. 45-53 (1987).
46. Hegedus, C.R. and Hirst, D.J., Naval Air Development Center Report No. NADC-88031-60, Warminster, PA, March 1987.
47. Eirich, F.R. (Ed.), Science and Technology of Rubber, Academic Press, New York (1978).
48. Damusis, A. (Ed.), Sealants, Reinhold, New York (1967).
49. Hirst, D.J., "Evaluation of Corrosion Resistant Coatings For Environmental Control System Ducts," NADC-83109-60, August 1983.
50. Boothe, V., Presentation at U.S. Environmental Protection Agency Aerospace CAAA CTG Hearing, Durham, NC, May 1993.

TABLE 1: PERFORMANCE CHARACTERISTICS OF AIRCRAFT COATINGS

<u>PROPERTY</u>	<u>PRIMER</u>	<u>TOPCOAT</u>	<u>SELF-PRIMING TOPCOAT</u>
GLOSS (60°)			
High Gloss Color	----	90 minimum	90 minimum
Low Gloss Color	----	6 maximum	6 maximum
WET TAPE ADHESION	No removal 1 day (23°C)	No removal 1 day (23°C)	No removal 7 day (49°C)
FLEXIBILITY			
GE Impact			
High Gloss Color	----	60 %	40 %
Low Gloss Color	10 %	20 %	20 %
Mandrel Bend (-51°C)			
High Gloss Color	----	0.95 cm	0.64 cm
Low Gloss Color	----	1.27 cm	0.64 cm
HUMIDITY RESISTANCE (95% RH & 49°C)	----	30 day	30 day
FLUID RESISTANCE			
Lubricating Oil	1 day (121°C)	1 day (121°C)	1 day (121°C)
Hydraulic Fluid	1 day (65°C)	1 day (65°C)	1 day (65°C)
Distilled Water	4 day (49°C)	4 day (49°C)	7 day (65 °C)
CORROSION RESISTANCE			
5% NaCl Salt Fog	2000 hr	2000 hr	2000 hr
SO ₂ /Salt Fog	----	----	500 hr
Filiform	1000 hr	1000 hr	1000 hr
WEATHER RESISTANCE			
Accelerated (ASTM G 26)	----	500 hr	500 hr
Outdoor Florida Exposure	----	1 year	1 year

**Figure 1. 2000 HOURS 5% SALT SPRAY
CHROMATE CONVERSION COATING**



Problems of Predicting Material Property Retention During Long Term Service

Yu.P. Gordeev and A.M. Khomutov

KOMPOZIT Corp.

4, ulitsa Pionerskaya

141070 Kaliningrad, Moscow Region, Russia

SUMMARY.

A procedure of materials-science studies accompanying the process of product development, manufacture and service is offered. It provides correct selection of materials, trustworthy prediction of their behavior, high reliability of their operation in products of space-rocket application. Reliable prediction of material behavior during long-term service is achieved by breaking up the complex effect of the environment into individual factors and by analyzing the effect of each factor on the properties of the material.

INTRODUCTION

Application of materials in space-rocket products is accompanied by a number of specific features, which makes them significantly different from other products of machine building including the aircraft industry.

First and foremost, these features include:

- particularly low safety factors;
- a very wide range of operating temperatures, a wide range of cyclic, vibratory and other force loads;
- rather long ground-service lives in various climatic zones or operation under space conditions;
- predominant application of high-strength materials;
- wide application of the welding and soldering processes in the assembling operations.

It is for this reason that the following steps are of particular importance to predict the serviceability of materials and to provide their high reliability in products:

firstly, preliminary comprehensive studies of their properties in the operating range of service factors;

secondly, preliminary determination or trustworthy prediction of the time dependencies of their properties under the action of service factors;

thirdly, preliminary testing of these materials under conditions as close to the service ones as possible;

fourthly, maximum possible ground bench testing of the materials in individual units of products during R & D works.

1. MAIN PRINCIPLES OF MATERIAL ASSIGNMENT AND APPLICATION.

All the above conditions we are to meet to provide high reliability of materials were allowed for when the procedure of material assignment and application used in the Russian space-rocket industry was developed. This procedure was legalized with a few standards and other standard technical documents. The procedure requires that the development of any product should be accompanied by materials-science studies. It does not allow unauthorized application of any insufficiently studied and tested material, on the one hand, and allows application of new and advanced materials which are well studied, on the other hand.

Fig. 1 shows this procedure in the form of a diagram.

The main stages of product development and manufacture characteristic of machine-building products of any kind are shown in the upper part of the diagram. They include the following basic stages: conceptual design, R & D to provide operational development of individual units and the product as a whole completed by issuing a detail design, then preparation and establishing of full-scale production and the stage of product operation including ground and flight operation follow.

The stages of the development of new materials or operational development of previously developed materials to use them in our products are shown in the lower part of Fig. 1.

Stages 2 and 3 include comprehensive tests of the materials, evaluation of their properties in a wide range of temperature, force, speed and other possible service loadings. These stages are completed by issuing material certificates: Stage 2 - a first-wording certificate, Stage 3 - a second-wording certificate.

Application of materials without certificates is not permitted.

Stages 4 and 5 include carrying out accelerated and full-scale environmental tests of the materials and individual units under concrete environmental conditions characteristic of a given product and assigned by the specifications of the product.

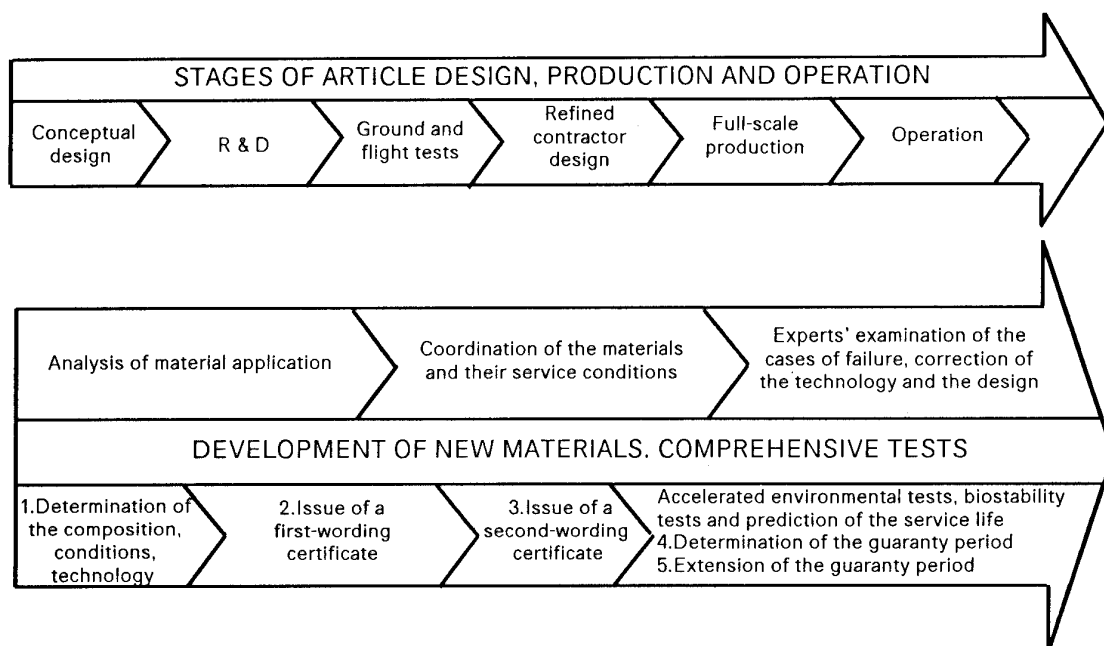


Fig.1 The procedure of material assignment and application

From the test results obtained the guaranty period is predicted for this material application in the given product under the conditions specified.

These periods are predictable and the reliability of the product as a whole depends on the trustworthiness of the prediction.

Analysis of standard technical documentation from the point of view of material-application correctness occupies a highly important place in the procedure at several stages of designing.

Another line of the materials-science studies accompanying this work is also of great importance. This is experts' examination of the causes of premature failures of the units and parts of products at various stages of R & D, ground and flight tests. This is usually referred to as "non-standard" operation of the unit or product. Such cases always take place but their number sharply decreases as the product is operationally developed.

In accordance with the results of experts' examinations a decision is made to change the technology, to change the design, to improve the technology and material-quality control system, and, very seldom, to replace the material.

Over a long period of time the procedure of materials-science studies accompanying the process of product development, manufacture and operation has been providing correct selection and reliable prediction of material serviceability and, as a result, high reliability of materials being developed for and used in products of space-rocket applications.

2. PRINCIPLES AND PROBLEMS OF PROPERTY-RETENTION PREDICTION FOR POLYMER-BASED MATERIALS

As illustrated in Fig. 1, one of a great number of problems of material-serviceability prediction is to predict permissible periods of material operation in a product, i.e., the problem of material-property retention in the process of long-term operation.

Solving the prediction problem is complicated by a number of factors: the variety and complexity of materials, multifactor conditions of their application in products, specific effect of these factors on different materials, the necessity of solving the problem for rather short periods of time, etc.

The problem of substantiated prediction consists in obtaining reliable information about the processes that occur in the material under the conditions prescribed and about the state of the material with respect to its physical-and-chemical properties and technical characteristics after the prescribed time of exposure (storage) or operation has passed, i.e., in determining the time dependences of its known initial properties after storage and operation under certain conditions.

There exist two idealized ways of predicting the periods of material-property retention:

- investigation of the properties of the material as a function of time by simulating its exposure (storage) and service conditions;
- detail study of the mechanisms of the processes occurring in the polymer composition, their physical nature and quantitative characteristics.

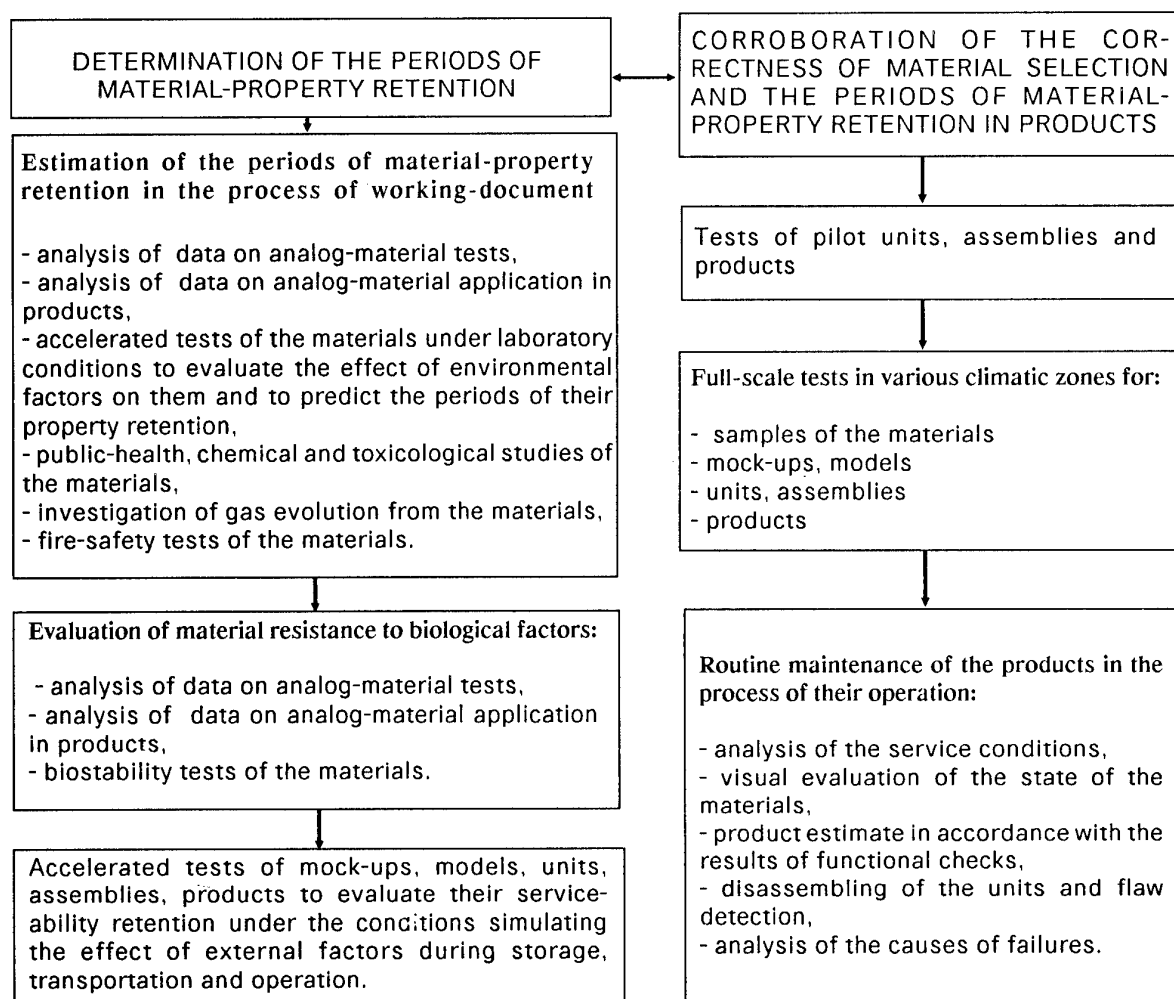


Fig.2. Procedure of testing materials to predict their application in products

In the former case the periods of material-property retention on exposure to a certain set of factors can be determined. However, it is practically impossible to simulate all the product exposure and service conditions in a laboratory because of their variety and variability.

In the latter case it could be possible to obtain the material-ageing function for any conditions by determining the mechanisms of the processes and by calculating all the parameters required. However, with this approach, often theoretical, used, the ageing function would become extremely complicated, including a great number of parameters that require special and complicated studies for each material. This way is feasible neither from scientific nor from practical positions under real conditions of product development and manufacture, especially when materials of complex compositions are used.

In practice, to solve the prediction problem, we combine both the ways, a great body of data on previously conducted tests and studies of the material being widely used.

A list of tests that can be used to predict permissible periods of material operation in products is given in Fig. 2.

As is evident from Fig. 2, the number of tests we have to conduct before issuing recommendation on material application is reasonably great.

The most objective data on the kinetics of possible changes in the material characteristics with time are obtained during accelerated tests of the given material.

The following problems are solved using accelerated tests:

- possible changes in the characteristics of the

materials during prescribed product exposure or service periods under assigned conditions are determined;

- the periods during which the material characteristics being tested decrease down to the level specified are determined;
- the characteristics of the material which are most sensitive to the effect of various factors and the factors that produce the strongest effect on the characteristics of the material are determined;
- recommendations related to material-composition and production-technology corrections are issued for industrial engineers.

In general terms, real prediction represents an extrapolation from the results of preliminary tests conducted using higher-value factors acting for shorter periods of time to milder service conditions acting for longer time.

The general scheme of accelerated tests provides for the following stages depending on the conditions prescribed:

- heat ageing;
- thermal-oxidative ageing;
- moisture-resistance tests;
- negative-temperature tests;
- thermal-cycling tests.

Thermal and thermal-oxidative ageing suggests that the changes occurring in the properties of materials during their exposure to or operation under the conditions of slightly changing positive temperatures should be predicted. For these conditions we use a semi-empirical prediction method including both some

elements of physical-and-chemical studies of the processes occurring in the material and experimental evaluation of the properties of the material (mechanical, electric, thermal ones) when exposed to higher temperatures as compared with the real ones.

However, it should be taken into account that acceleration of tests (an increase in the test temperature) can change the character of physical and physical-and-chemical processes in the material.

Fig. 3 give the data on the effect of temperatures of various levels on the behavior of materials of two compositions: phenol-rubber composition-based and chlorosulfonated polyethylene-based materials. As is evident from the pictures, an increase in temperature results in a considerable increase in the intensity of the processes in the material, which leads to the necessity of limiting the level of the accelerated-test temperature not to make a mistake while predicting the properties of the material under real exposure and service conditions.

To evaluate the permissible level of temperature increase, preliminary investigations of the material are conducted using physical-and-chemical methods: differential thermal, thermogravimetric, thermomechanical, spectroscopic analyses, etc. From the results of these studies the temperature of material-destruction onset, the temperatures of phase transitions (glassy, elastic state), the functional-group relation in the structure of the material are determined and the temperature of further thermal-ageing tests is specified.

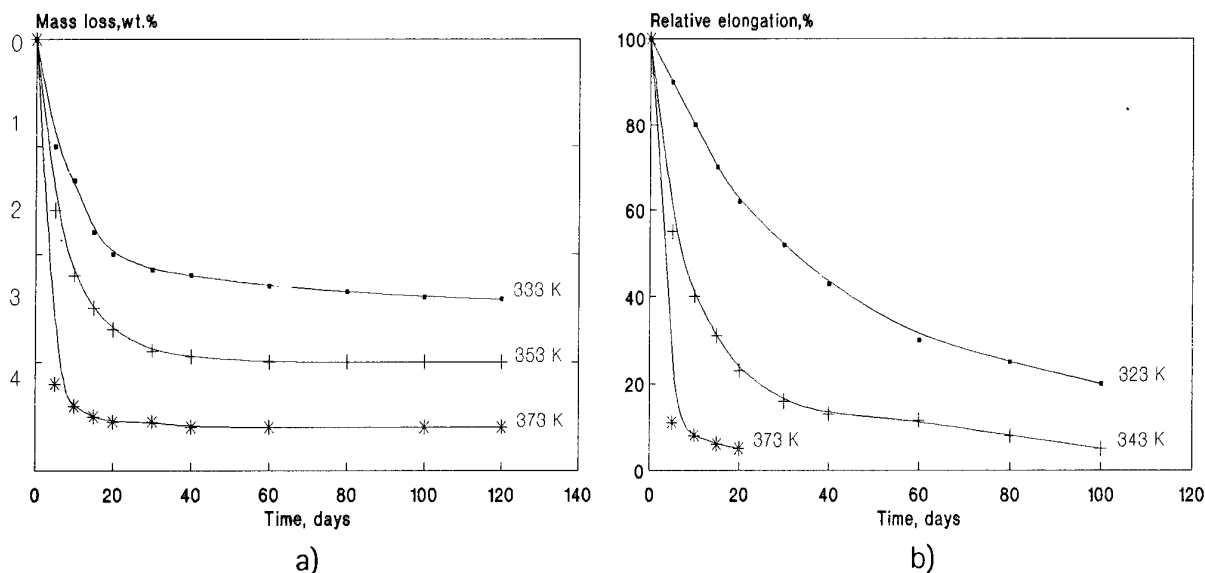


Fig. 3
Changes in the characteristics of the materials during ageing.
a) phenol-rubber -based material;
b) chlorosulfonated polyethylene- based material.

Table 1

Electric resistance of current-conducting materials and its recoverability as a function of the temperature-humidity conditions.

Testing conditions, temperature/humidity, %	ELECTRIC RESISTANCE		
	After testing	After additional holding under the following conditions:	
		temperature of 293 K, humidity of 40%, holding time of 2160 hours	temperature of 293 K, holding time of 1440 hours.
293 K / 98	+11	+6	+5
313 K / 98	+44	+32	+22
333 K / 98	+79	+63	+62

The time of testing is calculated based on the ageing model which suggests that the processes running during accelerated tests are equivalent to those under real exposure and service conditions of the products.

Assignment of the *moisture-content* level during accelerated tests seems to be a most complicated problem. This is conditioned by many factors, the structure and chemical nature of the material (hydrophilic or hydrophobic materials, the character of pores in the material, etc.), the character of moisture interaction with the structural elements of the material (chemical or physical interaction), the character of moisture sorption of the material, the value of the moisture-content parameter itself, the temperature level and other factors. As is shown in Table 1 and by the experimental data obtained, combined (simultaneous) effect of elevated temperatures and high humidity on current-conducting materials leads to a considerable change in their electric resistance as compared with the effect of high humidity at normal temperature (292K). Besides, after exposure to elevated temperatures and high moisture-content atmosphere (at 333K and the humidity of 98 to 100% the moisture content is approximately 10 times as high as that at 293K and the humidity of 98 to 100%) the recovery of the electric resistance of the material is impaired even after sufficiently long exposure of the material to low humidity. It indicates that both the character of moisture sorption and the character of moisture interaction with the structural elements of the material can change on exposure to severe temperature-humidity conditions, which won't correspond to real conditions.

Based on the above, when accelerated moisture-resistance tests are conducted, we hold the viewpoint that the test temperature should be at the level close to that under real conditions of product exposure and

service. Acceleration of the moisture effect is achieved by increasing the moisture content within the chamber.

The problem of moisture-effect evaluation can also be solved using pre-determined diffusion coefficients. With this, it should be mentioned that for materials of complex compositions and structures this characteristic of the material is somewhat conventional and determines some integral process of moisture diffusion.

When *negative temperatures* are selected and the conditions of thermal cycling are assigned, we are guided either by concrete requirements specified by the technical assignment to develop a material for some concrete product exposure and service conditions or by statistical data of the climate of the climatic zone where the product being developed is supposed to be used.

Reliability of the test results is an important aspect of the problem of predicting the periods of long-term retention of material properties. Initial materials even of the same compositions can have distinctions caused by the distinctions of the characteristics of the initial component parts, permissible departures from the manufacture conditions, variations in the level of the binder-polymerization degree, etc. Therefore, to obtain more objective data, it is reasonable to test a few lots of materials.

And at the same time it must be understood that none of the accelerated-test procedures can take into account all the diversity of factors affecting the behavior of a material under real conditions. No matter how reliable and substantiated the prediction could be, only real service can clear up the uncertainty and make the prediction true. This requires that the prediction should be corrected as new information on the object

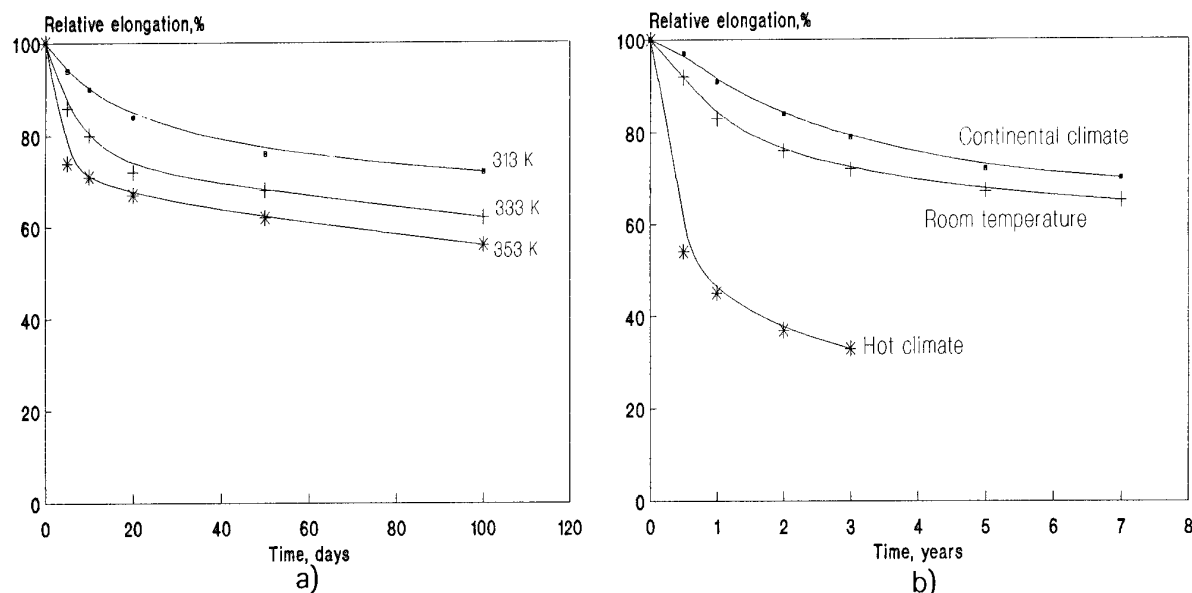


Fig. 4

Changes in the elongation of the phenol-rubber material under laboratory conditions (a) and under nature conditions (b).

being predicted is received, which is achieved in the process of routine maintenance of operating products.

Fig. 4 shows comparative data on changes in the elongation of the phenol-rubber composition in the process of thermal ageing under laboratory conditions (a) and under nature conditions in a fabric container. As follows from the data obtained, the character of changes in elongation is identical for all the testing conditions. Reasonably satisfactory agreement is obtained between the results of accelerated tests and those of environmental exposure under constant-temperature conditions ($T=293K$) and under continental-climate conditions where no long high-temperatures periods are available during a year. For the hot-climate zone these changes are much more

significant than those during accelerated ageing.

Furthermore, some results we got while testing a number of materials both by accelerated methods and under real conditions and some comments to them are brought to your notice.

In our report we have tried to give a general description of the methodical approaches we use and to show the problems arising when the periods of long-term property retention are predicted for polymer-based materials. The prediction problem involves the development, perfection and integration of the software that could provide systematization of the data-obtaining methods, development of data bases, and a system of mutually coordinated standards.

CORROSION DETECTION AND MONITORING OF AIRCRAFT STRUCTURES: AN OVERVIEW

V.S. Agarwala*, P.K. Bhagat**, G.L. Hardy***

*Naval Air Warfare Center, Aircraft Division
Warminster, Pennsylvania 18974
Aircraft Safety Directorate

**Federal Aviation Administration Technical Center
Atlantic City International Airport, New Jersey 08405

***Materials Directorate, Wright Laboratory
Wright Patterson AFB, Ohio 45433
U.S.A.

ABSTRACT

Corrosion occurs on both military and civilian aircraft as a result of operation in corrosive environments and utilization of less than optimum corrosion preventive measures during fabrication. For low usage rate systems such as military aircraft, corrosion treatment constitutes a high cost maintenance action because corrosion effects can be life limiting mainly due to the fact that current techniques require extensive material loss for reliable detection of corrosion. For high usage systems such as commercial aircraft, corrosion may constitute a safety problem. A recent study by the U. S. Air Force at Tinker Air Force Base has demonstrated that while off-the-shelf nondestructive inspection equipment has some capability for detecting and quantifying aircraft corrosion, significant improvements in both detection and quantification are still required. Results of this study will be briefly reviewed along with discussions relating to some new and innovative inspection technology for detecting corrosion. New concepts and techniques for corrosion monitoring, i.e., detection of onset of corrosion or breakdown of corrosion protection system, will also be discussed. Advances in electrochemical measurements, thermal imaging, and optical scanning for chemical changes are providing some new research and development opportunities. Finally, concepts relating to damage-revealing chemicals and coatings which may revolutionize the detection and management of corrosion in our systems will be discussed.

INTRODUCTION

To a certain extent, almost all environments can be classified as corrosive because moisture in the air along with its atmospheric contents (acids, salts, and organics) can condense on almost any metallic object to cause corrosion. Non-metallic materials can also absorb moisture and deteriorate with prolonged solar exposures and varying climatic conditions. Recent estimates indicate that corrosion related costs in the U. S. are as high as 4.2 percent of the GNP or about \$70 billion[1]. About \$4B of this cost is due to aircraft corrosion.

It is well known that military as well as civilian aircraft operators use a significant portion of their maintenance budget on corrosion related issues. These include costs attributed to corrosion detection,

prevention, repair, and control at both depot and field levels. A recent Air Force sponsored study concluded that approximately \$718 million per year can be attributed directly to corrosion related issues on the current inventory of operating military aircraft[2]. Approximately an equal amount of money is spent by the Navy in corrosion maintenance cost. The indirect use/nonuse, downtime etc., not including loss of life, could add another 0.5B dollars annually for the Department of Defense. It is interesting to note that the oldest aircraft C/KC-135, C-130, B-52, F-111, and C-141 account for approximately half of the total cost. US Navy experience indicates that 27 percent of life cycle cost of operational aircraft is in the ownership and support function. This is to be contrasted with 15 percent costs for R&D and 58 percent related to the procurement of the system. The higher percentage costs for the Navy maintenance are directly attributed to the highly corrosive environment its aircraft operate under. Even the use of advanced materials, such as graphite-epoxy and graphite/bismaleimide composites, to replace metallic structures does not alleviate environmental impacts on the aircraft. Concerns about polyimide degradations due to galvanic corrosion effects on airframe structures have recently been raised[3]. Damage detection in case of advanced materials is currently in the developmental stage and the reliability of techniques used are not well established. This can become a significant factor as today's planes containing composite material components age and get damaged.

Corrosion detection, prevention, and control issues have historically had low priority in weapon systems development. In systems such as the C/KC-135, material selection was primarily predicated upon reduced weight and improved mechanical performance. Scant attention was paid to the possibility of galvanic reactions due to contact of dissimilar conducting/metallic materials. Airframe designs, often inadvertently, provided locations for entrapment of corroding agents including moisture and sometimes precluded access to corrosion prone areas. In addition, corrosion prevention had lower priority than acquisition costs, weight, appearance, operational readiness, and safety of flight.

During the period of generous defense budgets with new systems promptly entering operational status to replace older systems, corrosion was not a seriously

impacting constraint on operational readiness. At the present time, however, with the current fleet aging, without newer aircraft entering the inventory, the deleterious effects of corrosion have become more acute in terms of readiness and quick response. This is due to the fact that corrosion is a much more severe problem for older aircraft. Preventive maintenance and repair actions require the affected system to be removed from service for long periods of time. In most cases, removal and replacement of skin is required, which is an expensive and time consuming proposition. Thus, the attendant cost of maintaining older aircraft is substantially higher and increases dramatically with age. Further, corrosion affects the fatigue life of airframes and, therefore, has implications related to life extension issues. Non-detectability of critical component damage due to corrosion may cause catastrophic failure since stress cracking susceptibilities are increased by a factor of ten or more[3].

In the current era of reduced budgets along with increased environmental constraints on chemicals currently in use for corrosion prevention, protection, and control, it is desirable that a fresh assessment of corrosion-related issues be undertaken. Efforts that are directed towards early detection, localization, and quantification of corrosion, if successful, can substantially reduce fleet operational costs. In addition, plans are also underway to store a number of acquired aircraft and other weapon systems for long periods of time. Since environmental effects on materials are cumulative, corrosion could be highly damaging to both the structural and electronic components. Thus, preservation of military hardware, does require continuous/periodic monitoring in terms of functional and structural integrity. Early and accurate detection of corrosion or material degradation is important because simpler repairs can be instituted for the damaged area yielding considerable savings in both material and labor costs.

CORROSION DETECTION

The most commonly used technique of surface corrosion detection is visual inspection. The inability to gain access for visual inspection of all possible has corrosion location sites led to the consideration of a host of instrument-based technologies such as eddy current, ultrasonic, and radiographic. These techniques require significant material loss to be effective, are somewhat quantitative, and are an improvement over visual methods for detection of hidden corrosion. In spite of the availability of a wide choice of nondestructive evaluation (NDE) technologies, questions regarding the accuracy and reliability of these techniques to detect, localize, and quantify corrosion remain. Some of the reasons include use of sensors which are not specific to corrosion products, area, or volumetric flaw detectors. In a recent state of the art review of NDE methods for corrosion detection, Beissner and Birring conclude that methods for hidden corrosion detection are not yet fully developed[4].

In a workshop on assessment of current corrosion research and development issues, it was noted that detection of corrosion in aircraft structures is complicated by geometrical constraints. Much of the earlier efforts in detection technology have, therefore, been directed at matching specific techniques to specific structural geometries. It was also reported that current methods of inspection for an operational aircraft can require over 1,000 man-hours of disassembly, inspection, and reassembly for areas that can not be inspected in-situ. Detection and quantification of corrosion without disassembly remains a high priority research and development issue for the Air Force. Improved means for detection and measurement of corrosion damage such as, paint property alterations, coating integrity assessment, new paint formulations, automated rapid inspection, field usability, and quantification were also reported as areas ripe for further research and development. Lack of funding as well as other priorities in the Air Force have precluded a long term and substantial effort to address all the needs and issues raised at this workshop[5].

In a more direct approach to assess the applicability of current NDE methods in corrosion detection, Tinker Air Force Base has embarked on a program of providing realistic samples of corroded specimen from C/KC-135 and B707 aircraft to the research community. Industry and other government agencies were invited to employ off-the-shelf technologies to detect and quantify hidden corrosion. To date over 50 organizations utilizing NDE technologies that include eddy current, ultrasonic, radiographic, and thermal wave imaging have voluntarily participated in this study at no cost to the Air Force. Major benefits to accrue from this program are that the effectiveness and applicability of current NDE equipment can be assessed and compared in a controlled environment. In a companion paper at this meeting, further details regarding the program are being presented[6].

It is generally known that while results from cut-up or inspection of a corroded aircraft will provide some generic data for corrosion control and prevention, more basic work will remain. In addition, the Air Force Corrosion Program Office is of the view that substantial savings will accrue from measures designed to prevent corrosion. Current corrosion control programs during preventive depot maintenance(PDM) involve rework or replacement of corroded structure and reapplication of corrosion prevention materials. Both the Air Force and Navy's current approach to control of corrosion effects have been through three levels of periodic maintenance: on equipment, intermediate, and depot.

In the civilian sector, the effects of corrosion were evident from the investigations into the causes of the Aloha Airlines accident in April 1988. The fuselage section in which a 20 ft long fracture occurred during flight was observed to be severely corroded with multi-site damage. Partly in response to this accident and also to enhance safety of the travelling public, Congress enacted the Aviation Safety Research Act of 1988. This Act has increased the scope of the

FAA's mission to include provision of funds for research and developmental efforts as assistance to industry towards maintaining continued airworthiness of the aging commercial fleet. In addition, Congress enacted the Aviation Research Grant Act of 1989, to enable colleges, universities, and nonprofit research organizations to apply for research grant awards from the FAA. A major focus of research funded by FAA has been in the area of corrosion detection and corrosion fatigue interactions. It is anticipated that the FAA funded research will lead to the development of a model for the corrosion process which will be integrated into a probabilistic model for service life predictions[7].

PLANNED PROGRAMS

Air Force and Navy are cooperating in the development of chemical sensors, which can be applied to aircraft structures via a paint based system, to identify and detect corrosion. As corrosion gets initiated chemical reaction of sensor material with corrosion products alters its optical characteristics. A suitable detector can, then, identify the affected areas[8].

Both the Air Force and the FAA have funded efforts in the area of thermal wave imaging for rapid assessment of aircraft structures for hidden corrosion. These techniques depend on thermal diffusivity mismatch and provide a temperature-time image of the inspected area. Disbond, material loss due to corrosion, and dissimilar material conductivities will provide a differing image which can be analyzed. The FAA Technical Center has encouraged investigations using this technology at the National Aging Aircraft NDE Validation Center on their Boeing 737 test-bed. At the time of this writing, lack of independent means of verifying the identified corrosion locations as well as their quantification remain still to be explored research and development issues.

Based on the results of a highly successful Air Force program in solid-state x-ray detection, a development project was initiated in FY93 to scale up this technology to provide an 8 in x 8 in field of inspection. The semi-automated prototype is geared towards depot/field assessment of airframe structure, and engine component degradation caused by corrosion. Some of the anticipated results are spatial resolution approaching 20 line pair/mm, dynamic range exceeding 3000:1, and wide operating energy range. Another program is to assess the applicability of back scattered tomography(BIT) to corrosion detection and quantification. This technology seeks to address the issue of structural inspection in areas of limited access requiring single side inspection. Other programs of interest include laser generated/detected ultrasonics, pulsed eddy current inspection[9].

FAA has been involved in contractual efforts to detect sub surface corrosion using a newly developed technology, magneto-optic imaging. Results from this Small Business Innovative Research (SBIR) funded

effort have been encouraging.

In addition, there have been activity in the eddy current, back-scatter radiography, and a visual inspection enhancement technique, retro-reflective light. This is a patented method to visualize surface distortions which can be applied to large area inspection, such as aircraft structures. A companion paper presented at this meeting provides details of this rapid area inspection technique [10].

EARLY DETECTION AND QUANTIFICATION EFFORTS

It is apparent from the foregoing that the development of an early warning corrosion detection device is highly desirable. In addition, if the sensors are micro-thin, they can readily be inserted into corrosion prone areas to provide the possibility of continuous monitoring of the functional and structural integrity of an aircraft.

A prototype micro sensor has recently been developed by the Navy which exploits the well-known galvanic corrosion process[11]. Two dissimilar metals with an insulating gap, such as Gold and Cadmium, in the presence of an electrolyte(moisture containing pollutants) bridging the gap form a galvanic cell when they are short circuited. The magnitude of the galvanic current depends on the thickness of the condensed film, its conductivity, and the extent to which the electrodes are polarized[12]. Monitoring of the sensor current output provides an early indication of corrosion initiation. A variety of sensors have been designed and fabricated on a 0.025 mm thick kapton or epoxy film using a photoresist process. The elements for sensors were micro dimensional strips(0.12 to 0.25 mm wide and 0.05 mm thick) of noble and active metals placed in alternative fashion concentrically (interdigitated). Some combinations used are gold and iron, gold and zinc, gold and cadmium, and gold and tin. These sensors have been used successfully in the evaluations of integrity of coatings, sealants, hidden structures, and organic composites under laboratory conditions[11]. These sensors are currently being tested for monitoring environmental corrosivity aboard carriers, aircraft, during aircraft preservation or storage, and on army ammunition storage sites.

FUTURE R&D NEEDS

What is needed in the near term is a program to provide realistic data related to managing the corrosion related maintenance and repair issues of aging aircraft. This program should address the following four basic needs in order to define the baseline for further research efforts. These are where to inspect, when to inspect, how often should it be done, and how accurately. Defining the most commonly occurring sites on aircraft structures for corrosion initiation can be done on the basis of available data related to service inspection of aircraft. The issue of when to inspect the aircraft relates to aspects of the environment the aircraft is operating under and its corrosive conditions, coating protection breakdown, corrosion initiation and growth rates, etc.

Growth rates of corrosion related damage and capability of current NDE instrumentation with respect to a specific aircraft type are important issues in this regard. Safety and economic considerations dominate the issue of how often the inspections should be done. Damage growth rate, interaction with environmental factors, material quality, and age of the aircraft are important parameters. In addition, the environment under which the aircraft operates also needs to be taken into account. Accuracy of a particular NDE technique to quantify corrosion damage needs to be compared against cost and manhour requirements.

A COORDINATED CORROSION R&D PROGRAM

It is apparent that there have been many efforts in detection, prevention, and control funded by various government agencies. However, there has been little or no coordination among the funding agencies on issues related to science base technology development and its eventual transition to field use. The issues in the development of a comprehensive program in corrosion per se are organizational, research and developmental, and prevention and control.

A centralized government wide working group with technical representation from corrosion, structures, and NDE areas with responsibility for coordinating research and development efforts should be established. This group should include representatives from the Navy, Air Force, FAA, National Institutes of Standards and Technology, and NASA. An interface with the aircraft industry, manufacturers and airlines, could provide a powerful organizational structure to effectively manage all issues related to corrosion.

Figure 1 shows a comprehensive research and development program addressing issues related to corrosion detection, prevention, and control. The basic research should address the issue of further technological developments needed for corrosion prevention and control. Analytic and quantitative corrosion investigation encompassing both basic and applied research should be initiated.

Quantification of effects of corrosion on electronic components and systems as a result of various chemicals being used for corrosion control is another important area of concern with in-service aircraft. Environmental aspects related to corrosion should be documented from available research data and publications. Corrosion standard samples should be developed so that accurate assessment of developed NDE technologies can be undertaken.

Basic and applied research related to subsurface corrosion identification, and quantification should be continued with both laboratory samples as well as actual structures. NDE technology development with the goal of reduction in the overall cost of inspection and reduction in man-hour requirements is needed. Reliability and accuracy of quantification of corrosion damage needs to be established. Further research in

established NDE technologies for corrosion detection, identification, and quantification should strengthen current programs in the areas of radiography both x-ray as well as neutron radiography. Real time radiography has the potential to reduce the time required for inspection and evaluation significantly. In addition, the development of film-free radiography and the possibility of digital image acquisition may provide a quantum leap in further usability of this technology. Research in issues related to further enhancing the capabilities of neutron radiography in terms of source flux and subsequent detection may yield good dividends. Further research is needed in thermal methods for rapid assessment of corrosion infested areas on aircraft structures. All these technologies require development of image and signal processing capabilities to unambiguously define corrosion related damage in structures.

Continued research efforts are needed in the development of chemical and electrochemical sensors which are specific to corrosion and their implementation in the operational fleet. These sensors are currently being envisioned for use in coatings and hidden/inaccessible areas of structures for in-situ detection and monitoring of damage due to corrosion. Integrity assessment of coatings and paints used for corrosion retardation and control is a fertile area for innovative R&D.

R&D issues in structural fatigue due to corrosion are: fatigue crack growth rates, stress intensity thresholds, environments, design strength based on corrosion impact on fracture toughness or structural strength, stress corrosion propagation rates, and fatigue life cycle analysis. Studies of damage assessment in advanced materials in corrosive environment are needed. Tradeoff studies of various structural alloy systems relating specific modulus and strength to corrosion resistance should provide important information relating to life extension issues in replacing corroded/degraded/damaged components.

While aluminum dominates the aging aircraft structures, studies related to corrosion should encompass all types of material structure and component such as aluminum and magnesium, honeycomb structures, composite structures, engine, electric/electronic component, and lubricant and hydraulic systems.

A systematic attempt at reducing the costly and man-hour intensive corrosion related damage should include prevention and control as a major factor. In this vein, studies related to the efficacy of preventive measures such as the use of corrosion prevention chemicals, identification of corrosion susceptible regions on aircraft structures, material selection, and construction methodologies are needed. Degradation of preventive coating systems as a result of environmental and service related causes needs to be quantified.

An important aspect related to life extension is the development of aircraft specific data base. This

should include development of a corrosion documentation system with data obtained from aircraft invasive disassembly and analysis. In addition, 'corrosion lessons learned' should be an important parameter.

SUMMARY

Air Force, Navy, and the FAA Tech Center are directly involved in understanding and developing new approaches to detect and quantify corrosion. Early identification of corrosion before significant material loss is important. The current R&D efforts pursued by various government agencies need to be enhanced for significant inroads in reducing costs attributed to corrosion. A program plan presented here envisioning closer cooperation and coordination of efforts can be a starting point for further action in this important area.

REFERENCES:

1. N. Hackerman, Plenary Lecture, 12th International Corrosion Congress, Houston, TX, 1993
2. G. Cooke, P. Vore, C. Gumeinny, G. Cooke Jr, E. Lunsford, and H. Kealy, "A study to determine the annual direct cost of corrosion maintenance for weapon systems and equipment in the United States Air Force", Final Report, September 1990, Contract #F09603-89-C-3016, Warner Robbins Air Logistics Center, GA.
3. V.S. Agarwala, "Electrochemical Concepts for BMI degradation", Proceedings 1992 Tri-Service Conference, May 1992, Plymouth, MA.
4. R. E. Beissner and A. S. Birring., "Nondestructive Evaluation Methods for Characterization of Corrosion- State of the Art Review, NTIAC-88-1, 1988
5. The AFWAL/ML workshop on nondestructive evaluation of aircraft corrosion: Requirements and Opportunities for research and development, Proceedings, 24-25 May 1983, Dayton, OH.
6. D. E. Nieser, "USAF Aging Aircraft Corrosion Program", 79th AGARD, Seville, Spain, October 1994, Paper 24.
7. National Aging Aircraft Research Program Plan, Federal Aviation Administration Technical Center, NJ, p 15, October 1993.
8. 1992 Materials Directorate and Manufacturing Technology Directorate Combined Roadmap Review, July 1992, Dayton Convention Center, Dayton, OH.
9. P. K. Bhagat, " Inspection and Evaluation of Aging Aircraft: Materials Directorate perspective", Proceedings, International Workshop on Inspection and Evaluation of Aging Aircraft, May 1994, Sandia National Laboratories, Albuquerque, NM.
10. J. P. Komorowski, K. Shankar, R. W. Gould, and O. L. Hageniers, " Double pass retroreflection for corrosion detection in aircraft structures", 79th AGARD, Seville, Spain, October 1994, Paper 7.
11. V.S. Agarwala and A. Fabiszewski, " Thin Film Microsensors for integrity of coatings, composites and hidden structures", Corrosion 94 conference, NACE international, March 94, Baltimore, MD.
12. V. S. Agarwala, " A probe for monitoring corrosion in marine environments", in Atmospheric Corrosion, W. H. Ailor(ed), John Wiley, NY, 183-192, 1982.

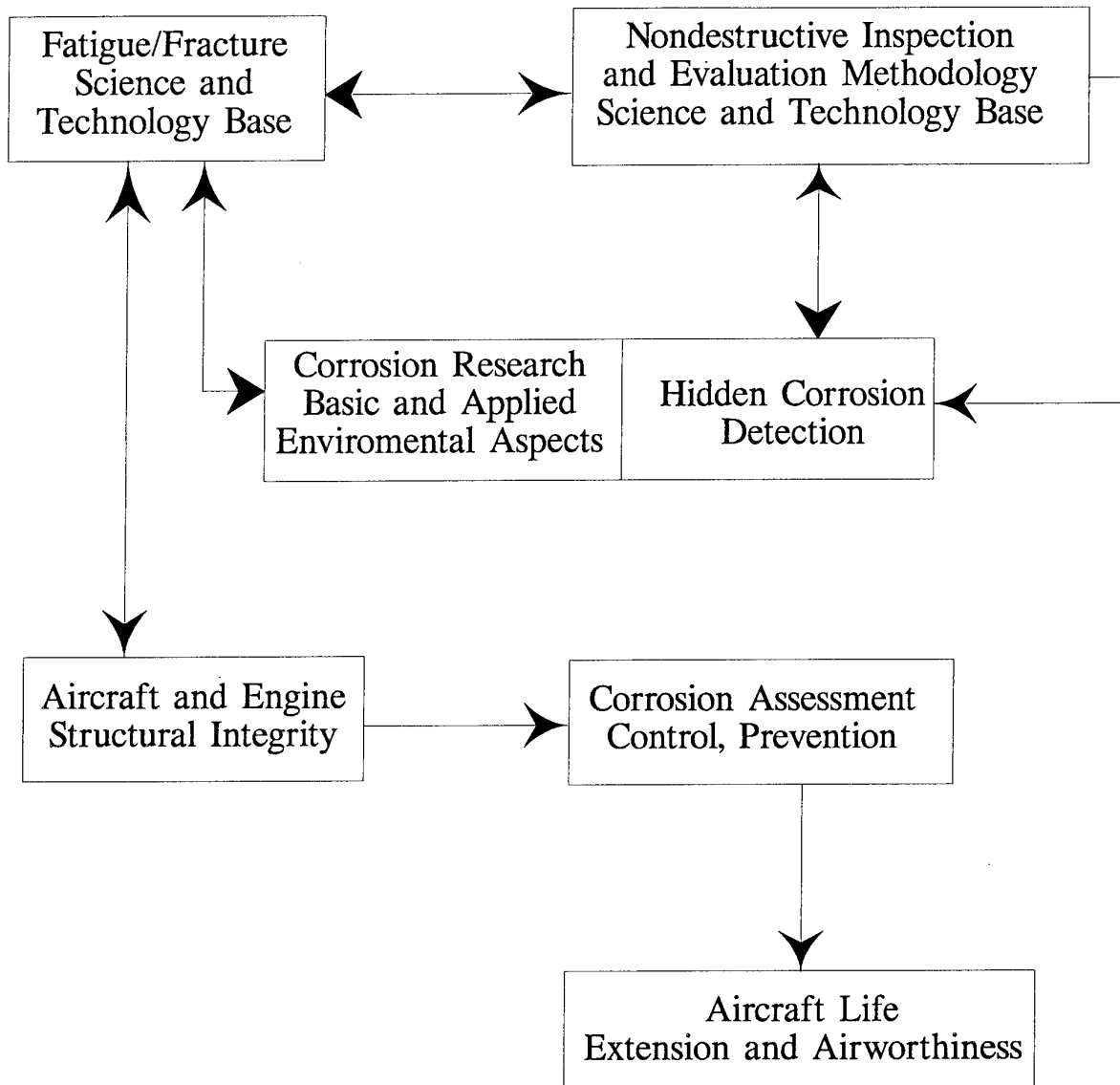


Figure 1. Corrosion Detection, Control, Prevention Model

EXPERIENCE OF IN-SERVICE CORROSION ON MILITARY AIRCRAFT

H.J. Voss
 Military Aircraft Division
 Deutsche Aerospace
 81663 München, Germany
 POSTFACH 801160

SUMMARY

To prevent corrosion of military aircraft the design has to be performed with respect to a careful material selection and an effective surface protection treatment of the materials. Protective treatment on aircraft against moisture, humidity, salty atmosphere, industrial environment, hydraulic fluids, fuel, de-icing fluids, combat chemicals etc. is necessary to meet the operation requirements of the aircraft throughout its operational life. Occurring corrosion detected during maintenance shows that not in every case the requirements above can avoid corrosion problems. This report will show some selected examples of in-service corrosion under investigation of the causes. Inspection and repair methods are shown, further recommendations for corrosion prevention and control to reduce corrosion problems based on practical experiences will be given.

1. INTRODUCTION

Due to Military Aircraft Design material selection and surface protection in general will be provided in accordance with defined standards as e.g. MIL-STD- 889, MIL-F-7179, MIL-STD-1568, MIL- S-5002, MIL-F-18264 or specially installed design standards.

The application of these standards is to ensure a comprehensive aircraft design resistant to corrosion attack. With respect to an operational life of at least 30- 40 years for a military aircraft this is a difficult task.

Corrosion experience obtained from maintenance and repair indicates that besides factors of common knowledge

influencing corrosion such as

- susceptibility to corrosion of high-strength materials
- assembly of dissimilar metals, generating electrochemical potentials
- atmosphere / humidity
- industrial environment

there are some other facts that also should be taken into account such as

- impracticable application of design standards due to manufacturing or other reasons
- in- service stresses / fatigue loads higher than originally calculated
- environmental pollution increased
- ageing of paint system, leading to embrittlement and cracks
- ageing of jointing compound
- manufacturing processes not in line with requirements

2. CORROSION DETECTION

Early detection of corrosion is very important to avoid further damages leading to cracks and to reduce the repair costs respectively down time during maintenance.

Besides visual inspection as a main method there is a number of non destructive testing techniques such as eddy current detection, ultrasonic inspection, radiography etc., being aware of the fact that the latter methods can be used and the results interpreted by experts only.

The detection methods used at the DASA Military Aircraft Maintenance and Repair Depot will be described within the following sections.

2.1 Visual Inspection

In general, corrosion damage will be detected by visual inspection, at first without paint removal, using a magnifier or adequate devices.

Areas of reduced accessibility will be inspected by use of endoscopic devices etc. As visual inspection only can detect corrosion already indicated by paint blistering, paint cracking, filiform etc. also the non indicated, but already existing corrosion below the paint system should be detected early to prevent further damage.

At GAF aircraft visual inspections of the skin have been performed before and after paint removal. Fig. 1 shows the increase of detected corrosion after paint removal, on average approximately 60 % is considered as a typical value.

2.2 Eddy Current Detection

The eddy current detection is a well established method not only suitable for detection of corrosion, cracks and other discontinuities, but also to determine the corrosion depth respectively residual wall thickness also at multi layer material, a method usable without paint removal.

There are two applications of probe guiding

- by hand and
- by scanner

The application of a scanner requires a two core- probe, also suitable for guiding by hand, because there are positions (e. g. edge of a wing) where it is difficult for a scanner to be fixed.

For calibration respectively test of an eddy current probe some test specimens of various material thickness incorporating slots, drills, fasteners and typical corrosion will be required.

Fig. 2 shows a plot of calibrated curves, generated by a stepped sheet, and an example of detected corrosion, showing a residual wall thickness of 0.6 mm.

To determine the corrosion depth, e.g. at a series of fasteners and to generate a monitoring picture an adequate

equipment of computer, software and scanner will be necessary.

In Fig. 3 a block scheme of the required equipment will be shown.

Fig. 4 shows the scanner, fixed on a wing panel, having detected some corrosion round a fastener.

2.3 Ultrasonic inspection

Ultrasonic inspection will be used for detection of exfoliation, cracks and for measurements of wall thicknesses.

This detection method, inspecting normal to damage extension will be preferably used for determination of residual wall thickness after removal of corrosion, giving more exact results than by EC-detection, but not applicable on multi layer material.

2.4 Radiography

X-ray or gamma radiation preferably will be used in areas of less accessibility to other detection methods, in order to detect discontinuities of materials, as pitting, also cracks, provided that the radiation will be directed along the crack. Hence, the application of this method especially will require rough knowledge of the damage.

3 EXAMPLES OF IN-SERVICE CORROSION

Obviously in most cases corrosion on the skin of an aircraft will occur near fasteners, usually countersunk type, also at edges and access panels. Minor corrosion will be found on uninterrupted parts of the panels, examples will show.

3.1 Air Intake

Fig. 5 shows an air intake of an a/c 8 years old with corrosion detected before and after paint stripping, corrosion is marked by circles.

Design data are:

Air intake panel made from 2024 T62, thin plate, stretch formed, with P.T. alodine, epoxy-primer chromate containing, polyurethane top coat, countersunks unprotected. Wet assembly of titanium fasteners, anodized, by jointing compound, corrosion inhibiting.

Contact corrosion between fasteners and air intake panel was caused by paint cracking round fasteners because of dynamic loads and paint ageing, the cracks leading to an ingress of humidity/salt, furthermore by embrittlement of jointing compound.

Modification of protection treatment in maintenance was performed by use of washprimer, epoxy-primer chromate free and acrylic top coat.

3.2 Wing trailing edge

Fig.6 shows a lower wing panel of an a/c 9 years old with corrosion detected before and after paint stripping, corrosion is marked by circles.

Design data are:

Wing panel made from 2024 T351, milled down from thick plate, with P.T. anodizing, epoxy-primer chromate containing, acrylic top coat. Countersunks unprotected, titanium screws anodized plus MoS_2 - coating, Non CRES-steel nuts, cadmium plated + MoS_2 .

Exfoliation form of intergranular corrosion near fasteners was determined, caused by high susceptibility to corrosion of this plate material, electro chemical potentials and permanent humidity ingressing from the upper region, from stress/fatigue requirements drainage holes not being permitted.

Fig. 7 shows a section of the wing trailing edge.

Modification of protection treatment in maintenance was performed as following: protection of countersunks by washprimer and epoxy-primer chromate free, wet assembly of hinge and fasteners by sealing compound, also sealing gaps and nuts. Additional application of water repellent compound.

Fig. 8 shows the post-mod version.

4. REPAIR

Repair of corroded a/c in general will be performed acc. to Repair Manuals resp. Technical orders containing manufacturers information and instructions of repair standards, being aware that increasing corrosion on ageing aircraft also may require the development of advanced repair methods.

4.1 Removal of Paint System

From a number of available devices for paint removal the following have been applied:

- paint stripper, chemical
- paint thinner, solvent and
- mechanical means.

Paint strippers must not be used near gaps, overlaps, holes because after ingress into the a/c structure the removability will be low, new corrosion is generated. As PU finishes are highly chemical resistant paint strippers are acting slowly, a mechanical postwork will be necessary. For health hazard and environmental reasons the application of paint strippers should be restricted. Removal of one pack acrylic finish will be possible by solvent, one of the reasons for the preferred application of this paint system. Also field repair can be done easily, being aware, that 2-pack primers cannot be removed by solvent. Mechanical paint removal is performed by brushing, grinding and abrasive blasting.

Preferably plastic media paint stripping the so-called dry stripping is a suitable, economical method for removing all paint systems, including polyurethane, partial or totally from aircraft skin, allowing visual inspection and excellent preparation for repainting. Plastic grains as a media will be used, existing in several grain sizes and hardness. Nearly 100 % of the blasting media can be recycled after being separated from paint dust which can be deposited without problems.

As the media will generate some residual compression stress on stripped surfaces, fatigue and crack propagation tests have been performed on stripped and unstripped sheet.

The results from fatigue tests of un-notched specimens, stripped and repainted up to five times, do not show a significant influence of the dry stripping process on the fatigue properties.[7].

Even crack propagation tests performed on specimens, stripped and repainted up to ten times do not show any influence [4].

Only the surface roughness will increase slightly.

In opposite to grinding, plastic media blasting will not remove clad coating. For the application of the dry stripping process special instructions due to each type of aircraft will be necessary, containing relevant process parameters as nozzle diameter, media flow, pressure, distance and angle of attack of the mouthpiece with respect to type of material and thickness.

Fig. 9 shows a GAF a/c subject to dry stripping.

4.2 Removal of Corrosion

Corrosion removal can be carried out by chemical or mechanical devices. As the application of chemical devices may lead

to an ingress into gaps, overlaps, countersunk holes etc. its usage will be restricted.

Hence mechanical devices such as scraping, grinding, hand milling, and blasting with glass beads respectively aluminium oxide will be used, with respect to the type of corrosion. As the removal of pitting corrosion or filiform is more easy, exfoliation requires alternating blasting and grinding. Blistering of the material due to blasting will show any remaining corrosion, which has to be removed totally in order to prevent new corrosion from forming. Since the material thickness of the structure must not be reduced more than necessary, this task requires comprehensive training and a lot of experience.

After removal of corrosion (up to mirror surface) the residual wall thickness will be determined, being required for decision of further procedure with respect to stress / fatigue requirements at the following categories:

- I. dimensional tolerances of parts not exceeded
 - repaint
- II. dimensional tolerances exceeded, but tolerable from stress / fatigue requirements
 - perform a concession and repaint
- III. dimensional tolerances exceeded not tolerable from stress / fatigue requirements
 - perform a repair / repair scheme, e.g. by doubler or equivalent and repaint
- IV. dimensional tolerances exceeded, not tolerable from stress / fatigue requirements, no repair possible
 - change of parts

Due to measures II to IV documentation will be necessary.

4.3 Repainting

As in the case of a total repainting the aircraft will stay unprotected 3-4 months between stripping and repainting, the question may occur if a temporary protection will be necessary.

Investigations of clad sheet, stripped and repainted immediately after stripping and stripped sheet, repainted after months did not show any difference of adhesion of paint systems. Therefore an interim protection for clad sheet will not be necessary, only around fasteners temporary protection of acrylic laquer will be applied, easily removable by solvent before repainting.

As pretreatment before repainting anodizing or chromate conversion coating would be required, giving excellent adhesion properties to the substrate and to following paint systems, but in maintenance only available as brush processes, not applicable near gaps, overlaps etc. because of generating new corrosion when ingressing into the structure.

For repainting of GAF Tornado a/c a paint system consisting of washprimer, epoxy-primer free of chromate, and acrylic top-coat will be applied. Subject to corrosion tests, this paint system (without top-coat) was passing salt spray tests of 1000 hours without showing any corrosion and also 42 cycles (i.e. 1000 hours) of humidity tests, the paint system including acrylic top-coat [6].

5. CORROSION PREVENTION AND CONTROL

Experience from maintenance shows that always corrosion will occur on military aircraft.

Through suitable means it should be possible to ensure the a/c performance not to be decreased by corrosion.

5.1 Design improvement

Corrosion prevention already starts during development phase of an a/c, by careful material selection, surface protection and design.

Airframe design includes high-strength aluminium alloys, high strength steels, titanium-alloys and magnesium-alloys.

Maintenance experience shows that due to design the strength properties of materials have to be considered versus inherent corrosion properties.

Hence, aluminium alloys extremely susceptible to corrosion should be eliminated from material selection lists or consequently applied in a heat treated condition less prone to exfoliation or SCC, such as overaged zinc-alloys.

For the application of steel CRES material should be preferred prior to NON-CRES material. As steels in general will be cadmium plated for compatibility with aluminium, cadmium plating of CRES may be replaced by painting, zinc or aluminium coatings, except for bushes, still to be cadmium plated before installation in aluminium structures.

Also the application of high strength steels should exclude tempers susceptible to stress corrosion cracking.

Since titanium alloys in general are not prone to corrosion but may generate corrosion when assembled to aluminium structures, sufficient protective treatment in area of touch has to be provided such as anodizing, painting, coating, wet assembly.

The application of those magnesium-alloys, tending to severe corrosion, should be eliminated consequently from structural design.

With respect to the requirements to surface protection, resulting from different categories of an aircraft a classification of several zones will be recommendable such as:

- Zone A: Interior surfaces, not to be subjected to permanent condensation
- Zone B: External and internal surfaces, to be exposed to wet environment
- Zone C: Fuel wetted surfaces

Due to each zone the protection treatment meeting the requirements may be selected.

Since the development of future primer systems will lead to products free of chromate, anodizing of aluminium-alloys should be applied as a pre-treatment giving more corrosion resistance, as investigations have shown.

As in most cases aluminium-alloys have been treated by conversion coating or anodizing prior to primer, in case of skin panels fitted with pilot holes, to be drilled up during a/c assembly, hence countersunk drills will be bare of any pre-treatment because protection post-treatment is not provided.

So, wet assembly of fasteners has to be obligatory, using sealing compounds only. Maintenance experience shows, that jointing compounds, although corrosion inhibitive, do not seem to meet the protection requirements over years because of progressing embrittlement and leaching.

The application of more flexible polyurethane top coat may improve corrosion resistance round countersunk fasteners but in the past no significant differences have been detected between corroded skins, painted either with acrylic or polyurethane top coat.

Provision of water repellent compounds as design means should be avoided because of difficult and time consuming removability due to paint removal, as well remaining particles will reduce adhesion of paint. Application may be provided in regions of wet environment and of less accessibility for repair and repainting (as bays, cavities etc), where paint systems are not sufficient, but being aware of the necessity of re-conservation yearly.

Further, sufficient drainage and ventilation of the interior airframe has to be provided, also the possibility of artificial ventilation by air of low humidity through an a/c during down time should be taken under consideration.

Humidity absorbing foam blocks inside of a/c should be avoided or sealed against ingress of moisture by adequate devices. Even the use of foam material releasing corrosion increasing substances should be prevented in a/c design.

5.2 Measures of maintenance

The installation of a Corrosion Prevention and Control Program for in-service aircraft will be suggested, this program containing all relevant measures, being aware that in maintenance preferably the symptoms of corrosion will be treated prior to causes.

As a part of the program above, all occurring corrosion damage will be documented in a Corrosion Control Register due to each aircraft. Statistical evaluation may show a single case or typical corrosion, often occurred at same parts.

Single corrosion will be removed followed by repainting, documentation depending from severity (see sect 4.2). Having detected part-typical, multiple corrosion the following will be performed:

- o Analysis of corrosion and determination of the causes
- o Development of remedial measures by improved surface protection, improved design etc.
- o Laboratory tests / flight tests
- o Interpretation of test results
- o Installation of T.O. / MOD and fitting to a/c.

Adequate devices as corrosion control data sheets, having been created for registration of corrosion, also computer programme for interpretation are available.

Fig. 10 shows a corrosion control data sheet of the lower wing panel.

By these means the effectiveness of maintenance and repair measures can be observed over years, the application of advanced methods inclusive.

6. CONCLUSIONS

Since maintenance experience shows that untreated corrosion will lead to an expensive change of parts, efficient corrosion control measures have to be provided.

As already outlined in sect. 2.1, repainting without removing the primer will not be suitable to detect 100% of corrosion.

Fig. 11 will explain the effectiveness of repair with and without the removal of the primer.

Hence paint removal from the a/c skin, also to detect the start of corrosion will be essential within defined intervals. To prevent major corrosion 5-8 years seem to be reasonable.

Fig. 12 schematically shows the exponential progress of untreated corrosion versus the improvement of the a/c condition by in-time repair within defined intervals. Corrosion prevention and control measures such as total paint stripping may appear to be expensive at the moment, but being long-term measures of high effectiveness the overall repair costs during a/c life will drop drastically.

7. REFERENCES

1. H. Unterreiner, DASA Manching,
"Dry Stripping Experience Gained
in Military Aircraft Overhaul and
Maintenance"
2. GAF, Luftwaffenwerft 13,
"Corrosion Prevention & Control
Program - TORNADO"
3. H. Grauvogl, DASA Manching,
Rep. N°. FQ154 / 45 / 08 / 91,
"Determination of Corrosion
Depth"
4. P. Steppe, MBB,
TN - ZTT61 - 17 / 86,
"Beeinflussung der
Rißfortschrittsgeschwindigkeit
durch Farbtragstrahlen"
5. H. J. Voss, DASA München
Rep. No. FE221-009/92
"Auftreten von Korrosion und
deren Behebung"
6. M. Weigand, MBB
TN-3465,
"Untersuchung von Anstrich-
stoffen mit chromatfreien
Grundanstrichen"
7. DASA Militärflugzeuge,
TN-S-318,
"Einfluß des Dry-Stripping
Verfahrens auf die Ermüdungs-
festigkeit von dünnen Al-Blechen"

		before	after
Fuselage	L / H	83 %	100 %
	R / H	80 %	100 %
	dorsal	77 %	100 %
	ventral	63 %	100 %
Fin		77 %	100 %
Taileron		25 %	100 %
Wing	upper	67 %	100 %
	lower	50 %	100 %
Air Intake		50 %	100 %

Fig. 1

Comparison of the volume of detected corrosion on the skin, before and after paint removal.

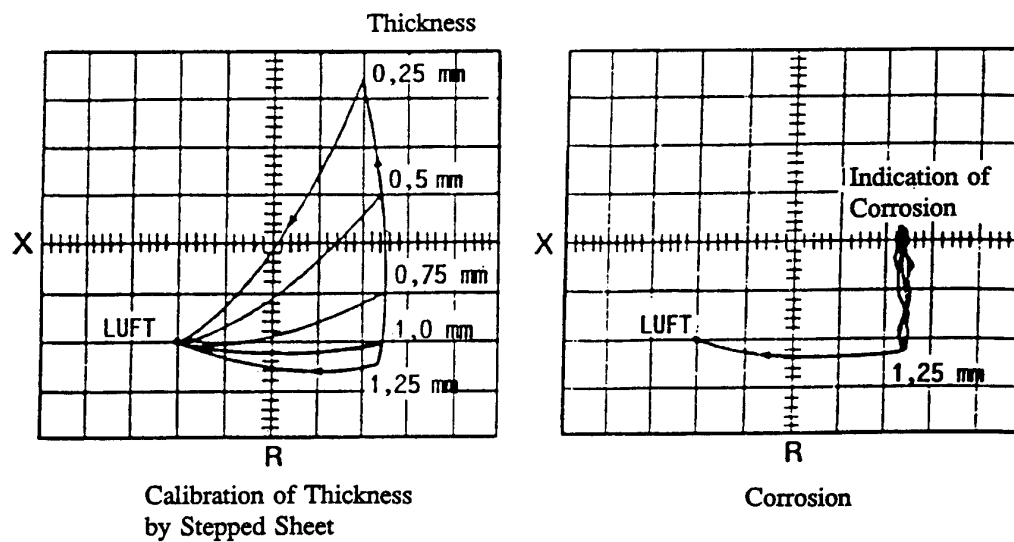


Fig. 2

Eddy current detection,, single frequency

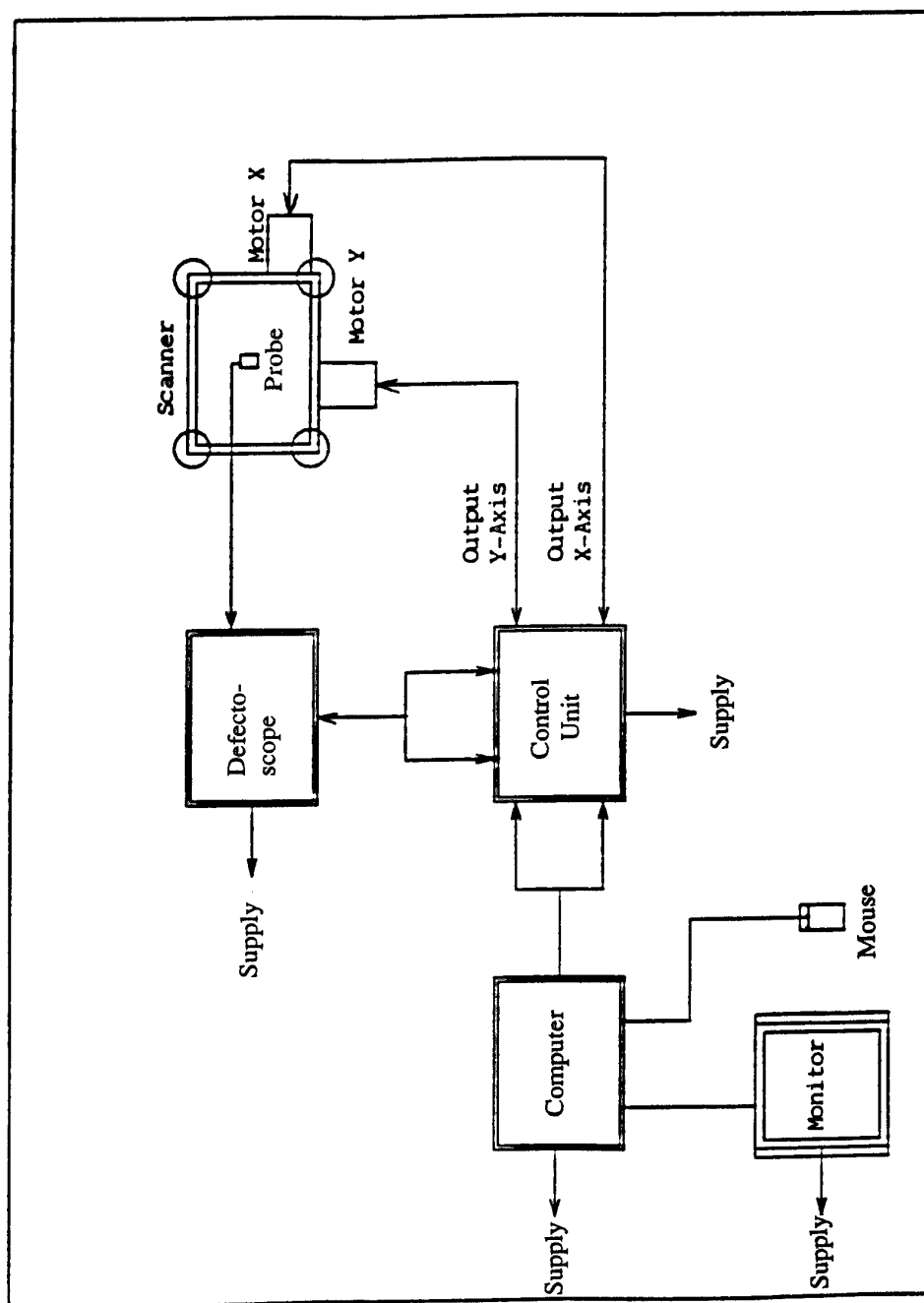
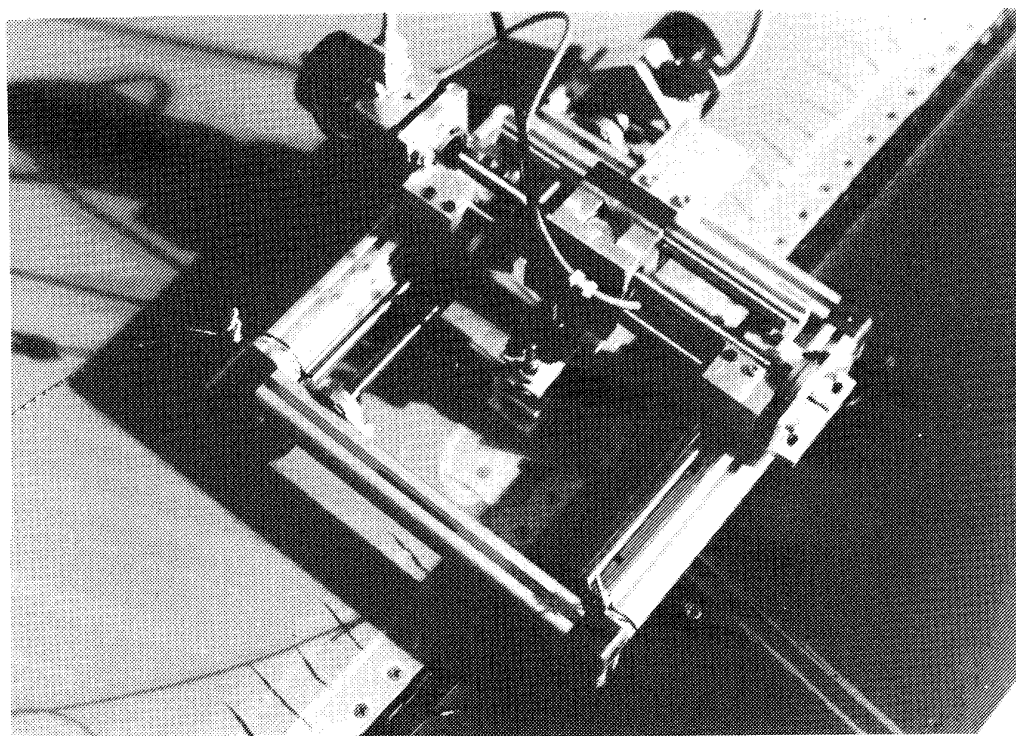
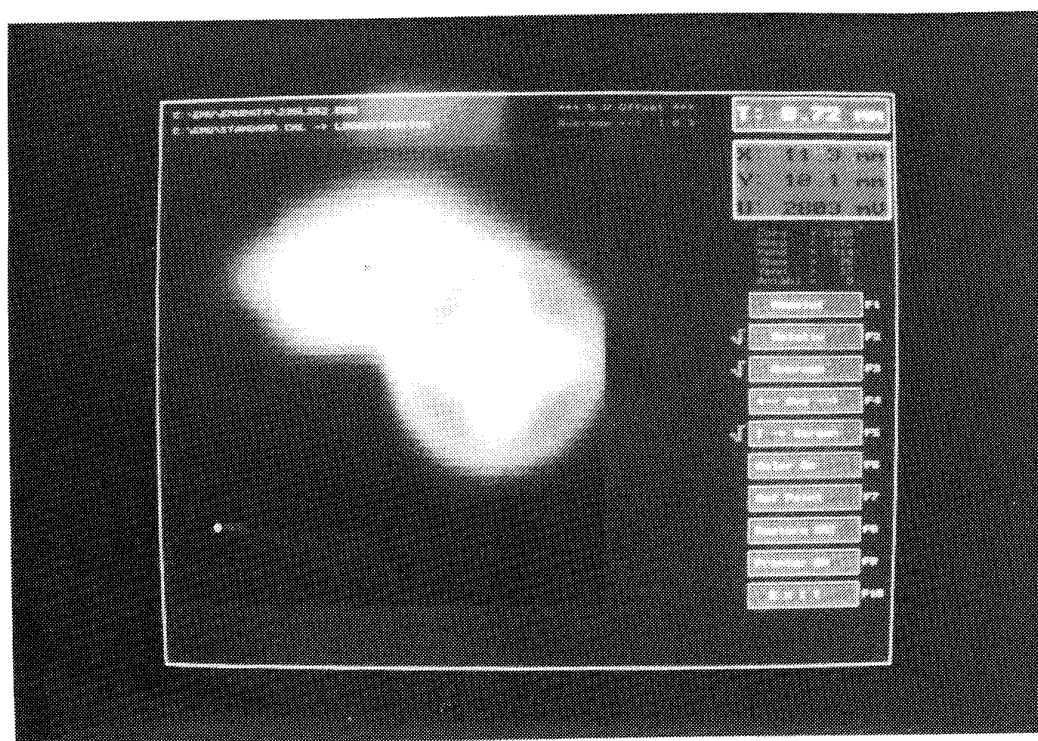


Fig. 3
EC-Detection of corrosion by scanner,
block scheme of the equipment

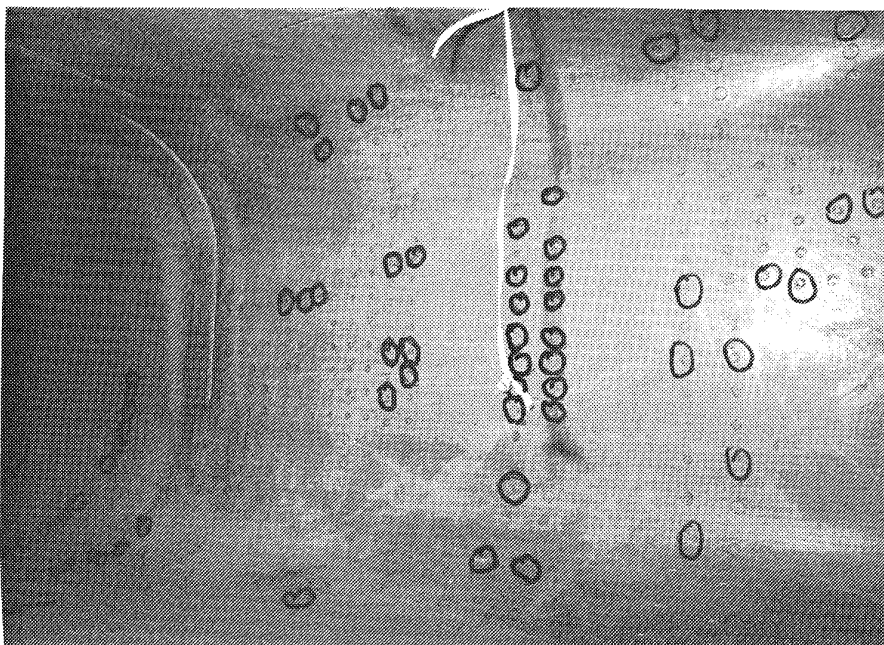


Corrosion detection by scanner

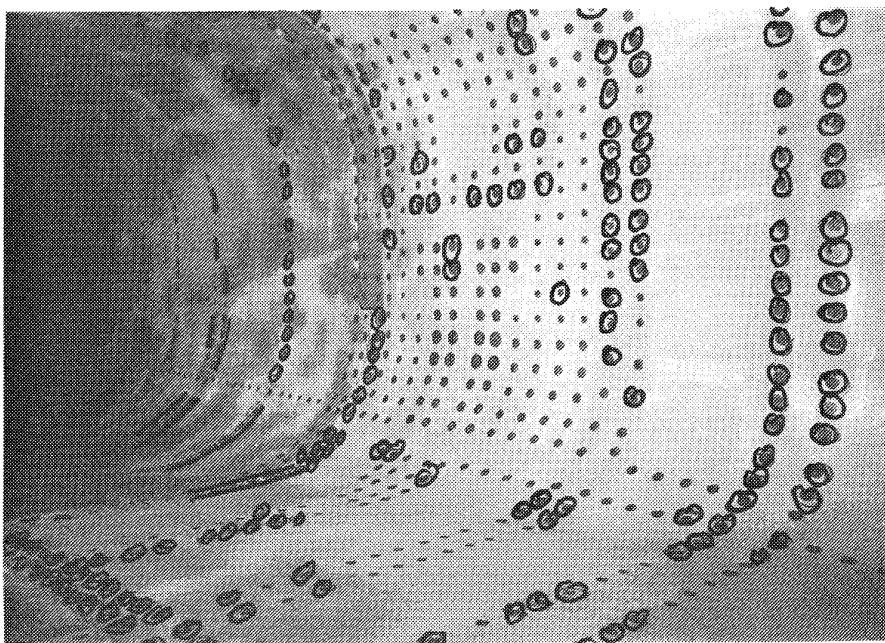


Monitoring of corrosion detected

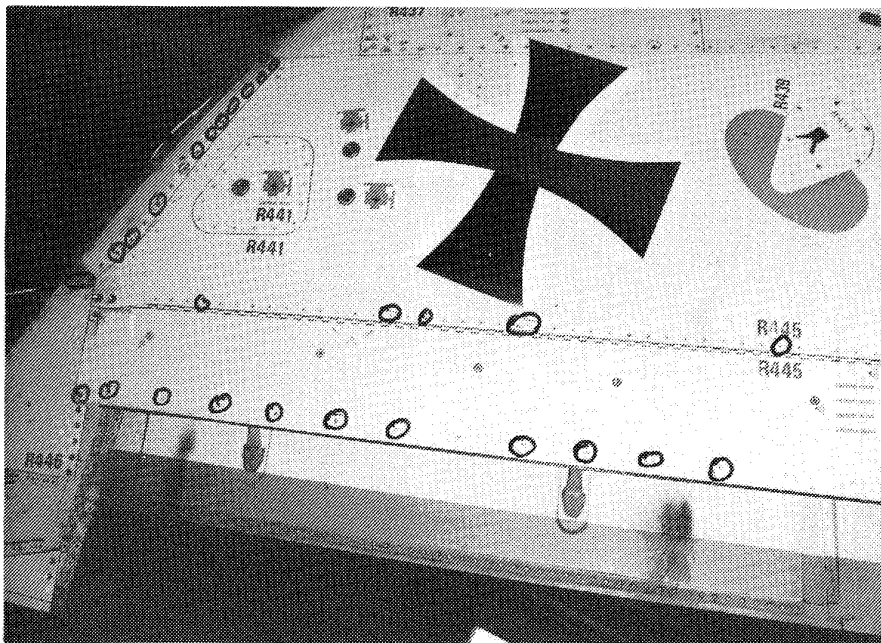
Fig. 4



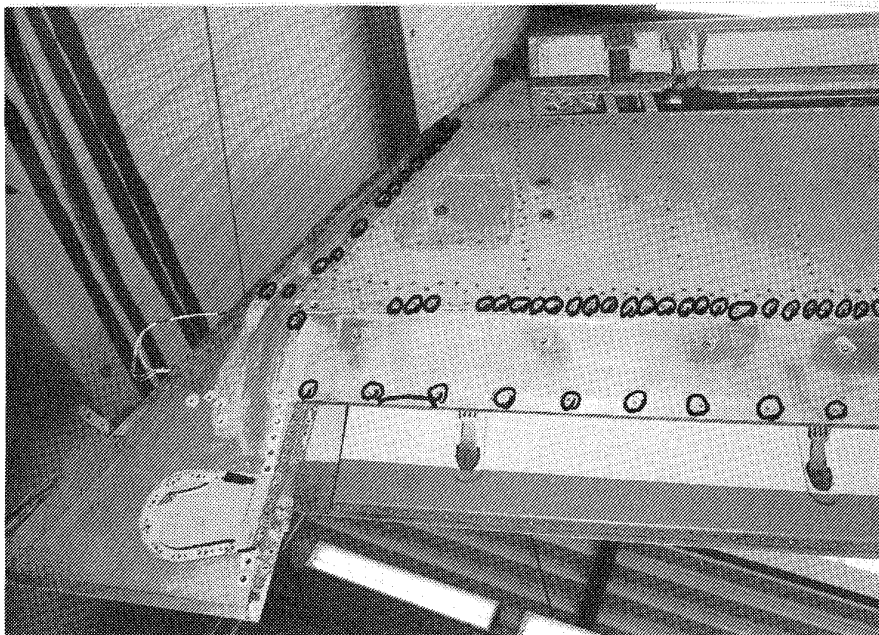
Air intake before paint removal



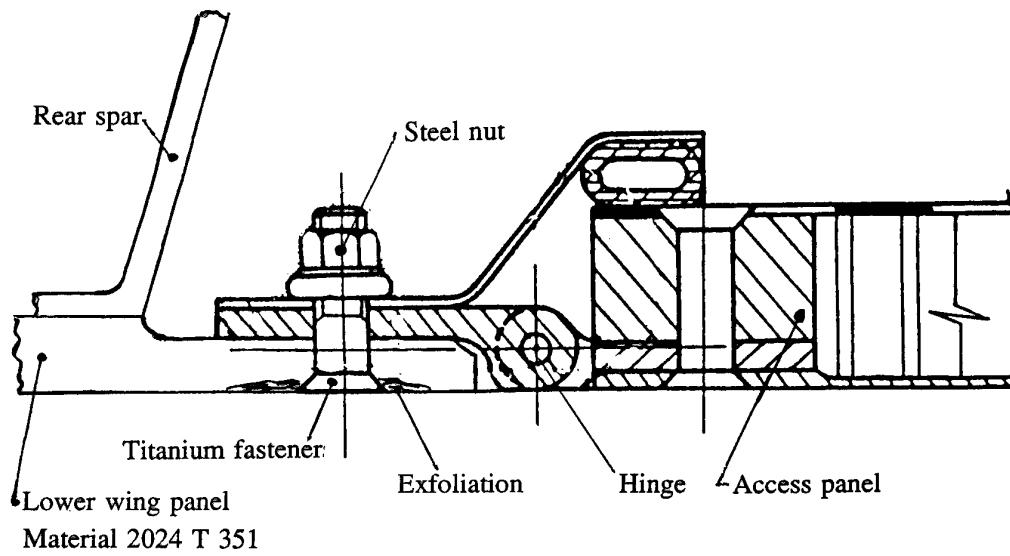
Air intake after paint removal



Lower wing panel before paint removal

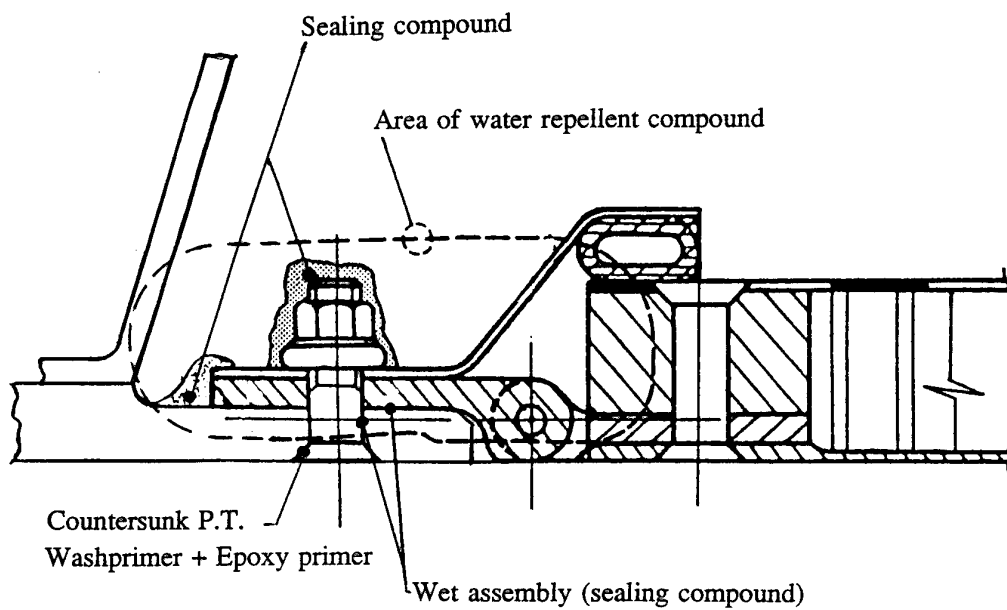


Lower wing panel after paint removal



WING TRAILING EDGE

Fig. 7



Post-MOD Version

WING TRAILING EDGE

Fig. 8



Dry stripping of GAF a/c

Fig. 9

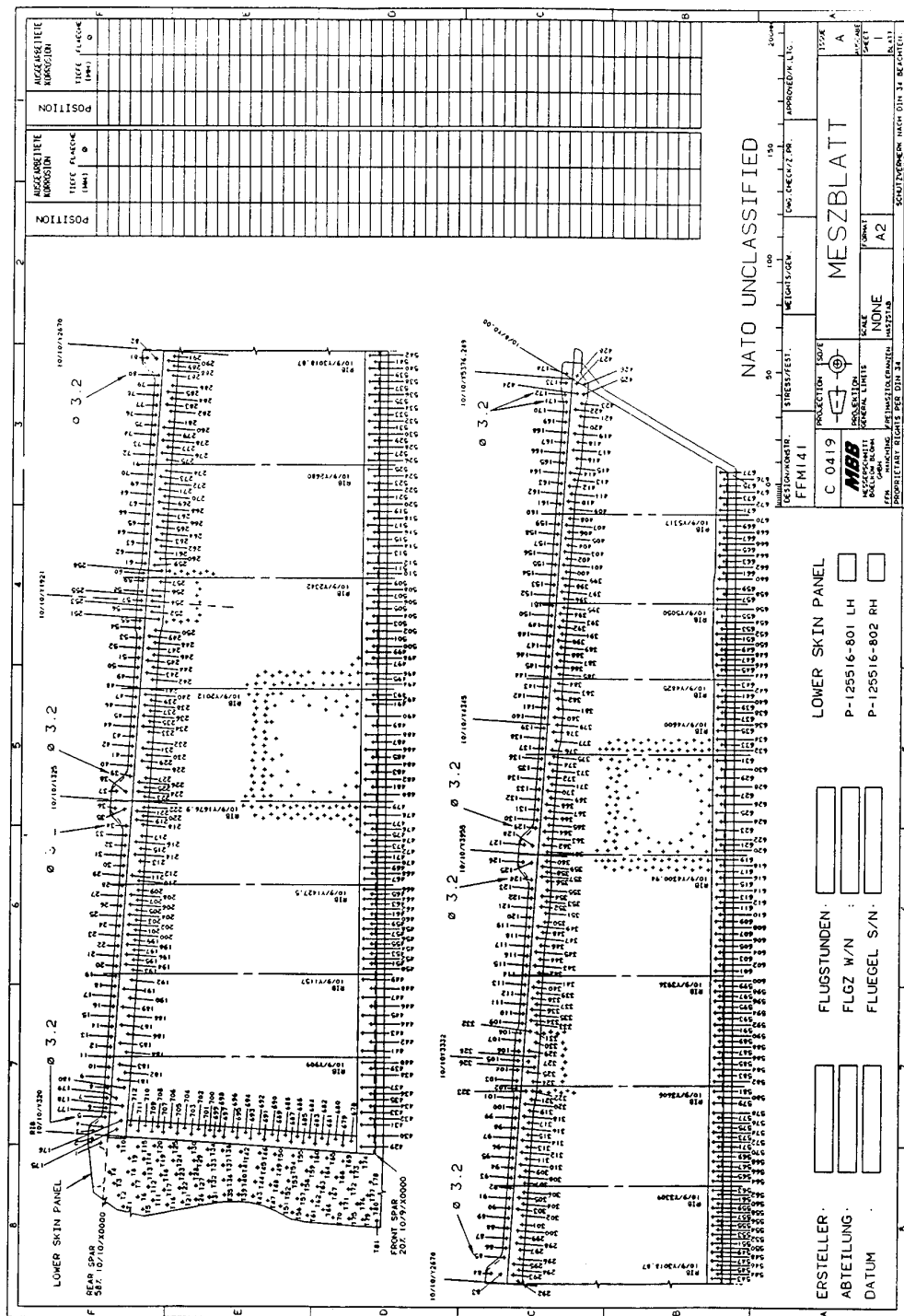
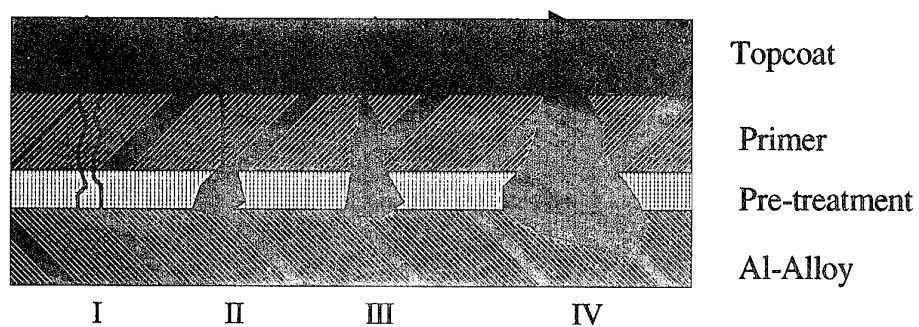


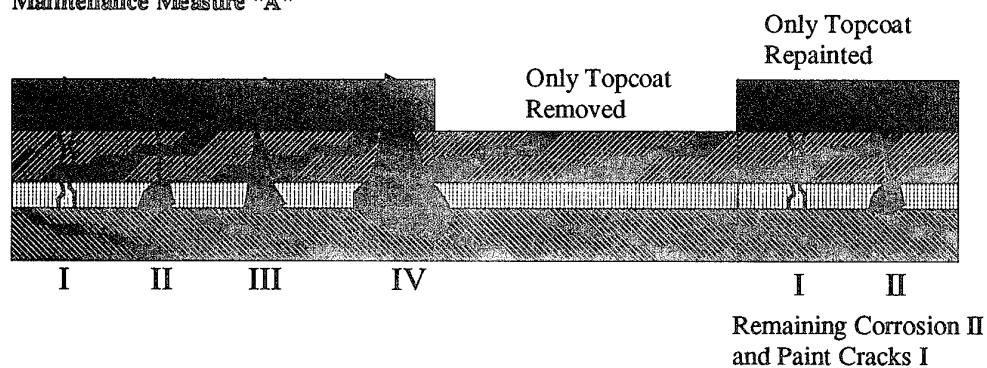
Fig. 10
Corrosion control data sheet of lower wing panel

Form of Corrosion

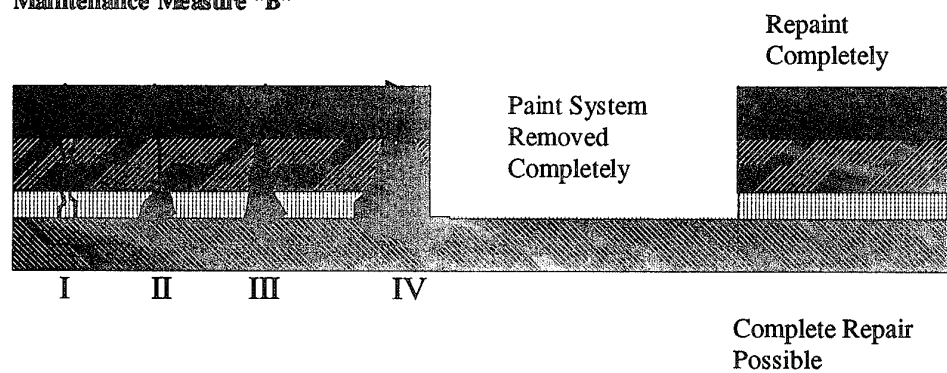


Form	Detectability	Damage
I	by Microsection	Paint Cracking, no Corrosion
II	on bare Substrate only	Low Corrosion
III	after Removal of Topcoat	Medium Corrosion
IV	Visible on Topcoat	Medium/Severe Corrosion

Maintenance Measure "A"

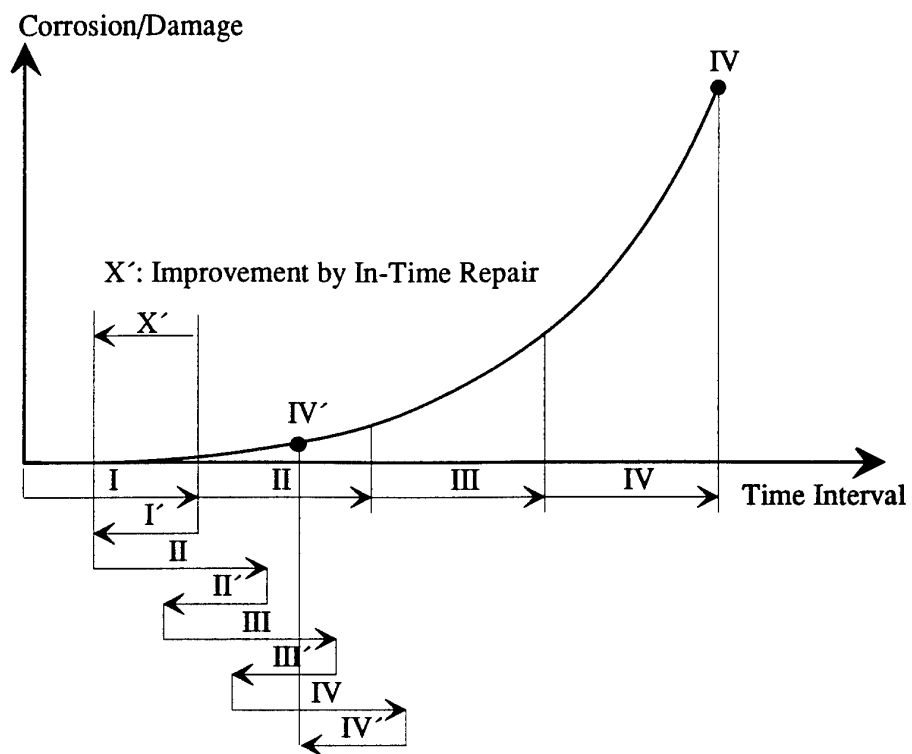


Maintenance Measure "B"



Effectiveness of repair with and without paint removal

Fig. 11



Progress of corrosion with and without in-time repair

Fig. 12

U.S. NAVY OPERATING EXPERIENCE WITH NEW AIRCRAFT CONSTRUCTION MATERIALS

G. T. Browne
Material Advisor
Commander Naval Air Force, U.S. Atlantic Fleet
Code 528
Naval Air Station
NORFOLK, VA 23511
UNITED STATES

This paper addresses the U.S. Navy's experience and problems encountered with new aircraft construction material in the highly corrosive naval operating environment, to include:

Experience with carbon bismaleimide (BMI) and epoxy matrices composite, new aluminum alloys and metal to composite joint repair of honeycomb and monolithic composite structure in fleet activities ashore and afloat.

Problems experienced with electromagnetic interference (EMI) protection, systems currently in use, and the development of corrosion inhibiting conductive (EMI) sealant.

Fastener compatibility for joining carbon composite to metals, H-60 and H-53 helicopter problems, and corrective actions.

1. The U.S. Navy is a premier organization that stays on the leading edge of material technology. Today, the U.S. Navy operates more aircraft containing carbon epoxy composite, new aluminum alloy/temper and steels in the naval operating environment than any other organization in the world. These aircraft operate anywhere on the globe.

Weather is always a factor in long term material performance. Sunny days with air temperatures of 70°F (21°C) and seas like glass, to temperature extremes with highs in excess of 100°F (37°C) and lows below 32°F (0°C) with high seas and strong winds resulting in water coming over the bow of a super carrier. Another factor of concern is the acid environment in which we live and operate. See reference (1). (Show Figures 1/2).

The naval operating environment provides a material testing laboratory that is second to none. We have seen many material problems which are discussed in this paper.

Note: When problems are discovered, fleet operators advise the Commander, Naval Air Systems Command (COMNAVAIRSYSCOM); Naval Air Warfare Center; Cognizant Field Activities (CFA); and aircraft manufacturers. COMNAVAIRSYSCOM initiates action to correct the problem in the most economical and expeditious manner. Commander Naval Air Force, U.S. Atlantic Fleet (COMNAVAIRLANT) ensures solutions are compatible with operational requirements and maintenance capacity.

Overall, the new materials introduced in F/A-18, AV-8B, H-60, and H-53E have performed well in the environments described above as individual materials. However, when the materials are joined, problems start and quickly advance in the harsh naval environment. For example:

2. The newest in aerospace materials, composites, and hybrid materials pose new problems when these materials are attached to the more conventional aerospace alloys. These new aerospace couples cause accelerated galvanic corrosion that can lead to rapid deterioration of critical aircraft parts, both metallic and non-metallic. It is well known that when carbon/graphite-epoxy composite materials are coupled to aluminum, steel, or titanium; the metal corrodes (in preference to the strong carbon/graphite cathode).

This type of corrosion is called galvanic corrosion. It should be realized that any carbon fiber reinforced composite will act as a cathode and thus accelerate the corrosion of the aerospace metal coupled to it. Thus, even the newer composites, such as carbon/graphite reinforced PolyEtherEtherKetone (PEEK), carbon Polyimide (PI), or Bismaleimide (BMI) will act to cause galvanic corrosion when coupled to metallic structures.

It should be emphasized that epoxy matrices are susceptible to water accumulation and hence degradation. Epoxies accumulate water. Even in the absence of galvanic corrosion, water absorption by the epoxy matrix can cause composite strength loss as well as act as a source of electrolyte for galvanic corrosion of metals to which it is attached. Therefore, carbon/graphite-epoxy composites that have suffered matrix degradation by water can be more damaging to metal couples, since the galvanic effect is augmented by the material carrying its own corrosive electrolyte.

Another matrix degradation phenomenon occurs when the cathodic reaction results in the reduction of water and oxygen, at the carbon/graphite fiber, to yield hydroxyl ions. The subsequent rise in pH the carbon/graphite imides matrix interfac may damage the imides matrix resin and reduce the structural integrity of the composite. This phenomenon has been repeatedly observed in matrices of bismaleimides.

3. High temperature composite, such as Polyimide (PI) and Bismaleimide (BMI) have seen little use to date in U.S. Navy aircraft. Some BMI panels are utilized on the AV-8B aircraft in the variable engine nozzle areas which have performed well.

Tests conducted by the NAVAIRWARCEN Warminster (reference 3) have shown that the imide based composite component in PI or BMI

cannot tolerate hydroxides (OH_2), which causes a breakdown of PI/BMI matrix. If used, PI/BMI should be protected from hydroxides. (Figures 3/4).

The following facts need to be emphasized when utilizing composite structure:

Carbon is the most stable of materials commonly used.

All epoxies will absorb water.

Fastener compatibility is a must when joining carbon epoxy composite to metal.

All metals joined to carbon epoxy composite become anodic.

Water absorbed into the composite matrix can become a potential electrolyte.

Fasteners alloys identified below (in a wide range of Ultimate Tensile Strength (UTS) are recommended (reference 4) for use when bolting composites to metal structures, to minimize corrosion problems.

Titanium Ti-6AL-4V
Inconel 718 180 KSI - 220 KS UTS
1240 MPa - 1515 MPa UTS
MP-35N/MP159 260 KSI UTS
159 MPa
(Used extensively in space shuttle)
See Figures 5., 5.5, 5.6

4. The first deployment of the F/A-18 aircraft was an eye opener. The carbon epoxy composite (FM300-3501-6) performance was flawless. Damaged composite components were usually repaired onboard the aircraft carrier using the NAVAIRSYSCOM designed Damage Engineering Disposition (DED) program. The area to be repaired is described in a naval message using an X to Y axis.

The message is transmitted to the CFA engineering activity, where detailed repair procedures are developed and sent to the requesting activity by naval message.

Typical repairs of a damaged honeycomb component range from 1 X 2 inches (3 to 6 cm) to 18 X 20 inches (45 to 50 cm). The technician will cut out the damaged skin and honeycomb, clean the area, and in some cases both top and bottom skins required replacement (the bottom skin is replaced first and cured). New skin can be metal, pre-preg or wet layup. The replacement honeycomb is bonded to the new skin, cured and shaved to the mole line of the component. The top skin is then bonded to the component, trimmed/sanded as required and painted back to original paint scheme. 423 plus of this type of repairs have been accomplished by Navy and Marine technicians since the F/A-18 has been deployed.

Damage and repair of monolithic skins/components are flush/lap bonded or bolted, depending on their location on the airframe and the aerodynamic requirement. Bolted repairs from 4 inches to 20 inches (10 cm to 50 cm) have been accomplished on monolithic components of AV-8B and F/A-18 using Ti-6AL-4V plates and fasteners (Composi-Lok II or a nut plate with bolts). Bolt alloys are Ti-6AL-4V for routine repairs for lightly loaded structures and Inconel 718 for high load carrying structure/components.

5. The strongest repair for monolithic structure seen to date is reported in reference (5) NASA proceedings. This report advised that an 18-1 scarf bonded repair provided the strongest repair to a monolithic component. This test consisted of a bolted bonded lap flush scarf, which was exposed to the elements for 10 years followed by 2.5 life cycles of fatigue testing followed by destructive testing. This 18-1 scarf strength exceeds all other repairs tested.

AV-8B has no honeycomb structure. All monolithic bonded and bolted repairs have been accomplished by depot and military technicians to the AV-8B structure, with no problems reported to date.

Overall, composites have performed very satisfactorily during nearly 10 years of service by naval aircraft with composite structures.

6. Corrosion of four types have been observed on metals/composite airframes, steel fasteners, and Al components crevice, galvanic, pitting, and rust. We will look at the rust problem first, as the other problems get more complicated.

Rust of fastener heads was reported shortly after the F/A-18 aircraft were deployed. Rusty fastener heads were visible through the paint system. The fastener was M013-8PH forming a protective oxide coating. The source of the electrolyte was believed to be the absorbed water in the matrix of the composite skin. Crevice corrosion has also been seen on some highly loaded skins when the fastener head failed. See figures 5/6. Corrective action for this problem consisted of replacing the fastener. Highly loaded fasteners were replaced with Inconel 718. Lesser loaded fasteners were replaced with titanium. Repairs were accomplished during depot rework of aircraft.

Since the F/A-18 is a fly by wire aircraft, there is concern about Electromagnetic Interference (EMI). An extensive EMI shielding effort was incorporated. History has shown that most efforts to make an aircraft EMI hard have failed, as the materials selected for this effort are good electrical conductors. They are not, however, compatible with the aircraft construction materials; and result in the establishment of galvanic cells. Water from any source will cause corrosion to be initiated. Once the corrosion process starts, the EMI protection system slowly degrades until there is no EMI protection, as you cannot maintain a ground in a corrosion product.

When the first F/A-18 was opened up at rework, exposing the dorsal longeron, rust galvanic pitting corrosion was noted on the dorsal longeron and attaching hardware.

The original EMI protection system installation consisted of the following: Longerons 7149-T76Al alloy with Class III chemical conversion coating and Sn/Zn metal spray with a Ti-6Al-4V shim bonded to the longeron using a silver (Ag) filled epoxy adhesive. A tin (Sn) plated ferrous brad was then bonded to the Ti-6Al-4V shim. The area around this installation was sealed with MIL-S-81733. The carbon epoxy composite cover panel had a like Al shim bonded along the panel edges that would make contact with the conducting brad when the panel was fastened in place with Ti-6Al-4V fasteners.

Electrolyte was provided by the presence of water in the composite matrix of the carbon epoxy longeron and cover panel. Rain, sea spray, and aircraft washing all contributed to the initiation of corrosion of this installation. This entire EMI installation was removed at the depot. Corrosion was removed and general cleanup of the dorsal longeron was accomplished followed by installation of an updated EMI protection system.

The updated EMI protection system consists of:

A Class III chemical conversion coating of the longeron

Followed by an adhesion promoter primer

A polysulfide sealant was put down in two strips leaving a trench 1/4" - 3/8" (6.3 - 9.4 mm) in width. A silver filled fluorosilicon rubber EMI seal is then bonded into the trench formed by the polysulfide, using a fluorosilicone RTV adhesive. (Fluorosilicone was chosen because it is resistant to hydrocarbons.) The contact surface on the carbon epoxy cover panel was retained. (See figures 6/7/8).

7. NAVAIRWATCENDWAR is developing a conductive corrosion inhibiting sealant, consisting of polythioether filled with Ni coated carbon fibers, and is in use on two test aircraft. All reports to date have been very positive. This new product will eliminate the need for most EMI seals as we know them today by providing both a conductive seal and a corrosion inhibitor in one. Reference (6) provided detailed information on this conductive sealant. See Figure 6-7.

Composite EMI hard/non-corrosive electronic boxes/connectors.

Because of the problem described above, an effort to develop avionic packaging and connectors that are independently EMI hard was initiated 5 to years back. Today, we have the packaging and connectors that can operate in an EMI environment, which will not corrode. This effort used PolyPropylene Sulfuron (PPS) plus Ni plated carbon fibers. PolyEtherEtherKetone (PEEK) is also now being investigated for use in high temperature packaging and connectors. Fabrication is via injection or compression molding, which makes this effort very economical in the long run.

As this program matures, the need for using good conducting cathodic material next to poor or non-conductor material should not be used to provide EMI protection in today's high technology aircraft as it will no longer be required. See Figures 8/9.

8. Ten Al Li 2090 alloy panels have been fabricated and installed on selected F/A-18 aircraft. To date, these panels have performed as well as the original 7075 T73 panels provided with the aircraft. The results of this service tour length evaluation will determine whether more Al Li panels/structures will be used on future Navy aircraft. As Al Li can provide as much as 11% weight reduction, it is being considered for numerous aircraft components/applications.

9. H-60 helicopter has experienced numerous corrosion problems in its early service life. This aircraft was originally procured under the U.S. Army Spec ADS-13, which, at the time, did not address corrosion prevention/control; as strongly as the U.S. Navy SD-24. This aircraft was procured a the U.S. Army Blackhawk attack helicopter. When the U.S. Navy procured this H-60, the Navy and contractor held several meetings to work out ways of improving the corrosion resistance of the helicopter, as the U.S. Navy plans to deploy H-60 primarily in the LAMPS role, exposing the aircraft to saltwater and sea spray on a continuing basis when deployed. All types of corrosion have been seen on Alum (al), Ma (Mg) and steel fasteners/ components have been seen during a standard operational cycle. LAMPS operational/ maintenance crews are aware of this problem.

Today, the corrosion is held to a minimum by a continuous corrosion prevention/control effort on their part, ensuring a high state of material readiness of H-60 aircraft. Composites used in the H-60 airframe are Kevlar, fiberglass, carbon and boron epoxies. To date, there have been no major problems reported with the composite structure. Some minor repairs have been accomplished at sea by LAMPS maintenance crews. As a back-up, the H-60 has a program similar to the F/A-18 DED program that provides engineering guidance to LAMPS crews when needed. This would cover areas not addressed in the aircraft Structural Repair Manual (SMR), i.e., repair that would normally be considered depot, requiring an engineering disposition. See Figures 8, 9, 10.

10. MH-53E aircraft is a state-of-the-art helicopter; however, we have seen some corrosion on the sponson fitting. The sponson fuel tanks are constructed from carbon epoxy composite; the aircraft skin and support fittings are fabricated from 7075-T3. Attaching bolts are not compatible. This combination of material and

insufficient corrosion inhibiting sealant in an electrolyte result in pitting corrosion, requiring replacement of the support fitting in several aircraft.

Two major sources of the electrolyte were identified as water in the carbon epoxy composite matrix and cold fuel being pumped into aircraft during hot weather, resulting in condensation forming on metal components. Corrective action for this problem was initiated by the CFA. During replacement of the support fitting, additional corrosion inhibiting sealant, MIL-S-81733 polysulfide, was applied to both sides of the new fitting and faying surfaces of aircraft skins. See Figure 11.

This effort may not stop all corrosion of the fitting; however, it should reduce the corrosion. We expect to see some corrosion around the attaching bolt holes, as the fastener will continue to be an electrical transmission path between the carbon epoxy composite and the Al sponson fuel tank support.

Ref: (1) AGARD-AG-278 Corrosion Handbook Vol (1)

(2) Dr. J. J. Deluccia, G. T. Browne
Tri-Service PC 1991 Present and Future Aircraft
Materials and Processes for Corrosion Prevention
and Control

(3) AGARD Report 785 R. C. Cochran
T. M. Donnellan R. E. Trabocco Naval Air
Warfare Center Aircraft Div Warminster PA

(4) NASA Welding Bonding Fastening
NASA CP2387 dated 1984

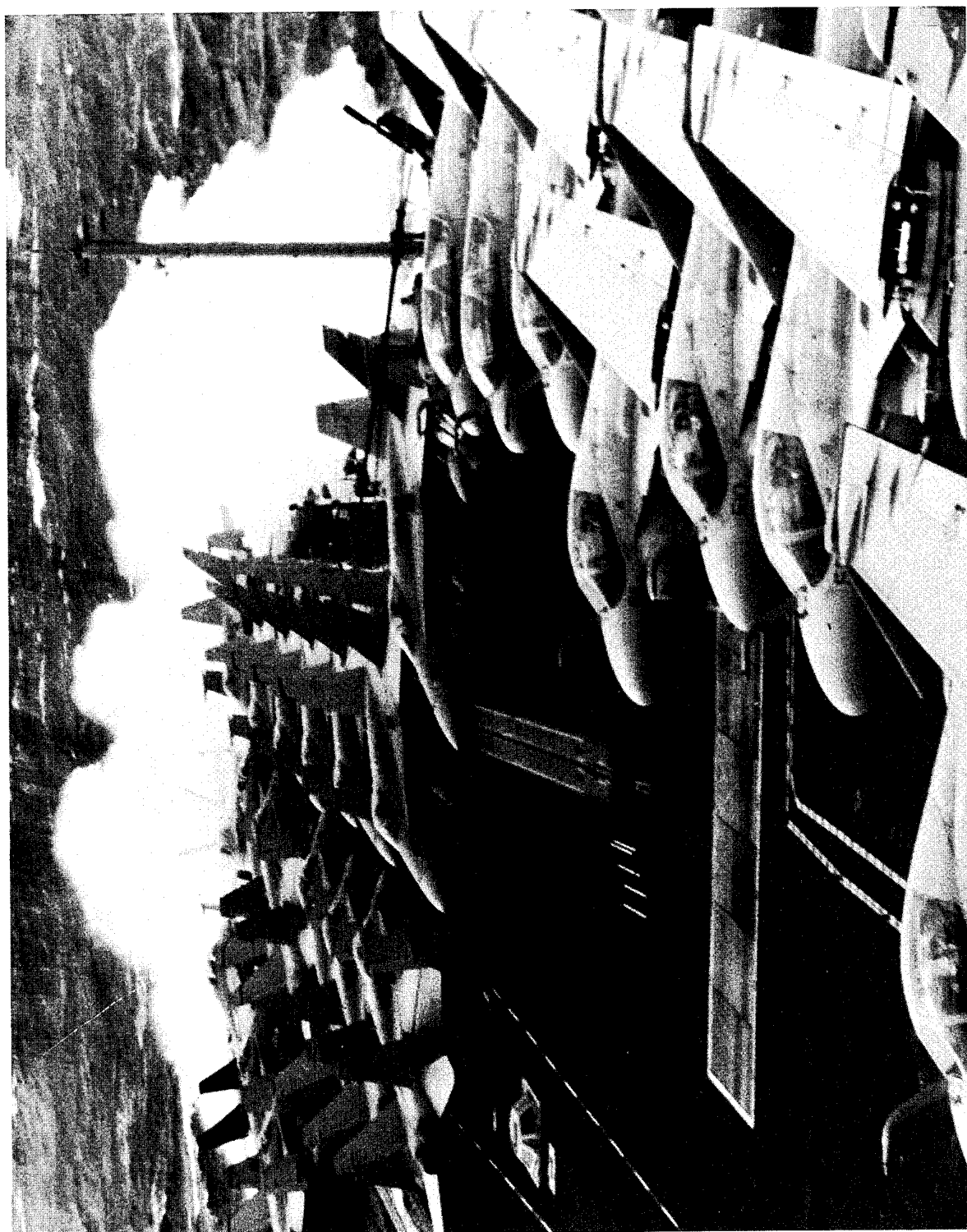
(5) Eighth DOD/NASA/FAA Conference of
Fibrous Composites in Structural Design (NASA
Conf Pub 3087 Part 2) dated Nov 28-30 1989

(6) J. T. Thompson, Wendy W. Lin Air
Vehicle & Crew System Technology Dept.
NAVAIRWARCENNADWARPA Report Nr
NADC8021-60

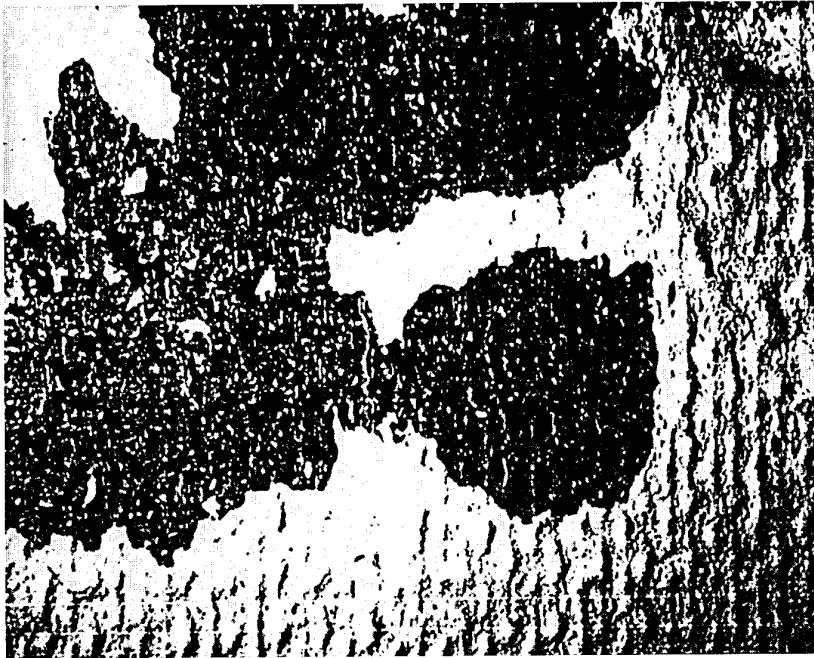
(7) G. T. Browne AGARD Report N0733
Workshop on Avionic Corrosion Control Oslo
Norway 1986

????? PROBLEM ?????

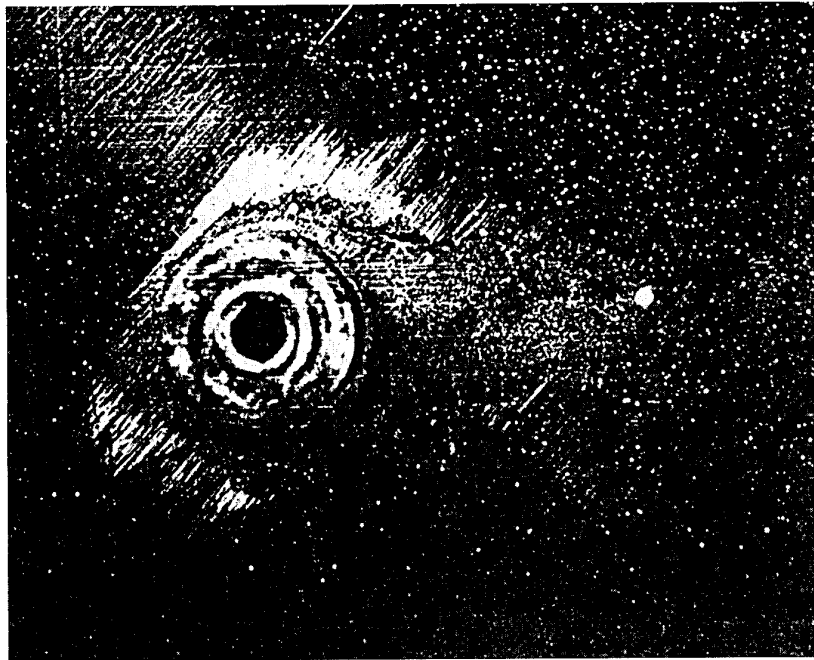
1. LACK OF COMMUNICATION BETWEEN ENGINEERING DISCIPLINES?
2. DO YOU KNOW HOW THE SELECTED MATERIAL WILL ACT WHEN EXPOSED TO THE OPERATING ENVIRONMENT WHERE THE MATERIAL IS USED?
 - a. AS IS?
 - b. MECHANICALLY ATTACHED TO ANOTHER MATERIAL?
 - c. BONDED TO ANOTHER MATERIAL?
 - d. IS THE BONDING ADHESIVE HYGROSCOPIC?
3. WHERE DO THE JOINED MATERIALS STAND IN THE GALVANIC SERIES?
 - a. HAVE YOU CONSTRUCTED A POTENTIAL BATTERY?
4. WHAT WILL BE THE RESULT OF CORROSION IN THE STRUCTURE WHEN EXPOSED TO CYCLIC LOADING?



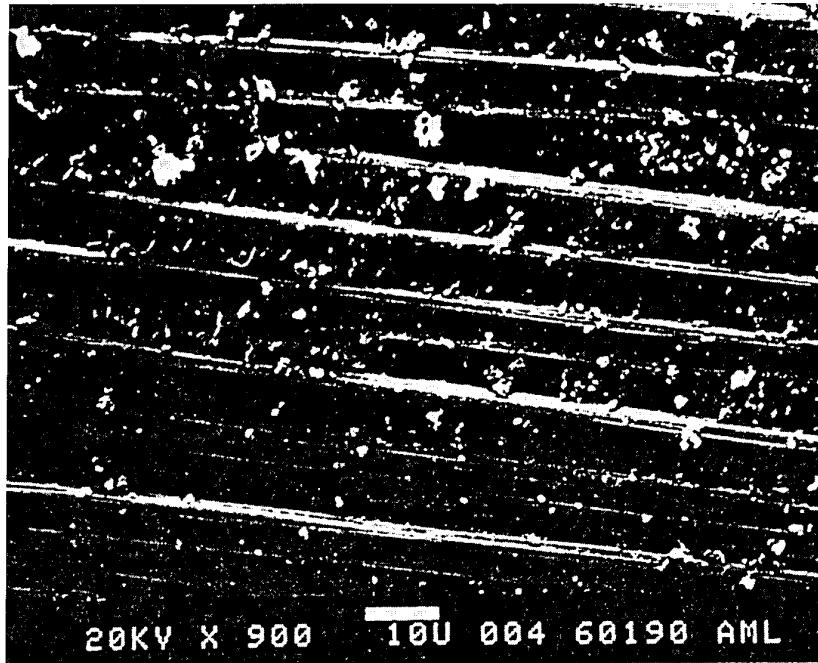




5250-4 BMI 30 Days Salt Spray



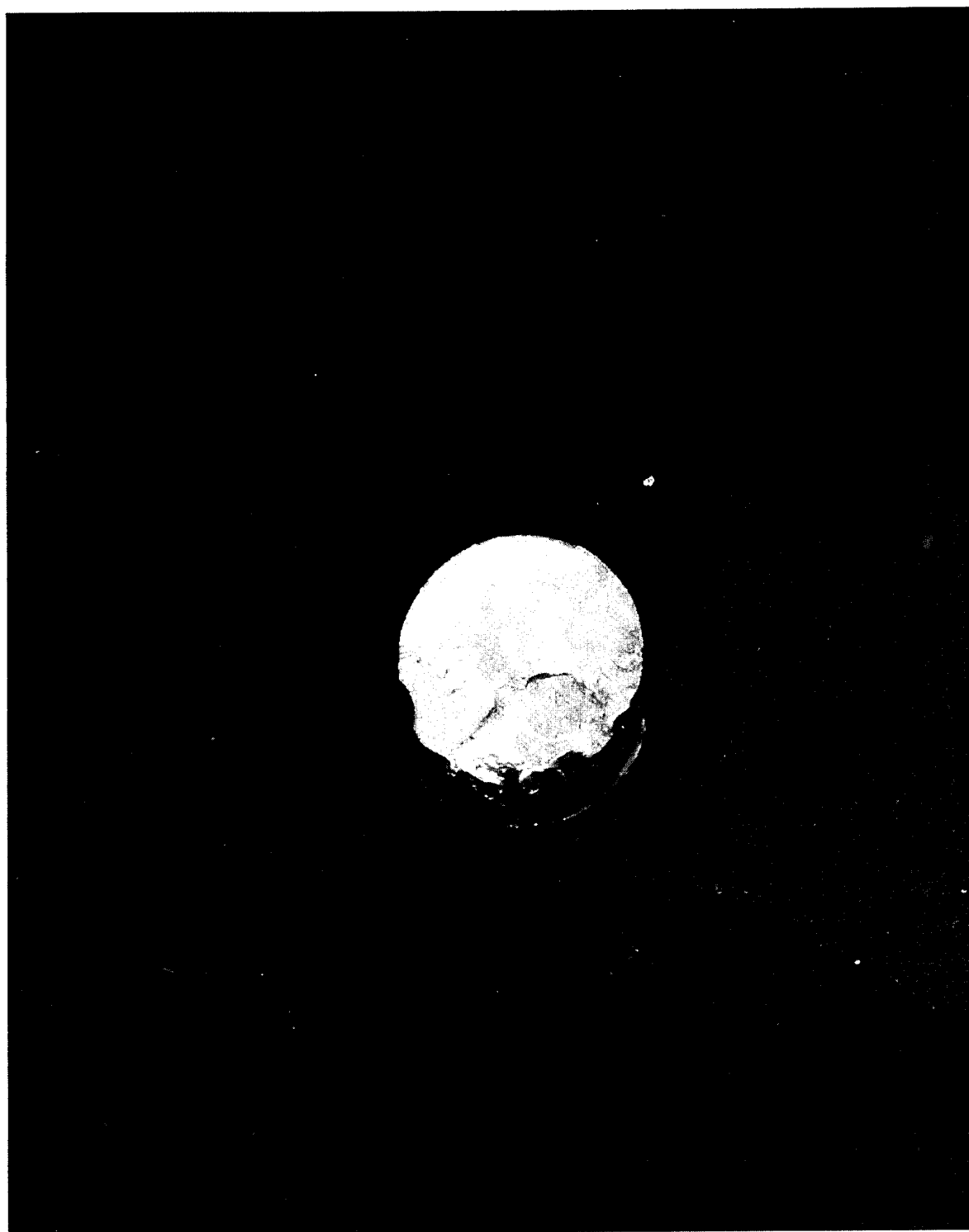
Front Side Primed & Topcoat Aluminum



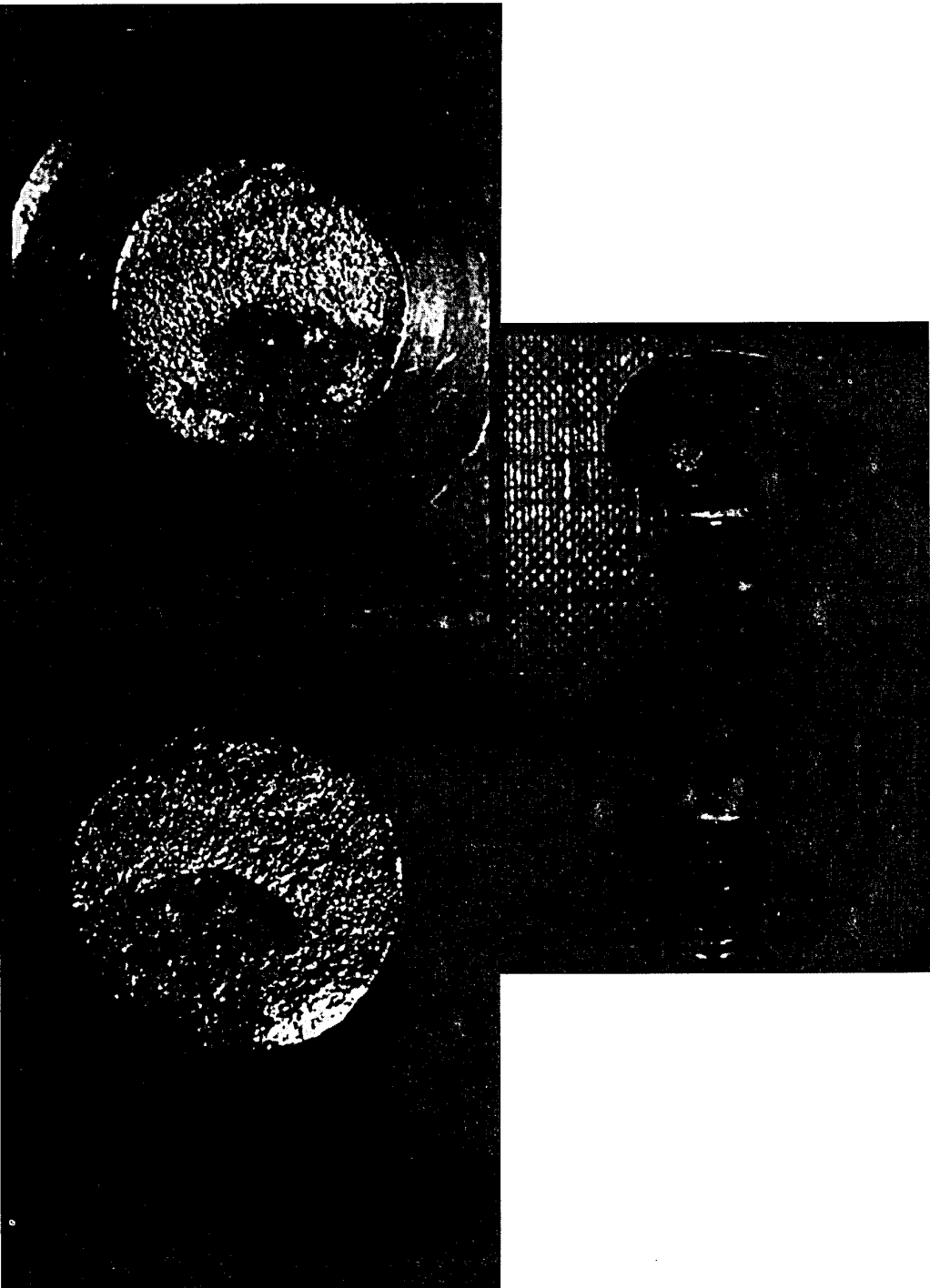
V-378 BMI Salt Water



V-378 Salt Water



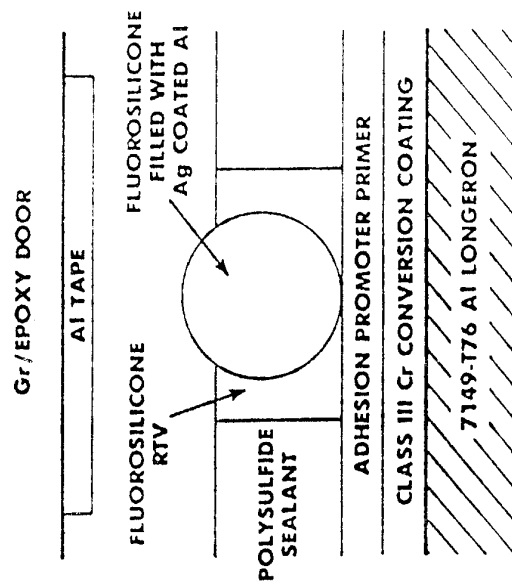




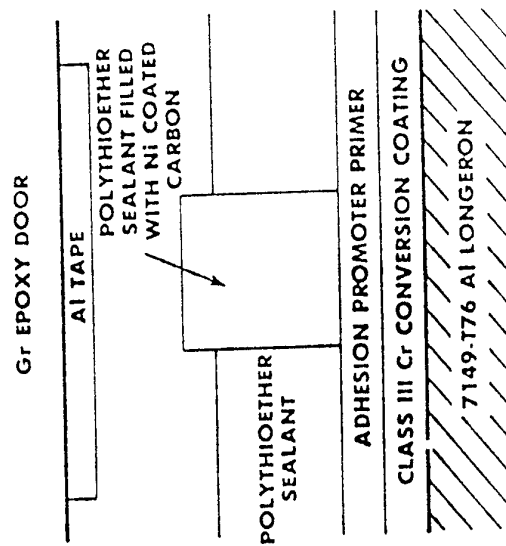
Stress Corrosion Cracking

13-8 Stainless Steel Fastener from outer wing panel of F-18

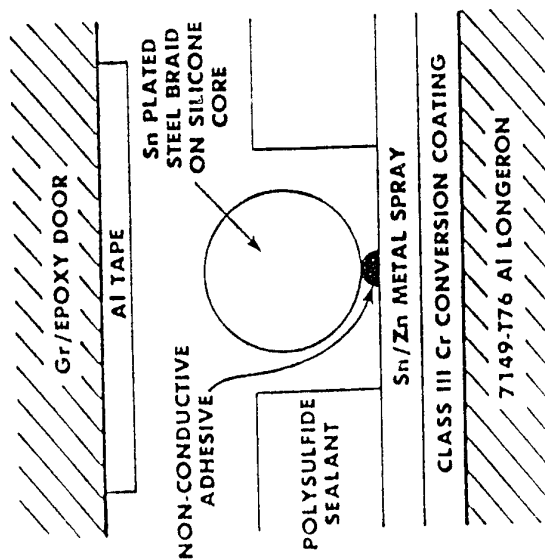


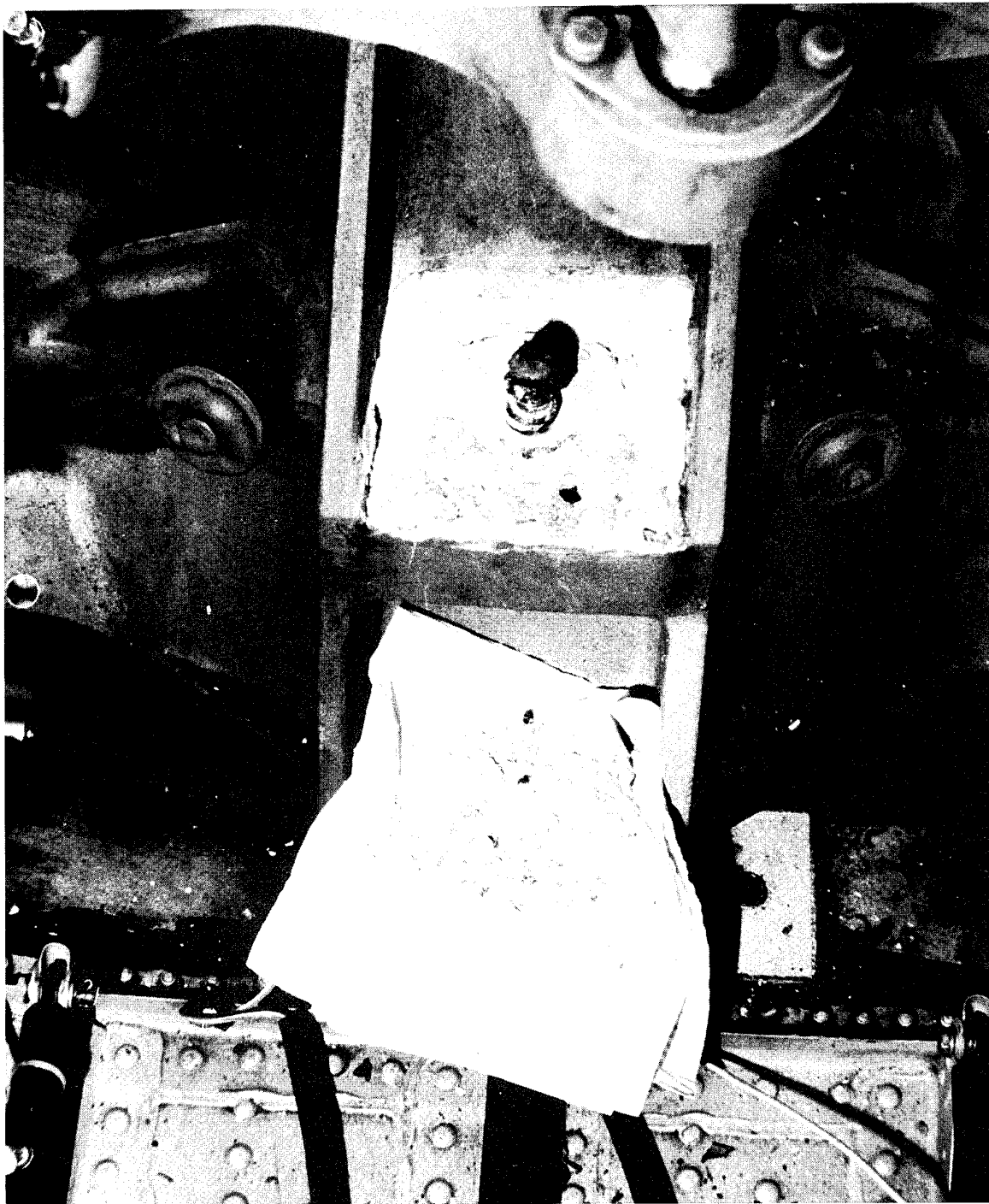


(b)



(a)





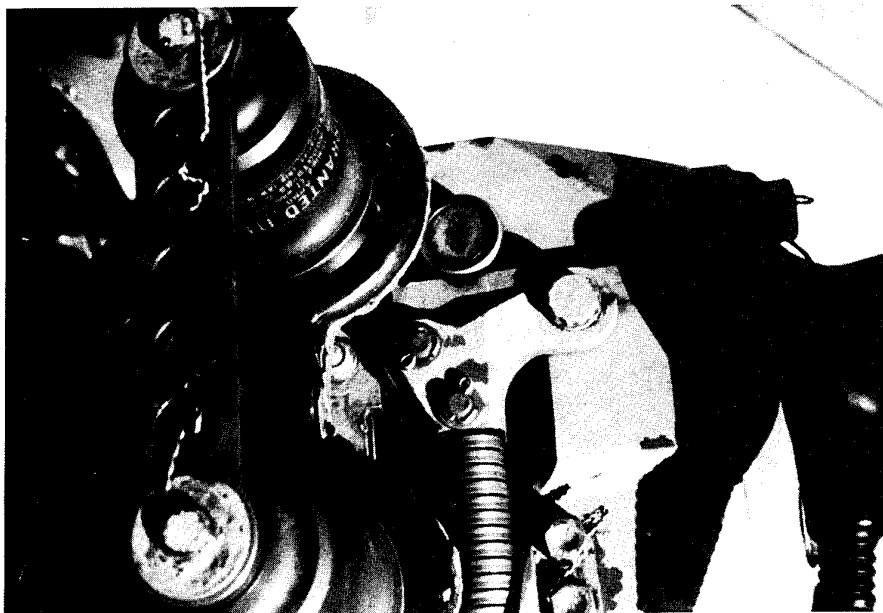
- Main Gearbox Fwd Flight Control Bridge Mounting Pad Corrosion
Resulting in Excessive Scrappage of Housings



- SH-60F LH Avionics Access Door Gasket Corrosion .
Typical of Corrosion Seen Under Other EMI Conductive Gaskets



MR TIP CAP CORROSION ADJACENT TO ATTACHMENT SCREW



MAIN ROTOR HEAD CORROSION



CORROSION IN SERVICE EXPERIENCE WITH AIRCRAFT IN FRANCE

M.J. FRUSTIE
AEROSPATIALE
Service Matériaux et Procédés
Division Avions

Mr. P. GAUTHIER
DCAe/CTMS
23, Avenue Henri Gillaumet
31056 TOULOUSE Cedex
FRANCE

1 - RESUME

Le but de cette communication est de présenter à partir d'une comparaison des corrosions observés sur avions modernes (Airbus, ATR) et des corrosions sur avions plus anciens (Transall, Caravelle) les progrès réalisés dans la maîtrise de la corrosion, grâce à l'adoption de matériaux et de protection plus performantes.

Pour bien appréhender l'avenir, il faut aujourd'hui que la technique s'adapte aux contraintes dues aux nouvelles dispositions législatives concernant l'environnement qui amènent à rechercher de nouveaux matériaux et système de protection.

2 - LE CONTEXTE

La corrosion est toujours un souci majeur des constructeurs d'avions civils ou militaires.

D'une part elle peut diminuer considérablement la durabilité des appareils ou parfois même affecter la sécurité, d'où une grande sensibilité des clients dans ce domaine.

D'autre part, la tenue à la corrosion est difficile à appréhender car :

- la prévision est difficile, le remède consiste à prévenir par des protections adéquates.
- Les solutions aux problèmes de corrosion sont à adapter à chaque nouvel appareil qui présentent des nouveautés de conception,

- les éventuelles inadaptations des protections anti-corrosion ne sont révélées qu'après plusieurs années d'exploitation,
- la durée de vie d'un avion est de plus en plus longue,
20 ans en 1960
30 ans et plus pour les avions développés plus récemment,
- les traitements de surface et produits anti-corrosion utilisés à ce jour sont amenés à disparaître suite à la mise en place de législations environnementales.

Le but de cette communication est de présenter la façon dont nous avons progressé dans la maîtrise de la corrosion, les résultats acquis et les orientations nouvelles.

3 - ACTIONS ENGAGEES VERS LA MAITRISE DE LA CORROSION

Pour progresser dans la maîtrise de la corrosion, nous avons mis en place il y a une douzaine d'années une série de mesures visant à :

- prendre en compte, dès la conception, les risques de corrosion,
- améliorer nos traitements de surface et nos produits anti-corrosion,
- renforcer les dispositions et notamment prendre en compte les recommandations IATA GEN2637

- animer des séances de sensibilisation auprès de nos personnels de production et de nos sous-traitants,

Tout récemment, nous avons lancé avec le support du STPA/CTMS une vaste étude qui nous a permis de faire le point de la situation, vérifier l'efficacité de ce plan d'actions et mettre en exergue les points sur lesquels devaient encore porter nos efforts.

La démarche adoptée a consisté à

- dresser un inventaire de tous les cas de corrosion* observés en service et connus de l'Aérospatiale sur les avions modernes tels que A310, A300-600, A320 et ATR,
- étudier tous ces cas de corrosion en détail, chaque cas de corrosion* faisant l'objet d'un dossier précisant la zone affectée, le nombre d'appareils concernés, le délai d'apparition de la corrosion, les matériaux et protections en présence, l'origine de la corrosion, les modifications apportées, l'efficacité des remèdes apportés après quelques années en service,
- identifier les zones les plus sensibles à la corrosion,
- analyser l'évolution des types de corrosion constatée,
- conclure sur les améliorations apportées sur les avions modernes.

4 - ANALYSE

Une comparaison des corrosions observées sur nos avions modernes avec celles constatées traditionnellement par exemple sur Transall, Caravelle nous ont permis de tirer un certain nombre de conclusions.

4.1 Les zones concernées par la corrosion se trouvent toujours préférentiellement dans les parties basses du fuselage, au niveau des portes et au voisinage des toilettes et galleys

Ces corrosions sont dues à la présence d'eau, de fluides hydrauliques, liquides de nettoyage etc ... qui se répandent et stagnent.

Par contre, dans les zones carburant, les problèmes de corrosion ont disparu. Le seul cas rencontré se situe au niveau des portes trou d'homme de voilure doivent être métallisées et ne peuvent donc recevoir la protection standard OAC + primaire anti-corrosion et montage au mastic lors de l'assemblage.

4.2 Parmi les corrosions observées sur nos avions modernes, les cas de corrosion les plus fréquents sont d'origine galvanique ou intergranulaire (voir planche 1) et on peut constater qu'un certain nombre de types de corrosion traditionnels n'existe plus sur les avions nouvelle génération grâce aux améliorations apportées. (Voir tableau suivant).

* On parle de cas de corrosion lorsqu'il y a apparition d'un même type de corrosion dans une même zone sur différents appareils.

Types de corrosion observés sur avion ancienne génération	Constat sur nos avions modernes	Observations
Corrosion par piqûre	Nombre de cas en régression mais problème encore présent	La régression est due à : - la généralisation de l'OAC - l'adoption de primaires peinture plus performant - la présence de mastic d'étanchéité
Corrosion intergranulaire (d'origine non galvanique)	Problème encore présent en présence du 2024 tôle épaisse	Le remplacement par du 7175 T7351 permet de remédier à ce problème
Corrosion par confinement	Problème maîtrisé	Maîtrisé grâce aux directives données pour concevoir le drainage et l'installation des matelas d'isolation thermique et grâce aux protections anti-corrosion
Corrosion filiforme	Problème maîtrisé	- se manifestait essentiellement en surfaces extérieures, - maîtrisé depuis l'adoption de l'OAC à l'extérieur et de gamme de peinture résistant à la corrosion filiforme
Corrosion microbienne	Problème maîtrisé	Maîtrisé grâce à l'adoption en milieu réservoir d'OAC et primaire anti-corrosion
Corrosion sous-contrainte	Problème maîtrisé	Maîtrisé par l'utilisation de matériaux plus performants et une meilleure connaissance de ceux-ci.
Fretting corrosion	Problème encore présent localement	Des améliorations sont à l'étude
Corrosion galvanique	Toujours présent	Encore très présent notamment dans le cas de structures démontables ou de métallisation car dans ces cas on ne peut utiliser de mastic intercalaire pour isoler et éviter le phénomène de pile

4.3 Les corrosions galvaniques observées proviennent le plus souvent de couplage inox/aluminium mais plus récemment on commence à trouver des cas de corrosion carbone/aluminium (voir planche 2).

4.4 L'ensemble des modifications apportées en service et en production visant à corriger les problèmes de corrosion par changements de matériaux et/ou de protection, renforcement de l'étanchéité et parfois modification de conception, s'est avéré après quelques années d'exploitation efficace dans tous les cas.

4.5 Conclusions :

L'étude réalisée montre que l'on maîtrise de mieux en mieux les phénomènes de corrosion et que le plan d'action mis en place a été efficace : certaines corrosions telles que les corrosions microbiennes et filiformes qui ont beaucoup sévi dans le passé ont maintenant disparu.

5 - ORIENTATION NOUVELLES

Pour bien appréhender l'avenir, il faut aujourd'hui que la technique s'adapte aux contraintes dues aux nouvelles dispositions législatives concernant l'environnement.

Bon nombre de traitements de surface et de produits anti-corrosion ne pourront plus être utilisés soit parce qu'ils mettent la santé des opérateurs en jeu lors de leur mise en œuvre soit qu'ils peuvent être source de dégradation de l'atmosphère.

Nombreuses sont les directives prises par les gouvernements concernant les substances polluantes. L'une des plus sévères est sans nul doute l'amendement sur la propreté de l'air (Clean Air Act) promulguée en 90 aux USA. Cette loi qui concernait au départ les CFC a porté de 8 à 189 le nombre de substances polluantes devant être réglementé (règlement NESHAP : National Emission Standard For Hazardous Air Polluant).

Ce règlement applicable d'ici fin 98 vise à interdire, en particulier : le méthylethylcétone, chlorure de méthylène, l'hexane, le toluène, les composés chromiques etc ... ce qui va nous conduire à remplacer toutes nos peintures, tous nos mastics, tous nos décapants, tous nos revêtements spéciaux, nos traitements de surface : OAC, chromatation, Nickelage, Chromage, ou bien à repenser entièrement notre système anti-corrosion.

D'où 2 voies de recherche menées en parallèle :

1ère voie : Recherche de produits de remplacement :

Le travail s'avère difficile, long et coûteux. En effet, ce travail va non seulement entraîner de nouvelles qualifications mais va également demander la modification des procédés de mise en œuvre et des moyens industriels ainsi que la mise en place d'équipements de contrôle de la pollution.

De plus, les produits de remplacement, pour nos applications, n'existent pas toujours sur le marché et quand ils existent, ils ont des performances inférieures aux produits actuellement utilisés, ce qui va à l'encontre de notre souci permanent d'améliorer la tenue à la corrosion de nos structures.

2ème voie : Repenser notre système anti-corrosion :

Par adoption de matériau alliage d'aluminium plus performant à la corrosion que les alliages conventionnels 2024 et 7075, et qui n'auraient pas besoin de revêtement anti-corrosion.

Nous avons engagé des travaux dans ce sens d'une part avec Rhénalu, d'autre part avec Alcoa.

Les premiers résultats de laboratoire sont encourageants mais beaucoup de travail reste à réaliser avant de passer au stade industriel.

5 - CONCLUSIONS

Pour mener à bien ces travaux de recherche, conciliant contraintes environnementales et tenue à la corrosion, et adopter dans les meilleurs délais des dispositions acceptables Aerospatiale a mis en place des dispositions nouvelles.

- travail en équipe composée de spécialistes bureau d'études/production/toxicologues et juristes,
- hiérarchisation des priorités
- coopération nombreuses aéronautiques et hors aéronautiques.

PLANCHE 1

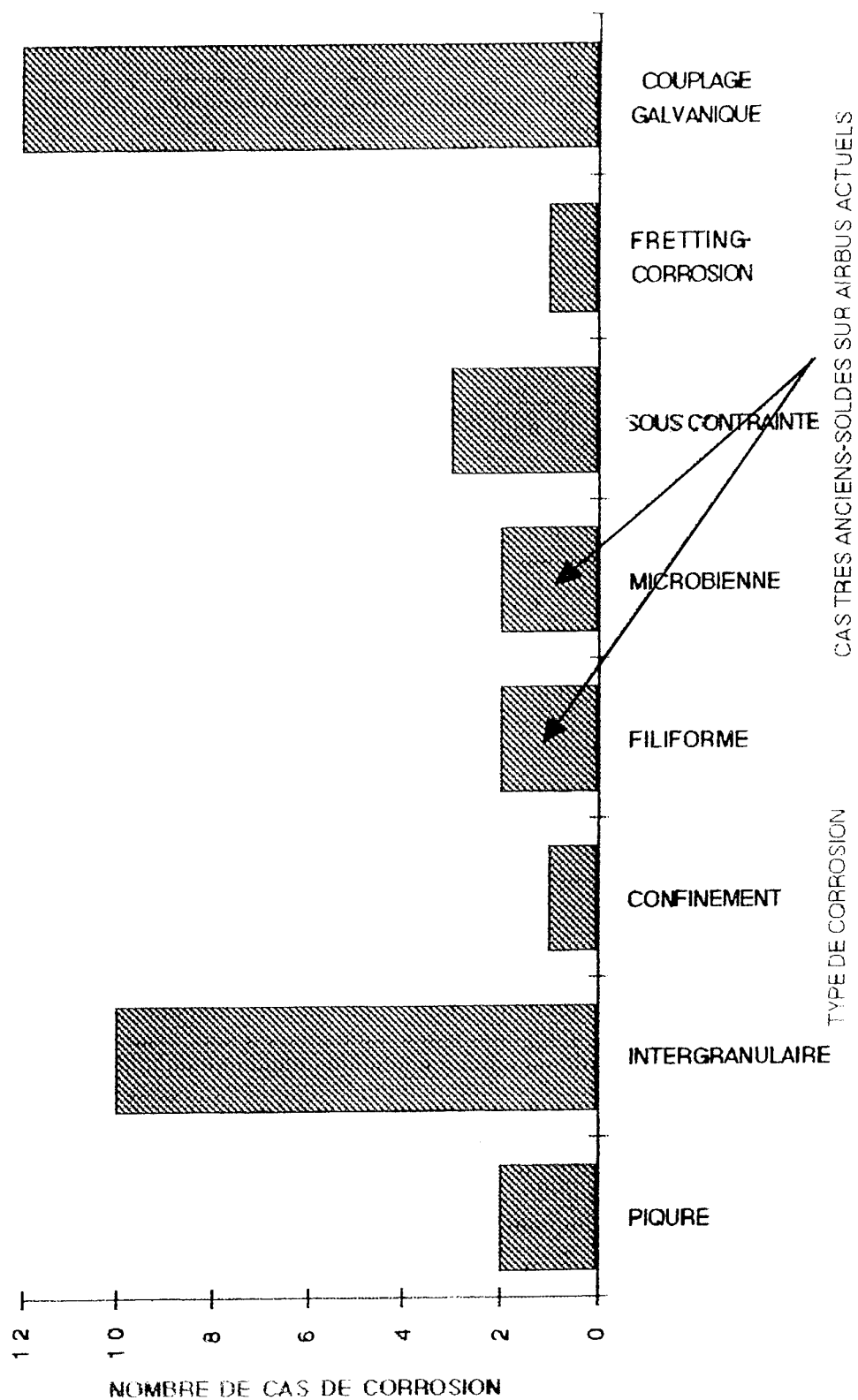
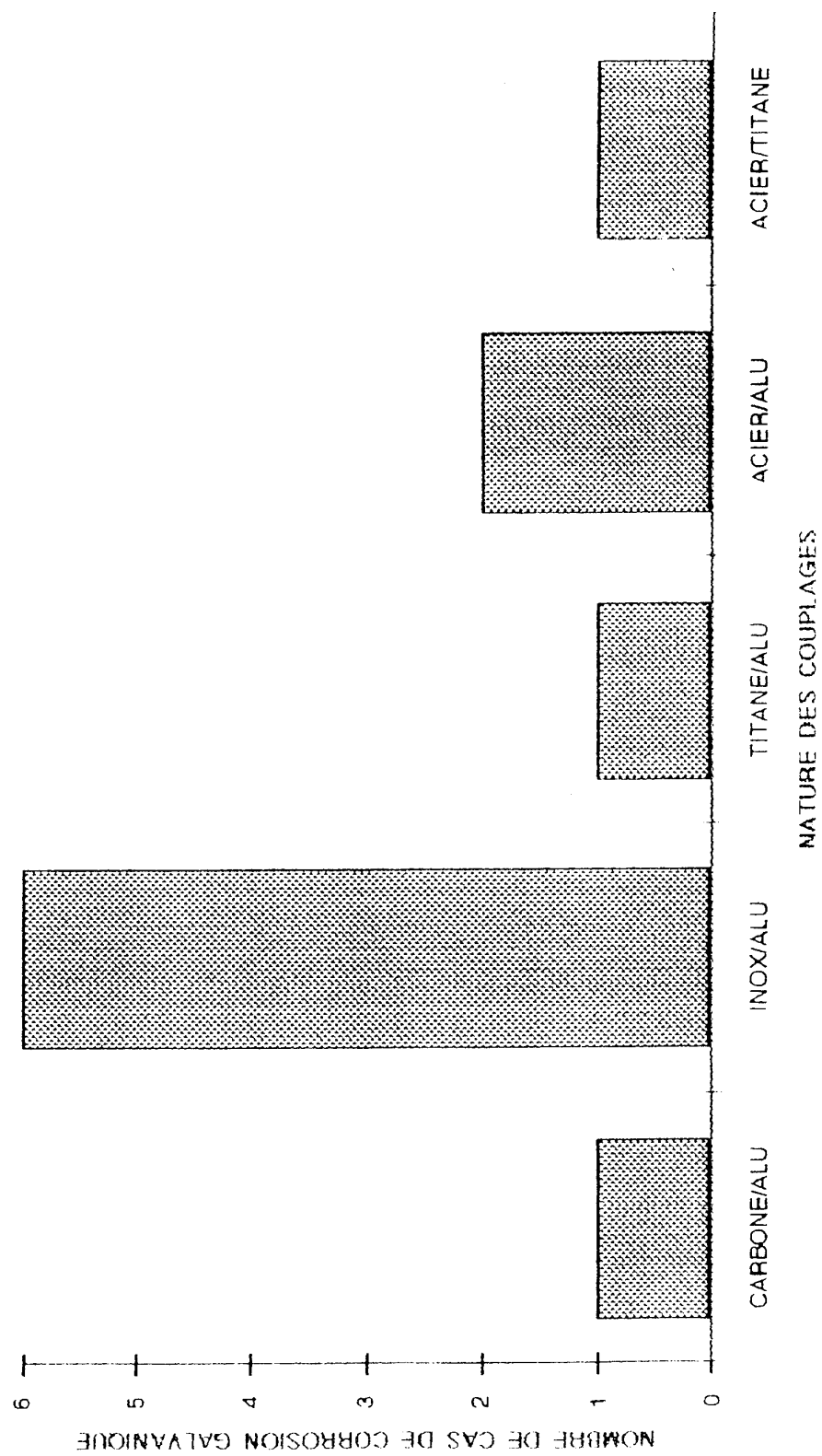


PLANCHE 2



OKLAHOMA CITY AIR LOGISTICS CENTER
(USAF) AGING AIRCRAFT CORROSION PROGRAM

Donald E. Nieser, P. E.
U S Air Force
OC-ALC/LACRA
3001 Staff Dr Ste 2AC489D
Tinker AFB OK 73145-3019

SUMMARY

Because of projected reductions in future defense budgets, less money will be available for new aircraft acquisitions. Consequently, many of the current aircraft will have to be maintained well into the twenty-first century. As they continue to age, the time-dependent effects of material degradation, due to corrosion, will become more significant. Having to maintain aircraft three to four times their original design life presents a unique new set of complex technical problems and challenges. The primary concern is the reduction of airframe fatigue life and static strength due to widespread corrosion damage, fatigue, embrittlement, material loss due to corrosion, intergranular corrosion attack, fretting and stress concentrations.

In an effort to ensure continued airworthiness and flight safety, an aggressive program plan has been developed and implemented at Tinker AFB to try to solve the corrosion problems and fatigue related problems to prevent the occurrence of catastrophic structural failures. The program consists of (a) invasive disassembly of a complete C/KC-135 and sections of B-52 and Boeing 707 aircraft, (b) corrosion documentation/information system development, (c) analysis and testing the effects of corrosion on structural integrity, as well as corrosion growth rates, (d) corrosion modeling and development of C/KC-135 service life extension strategies, (e) and comprehensive evaluation of nondestructive inspection/testing (NDI/NDT) equipment for hidden corrosion detection and quantification. This program has been extensively coordinated with USAF Wright Labs, AFOSR, Naval Air Warfare Center, FAA Aging Aircraft Center, NASA Langley, industry and academia.

INTRODUCTION

As a result of decreasing future defense budgets, procurement of a limited number of replacement aircraft is projected for the U S Air Force. Limiting the number of aircraft acquisitions is, therefore, a de facto decision to extend the life of existing aircraft, assuming constant mission requirements. Current phase-out projections of many USAF aircraft reveal life spans of

unprecedented length. Some will be in the 60- to 80-year-old range. Out to year 2010, most C/KC-135s, B-52s, C-5As, C-141s, older C-130s, T-37s, and T-38s will still be in service. The average age of all of these aircraft will be between 40 and 50 years old.

The reality of trying to maintain aircraft airworthiness over an unprecedented 60- to 80-year life span presents a whole new set of technical problems/issues that the original design did not have to meet. It cannot be treated as business as usual, and is neither cost, nor risk free. Future operational readiness, availability, and flight safety are at risk. These aircraft were designed for a finite life span of approximately 20 to 30 years, and corrosion-induced material degradation was not considered. Original aircraft life spans assumed preventative maintenance up to, and including, depot level maintenance. The original manufacturers caution that to maintain structural airworthiness for three to four times original design life, some type of major structural modifications or life extension update would be required.

Because of a lack of data related to aging aircraft corrosion, and in an effort to answer questions concerning C/KC-135 structural life, as well as trying to determine the structural modifications and refurbishment required to ensure airworthiness out to 2040, an extensive and comprehensive program was planned and implemented. This OC-ALC Aging Aircraft Disassembly and Hidden Corrosion Detection Program (OC-ALC Aging Aircraft Corrosion Program, short title) was started in FY92. Because no other USAF aging aircraft corrosion efforts existed, but extensive efforts did exist concerning wide spread fatigue damage and multi-site damage (MSD), it was recognized that many areas of corrosion investigation and evaluation would have to be conducted. These efforts were driven by necessity and the cognitive identification of potential structural integrity problems and proactive drive to solve them before aircraft were lost due to catastrophic structural failures.

The program plan consists of: (1) evaluation, identification and development of nondestructive

inspection /testing (NDI) (NDT) equipment to detect and quantify hidden corrosion, (2) invasive disassembly of C/KC-135 aircraft to determine and map the location and severity of hidden and inaccessible corrosion, (3) testing and analysis to determine the effects of corrosion and fatigue on aircraft structural integrity, (4) determination of corrosion growth rates, (5) development of empirical corrosion prediction models, (6) development of a computer data base to document aircraft corrosion and maintenance history (7) development of modifications and maintenance actions to ensure C/KC-135 airworthiness to 2040 along with cost benefit analyses. This paper includes a discussion of all areas of the OC-ALC Corrosion Program and some of the test data already collected.

C/KC-135 AIRCRAFT

One of the most critical aircraft in the USAF fleet, in terms of aging aircraft corrosion, is the fleet of C/KC-135 air refueling tankers and special purpose aircraft. There are approximately 600 C/KC-135 aircraft of 32 different types operating around the world. As of 1994, the average age was approximately 34 years, with some 39-year-old aircraft still operating as shown in Figure 1. C/KC-135 aircraft are projected to be in service until 2040. In fact, calculations using a predicted minimum fatigue life of 43,200 flight hours for the upper wing skin and fuselage skin and based on current annual flight hours, reveal a notional service life of over 80 years. However, these numbers taken alone are misleading or unconservative as they do not include the material strength degradation effects of corrosion. It is predicted that corrosion induced material strength degradation and the combined effects of corrosion and fatigue will limit structural life to less than 2040.

Because of the unique fuselage construction (spot-welded lap joints and spot-welded doublers), the C/KC-135 fuselage is probably more susceptible to hidden crevice type corrosion than any other USAF aircraft. Two layers of bare aluminum were joined together without primer or sealant protection. Only a slight amount of moisture can create the corrosion galvanic couple. A portion of the fuselage surface area contains spot-welds. Figures 2 and 3 show a typical riveted lap joint with associated corrosion.

MAJOR PROGRAM ELEMENTS

1. Evaluation/Identification of Non-Destructive Inspection Equipment (NDI)

Because of the C/KC-135 spot welded fuselage lap joint and doubler construction, some effective means of detecting hidden corrosion is urgently needed. Non-destructive evaluation/inspection efforts within the FAA Aging Aircraft program, NASA and the Materials Directorate of Wright

Labs was investigated, but none of these were directly applicable. Therefore, a systematic trade-off study was implemented to review off-the-shelf NDI equipment to determine applicability and capability to effectively detect and accurately quantify hidden corrosion. The scope was narrowed initially to include the two most important problems on the C/KC-135, E-3 and B-52, corrosion between layers of fuselage lap joint skins and corrosion around and adjacent to wing skin fasteners. Figure 4 depicts the type of corrosion encountered around wing skin fasteners.

In conjunction with the complete invasive disassembly of the first C/KC-135 aircraft retired, the unique opportunity was seized to prove or disprove the effectiveness of NDI equipment in detecting hidden corrosion by comparing NDI equipment inspection results with the actual corrosion found when the aircraft structure was disassembled. Coupons or specimens were cut from the disassembled aircraft and used for the NDI equipment evaluations.

Scope

The effort to identify and evaluate off-the-shelf NDI equipment that required little or no modification included the following tasks: (Task 1) Conduct a survey of available off-the-shelf NDI equipment capable of detecting hidden corrosion, (Task 2) Determine desired NDI equipment characteristics, determine trade-offs, and develop criteria for evaluating the ability of NDI equipment to detect hidden corrosion, (Task 3) Identify and compare NDI equipment candidates suitable for test and evaluation, (Task 4) Evaluate off-the-shelf NDI equipment at two demonstrations (the first demonstration, evaluate the capability of the equipment to detect hidden corrosion on representative aircraft coupons test samples taken from retired Air Force aircraft and in the second demonstration, evaluate the capability of equipment that performed well in the first demonstration to inspect an actual aircraft containing hidden corrosion), (Task 5) Analyze demonstration results, identify the highest rated NDI equipment and make recommendations.

First Demonstration (Laboratory Coupons)

The objective of the first demonstration was to evaluate the capability of off-the-shelf NDI equipment to detect hidden corrosion in fuselage lap joints and in wing skin adjacent to and under wing fasteners. Twenty vendors participated in the demonstration, which was conducted by ARINC Research Corp from 29 Jun through 24 Jul 92 at the Metro-Tech Aviation Career Center in Oklahoma City OK. Three primary Scoring parameters were identified: Corrosion detection, false calls, and scan rates.

The demonstrated equipment represented six types of technologies: eddy current, ultrasonic, thermal imaging, shearography, acoustic emission, and enhanced visual inspection. Depending on the capability of their equipment, vendors inspected samples of aircraft structures (coupons) from lap joints of C/KC-135 aircraft or coupons from wing skin of B-707 aircraft (representative of E-3 AWACS) and from B-52 aircraft. Equipment that rapidly inspects large areas (large-area rapid scan equipment) inspected an intact lap joint on a retired Boeing 727 aircraft.

Vendors inspected the coupons and marked their estimates of the location and extent of corrosion on a Mylar sheet. The vendors that inspected the B-727 lap joint marked their results on the aircraft, using erasable marking pencils. The marks were photographed and videotaped, then erased before the next inspection. After the inspections, the coupons were invasively disassembled by Boeing Wichita to determine actual hidden corrosion, but the B-727 was not disassembled.

Results

In terms of the most important scoring parameter, corrosion detection, only four vendors did well (Figure 5). These vendors were invited back for the second demonstration. The low percentage of accurate identifications of corrosion for all inspecting the wing skin coupons rendered the results of the wing skin coupon inspections inconclusive (Figure 6). Only two of the five vendors that inspected the B-727 lap joints were able to detect corrosion in the lap joints; the other three were unable to successfully complete the demonstration.

Second Demonstration (On-Aircraft)

The demonstration was conducted by ARINC Research Corp, 10-26 May 94, at Tinker AFB OK and objectives were as follows: (1) Determine the capability of NDI equipment to detect hidden corrosion in fuselage lap joints of C/KC-135 and E-3A aircraft, (2) Determine the capability of NDI equipment to detect hidden corrosion in wing skin adjacent to and under wing fasteners of C/KC-135, E-3A, and B-52 aircraft, (3) Evaluate the human factors associated with using the NDI equipment.

Eight of the invited vendors participated, demonstrating equipment representing four types of technologies: eddy current, ultrasonic, thermal imaging, and enhanced visual inspection. They inspected lap joints and wing skin fasteners on actual aircraft undergoing depot overhaul. The procedure for recording results was similar to that used in the first demonstration, with the addition of a final step. Results were recorded on an ARINC developed computer representation of the inspection area, allowing for fully computerized

scoring. After the inspections, two lap joint inspection areas and one wing skin fastener inspection area was cut from the C/KC-135 and subjected to invasive disassembly. The results were scored in terms of the most important scoring parameter, corrosion detection. Corrosion detection encompasses the accuracy and sensitivity of corrosion detection and was scored on the basis of hidden corrosion actually detected.

Inspection Results

The chart in Figure 7, represents the comparison of the vendor corrosion detection results for the on-aircraft demonstration on Baseline Lap Joint Sample #1 to the actual corrosion found in the sample. The "Actual" strip was produced by the Topographic Radiscopy corrosion mapping technique developed by the Materials Directorate at Wright Laboratories.

The output from the computerized data comparison is the bar charts in Figure 8 which show the detection and false call results for Baseline Lap Joint Sample #1. The optimum result would be 100% detection rate and 0% false call percentage. While the lap joint results were encouraging and lead to recommendations for system prototyping, wing skin results were again discouraging, and no systems were recommended. The systems recommended for lap joint inspection and purchased for prototyping were two dual frequency eddy current systems, one with C-SCAN display and one impedance plane display. An enhanced visual imaging system was also purchased. These three systems and associated inspection procedures are currently undergoing corrosion detection reliability testing and Air Force verification testing. This equipment will be used on the depot maintenance line starting in early 1995.

Future

Implementation of the long-term phase of the NDI project has begun. This phase will evaluate NDI technologies and techniques that are newly developed or advanced since the evaluation of "off-the-shelf" equipment and may provide significant improvement in detection of corrosion. A series of these evaluations are planned in order to continually capture NDI improvements that may be in various stages of development. The first evaluation is scheduled for mid 1995.

2. Aircraft Disassembly and Corrosion Documentation/Mapping

In an effort to determine if there is hidden/inaccessible corrosion on the C/KC-135 aircraft that is not detected and, therefore, not fixed or treated during depot maintenance, it was decided to completely cut up and disassemble a whole aircraft. Coincidentally, the first C/KC-135 retired was the aircraft offered for

disassembly. It was an EC-135H (S/N 61-10291), had spent most of its life at Mildenhall AB England and had a history of corrosion problems. The objectives were: (1) Map and document the location and severity of corrosion and/or fatigue cracks, (2) Use specimens in the evaluation of non-destructive inspection equipment to detect the hidden corrosion, (3) Use these naturally corroded specimens for accelerated fatigue testing to determine the effects of corrosion on structural integrity, (4) Help in the identification of structural components that may be candidates for life extension/ major modification, repair or replacement.

Data from the 1972 teardown inspection of the KC-135 cyclic test aircraft, C/KC-135 history, commercial teardown inspections of Boeing 707/Boeing 737 airplanes, and Commercial Aging Fleet Service Bulletins were reviewed to help identify potential sections on a KC-135 aircraft which would be most likely to exhibit corrosion, stress corrosion and fatigue damage. Particular emphasis was put on sections of the aircraft that are difficult to inspect or which have no access for visual inspection. As a result of this review, a list of 300 aircraft sections (approximate size 4' by 4') was developed and rated based on damage mechanism, probability of damage and inspection accessibility.

The sections to be disassembled were marked on the aircraft that was located at Davis Monthan AFB AZ (Figure 9). The sections were cut and shipped to Boeing Defense and Space Group, Wichita, KS, for further processing. At Boeing, the sections were photographed, disassembled, all the paint stripped and all corrosion and cracks found were entered into a database and the results are being published in a series of documents. To date, 230 of the sections have been disassembled with the results of 218 of these released in 8 documents. It is expected that the remaining sections will be completed in early 1995.

Corrosion on the parts is being classified as light, light to moderate, moderate, moderate to severe and severe, with the corresponding depths of this corrosion being defined as less than .001, .001 to .003, .001 to .01, .008 to .012, and greater than .01, respectively. From the 230 sections documented to date, there were 966 records generated in the database detailing results. One hundred forty-nine of these records had instances of severe corrosion, 99 records had moderate to severe corrosion, 475 had moderate corrosion, 619 had light to moderate corrosion and 795 had light corrosion. There were 16 instances of stress corrosion cracking and 17 instances of fatigue cracking on the sections documented to date. Over 70 areas of the aircraft have been identified as needing better repair techniques, more rework allowables, and better maintenance procedures, or have been identified as potential service life extension program

candidates. A few of the additional and/or increased inspections and repairs added to the Programmed Depot Maintenance (PDM) Statement of Work (SOW) are: cockpit window frame corrosion, expanded wing skin corrosion inspections, radome bulkhead corrosion and corrosion between fuselage skin and steel doublers below pilot's side windows. Some areas of serious hidden/inaccessible severe corrosion were found that had not been previously identified:

1. Inside surface of lower wing skin where the steel main landing gear support trunnion is attached. Figure 10 is a photograph of the severe pitting corrosion on the top surface of the "new" lower wing skin where the steel main landing gear trunnion is bolted between the top and bottom wing skins. The deepest pits were approximately 0.06 inch deep in the 0.54-inch thick skin.

2. Faying surfaces of wing skins and wing spar caps where upper and lower wing skins are attached to the front and rear spar. Figure 11 is a photograph of corrosion between the lower skin and the wing spar caps.

3. Buried intergranular corrosion around wing skin fasteners. Disassembly experience showed that there is layered intergranular corrosion when corrosion is present on the wing skin surfaces and is often present even when no surface corrosion is observed. Figure 12 is a cross-sectional cut through a wing skin fastener hole showing surface corrosion, as well as under the fastener hole.

Since it has been confirmed that severe hidden/inaccessible corrosion was found on the disassembled aircraft, it can be assumed that it also exists on other aircraft in the fleet. As a result, the following major issues/questions arise: (a) methodologies to detect and quantify this hidden/inaccessible corrosion are urgently needed, (b) to what degree does this corrosion degrade the structural integrity? (c) what are the growth rates of this corrosion? and (d) what is the actual structural life or economic life of the aircraft with the effects of corrosion now included?

3. Corrosion/Structural Integrity Testing and Analysis

The estimates of structural life/fatigue life presented by aircraft manufacturers do not include the material strength degradation effects of corrosion. Tests and analyses are based on pristine aluminum structure. Also, the USAF Aircraft Structural Integrity Program (ASIP) and Damage Tolerance Analysis (DTA) procedures do not include considerations of how corrosion may alter fatigue crack nucleation (initiation) and accelerate crack growth rates. It is recognized

that to be able to maintain C/KC-135 structural integrity to 2040 the effects of corrosion and combined effects of corrosion and fatigue need to be determined. Therefore, the objectives of this element are to access the effects of corrosion on fatigue life and crack growth rates of C/KC-135 fuselage lap joints and upper wing skins.

Strategy

Initially, it is planned to conduct two types of test, stress vs. fatigue cycles to failure (S-N) and crack propagation fatigue tests (da/dn vs. K) in corroded material. The (S-N) test data will be used to determine a preliminary fuselage lap joint relative life factor. Boeing will use the relative life factor to revise C/KC-135 fuselage structural/economic life estimates. Specimens will be cut from old C/KC-135 aircraft with and without natural corrosion, as well as lab grown severe corrosion. Fuselage lap joint specimens will be from 2024-T3, 2024-T4 and 7075-T6 materials. Wing skin specimens will be from 7178-T6 material. Complete fractographic and corrosion quantification analysis will also be conducted.

S-N Fatigue Testing

The S-N fatigue testing of select C/KC-135 fuselage lap joint structure is for the purpose of determining a preliminary assessment of fatigue life degradation due to faying surface corrosion. Test results will provide an initial estimate of aircraft service life reduction due to corrosion.

"Natural" (as-received) and "severe" (artificial) corrosion life reduction effects will be assessed through interpretation of resulting S-N curves (Figure 13). Specimen relative life ratios will be applied (as a first approximation) to actual uncorroded aircraft service life to calculate corroded service life. Subsequent testing may refine this estimate if this test effort demonstrates that life reduction effects are significant or cannot be accounted for by simple stress level adjustments.

Test specimens are TYPE 1 joint structure as defined in Figure 14, and will be the only joint configuration tested due to current material availability. Depicted is the top 10 of a possible 195 unique C/KC-135 fuselage lap joint types. These 10 types have been identified as comprising approximately 56% of the total length of all fuselage lap joints and reflect different skin/doubler configurations, aluminum alloys, heat treatment conditions, skin thicknesses, number of fastener rows, fastener types, fastener diameters, and fastener patterns. The TYPE 1 configuration has been selected based on material availability alone, and not as being any more susceptible or prone to corrosion problems than any other lap joint type. A total of

forty-eight fuselage lap joint specimens will be fabricated per Figure 15.

All specimens will be NDI inspected after final fabrication to establish NDI baselines for the uncorroded specimens and to aid in selecting the specimens for artificial corrosion. Artificially corroded specimens will be NDI inspected a second time prior to test to establish NDI baselines. Constant amplitude testing will be conducted with three different maximum cyclic stress levels (9, 12, 15), R-ratio = +0.1, room temperature (65-85 degrees F), 85% minimum non-condensing relative humidity, and 10hz sine wave loading. Between four and six replications will be initially tested for each data point. All specimens will be disassembled after testing for a visual and fractographic examination to define the onset of "failure", and to supply NDI verification data.

Crack Growth Rate/Crack Propagation Testing

This test plan details the constant load fatigue crack growth rate test requirements of "as-received" and "artificially corroded" C/KC-135 fuselage and upper wing skin materials. "As-received" and "artificially corroded" fatigue crack growth rate data for four materials, two degrees of humidity and two cyclic frequencies will be recorded. Comparisons within this contemporary data set, as well as to existing data, will provide the basis for calculating analytical crack growth parameters for corroded and uncorroded C/KC-135 aircraft fuselage and upper wing skin material. Testing will be conducted at multiple laboratories, and Boeing Wichita will fabricate all test specimens. General testing practices and procedures will conform to ASTM E647-93. The test specimens will be ASTM E647-93 Middle Tension specimen fabricated from C/KC-135 material. Sufficient grip end area is provided to facilitate hydraulic gripping. The specimens will be locally polished to facilitate optical crack length measurements (two sides of the "as-received" and one side of the "artificially corroded"). The starter notch will be wire cut. Artificial corrosion will be on the "exterior" (relative to the airplane) surface only. Test specimen material is from U S Air Force provided retired C/KC-135 aircraft. Specifically, 2024-T3, 2024-T4, and 7075-T6 fuselage skin material and 7178-T6 upper wing skin material will be tested. Nominal fuselage skin thicknesses range from approximately 0.040" to 0.100". Nominal upper wing skin thicknesses range from approximately 0.060" to 0.350".

Corrosion Degree and Type

Specimens will be tested in the "as-received" and "artificially corroded" corrosion states. An attempt will be made to find and test specimens with natural corrosion. The problem is trying to

find large enough naturally corroded panels to make specimens that are free of fastener holes.

Test and Loading

All testing will be continuous and at room temperature (65-85 degrees F). "Dry" environment is defined as being less than 15% relative humidity. "Wet" environment is defined as being non-condensing and greater than 85% relative humidity. All humidity data should be at the environmental chamber exhaust. High humidity vapor should be provided by bubbling "clean" laboratory air through a column of ASTM D1193 Type III or better reagent water. Loading will be constant amplitude sine wave. Pre-cracking cyclic stress levels shall be 75% of the maximum cyclic stress levels, and extend the starter notch from 0.350 inch to 0.450 inch.

Future Test Plans

A number of tests are planned and will be implemented as funding becomes available; Natural Corroded Specimen Testing, Spectrum Loading Tests, Full Scale Fuselage Panel Tests, Full Scale Wing Section Tests, Residual Strength Tests of Corroded Specimens.

4. Corrosion Growth Rate Testing and Analysis

It is imperative that corrosion growth rates be determined to be able to predict the future occurrence and severity in areas like the faying surfaces of lap joints on C/KC-135 aircraft. Attendant with determining growth rates is the identification of the variables that influence growth rates such as material and environment.

To conduct the required corrosion growth rate testing, lap joint specimens will be manufactured from new material and material taken from retired C/KC-135 aircraft and placed in locations worldwide that coincide with C/KC-135 aircraft operations. The specimens will be examined at the test location and selected specimens will be returned periodically for invasive examination. Data will be collected and analyzed to determine the corrosion growth rates in the lap joint specimens. Tests will generally follow the guidelines of ASTM G-50. Modifications have been made where necessary to accommodate the specifics of this test. If available, new technology corrosion sensors and detectors will also be installed on the specimens to record additional corrosion data.

In determining which sites to use for this test, three factors were considered: first, presence of an active runway; second, environmental conditions and expected corrosion damage (based upon "PACER LIME" an Environmental Corrosion Severity Classification System"); and third, whether C/KC-135 aircraft operate at the location.

Kure Beach, North Carolina, was selected, but does not meet the criteria listed above. It was selected since it is a commercial corrosion test facility. All of the other sites selected have been determined to be representative of worldwide C/KC-135 operating environments. The following sites have been tentatively selected:

Expected Very Severe Corrosion Sites:

a. Elmendorf AFB, Alaska, b. Kure Beach, North Carolina, c. Hickam AFB, Hawaii, d. Kadena AB, Japan

Expected Severe Corrosion Site:

Aviano AB, Italy

Expected Moderate Corrosion Sites:

a. Fairchild AFB, Washington, b. Howard AFB, Canal Zone, c. Ramstein AB, Germany, d. Tinker AFB, Oklahoma

Expected Mild Corrosion Sites:

a. Davis Monthan AFB, Arizona, b. O'Hare AFB, Illinois.

An initial test involves placement of specimens representative of C/KC-135 lap joints and upper wing surfaces in Riyadh and Jedda, Saudi Arabia. While the test is programmed for five years, a ten year supply of specimens will be put in place to allow for a five year extension to the program. Each year a predetermined number of specimens will be returned, nondestructively inspected, disassembled, analyzed, and assessed.

5. Integrated Corrosion Data Base (ICDB):

The integrated Corrosion Data Base (ICDB) is essentially an information management system. It will store only that data that is not stored on other systems and devote the remainder of its functions to accessing and retrieving information from other "legacy" systems. It will provide for information collection from the Program Depot Maintenance (PDM) line via the Boeing built Graphically Enhanced Corrosion Information System (GECIS) and be able to handle the automated processing of the engineering discrepancy forms, AFMC Form 202. It will house and manipulate all the information collected in the test programs to allow for analysis of that information. In turn, this information will be feed into the predictive models for corrosion formation that will also be housed in ICDB. ICDB will also provide "by-tail-number" comparisons of damage and previous repairs as well as tracking of parts required for upcoming PDMs.

It leverages a number of systems already in place and programs currently in operation in order to minimize the cost associated with the ICDB. All of the equipment and legacy systems from which it will draw information are already in place.

This includes the primary sever. Also, the resources of other programs such as the Integrated Data Strategy (IDS) are being taped to obtain funding for additional equipment and functions.

The complete ICDB has not yet gone on contract, but will be a valuable asset to the C/KC-135 engineering office, and will be completely transportable to other weapon systems.

The KC-135 has been around for over thirty years, but virtually very little maintenance data has been collected over these years that is sufficient to assess the overall corrosion condition.. A system is currently being developed by Boeing Wichita to insure more accurate data input without increasing the workload of maintenance personnel. This system is called GECIS (Graphically Enhanced Corrosion Information System). GECIS utilizes graphical images of the aircraft to allow the aircraft inspector to point and click to the particular part of the aircraft of interest before going to the data input screen. The computer will identify the work unit code at this location and automatically log it into the form. A graphical interface is used throughout this system to help reduce the reliance on the mechanic/inspectors ability to accurately lookup and input data. In addition, the system will have tables of information in the database to link particular location of the aircraft with the Illustrated Parts Breakdown, Repair Manuals and Rework Manuals. The development of this system is currently in progress and a prototype should be completed in early 1996.

6. Corrosion Predictive Modeling

Concept Development

There has been virtually little work in the field of corrosion modeling and prediction which can be directly applied to prediction and modeling of environmental corrosion of C/KC-135 aircraft structure. Specific corrosion data for C/KC-135 structure, or any aircraft structure, is not readily available. However, a variety of existing information sources exist, including Depot overhaul inspection/repair information and individual C/KC-135 operational and maintenance reports that could be used to provide some insight concerning the occurrence of corrosion on C/KC-135 aircraft.

This approach, developed by ARINC Research Corp, will consist of the concurrent development of a Statistical Model (SM), a Mechanistic Model (MM), and a Probabilistic Model (PM), Figure 16. Generally, the SM will address corrosion at the aircraft fleet level and will use actual aircraft data to determine the probability of corrosion occurring on specific C/KC-135 components (e.g., Stringer 19, Bulkhead Station 360-420 RH) based on the number of ground-air-

ground (GAG) cycles, environmental exposure experienced by the aircraft, and other measurable variables. If there is information from aircraft disassembly, assumptions will be made based on information availability. The MM will address corrosion at the material and component (e.g., lap seams) levels to determine the rate of corrosion, the extent of corrosion, where corrosion can be expected to occur in relation to environment (e.g., temperature, pH), and the effect of corrosion on the structural integrity of the aircraft based on material properties, including corroded and virgin material, and structural configuration. The PM will integrate information on the C/KC-135 corrosion process from the SM and MM to develop the probability distribution functions which will relate certain measurable variables with the probability, over time, of certain levels of corrosion.

Assumptions

The magnitude of modeling corrosion on the C/KC-135 is such that certain assumptions must be made to place bounds on the problem so that work can progress in a timely manner. The assumptions and guidelines necessary to limit the initial scope of model development are: Only worst case scenarios of corrosion will be addressed, and the aircraft component studied will be the simple lap seam.

CONCLUSIONS

Corrosion currently is a serious maintenance problem on many U S Air Force aircraft and especially the C/KC-135 and it is getting worse. If the C/KC-135 and many other aircraft are expected to remain airworthy three to four times their original design life, then the combined effects of corrosion and fatigue will reduce structural integrity and catastrophic structural failures are predicted unless the corrosion is found, fixed and/or eliminated. Corrosion may very well prove to be one of the major life limiters of aging aircraft.

In this OC-ALC Aging Aircraft Corrosion Program, a plan has been developed to acquire the necessary engineering data to determine the location and severity of C/KC-135 corrosion, determine corrosion growth rates, determine the effects of corrosion on structural integrity, develop models to predict future corrosion, document corrosion occurrences and finally provide information to support a C/KC-135 Service Life Extension Program. Many of the results of this program are, and will be, applicable to other aircraft and will benefit the worldwide aviation community.

NUMBER OF AIRCRAFT

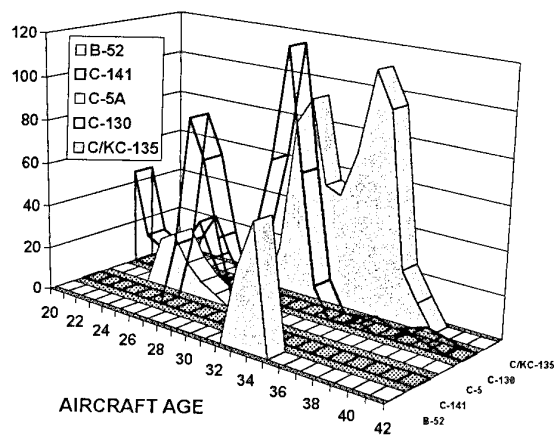


FIGURE 1. USAF Aging Aircraft Fleets

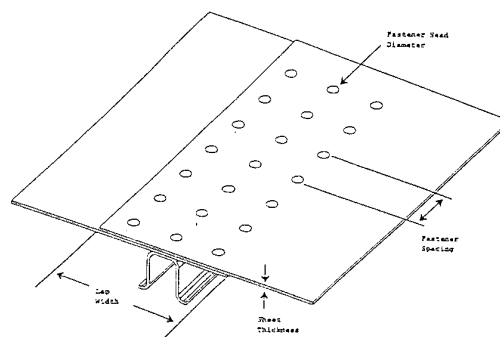


FIGURE 2. Typical Fuselage Lap Joint Configuration

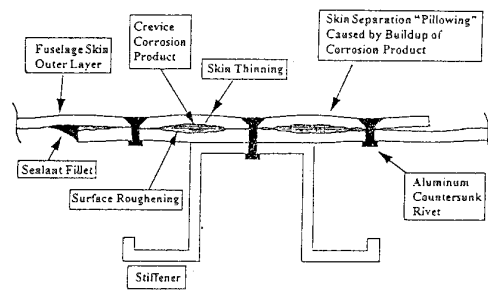


FIGURE 3. Cross Section Through Lap Joint

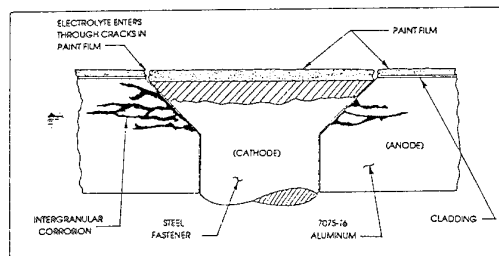


FIGURE 4. Intergranular Wing Skin Corrosion

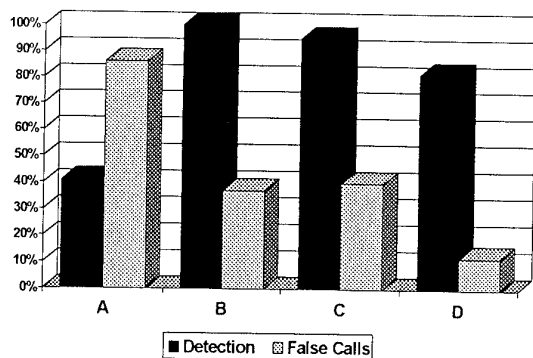


FIGURE 5. Detection vs False Call Results

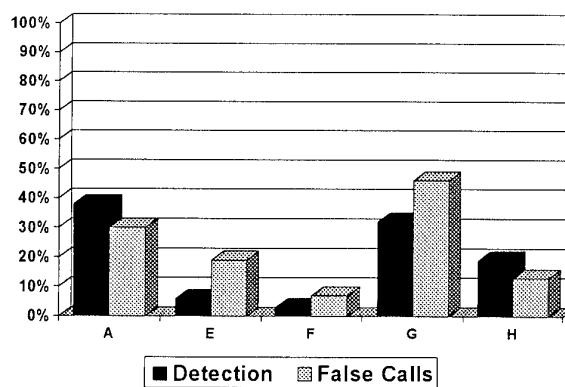


FIGURE 6. Wing Skin Corrosion Detection Results

AREA 1, SHEET 1

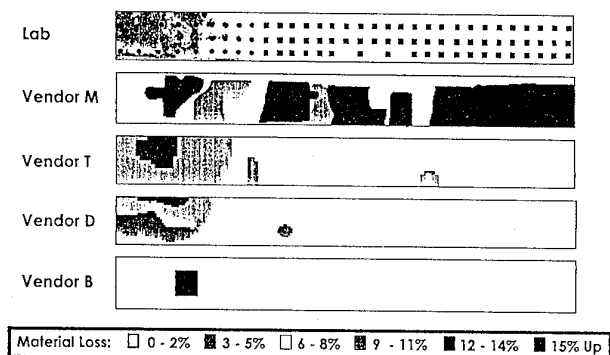


FIGURE 7. Actual Corrosion and NDI Images

AREA 1 RESULTS

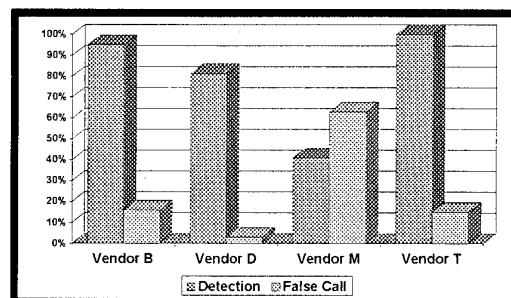


FIGURE 8. Area 1 Corrosion Detection Results

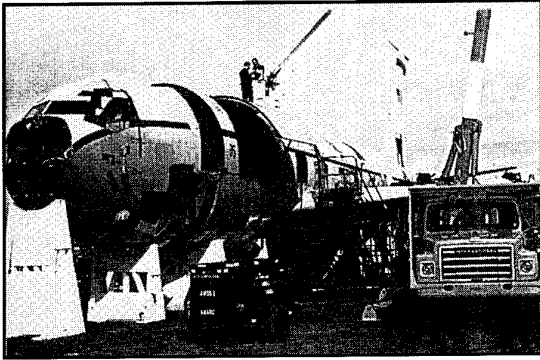


FIGURE 9. EC-135H Aircraft Marked for Cutting

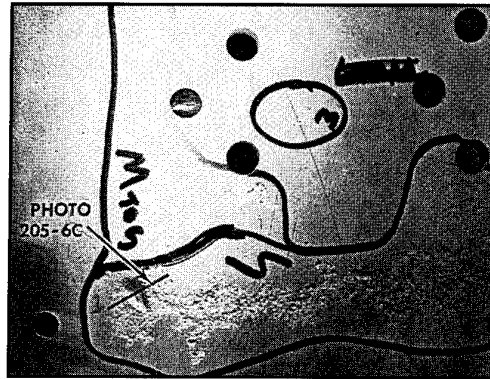


FIGURE 10. Severe Corrosion on Lower Wing Skin

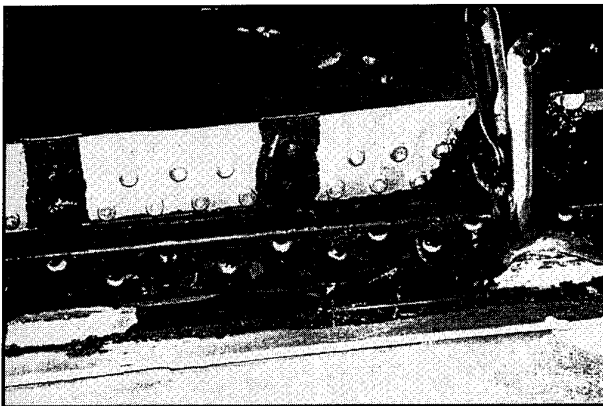


FIGURE 11. Corrosion between Wing Skin and Spar

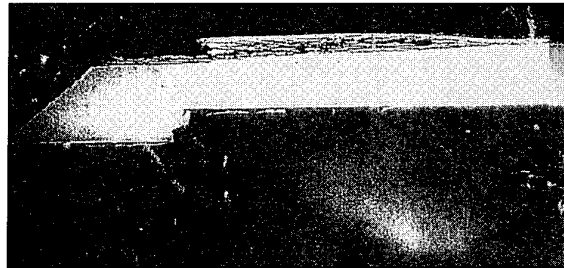


FIGURE 12. Intergranular Corrosion on Wing Skin

S/N Fatigue Relative Life

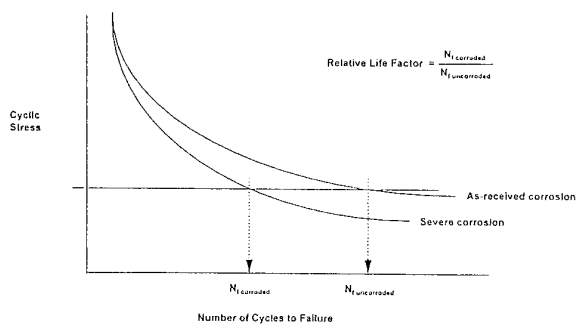


FIGURE 13. Relative Corrosion "Life Factor"

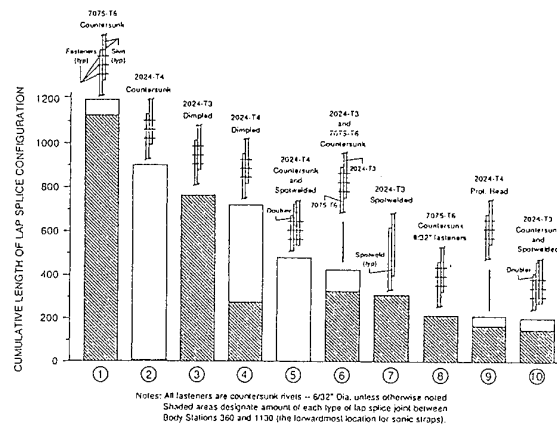


FIGURE 14. C/KC-135 Fuselage Lap Joint Types

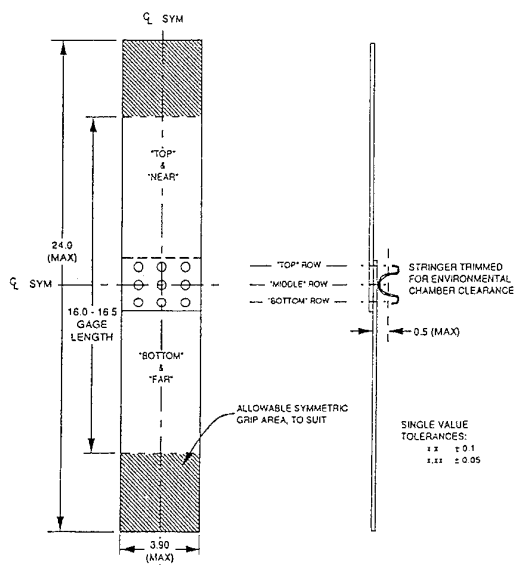


FIGURE 15. Typical Fuselage Lap Joint Test Coupon

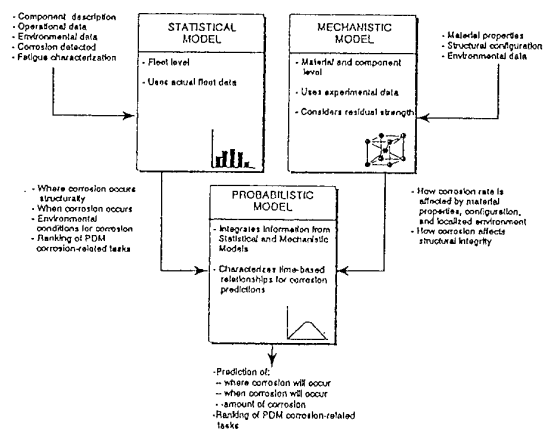


FIGURE 16. Three-Part Corrosion Model

REPORT DOCUMENTATION PAGE

1. Recipient's Reference	2. Originator's Reference AGARD CP-565	3. Further Reference ISBN 92-836-1011-3	4. Security Classification of Document UNCLASSIFIED
5. Originator Advisory Group for Aerospace Research and Development North Atlantic Treaty Organization 7 rue Ancelle, 92200 Neuilly-sur-Seine, France			
6. Title Corrosion Detection and Management of Advanced Airframe Materials			
7. Presented at The 79th Meeting of the AGARD Structures and Materials Panel, held in Seville, Spain, 5-6 October 1994			
8. Author(s)/Editor(s) Multiple			9. Date January 1995
10. Author's/Editor's Address Multiple			11. Pages 250
12. Distribution Statement There are no restrictions on the distribution of this document. Information about the availability of this and other AGARD unclassified publications is given on the back cover.			
13. Keywords/Descriptors Airframes Aircraft maintenance Corrosion prevention Corrosion tests Degradation Service life			
14. Abstract <p>A Specialists' Meeting on Corrosion Detection and Management of Advanced Airframe Materials was held to present the current knowledge base of corrosion, degradation, detection and prevention and to identify the research and development issues which must be addressed in order to ensure long service life and low maintenance costs of NATO aircraft. The Meeting concentrated on Corrosion Detection, Test Methodology for Environmental Assessment, Mechanistic Evaluation, Corrosion Prevention Methods, and Materials Selection and Design to Prevent Environmental Degradation.</p>			

<p>AGARD Conference Proceedings 565 Advisory Group for Aerospace Research and Development North Atlantic Treaty Organization CORROSION DETECTION AND MANAGEMENT OF ADVANCED AIRFRAME MATERIALS Published January 1995 250 pages</p> <p>A Specialists' Meeting on Corrosion Detection and Management of Advanced Airframe Materials was held to present the current knowledge base of corrosion, degradation, detection and prevention and to identify the research and development issues which must be addressed in order to ensure long service life and low maintenance costs of NATO aircraft. The Meeting concentrated on Corrosion Detection, Test Methodology for Environmental Assessment, Mechanistic Evaluation,</p>	<p>AGARD CP-565</p> <p>Airframes Aircraft maintenance Corrosion prevention Corrosion tests Degradation Service life</p>	<p>AGARD Conference Proceedings 565 Advisory Group for Aerospace Research and Development North Atlantic Treaty Organization CORROSION DETECTION AND MANAGEMENT OF ADVANCED AIRFRAME MATERIALS Published January 1995 250 pages</p> <p>A Specialists' Meeting on Corrosion Detection and Management of Advanced Airframe Materials was held to present the current knowledge base of corrosion, degradation, detection and prevention and to identify the research and development issues which must be addressed in order to ensure long service life and low maintenance costs of NATO aircraft. The Meeting concentrated on Corrosion Detection, Test Methodology for Environmental Assessment, Mechanistic Evaluation,</p>	<p>AGARD CP-565</p> <p>Airframes Aircraft maintenance Corrosion prevention Corrosion tests Degradation Service life</p>
<p>AGARD Conference Proceedings 565 Advisory Group for Aerospace Research and Development North Atlantic Treaty Organization CORROSION DETECTION AND MANAGEMENT OF ADVANCED AIRFRAME MATERIALS Published January 1995 250 pages</p> <p>A Specialists' Meeting on Corrosion Detection and Management of Advanced Airframe Materials was held to present the current knowledge base of corrosion, degradation, detection and prevention and to identify the research and development issues which must be addressed in order to ensure long service life and low maintenance costs of NATO aircraft. The Meeting concentrated on Corrosion Detection, Test Methodology for Environmental Assessment, Mechanistic Evaluation,</p>	<p>AGARD CP-565</p> <p>Airframes Aircraft maintenance Corrosion prevention Corrosion tests Degradation Service life</p>	<p>AGARD Conference Proceedings 565 Advisory Group for Aerospace Research and Development North Atlantic Treaty Organization CORROSION DETECTION AND MANAGEMENT OF ADVANCED AIRFRAME MATERIALS Published January 1995 250 pages</p> <p>A Specialists' Meeting on Corrosion Detection and Management of Advanced Airframe Materials was held to present the current knowledge base of corrosion, degradation, detection and prevention and to identify the research and development issues which must be addressed in order to ensure long service life and low maintenance costs of NATO aircraft. The Meeting concentrated on Corrosion Detection, Test Methodology for Environmental Assessment, Mechanistic Evaluation,</p>	<p>AGARD CP-565</p> <p>Airframes Aircraft maintenance Corrosion prevention Corrosion tests Degradation Service life</p>

Corrosion Prevention Methods, and Materials Selection and Design to Prevent Environmental Degradation.	Corrosion Prevention Methods, and Materials Selection and Design to Prevent Environmental Degradation.
ISBN 92-836-1011-3	ISBN 92-836-1011-3
Corrosion Prevention Methods, and Materials Selection and Design to Prevent Environmental Degradation.	Corrosion Prevention Methods, and Materials Selection and Design to Prevent Environmental Degradation.
ISBN 92-836-1011-3	ISBN 92-836-1011-3

Aucun stock de publications n'a existé à AGARD. A partir de 1993, AGARD détiendra un stock limité des publications associées aux cycles de conférences et cours spéciaux ainsi que les AGARDographies et les rapports des groupes de travail, organisés et publiés à partir de 1993 inclus. Les demandes de renseignements doivent être adressées à AGARD par lettre ou par fax à l'adresse indiquée ci-dessus. *Veuillez ne pas téléphoner.* La diffusion initiale de toutes les publications de l'AGARD est effectuée auprès des pays membres de l'OTAN par l'intermédiaire des centres de distribution nationaux indiqués ci-dessous. Des exemplaires supplémentaires peuvent parfois être obtenus auprès de ces centres (à l'exception des Etats-Unis). Si vous souhaitez recevoir toutes les publications de l'AGARD, ou simplement celles qui concernent certains Panels, vous pouvez demander à être inclu sur la liste d'envoi de l'un de ces centres. Les publications de l'AGARD sont en vente auprès des agences indiquées ci-dessous, sous forme de photocopie ou de microfiche.

CENTRES DE DIFFUSION NATIONAUX

ALLEMAGNE

Fachinformationszentrum,
Karlsruhe
D-76344 Eggenstein-Leopoldshafen 2

BELGIQUE

Coordonnateur AGARD-VSL
Etat-major de la Force aérienne
Quartier Reine Elisabeth
Rue d'Evere, 1140 Bruxelles

CANADA

Directeur, Services d'information scientifique
Ministère de la Défense nationale
Ottawa, Ontario K1A 0K2

DANEMARK

Danish Defence Research Establishment
Ryvangs Allé 1
P.O. Box 2715
DK-2100 Copenhagen Ø

ESPAGNE

INTA (AGARD Publications)
Pintor Rosales 34
28008 Madrid

ETATS-UNIS

NASA Headquarters
Code JOB-1
Washington, D.C. 20546

FRANCE

O.N.E.R.A. (Direction)
29, Avenue de la Division Leclerc
92322 Châtillon Cedex

GRECE

Hellenic Air Force
Air War College
Scientific and Technical Library
Dekelia Air Force Base
Dekelia, Athens TGA 1010

ISLANDE

Director of Aviation
c/o Flugrad
Reykjavik

ITALIE

Aeronautica Militare
Ufficio del Delegato Nazionale all'AGARD
Aeroporto Pratica di Mare
00040 Pomezia (Roma)

LUXEMBOURG

Voir Belgique

NORVEGE

Norwegian Defence Research Establishment
Attn: Biblioteket
P.O. Box 25
N-2007 Kjeller

PAYS-BAS

Netherlands Delegation to AGARD
National Aerospace Laboratory NLR
P.O. Box 90502
1006 BM Amsterdam

PORTUGAL

Força Aérea Portuguesa
Centro de Documentação e Informação
Alfragide
2700 Amadora

ROYAUME-UNI

Defence Research Information Centre
Kentigern House
65 Brown Street
Glasgow G2 8EX

TURQUIE

Millî Savunma Başkanlığı (MSB)
ARGE Dairesi Başkanlığı (MSB)
06650 Bakanlıklar-Ankara

Le centre de distribution national des Etats-Unis ne détient PAS de stocks des publications de l'AGARD.

D'éventuelles demandes de photocopies doivent être formulées directement auprès du NASA Center for AeroSpace Information (CASI) à l'adresse ci-dessous. Toute notification de changement d'adresse doit être fait également auprès de CASI.

AGENCES DE VENTE

NASA Center for
AeroSpace Information (CASI)
800 Elkridge Landing Road
Linthicum Heights, MD 21090-2934
Etats-Unis

ESA/Information Retrieval Service
European Space Agency
10, rue Mario Nikis
75015 Paris
France

The British Library
Document Supply Division
Boston Spa, Wetherby
West Yorkshire LS23 7BQ
Royaume-Uni

Les demandes de microfiches ou de photocopies de documents AGARD (y compris les demandes faites auprès du CASI) doivent comporter la dénomination AGARD, ainsi que le numéro de série d'AGARD (par exemple AGARD-AG-315). Des informations analogues, telles que le titre et la date de publication sont souhaitables. Veuillez noter qu'il y a lieu de spécifier AGARD-R-nnn et AGARD-AR-nnn lors de la commande des rapports AGARD et des rapports consultatifs AGARD respectivement. Des références bibliographiques complètes ainsi que des résumés des publications AGARD figurent dans les journaux suivants:

Scientific and Technical Aerospace Reports (STAR)
publié par la NASA Scientific and Technical
Information Division
NASA Headquarters (JTT)
Washington D.C. 20546
Etats-Unis

Government Reports Announcements and Index (GRA&I)
publié par le National Technical Information Service
Springfield
Virginia 22161
Etats-Unis
(accessible également en mode interactif dans la base de
données bibliographiques en ligne du NTIS, et sur CD-ROM)



AGARD holds limited quantities of the publications that accompanied Lecture Series and Special Courses held in 1993 or later, and of AGARDographs and Working Group reports published from 1993 onward. For details, write or send a telefax to the address given above. *Please do not telephone.*

AGARD does not hold stocks of publications that accompanied earlier Lecture Series or Courses or of any other publications. Initial distribution of all AGARD publications is made to NATO nations through the National Distribution Centres listed below. Further copies are sometimes available from these centres (except in the United States). If you have a need to receive all AGARD publications, or just those relating to one or more specific AGARD Panels, they may be willing to include you (or your organisation) on their distribution list. AGARD publications may be purchased from the Sales Agencies listed below, in photocopy or microfiche form.

NATIONAL DISTRIBUTION CENTRES

BELGIUM

Coordonnateur AGARD — VSL
Etat-major de la Force aérienne
Quartier Reine Elisabeth
Rue d'Evere, 1140 Bruxelles

CANADA

Director Scientific Information Services
Dept of National Defence
Ottawa, Ontario K1A 0K2

DENMARK

Danish Defence Research Establishment
Ryvangs Allé 1
P.O. Box 2715
DK-2100 Copenhagen Ø

FRANCE

O.N.E.R.A. (Direction)
29 Avenue de la Division Leclerc
92322 Châtillon Cedex

GERMANY

Fachinformationszentrum
Karlsruhe
D-76344 Eggenstein-Leopoldshafen 2

GREECE

Hellenic Air Force
Air War College
Scientific and Technical Library
Dekelia Air Force Base
Dekelia, Athens TGA 1010

ICELAND

Director of Aviation
c/o Flugrad
Reykjavik

ITALY

Aeronautica Militare
Ufficio del Delegato Nazionale all'AGARD
Aeroporto Pratica di Mare
00040 Pomezia (Roma)

LUXEMBOURG

See Belgium

NETHERLANDS

Netherlands Delegation to AGARD
National Aerospace Laboratory, NLR
P.O. Box 90502
1006 BM Amsterdam

NORWAY

Norwegian Defence Research Establishment
Attn: Biblioteket
P.O. Box 25
N-2007 Kjeller

PORTUGAL

Força Aérea Portuguesa
Centro de Documentação e Informação
Alfragide
2700 Amadora

SPAIN

INTA (AGARD Publications)
Pintor Rosales 34
28008 Madrid

TURKEY

Millî Savunma Başkanlığı (MSB)
ARGE Dairesi Başkanlığı (MSB)
06650 Bakanlıklar-Ankara

UNITED KINGDOM

Defence Research Information Centre
Kentigern House
65 Brown Street
Glasgow G2 8EX

UNITED STATES

NASA Headquarters
Code JOB-1
Washington, D.C. 20546

The United States National Distribution Centre does NOT hold stocks of AGARD publications.

Applications for copies should be made direct to the NASA Center for AeroSpace Information (CASI) at the address below.

Change of address requests should also go to CASI.

SALES AGENCIES

NASA Center for
AeroSpace Information (CASI)
800 Elkridge Landing Road
Linthicum Heights, MD 21090-2934
United States

ESA/Information Retrieval Service
European Space Agency
10, rue Mario Nikis
75015 Paris
France

The British Library
Document Supply Centre
Boston Spa, Wetherby
West Yorkshire LS23 7BQ
United Kingdom

Requests for microfiches or photocopies of AGARD documents (including requests to CASI) should include the word 'AGARD' and the AGARD serial number (for example AGARD-AG-315). Collateral information such as title and publication date is desirable. Note that AGARD Reports and Advisory Reports should be specified as AGARD-R-nnn and AGARD-LS-AR-nnn, respectively. Full bibliographical references and abstracts of AGARD publications are given in the following journals:

Scientific and Technical Aerospace Reports (STAR)
published by NASA Scientific and Technical
Information Division
NASA Headquarters (JTT)
Washington D.C. 20546
United States

Government Reports Announcements and Index (GRA&I)
published by the National Technical Information Service
Springfield
Virginia 22161
United States
(also available online in the NTIS Bibliographic
Database or on CD-ROM)



Printed by Canada Communication Group
45 Sacré-Cœur Blvd., Hull (Québec), Canada K1A 0S7